TECTONIC EVOLUTION OF THE CALEDONIAN COLLISIONAL SYSTEM, OFOTEN-EFJORDEN, NORTH NORWAY

by

Clyde J. Northrup

B.S. Geology
the University of New Mexico
1989

M.S., Geosciences
the University of Arizona
1991

Submitted to the Department of Earth, Atmospheric and Planetary Sciences in Partial Fulfillment of the Requirements for the Degree of

DOCTOR OF PHILOSOPHY

at the
MASSACHUSETTS INSTITUTE OF TECHNOLOGY
JUNE, 1996

Signature of Author.....
Department of Earth, Atmospheric and Planetary Sciences
May 21, 1996

Certified by.....
B. C. Burchfiel
Thesis Supervisor

Accepted by.....
Thomas H. Jordan
Department Head

Tectonic Evolution of the Caledonian Collisional System, Ofoten-Efjorden, north Norway

by
Clyde J. Northrup

Submitted to the Department of Earth, Atmospheric, and Planetary Sciences on May 21, 1996 in Partial Fulfillment of the Requirements for the Degree of Doctor of Philosophy

ABSTRACT

The Ofoten-Efjorden region of north Norway contains exposures of mid-crustal levels of the Caledonian collisional system, including the lower portions of the Caledonian nappe stack and the upper part of the structural basement onto which the nappes were emplaced. This study combines field mapping, structural/kinematic analyses, metamorphic petrology, and radiometric isotope geochronology to examine the Caledonian tectonothermal history of the region. Amphibolite facies metamorphism and strong penetrative strain occurred at deep levels of the nappe stack as it was emplaced onto the western margin of Baltica. Deformation within the rock mass reflects components of foreland-directed simple-shear and sub-vertically shortened pure-shear, a pattern of deformation consistent with spreading of the allochthon during emplacement.

Peak metamorphic mineral assemblages in metasedimentary rocks beneath the basal thrust of the allochthon contain garnet + kyanite + biotite ± staurolite, indicating that amphibolite facies conditions were attained by the footwall. The coexistence of rutile + almandine-rich garnet and zoisite + kyanite in these rocks is consistent with moderately high pressures, (9-10 kbar), suggesting that the portion of the Baltic craton now exposed in the western Ofoten area was subducted to 34-40 km depth beneath the nappe stack. Syntectonic to post-tectonic resorption of garnet and growth of plagioclase provides textural evidence for high-temperature decompression of the footwall.

Kyanite schist and local anatectic melts in the Narvik Nappe Complex yield U-Pb monazite and zircon with crystallization ages of ca. 432 ± 2 Ma, interpreted as the age of peak metamorphism. Cooling data from the area indicate time-integrated cooling rates of ca. 8-10°C/My from 432 to 400 Ma and ca. 2-3°C/My from 400 to 360 Ma. Combining these data with published information about the local P-T history indicates that rocks at this structural level underwent tectonic burial at an integrated rate of ca. 7 mm/yr from 437 to 432 Ma, followed by unroofing at an integrated rate of ca. 1 mm/yr from 432 to 405 Ma.

Tectonically significant findings of this study include the following: (1) the emplacement of the Caledonian allochthon resulted from a dynamic interaction between extensional and contractional processes; and (2) rocks in the footwall of the basal thrust of the allochthon underwent high-temperature decompression during the peak to early retrograde segment of their metamorphic evolution, consistent with extensional modification of the overlying nappe complex.

Thesis Advisor: B. C. Burchfiel, Professor of Geology

ACKNOWLEDGMENTS

As I look back and try to think of everyone I should acknowledge, it seems almost overwhelming to me the number of people who have contributed to the completion of this thesis in ways large and small. I will almost certainly forget to mention some individuals who deserve recognition, so let me begin by simply offering a collective "thank you" to the many people who have shaped my experience over the last decade or so. Thanks to Dr. Ed Grey for first pointing me in the direction of geology by allowing me to work with him as a field assistant in California back when I wasn't sure what I wanted to do with my life. Ed's love of his work and the wonders of the Owens Valley region convinced met to give Earth sciences a try. In addition to geology, Ed also introduced me to Chris Kaye (now Chris Northrup), so Ed's affect on my life has been profound and multifaceted.

After deciding to study geology, I re-entered the world of academia, first at the University of New Mexico and then at the University of Arizona. In many ways, the fact that I am now completing a Ph.D. is testimony to the strength of the undergraduate geology program at UNM and the geosciences curriculum at U of A. The boundless enthusiasm of fellow students and broad scientific curiosity of many faculty members with whom I have interacted at both institutions exerted a lasting influence. People like Chris Mawer, Rod Ewing, Jeff Grambling, and John Geissman at UNM and Spence Titley, Joaquin Ruiz, Peter Coney, and Dennis Norton at U of A all helped to begin the process of turning me into something of an Earth scientist. Brooke Clements, Tom McCandless, and many other graduate students at U of A provided the friendship, encouragement, and solace necessary to get me through a fairly rigorous M.S. program in a timely manner — thanks to all.

I will always remember the feeling of driving out of Tucson in a U-Haul truck headed for Boston and MIT in the summer of 1991. As someone raised in New Mexico, anything east of Missouri was considered a foreign country filled with strange, unpredictable people. Having now lived in the Boston area for several years, I can say with the clarity of first-hand knowledge that my preconceptions were entirely justified. Actually, life here has been full(!) and enjoyable, due in no small part to the community of folks I've worked with at MIT.

As thesis advisor, Clark Burchfiel deserves high praise for giving close guidance when necessary and yet providing enough room for me to grow scientifically. Clark gave me a lot of freedom to define the scope of this project, and shared his incredible insight into the workings of orogenic systems around the world. If I have learned anything from Clark about how to study mountain belts, it is the value of careful field work, asking important questions, and knowing where to look for the answers.

One of the great strengths of studying tectonics at MIT is that you have the opportunity to interact with a relatively large number of people who are interested in tectonic problems. Thanks to Sam Bowring, Kip Hodges, and Wikki Royden for teaching me the finer points of quantitative research, for serving as my "other advisors", and for many interesting discussions about tectonic issues great and small. Sam, in particular, gave me free run of

the U-Pb lab for my thesis work, and has spent a great deal of time, energy, and resources allowing me to do research in the Archean Slave Province in Canada as a side project, an opportunity for which I am very grateful. Thanks to John Bartley, from the University of Utah, for providing extremely useful critical feedback on all of the thesis chapters and for serving as a member of my committee. I continue to be amazed and inspired by the diversity and depth of John's knowledge in the Earth sciences. Jane Selverstone (now at UNM!) is one of my scientific heroes, and her class in metamorphic petrology reopened my eyes to the importance of careful petrography. It is truly amazing what one can learn about the evolution of a mountain belt by looking carefully at a suite of thin sections — thanks Jane.

Nancy Dalaire kept me out of trouble on numerous occasions when I had to deal with things bureaucratic or financial at MIT. Her patient answers to my endless questions and maneuvering in the world of paper and computer circuitry that is MIT kept me on track. Field assistants Bo Lawler and Dave Root provided excellent service during field seasons in Scandinavia, and deserve some kind of medal for keeping their *Esprit de Corps* in spite of the sometimes adverse conditions (i.e., becoming engulfed in fog so thick you can't see your feet while scrambling down a shear granite cliff; or wading through chest-high ferns which conceal wet, slippery fallen logs; or being overwhelmed by seething masses of flies; or...)

Graduate study at MIT is a fairly rigorous experience, and the encouragement, camaraderie, and scientific input of my student colleagues has made it worthwhile and enjoyable. Dave Applegate, Allison MacFarlane, Dave Dinter, Meg Coleman, Dave Hawkins, and many others have spent a lot of hours helping me not only to learn a great deal, but also to keep a balanced perspective; much love and thanks to all of them.

Speaking of much love and keeping a balanced perspective, the people who deserve the most credit for making this all possible are the many members of my family. While growing up in New Mexico, my parents provided an atmosphere which encouraged observation, asking questions, and exploring the environment — Earth science at its best. I remember the many weekend trips we took, stopping to collect rocks, or flowers, or bugs, or whatever the current subject of fascination might have been. Thanks to my parents, Clyde and Lu Northrup, for investing so much in their children.

Finally, let me acknowledge the love and support of Chris Northrup, my wife and partner, who has sacrificed a lot during the last several years to give me the opportunity to work toward a Ph.D. Through it all, her support has been unwavering. There is no way I could have accomplished this task without her walking with me every step of the way. More recently, Daniel Northrup has come into the picture, giving further proof of life beyond geology. Apart from an overwhelming need to help type on the keyboard as I write this, Daniel's core contribution to this thesis has been to maintain my perspective during the last 7 months as I completed the research, wrote and defended this thesis. Thanks Daniel.

Dedicated to:

Clyde and Lu Northrup

and to

Chris and Daniel Northrup

whose sacrifice and support have made it possible.

dvrggefggtc f hgggggggggggggggggggggggggggggggggggggggggggggggggg ttyn bbb nj g ghbbtnnnn yf5rtnbgi.....ft mnbhkkkkkkkkkkkkkkkkcg bhjkjgtbyhggngtllllll

- contributed by D. C. N.

Table of Contents

Chapter 1

Introduction and overview

INTRODUCTION

This chapter has three main purposes: first, it provides a general introduction to the history of the Caledonian Orogen as context for the geology of the Ofoten-Efjorden region; second, it gives an overview and synthesis of the results of this study; and third, it describes the rock units shown on the geologic maps that accompany this volume. Each of the other chapters contain enough background material to frame the specific questions addressed, and they can be read independently. Nevertheless, a more complete review of Caledonian tectonics might be beneficial to people not already familiar with the orogen, and such an overview seems an appropriate way to begin.

THE CALEDONIAN OROGEN

The Caledonian mountain belt contains the geologic record of the opening and closing of the Iapetus Ocean basin — a Wilson Cycle that spanned late-Proterozoic to early-Paleozoic time (Figures 1 and 2; Harland and Gayer, 1972). Due in part to the strong overprint of later tectonic activity, the early history of Iapetus is poorly known. Estimates of the age of rifting along the Baltic margin as the ocean basin opened vary from ca., 750 to 600 Ma, and the continent that rifted away from Baltica has not been clearly identified (Krill, 1986; Zwaan and Van Roermund, 1990; Svenningsen, 1993). However, from the perspective of Caledonian tectonics, the subduction and closure of

Iapetus are far more important than its formation. Arc-volcanic rocks with crystallization ages of ca. 500 Ma are found in oceanic-affinity thrust sheets in many parts of the orogen, indicating that subduction of the ocean basin had initiated by late Cambrian time (Dunning and Pedersen, 1988; Claesson et al. 1987; Stephens et al. 1993).

A long-standing controversy in Caledonian tectonics is whether or not an early episode of tectonic activity affected the western margin of Baltica in late Cambrian to early Ordovician time, 40 to 80 million years prior to the main Caledonian tectonothermal event (the 'Finnmarkian' phase of orogeny; Sturt et al. 1975; Sturt et al. 1978). Although the original relationships in Finnmark that led to the proposal of such activity have been questioned by some workers (see Krill and Zwaan, 1987; Krill et al., 1988), recent studies of the Seve nappes in other parts of the orogen suggest that Cambro-Ordovician metamorphism and deformation did occur elsewhere along the Baltoscandian margin (Dallmeyer and Gee, 1988; Dallmeyer, 1990; Dallmeyer et al. 1991). Thus, "Finnmarkian" tectonism may not have affected the type locality in Finnmark, but it seems to have taken place in other locations. Unfortunately, the term 'Finnmarkian' is deeply rooted in the literature and is still widely used despite its paradoxical origins. The causes of Cambro-Ordovician metamorphism and deformation along the continental margin are enigmatic. One possibility is that a volcanic arc collided with Baltica during early stages of the closure of Iapetus (Dallmeyer, 1990, others), but more work will be necessary before this part of the tectonic history can be resolved with confidence.

Final closure of Iapetus in Siluro-Devonian time resulted in the collision of Baltica and Laurentia and produced the main "Scandian" phase of Caledonian orogenesis (Gee and Wilson, 1974; Gee, 1975). As a consequence of the collision, a composite

nappe-stack was thrust eastward over the western margin of Baltica (Figures 2 and 3; Gee, 1975; Stephens and Gee, 1989). The nappe stack consisted of thrust sheets derived from the Baltic craton and its cover (the Lower and Middle Allochthons), overlain by thrust sheets from the distal margin of Baltica and the Iapetus Ocean basin (Seve and Köli nappes of the Upper Allochthon), overlain structurally by rocks of Laurentian continental affinity (Uppermost Allochthon; see Roberts and Gee, 1985). Strong penetrative deformation and high-grade metamorphism occurred at deep levels of the orogen as the allochthon was thrust eastward over the Baltoscandian margin. A-type subduction of the western portion of the Baltic craton to significant depths beneath the allochthon produced widespread high-P metamorphism in the cratonal rocks of southwestern Norway (Griffin, 1987, and references therein).

Extensional processes began to modify the architecture of the nappe stack during late stages of its emplacement (see chapter 2; Gee et al. 1994), and extension became the dominant tectonic mode (at least in the central and southern Caledonides) by early to middle Devonian time (Andersen et al. 1991; Norton, 1986). Late Caledonian extensional denudation and subsequent erosion have removed much of the allochthon and exposed deep levels of the orogen in Scandinavia. Today, the mountain belt consists of a relatively thin veneer of the original allochthonous thrust-stack lying over autochthonous or parautochthonous rocks of the Baltic craton (Figures 1 and 3). The present erosional surface essentially follows the structural level of the Caledonian A-type subduction zone across the orogen, so basal parts of the allochthon and the upper part of the structural basement are well exposed and can be studied directly in many parts of the orogen.

THE OFOTEN-EFJORDEN AREA

The general geology and regional context of Ofoten-Efjorden are illustrated in Figures 4 and 5. Outcrops in the study area comprise some of the westernmost, and therefore deepest, exposures of the Caledonian allochthon on the Norwegian mainland at this latitude. Two sets of late-Caledonian folds, one trending NNE and another trending ESE, control the regional map pattern (Figure 5; Steltenpohl and Bartley, 1988). The folds rotate the structural section into variably dipping orientations, so the fold limbs provide oblique cross-sectional views through the lower part of the allochthon and the upper part of the structural basement.

This part of the Caledonides has enjoyed a relatively long history of geologic investigation. Reconaissance mapping by Vogt (1942, 1950) and Foslie (1941, 1949) produced a remarkably complete and accurate inventory of rocks in the allochthon. More recent studies by Bartley (1980), Hodges (1982), Steltenpohl (1983, 1985) and others have evaluated various aspects of the tectonothermal history of the area. Three general phases of deformation are recognized: Early deformation (D1) included the thrusting, folding, and bulk shortening associated with assembly of the composite allochthon prior to the metamorphic peak in the allochthon. D1 structures are commonly cryptic due to the intensity of later deformation and metamorphism. The second phase of deformation (D2) involved the eastward emplacement of the assembled allochthon onto the margin of the Baltic craton, perhaps accompanied by continued imbrication and tectonic shuffling of nappes in the allochthon. D2 thrusting was accompanied by epidote-amphibolite facies metamorphism and intense penetrative strain at deep levels of the allochthon.

Late-Caledonian deformation (D3) resulted in the NE- and SE-trending folds, local crenulation and transposition of early fabric, and some additional motion across ductile fault zones during the retrograde portion of the P-T path. ESE-directed transport of allochthonous tectonic elements occurred throughout the early phases of deformation and continued into the early part of D3. Post-orogenic top-W extensional reactivation of thrusts occurred locally in the eastern portion of the region during D3 (Fossen and Rykkelid 1992; Rykkelid and Andresen 1994).

KEY RESULTS OF THE PRESENT STUDY

My work focused primarily on the kinematic characteristics and patterns of deformation associated with the assembly and emplacement of the nappe stack in the region. Specifically, I examined the following: (1) the structural development of the ductile faults that constitute the basal shear zone of the Caledonian allochthon; (2) kinematic characteristics of penetrative deformation and its role in the evolution of the nappe stack; (3) metamorphism and deformation in the footwall of the basal shear zone; and (4) the absolute ages of deformation, metamorphism, and cooling at various structural levels. Geologic mapping and field work focused on the contact between the basement and tectonic cover from East Hinnøya southward to Efjorden (Figure 5; Plates 1-3), and linked areas studied previously by Bartley (1981) and Hodges (1982).

Tectonostratigraphy

A wide variety of rocks were mapped in the region during the course of this study. The lithologic units found on the geologic maps (Plates 1-3) are keyed to the descriptions presented below.

Cratonal Basement

Proterozoic granite **(pCg)** forms the dominant rock type within the Baltic craton of the region. In most locations, the granite is coarse grained and contains abundant K feldspar megacrysts; local aplitic zones are present as well, commonly in the form of dikes. The Proterozoic granite contains sporadic xenoliths and screens of older Precambrian supracrustal rocks including amphibolite, quartzite, and schist **(pCs)**. Such rocks are particularly common in the craton between Ofotfjord and Efjord, and in the basement on East Hinnøya near Storvann.

Storvann Group

Working on East Hinnøya, Bartley (1981) recognized a laterally persistent sequence of metasedimentary rocks above the cratonal basement of Baltica but beneath the nappes of the Allochthon, and he interpreted these rocks as a tectonized remnant of the early Paleozoic cover on Baltica (the Storvann Group; see chapter 5). The base of the Storvann group consists of a heterogeneous quartzite layer that varies in thickness from a few cm up to more than 200 m and ranges in character from vitreous quartzite **(sq)**, to sugary arkosic quartzite **(sa)** ± quartzofeldspathic schist. South of Ofotfjorden, much of the quartzite is arkosic, with sporadic layers of white vitreous quartzite or quartzofeldspathic schist up to 10 m thick.

Psammitic schist **(sg)** overlies the quartzite, and it represents the most widespread and volumetrically significant lithology within the Storvann Group. Garnet is present as 1-10 mm porphyroblasts within a quartz-plagioclase-muscovite-biotite matrix. Muscovite and biotite commonly form lenticular segregations within the schist, lending a distinctive appearance to outcrops of this unit. In places, the psammitic schist becomes calcareous near its base or its top, producing discontinuous marble horizons **(sm)**. Where different marbles can be recognized, they have been designated sm1 near the base of the psammitic schist, and sm2 near the top of the schist.

The stratigraphically highest rock type recognized in the metasedimentary cover is a rusty-weathering calc-pelitic schist **(sp)**. This unit is more aluminous than the psammitic schist. It contains kyanite and large garnet porphyroblasts up to 3 cm in diameter in a muscovite-rich matrix. The stratigraphic thickness of the calc-pelitic schist is highly variable due to complex internal deformation. In most of the area mapped, it is present only as discontinuous outcrops or lenses up to 50 m in thickness directly beneath the Caledonian allochthon.

sliver zone

In some places, the shear zone at the base of the allochthon consists of structurally interleaved mylonitic rocks of uncertain tectonic affinity and heterogeneous lithologic character. This mylonitic sliver zone **(mz)** forms a fundamental structural and tectonostratigraphic break — it marks the transition between Baltic affinity rocks below and far-traveled oceanic affinity rocks above.

Narvik Nappe Complex

The Caledonian allochthon in Ofoten-Efjorden contains a complex assemblage of far-traveled nappes which were emplaced to the ESE onto the margin of the Baltic craton as the continental margin was subducted westward during the culmination of the Caledonian collision. The structurally lowest thrust sheets in the allochthon form the Narvik Nappe Complex (NNC), and these rocks crop out chiefly south of Ofotfjord in the area examined by this study. Four units have been recognized for purposes of mapping. A basal unit composed of amphibolite and biotite schist **(nb)** forms the lower 100-300 m of the NNC. Due to its structural position in the hangingwall of the basal shear zone, this unit constains strong internal deformation. Lenses of ultramafic rocks **(nu)** and impure marbles **(nm)** can be found in mafic and pelitic schist in the lower parts of the NNC. Relatively large lenses of these rocks types are indicated on the map, but smaller outcrops of ultramafic rocks and impure marbles (<10 m) are present sporadically. Pelitic schist **(np)** represents by far the most significant lithology within the NNC. In most outcrops, kyanite forms obvious bladed crystals up to 2 cm in length. Strongly deformed granitic dikes are ubiquitous in the schists of the NNC, and are characteristic of this tectonostratigraphic package.

Ofoten Nappe Complex

Structurally above the NNC lies the Ofoten Nappe Complex (ONC). The present study focused primarily on mapping the relationships and rock units below the ONC, so these rocks were not examined in detail. The parts of the ONC mapped have been divided into three units. A thin (25 - 100 m thick) layer of amphibolite ± tonalite **(oa)** occurs

discontinuously at the base of the ONC and is overlain by heterogeneous clastic sediments **(oc)** including quartzite, biotite schist, and para-amphibolite. The clastic sediments contain sporadic conglomerate lenses with clasts of amphibolite and tonalite in a quartzite or amphibolite matrix. The Evenes marbles **(oe)** overly the clastic sediments, and are composed of relatively pure calcite marble with intercalated horizons of calcareous shist and minor amphibolite layers.

Structural Development

Shear-sense indicators such as shear bands, S-C fabric, and asymmetric porphyroclasts are ubiquitous in the tectonites of the basal thrust, and they yield a consistent top-to-the-ESE sense of structural transport across the shear zone at the base of the nappes in the areas examined in this study. Deep levels of the nappe stack underwent amphibolite facies metamorphism and strong penetrative strain as the nappes were emplaced. Bulk deformation included components of foreland-directed (top-to-the-ESE) simple-shear and sub-vertically shortened pure-shear, a pattern of ductile flow which resulted in foreland-directed structural transport, sub-vertical thinning, and transport-parallel elongation of the rock mass at deep levels of the nappes. Such deformation is consistent with spreading of the allochthon during emplacement (Chapter 2).

Nappe emplacement in northern Scandinavia was generally ESE-directed, an orientation nearly perpendicular to the trend of the orogen. In the Efjord area, however, orogenesis also produced top-to-the-SSW motion on N-dipping thrust faults in the cratonal basement beneath the allochthon. Some of the SSW-directed thrust-sheets moved upward into the overlying metasedimentary cover and formed the cores of S-

verging recumbent folds at the base of the Caledonian allochthon. As deformation continued, these fold nappes became entrained in the top-to-the-ESE transport of the overlying allochthon. Thus, structures in the area suggest vertical partitioning of strain into components with nearly orthogonal displacement directions at different structural levels. Collectively, the top-to-the-SSW (orogen-parallel) and top-to-the-ESE (orogen perpendicular) components of transport are consistent with overall sinistral-oblique, post-collisional convergence between Baltica and Laurentia (Chapter 3).

Metamorphism

Metamorphic studies focused on the thermobarometric history of rocks that constitute the footwall of the Caledonian A-type subduction zone in the region. Some of the metasedimentary rocks in the footwall of the basal thrust of the allochthon are a strongly tectonized remnant of the early Paleozoic cover sequence on Baltica, and their metamorphic and deformational history provide a record of the progressive movement of the structural basement through the Caledonian A-type subduction system. Peak metamorphic mineral assemblages contain garnet + kyanite + biotite ± staurolite, indicating that amphibolite facies conditions were attained. In addition, the coexistence of rutile + almandine-rich garnet and zoisite + kyanite in these rocks is consistent with moderately high pressures (ca. 9-10 kbar). Such pressures suggest that the portion of the Baltic craton now exposed in the western Ofoten area was subducted to 35-40 km depth during Caledonian orogenesis. Syntectonic to post-tectonic resorption of garnet and growth of plagioclase provides textural evidence for high-temperature decompression of

the footwall (Chapter 5), and this decompression may be related to extensional processes recognized in the overlying nappe complex.

Timing Relations

U-Pb and $^{40}Ar/^{39}Ar$ geochronologic analyses (Chapter 4) were done to determine the age of amphibolite facies metamorphism, penetrative deformation, and subsequent cooling of rocks at deep levels of the allochthon, primarily within the Narvik Nappe Complex (NNC). Strongly deformed granitic dikes in the NNC yield U-Pb zircon ages of 437 ± 1 Ma, giving a maximum age for the thrust assembly, amphibolite facies metamorphism, and concomitant penetrative deformation at this structural level. Monazite and zircon from garnet + kyanite schist and local anatectic melts in the NNC yield crystallization ages of ca. 432 ± 2 Ma, and this is interpreted to reflect the age of peak metamorphism. The cooling history of the NNC is delineated by the isotopic ages of a series of minerals with different closure temperatures, including: U-Pb monazite (432 Ma), $^{40}Ar/^{39}Ar$ hornblende (410-405 Ma), $^{40}Ar/^{39}Ar$ muscovite (400-395 Ma), U-Pb rutile (ca. 382 Ma), and Rb-Sr biotite (ca. 360 Ma; Chapter 4). Data from the area indicate a time integrated cooling rate of ca. 8-10°C/My from 432 to 400 Ma, followed by slower cooling (2-3°C/My) from 400 to 360 Ma. Combining this T-t information with published information about the P-T history of the NNC allows estimation of time-integrated rates of tectonic burial and denudation. Such an analysis indicates that rocks at this structrual level underwent tectonic burial at an integrated rate of ca. 7 mm/yr from 437 to 432 Ma, followed by unroofing at an integrated rate of ca. 1 mm/yr until 405 Ma.

Tectonic Synthesis

Collectively, the data and observations presented in this study form the basis for a tectonic model of the evolution of the Caledonian collisional system in this region. Early thrusting, folding, and bulk shortening assembled a thick, composite nappe stack west of the present study area during final stages of the closure of Iapetus. As a consequence of imbrication and crustal thickening, the temperature at deep levels of the allochthon increased. Prograde thermal evolution culminated with amphibolite facies metamorphism in rocks at deep levels of the nappe stack (the NNC) at ca. 432 Ma. Relatively high temperatures and prograde devolatilization caused a decrease in the internal strength and basal coupling of the nappe stack, and these changes in the rheologic structure resulted in extensional failure of the nappes during their emplacement. Extension at midcrustal levels was accommodated by a combination of ductile faulting and heterogeneous flow. These modes of deformation occurred while the rocks remained at relatively high temperatures and, therefore, such deformation happened prior to cooling through about 500°C at 405-410 Ma (the nominal range of $^{40}Ar/^{39}Ar$ ages of hornblende at this structural level).

Following A-type subduction of the cratonal basement of Baltica to depths of 35-40 km beneath the nappe stack in the Ofoten-Efjorden region, extensional thinning of the overlying nappes produced decompression of the footwall. Textural relations in the metasedimentary rocks in the footwall of the basal thrust provide evidence for resorption of garnet and growth of plagioclase, consistent with high-temperature decompression. Foreland-directed extensional transport and ductile flow of midcrustal rocks in the nappe

stack may have contributed to the unroofing of the regionally significant basement culmination exposed in the western part of the Ofoten-Efjorden study area and on the Lofoten Islands, and this deformation provided a kinematic link between extension in the Caledonian hinterland and continued shortening in the foreland. If so, then decompression of the footwall was contemporaneous with the high-temperature attenuation of the overlying nappe stack sometime in the interval of time between ca. 430 and 410 Ma. Thus, emplacement of the Caledonian allochthon was achieved by an evolving interaction of extensional and contractional processes operative in different locations or structural levels within the orogen over an interval of time spanining ca. 430-410 Ma.

Relatively slow cooling (ca. 2-3°C/My) from 400 to 360 Ma suggests relatively slow, steady unroofing in this region during early to middle Devonian time. Such an interpretation is in marked contrast to the apparently rapid and active tectonic denudation of midcrustal rocks documented in the central and southern parts of the orogen at this time, and it suggests that the character of Siluro-Devonian tectonism may have varied significantly in different parts of the Caledonides.

One aspect of the tectonic evolution in the region that deserved emphasis is the apparently fundamental role played by mechanical decoupling between rocks at various crustal and structural levels in the overall evolution of the system. Such decoupling seems to have allowed seemingly disparate patterns of deformation to develop at different structural levels and produced significant vertical partitioning of the midcrustal strain field (Chapers 2 and 3). These observations highlight the potential three-dimensional

complexity of nappe emplacement kinematics in environments with partitioned deformation, evolving rheologic structure, and significant decoupling between structural levels.

CONCLUSION

The preceding discussion introduces the tectonic evolution of the Caledonian Orogen, provides a brief description of the rock units found within the Ofoten-Efjorden area, and gives an overview of some of the results of this study. More detailed descriptions of rock types, field relations, analytical data, and interpretations can be found in each of the following chapters which focus on specific questions addressed by this study.

REFERENCES

Bartley, J., M., 1981, Structural geology, metamorphism, and Rb/Sr geochronology of east Hinnøy, north Norway, Ph.D. thesis, Massachusetts Institute of Technology, Cambridge, MA.

Claesson, S., Stephens, M. B., and Klingspor, I., 1987, U-Pb zircon dating of felsic intrusions, Middle Köli Nappes, central Scandinavian Caledonides. *Norsk Geol. Tidsskr.* **67**, 89-97.

Crowley, P. D., 1985, The structural and metamorphic evolution of the Sitas area, northern Norway and Sweden, Ph.D. thesis, M.I.T., Cambridge, MA, 253pp.

Dallmeyer, D., 1990, 40Ar/39Ar mineral age record of a polyorogenic evolution within the Seve and Köli nappes, Trøndelag, Norway. Tectonophysics, 179, 199-226.

Dalmeyer, D., and Gee, D. G., 1988, Polyorogenic 40Ar/39Ar mineral age record in the Seve and Köli nappes of the Gåddede area, northwestern Jämtland, Central Scandinavian Caledonides, *J. of Geology,* **96,** 181-198.

Dallmeyer, R. D., Andreasson, P. G., and Svenningsen, O. M., 1991, Initial tectonothermal evolution within the Scandinavian Caledonide Accretionary Prism: constraints from 40Ar/39Ar mineral ages within the Seve Nappe Complex, Sarek mountains, Sweden. J. Metamorphic Geol. 9, 203-218.

Dunning, G. R., and Pedersen, R. B., 1988, U/Pb ages of ophiolites and arc-related plutons of the Norwegian Caledonide: implications for the development of Iapetus. *Contrib. Mineral. Petrol.*, **98**, 13-23.

Foslie, S., 1941, Tysfjords Geologi. *Norges Geol. Unders.* 149, 298 pp.

Foslie, S., 1949, Haafjells-Mulden I Ofoten. *Norges Geol. Unders.* 174, 129 pp.

Fossen, H., and Rykkelid, E., 1992, Postcollisional extension of the Caledonide orogen in Scandinavia: Structural expressions and tectonic significance, Geology, 20, 737-740.

Gee, D. G., 1975, A tectonic model for the central part of the Scandinavian Caledonides, *Am. J. Sci.*, **275-A**, 468-515.

Gee, D.G., R. Kumpulainen, D. Roberts, M. B. Stephens, A. Thon, and E. Zachrisson, 1985, Tectonostratigraphic map of the Scandinavian Caledonides: in D. G. Gee and B. A. Sturt, eds., *The Caledonian Orogen - Scandinavia and related areas*, J. Wiley and Sons, Chichester, England.

Gee, D. G., Lobkowicz, M., and Singh, S., 1994, Late Caledonian extension in the Scandinavian Caledonides - the Roragen Detachment revisited. *Tectonophysics,* **231**, 139-155.

Gee, D. G., and M. R. Wilson, 1974, The age of orogenic deformation in the Swedish Caledonides, *Am. J. Sci.*, **274**, 1-9.

Griffin, W. L., 1987, On the Eclogites of Norway - 65 years later. Mineral Mag., 51, 333-343.

Harland, W. B., and R. A. Gayer, 1972, The Arctic Caledonides and earlier oceans, *Geol. Mag.*, **109,** 289-314.

Hodges, K. V., 1982, Tectonic evolution of the Aefjord-Sitas area, Norway-Sweden, Ph.D. thesis, Massachusetts Institute of Technology, Cambridge, MA.

Krill, A. G., 1986, Eidsvoll Quarry, Oppdal, south Norway: a one-outcrop model for some aspects of Trollheimen-Dovrefjell tectonics. *Nor. Geol. Unders. Bull.* **404**, 23-32.

Krill, A. G., and Zwaan, B., 1987, Reinterpretation of Finnmarkian deformation on western Sørøy, northern Norway. *Norsk Geol. Tidsskr.*, **67,** 15-24.

Krill, A. G., Rodgers, J. and Sundvoll, B., 1988, Alternative to the Finnmarkian-Scandian interpretation on Magerøya, northern Norway. *Norsk Geol. Tidsskr.* **68,** 171-185.

Norton, M. G., 1986, Late Caledonian extension in western Norway: A response to extreme crustal thickening. *Tectonics*, **5**, 195-204.

Rykkelid, E., and Andresen, A., 1994, Late Caledonian extension in the Ofoten area, northern Norway, Tectonophysics, 231, 157-169.

Roberts, D., and Gee, D. G., 1985, An introduction to the structure of the Scandinavian Caledonides, in: D.G. Gee and B. A. Sturt, eds., *The Caledonian Orogen - Scandinavia and Related Areas*, John Wiley, New York, p. 55-68.

Steltenpohl, M. G., 1983, The structure and stratigraphy of the Ofoten synform, North Norway, M.S. thesis, University of Alabama, University, AL.

Steltenpohl, M. G., 1985, The structural and metamorphic history of Skanland, north Norway, and its significance for tectonics in Scandinavia, Ph.D. thesis, University of North Carolina, Chapel Hill, NC.

Steltenpohl, M. G., and J. M. Bartley, 1988, Crossfolds and backfolds in the Ofoten-Tysfjord area, Norway and their significance for Caledonian tectonics, *Geol. Soc. Am. Bull.*, **100,** 140-151.

Stephens, M. B., and D. G. Gee, 1989, Terranes and polyphase accretionary history in the Scandinavian Caledonides, *Geol. Soc. Am. Spec. Paper,* **230,** 17-30.

Stephens, M. B., Kullerud, K., and Claesson, S., 1993, Early Caledonian tectonothermal evolution in outboard terranes, central Scandinavian Caledonides: new constraints from U-Pb zircon dates. *J. Geol. Soc. Lond.*, **150**, 51-56.

Sturt, B. A., Pringle, I. R., and Roberts, D., 1975, Caledonian nappe sequence of Finnmark, northern Norway, and the timing of orogenic deformation and metamorphism. *Geol. Soc. Amer. Bull.* **86**, 710-718.

Sturt, B. A., Pringle, I. R., and Ramsay, D. M., 1978, the Finnmarkian phase of the Caledonian orogeny. *J. Geol. Soc. London*, **135**, 597-610.

Svenningsen, O. M., 1993, Tectonic evolution of the Sarektjåkkå Nappe, northern Swedish Caledonides. Ph.D. thesis, Geological Institute, Univ. of Lund, Sweden.

Vogt, T., 1942, Trekk av Narvik - Ofoten traktens geologi. *Norges Geol. Unders.* **21**, 198-213.

Vogt, T., 1950, Map sheet Narvik, 1:100,000. Norges Geol. Unders., Trondheim.

Zwaan, B. Z., and Van Roermund, H. L. M., 1990, A rift-related mafic dike swarm in hte Corrovarre Nappe of the Caledonian Middle Allochthon, Troms, North Norway,and its tectonometamorphic evolution. *Nor. Geol. Unders. Bull.* **419**, 25-44.

FIGURES FOR CHAPTER 1

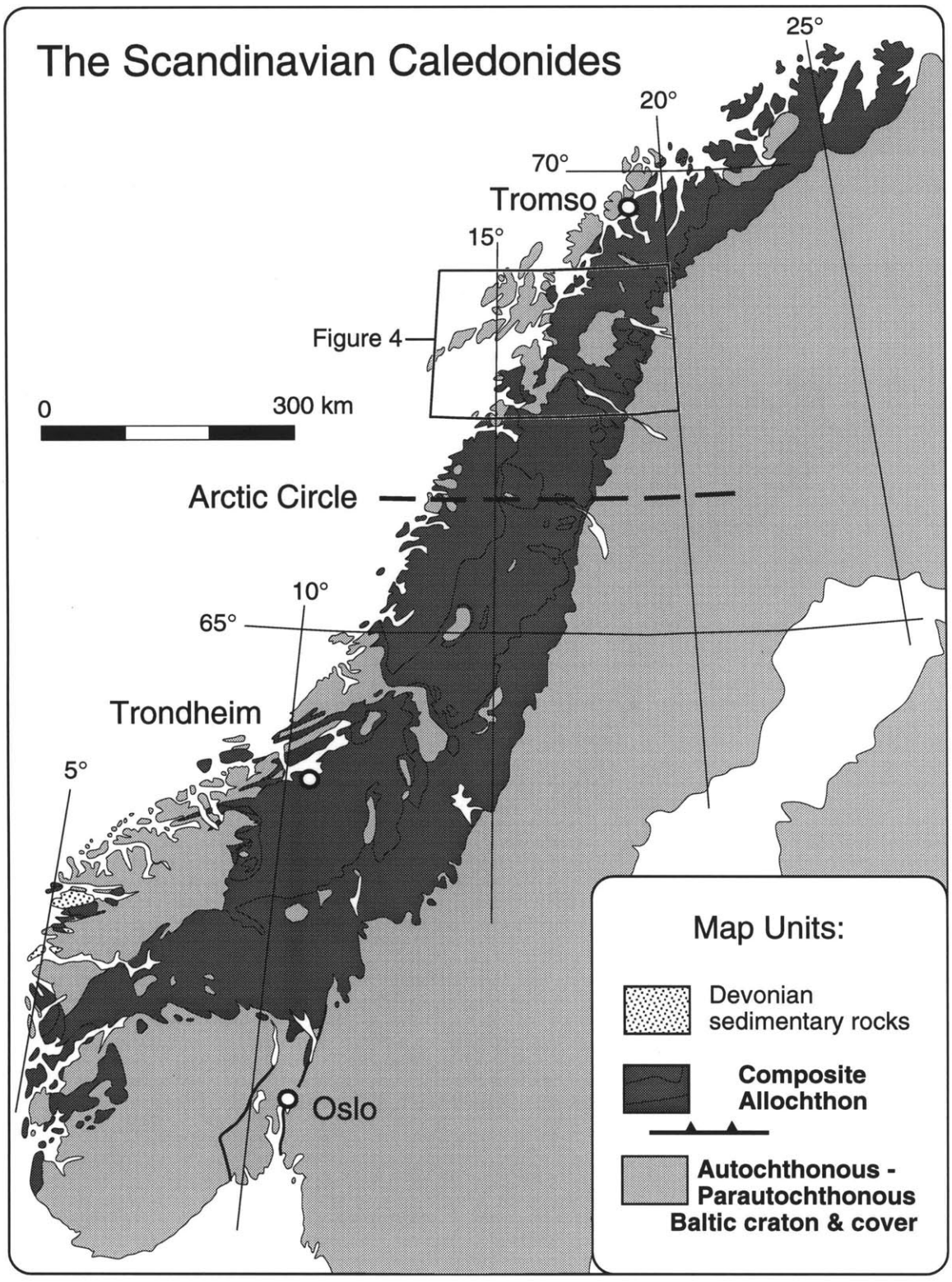

Figure 1: Simplified geologic map of the Scandinavian Caledonides (modified from Gee et al. 1985).

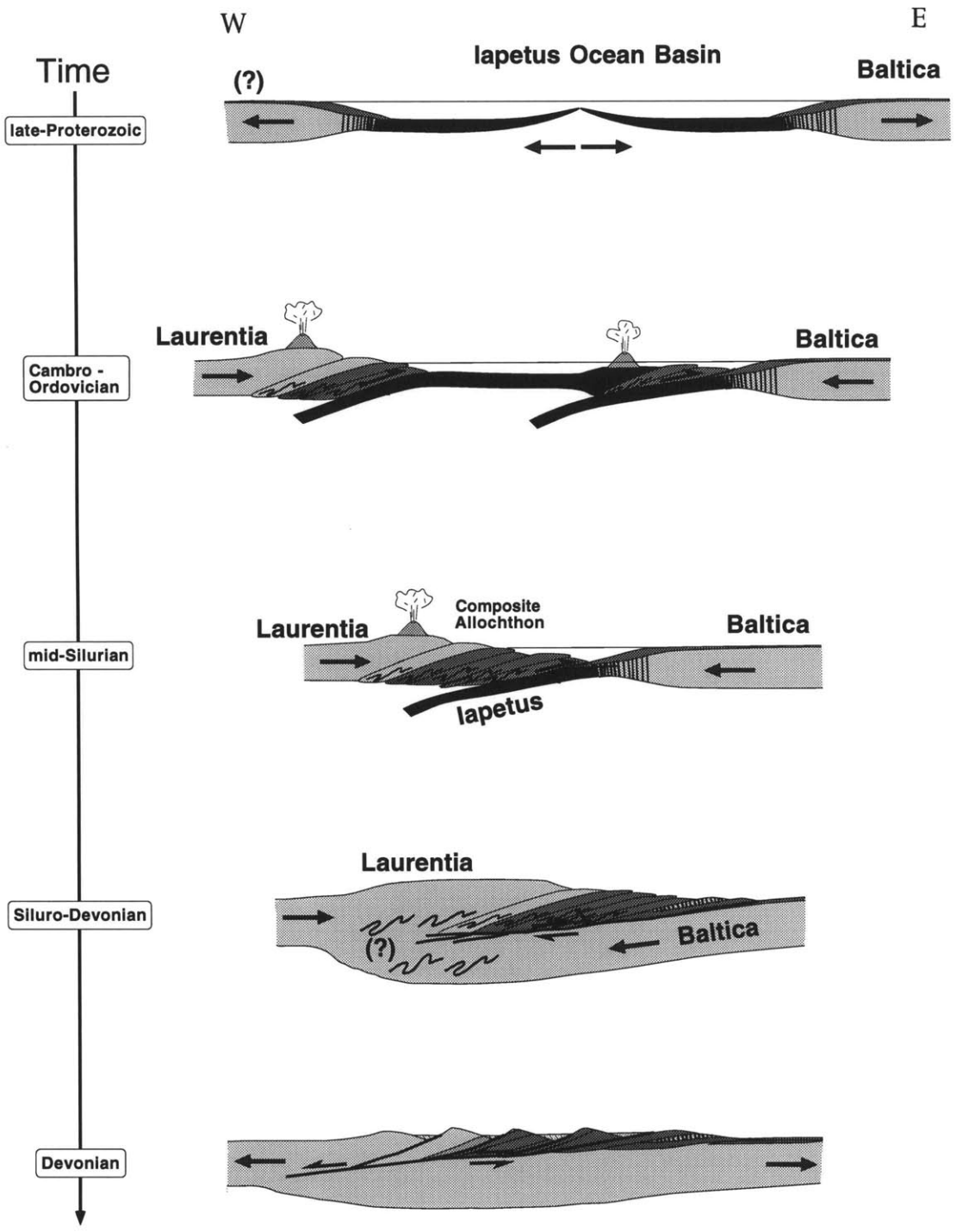

Figure 2: Schematic cross-sections illustrating the evolution of the Iapetus Ocean basin and the development of the Caledonian Orogen during late-Proterozoic through Devonian time.

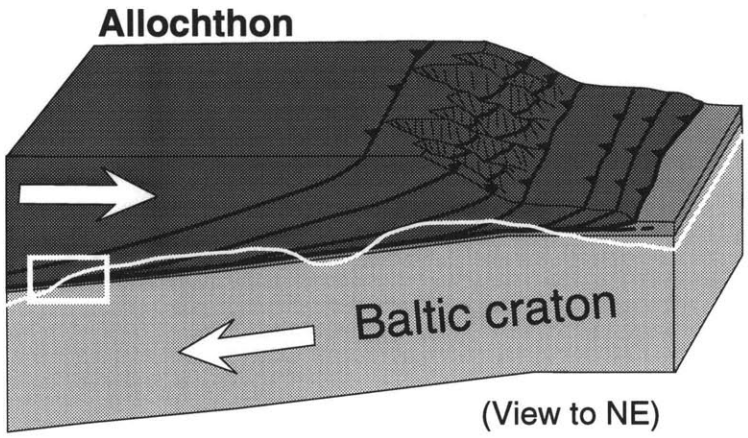

Figure 3: A schematic block diagram illustrating the emplacement of the composite allochthon during the culmination of the Caledonian collision. The white line shows the general level of exposure today, and the white box indicates the structural position inferred for rocks in the study area.

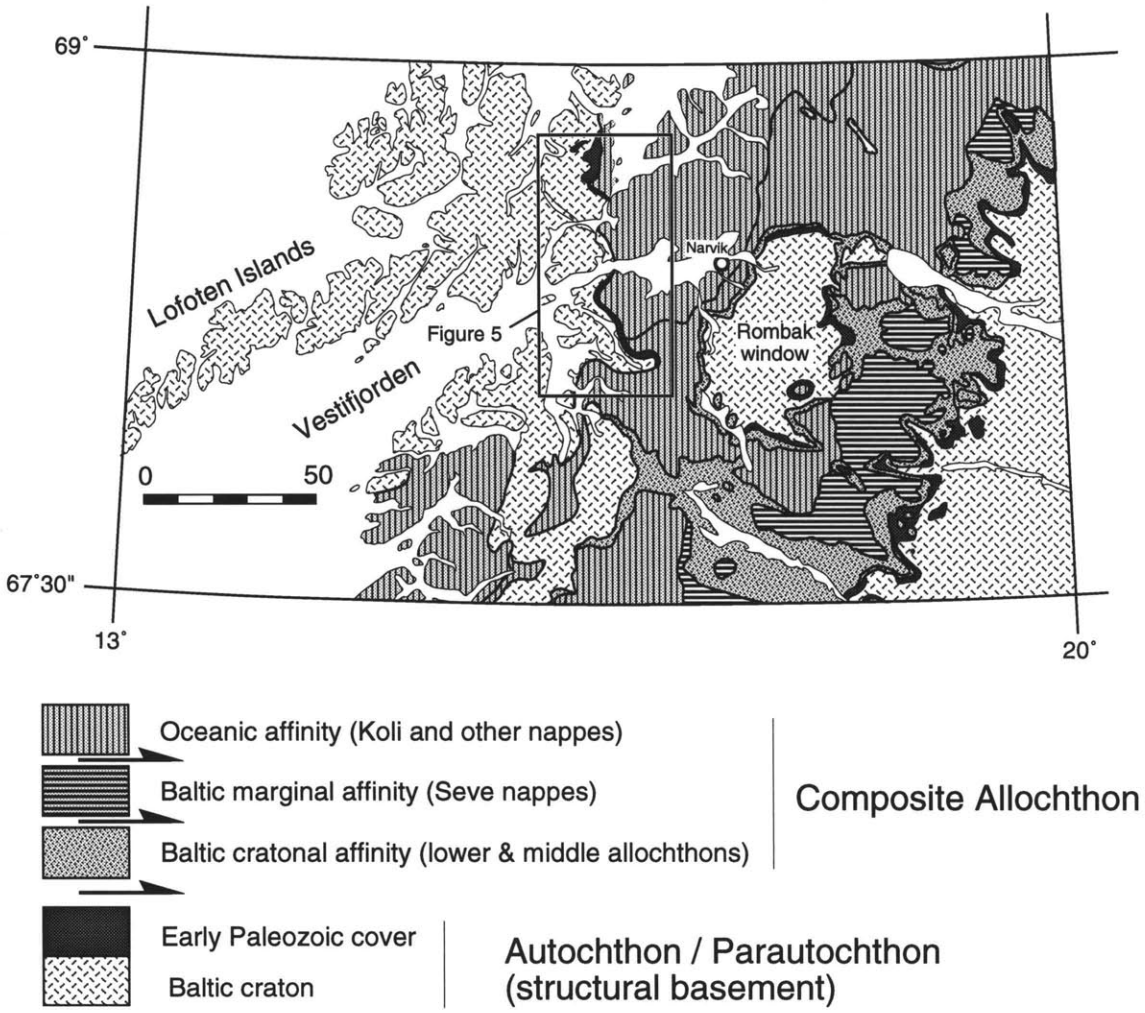

Figure 4: simplified geologic map showing the regional context of the study area.

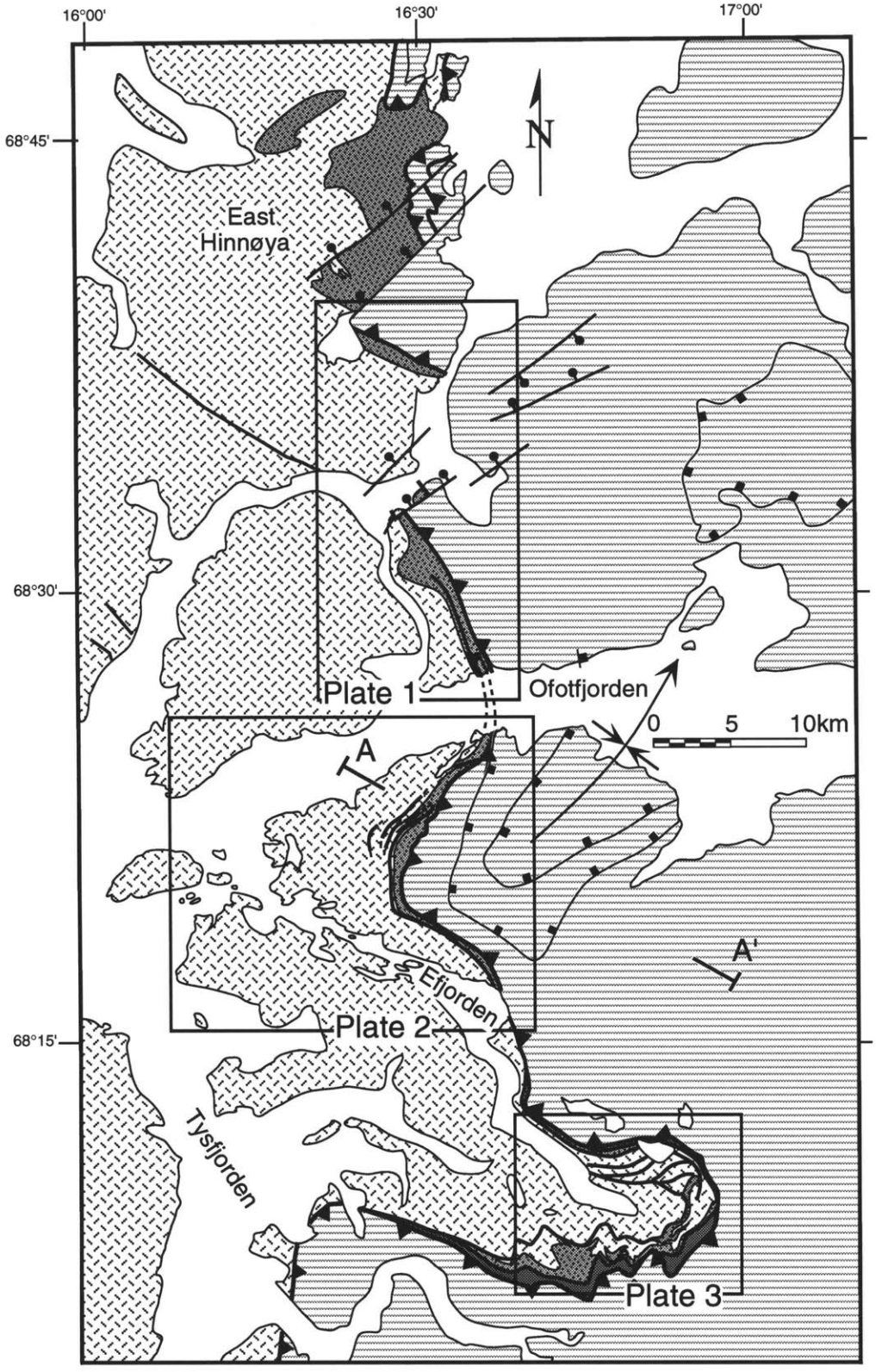

Figure 5: simplified geologic map of the Ofoten-Efjorden region, showing the locations of areas examined in this study.

Chapter 2

General non-coaxial flow in the midcrust of a collisional orogen: the northern Scandinavian Caledonides

ABSTRACT

Mapping and strain analysis in the northern Scandinavian Caledonides indicates that one way in which contemporaneous upper-crustal extension and deeper thrusting within collisional orogens may be linked in a kinematically compatible manner is through the ductile flow of rocks in the midcrust of these mountain belts. In the Ofoten-Efjorden region of north Norway, amphibolite facies metamorphism and strong penetrative strain occurred at deep levels of the Caledonian nappe stack as it was thrust eastward onto the western margin of Baltica. Kinematic analysis of deformation in the lower portion of the Caledonian nappes indicates that the rock mass underwent heterogeneous non-coaxial flow, with components of foreland-directed simple-shear and sub-vertically shortened pure-shear. General non-coaxial flow (simultaneous simple shear + pure shear) can accomplish foreland-directed tectonic transport, sub-vertical thinning, and transport-parallel elongation at deep levels of a nappe stack. This pattern of flow is significant tectonically for two reasons — first, it suggests spreading of the Caledonian allochthon during thrust emplacement, and second, it can form a kinematic link between normal faulting at shallower structural levels and thrusting at the base of the nappes. By analogy with the Caledonides, general non-coaxial flow of midcrustal rocks may be a tectonically

important process in other collisional and contractional orogens, particularly in those that have undergone upper crustal extension while thrusting continued in the foreland.

INTRODUCTION

The structural evolution of collisional orogens reflects the dynamic interaction between contractional and extensional processes operative at different structural levels or location within such orogens. Recent studies have demonstrated that extension in the upper crust developed contemporaneously with continued thrusting either at deeper structural levels or in the forelands of several contractional mountain belts. Examples include the Himalayas (Burchfiel et al. 1992, and references therein), Appenines (Carmignani and Kligfield, 1990), Betic Cordillera (Vissers et al., 1995), Scandinavian Caledonides (Andersen et al. 1991; Gee et al. 1994), and the North American Cordillera (Hodges and Walker, 1992). Extension within the context of contractional orogeny poses an interesting kinematic problem — how do these tectonic processes interact dynamically, and what structures or patterns of strain at mid to deep crustal levels of collisional orogens form the kinematic links between contemporaneous upper-crustal extension and continued thrusting?

One way to address this problem is to examine middle and deep crustal levels of collisional orogens and look for modes of deformation that can accommodate simultaneous extension and thrusting. The Scandinavian Caledonides provide an excellent field laboratory for such studies because relatively deep structural levels of this Paleozoic collisional orogen are now well exposed. The purpose of this paper is to present a kinematic analysis of penetrative strain at deep levels of the Caledonian

allochthon in the Ofoten-Efjorden area of north Norway (Fig. 1), and to examine the role of heterogeneous ductile flow in the overall tectonic evolution of the nappe stack. Although the structural observations and discussion center around part of the Caledonian mountain belt, the tectonic processes described may have been important in the development of other collisional/contractional orogens as well.

TECTONIC SETTING

The Scandinavian Caledonides are a classic example of an old, deeply exposed collisional orogen (Figure 1). Closure of the Iapetus Ocean basin resulted in the collision of Baltica and Laurentia in late-Silurian to early-Devonian time (Harland and Gayer, 1972; Gee and Wilson, 1974). During the climax of the Caledonian collision (ca. 430-400 Ma), the western margin of Baltica was subducted to deep levels of the orogen, and a crustal-scale composite allochthon was thrust eastward onto the Baltic craton (Griffin and Brueckner, 1980; Hodges et al., 1982; Stephens and Gee, 1989). The allochthon was formed by thrust imbrication of rocks derived from the Vendian rifted margin of Baltica, the Iapetus Ocean basin, and rocks of Laurentian affinity (Roberts and Gee, 1985).

Erosion has removed much of the original composite allochthon and exposed deep structural levels of the Caledonian orogen. The present-day mountain belt in Scandinavia consists of a relatively thin but regionally extensive remnant of the original nappe-stack lying structurally over autochthonous or parautochthonous rocks of the Baltic craton and its pre-Caledonian sedimentary cover (Figure 1; Roberts and Gee, 1985). Because the present erosional surface cuts the Caledonian orogen near the base of the nappe stack, the

structural development and patterns of strain in the lower few km of the Caledonian nappe stack can be examined directly.

GEOLOGY OF OFOTEN-EFJORDEN

Work reported in this paper was conducted in the Ofoten-Efjorden region of north Norway, approximately 200 km north of the Arctic circle (Figures 1 & 2). Outcrops in the study area comprise some of the westernmost, and therefore deepest, exposures of the Caledonian allochthon on the Norwegian mainland at this latitude. Two orthogonal sets of late-Caledonian folds control the present-day map pattern (Figure 2; Steltenpohl and Bartley, 1988). Regionally significant manifestations of these fold sets in the study area include the gently NNE-plunging Ofoten synform and the gently ESE-plunging Efjord culmination. The folds rotate the structural section into variably dipping orientations, so portions of the geologic map covering the fold limbs represent oblique cross-sections through several kilometers of section in the lower part of the allochthon and the upper part of the structural basement.

In the Ofoten-Efjorden region, Precambrian granite of the Baltic craton and a thin but persistent remnant of its metasedimentary cover form the structural basement onto which the allochthon was emplaced (Figure 2). All parts of the metasedimentary cover sequence (a basal quartzite and garnet-grade quartzofeldspathic schists of the Storvann Group; Bartley, 1980), have been strongly tectonized, and considerable dynamic recrystallization and grain-size reduction occurred in the Precambrian granite near the base of the allochthon. The intensity of fabric in the granite, however, decreases significantly over a distance of 500 to 1000 m structurally downward, leaving a moderate

L-S fabric (L>S). Localized zones of increased finite strain can be found sporadically at various structural levels of the basement, and increased strain is particularly prominent near large xenoliths or screens of Precambrian mafic schist and epidote-amphibolite gneiss in the granite which may have acted as stress risers. For the most part, however, these localized zones are discontinuous along strike and do not indicate significant displacement. Because the high strain zones in the cratonal basement are confined to Precambrian rocks, their age and significance are poorly constrained. Ductile faults with clear Caledonian motion are present in the basement north and west of the study area (e.g., Tull, 1972), and they provide evidence for some internal shortening of the Baltic craton. On the whole, however, the intensity of deformation in the deep parts of the structural basement is significantly less than in the overlying allochthon (Bartley, 1982).

The Caledonian allochthon in Ofoten-Efjorden contains a complex assemblage of far-traveled nappes which were emplaced to the ESE onto the margin of the Baltic craton as the continental margin was subducted westward during the culmination of the Caledonian collision (Hodges et al., 1982). The tectonostratigraphy of the allochthon in the region was reviewed and reinterpreted recently by Andresen and Steltenpohl (1994), and the general terminology they proposed will be used here. In most of Ofoten-Efjorden, the lower portion of the allochthon is composed of the Narvik Nappe Complex, a sequence of pelitic and mafic schist up to 3 or 4 km thick with rare marble and quartzite. Above the Narvik Complex is a sequence of rocks consisting of marble and schist which forms the Ofoten Nappe Complex. Quantitative thermobarometry of garnet-kyanite schists in the allochthon indicate peak metamorphic temperatures of 650 to 700

°C, at pressures of 9 to 10 kb, consistent with paleodepths of 35 to 40 km during the collision (Hodges and Royden, 1984; Steltenpohl and Bartley, 1987).

Based on a large body of previous work in the region (including Foslie, 1941; Gustavson, 1974; Bartley, 1980, 1984; Hodges, 1982, 1985; Steltenpohl, 1983, 1985; and others) the Siluro-Devonian deformational history of the area can be divided into three general phases. Early deformation (D_1) included the thrusting, folding, and bulk shortening associated with assembly of the composite allochthon prior to the metamorphic peak in the allochthon. D_1 structures are commonly cryptic due to the intensity of later deformation and metamorphism. The second phase of deformation (D_2) involved the emplacement of the assembled allochthon onto the margin of the Baltic craton. Emplacement was accompanied by metamorphism to epidote-amphibolite facies conditions and intense penetrative strain at deep crustal levels of the allochthon. Much of the penetrative strain in the area was produced during this phase of deformation. Late-Caledonian deformation (D_3) resulted in the NE- and SE-trending folds, local crenulation and transposition of early fabric, and some additional motion on ductile fault zones during the retrograde portion of the P-T path. ESE-directed transport of allochthonous tectonic elements occurred throughout the early phases of deformation and continued into the early part of D_3. Fossen and Rykkelid (1992), and Rykkelid and Andresen (1994) documented post-orogenic top-W extensional reactivation of thrusts farther to the East, but such reactivation has not been found at deep levels of the nappe stack in the present study area.

This paper focuses on the nature and significance of D_2 penetrative strain that developed at deep crustal levels of the allochthon as it was emplaced on the Baltic craton.

The kinematic analysis presented is based on the geometry and orientations of deformational fabric, folds, boudinage, and discontinuous shear zones or shear bands within the rock mass at deep levels of the nappe stack, and these structural elements are described in the next section.

STRUCTURAL OBSERVATIONS

Basal Shear Zone

The basal shear zone separates rocks of the Caledonian allochthon exposed in the eastern part of the area from parautochthonous structural basement exposed in the western part of the area (Figure 2). In most places the basal shear zone is composed of a series of narrowly spaced (5-50 m), anastomosing ductile faults that separate thin structural slices of mylonitic granite and schist derived from the footwall. Mylonite in the basal shear zone contains well-developed L-S deformational fabric (Fig 3). The mylonitic foliation is parallel to the structural contact at the base of the allochthon and is defined by a preferred alignment of micas and mm-scale compositional layering. Foliation orientations in the basal shear zone are uniform locally, but they vary from location to location within the area due to reorientation by NE- and SE-trending, late-Caledonian folds. Originally, the basal shear zone may have dipped shallowly to the west or northwest, consistent with its orientation farther east in the orogen where late folding is weak or absent. Now it dips moderately (50°-60°) to the southeast along the western limb of the Ofoten synform and is nearly vertical in the western part of the north limb of the Efjord antiform.

Stretching lineation in the basal shear zone plunges variably but trends consistently ESE. Late folds have little affect the trend of the lineation because the fold sets are nearly parallel and perpendicular to the lineation. Outcrop surfaces oriented parallel to the lineation and perpendicular to the foliation in the basal shear zone display abundant shear-sense indicators which yield a regionally consistent, top-ESE sense of tectonic transport (Figure 4).

Penetrative Strain in the Allochthon

Throughout the erosional remnant of the allochthon, penetrative deformational fabric is well developed. The dominant foliation in the area (S_2) is a ubiquitous schistosity that can be found continuously from the basal shear zone structurally upward into the Narvik and Ofoten Nappe Complexes. The foliation contains a stretching lineation (L_2) defined by an alignment of elongate minerals, ellipsoidal mineral-aggregates, stretched clasts in rare metaconglomerates, and strain shadows around garnet porphyroblasts.

Scatter of poles to foliation in three structural domains in the allochthon (Fig 3d-f) results largely from local rotation of the foliation by late-Caledonian NE- and SE-trending folds with variable wavelengths and amplitudes. Late-phase deformation is heterogeneous, and its effects are particularly strong near the hinge of the Ofoten synform (Figs. 3b and 3e) and along the north limb of the Efjord culmination (Figs.3c and 3f). In these areas, the S_2 foliation is folded by ESE-plunging, north-inclined folds with 10 to 100 m wavelengths and tight fold geometries. The folds are associated with a south-dipping crenulation cleavage (S_3) that variably transposed S_2, and caused local retrograde

recrystallization to chlorite-bearing mineral assemblages. Relatively strong late-phase deformation along the north limb of the Efjord antiform obscures the original orientations and geometric relationships among D_2 deformational features in this part of the study area. Late-phase strain is less intense, however, on the west limb of the Ofoten synform (Figs. 3a and 3b). In this portion of the area, the original geometry of earlier deformational features is better preserved. Late NE- and SE-trending mesoscopic folds with more open geometries still cause scatter in the orientation data, but the mean orientation of foliation gives a reasonable approximation of the enveloping surfaces of the folds.

The S_2 foliation in the allochthon is sub-parallel to the thrust contact at the base of the allochthon. In the western limb of the Ofoten synform, where early deformational features are preserved best, the mean orientation of poles to S_2 foliation in the allochthon differs from the mean orientation of poles to mylonitic foliation in the basal shear zone by about 7^{o}, but the difference is barely resolvable at the 95% confidence interval (Figs. 3a and 3d). Furthermore, the measurements in the allochthon were made closer to the core of the Ofoten Synform, so some of the apparent difference in orientation is due to the curvature of the regional-scale fold.

Tabular bodies of more competent rock within the nappe complex serve as active strain markers that indicate the character of finite longitudinal strain in various orientations, at the scale of a given outcrop. Pre- and syn-kinematic granitic dikes exist in the Narvik Nappe Complex, and relatively competent amphibolite layers exist in the marble-dominated lower portion of the Ofoten Nappe Complex. Boudinage, pinch-and-swell geometry, and folds in these competent layers are displayed in outcrop surfaces

oriented parallel to lineation and perpendicular to foliation (Figure 5). Consistently, dikes oriented at a high angle to foliation have been shortened and those at low angles to the foliation have been stretched. The general pattern of dike deformation suggests that S_2 approximates the X-Y plane of finite strain, an interpretation supported by the ubiquitous alignment of strain-shadows on garnet porphyroblasts parallel to foliation, and the elongation of cobbles in rare metaconglomerates parallel to the foliation.

Strain analysis of boudinage and folding in dikes and competent layers provides semiquantitative information about the magnitude and heterogeneity of strain at mesoscopic scale. In order to explore these aspects of the deformation, I examined outcrop surfaces oriented perpendicular to foliation and parallel to lineation (the inferred X-Z plane of finite strain), and estimated the longitudinal strain of material lines, as indicated by boudinage or ptygmatically folded dikes. Longitudinal strains were estimated from boudinage by comparing the length of a boudin train (from the center of the first to the center of the last in a train) to the to the sum of the lengths of individual boudins. Boudin trains contained between 3 and 7 boudins Alternatively, strains were estimated from ptygmatically folded dikes by measuring the linear distance between two points on a dike and comparing it to the folded length of dike connecting the points. S_2 foliation was used as an internal frame of reference in each outcrop, and the orientations of material lines were measured with respect to it. Granitic dikes and amphibolite layers exhibiting maximum competency contrast relative to the schist or marble matrix were preferentially selected in order to diminish the effects of deformation within the strain markers, but all contained some internal deformation. Longitudinal strain estimates are presented in Table 1 and illustrated in figure 6a.

A finite strain ellipse can be calculated from two differently oriented observations of longitudinal strain if the orientations of principal strain axes are known independently (see Ramsay and Huber, 1983). Because S_2 foliation marks the X-Y plane of finite strain at outcrop scale and the orientation of the stretching lineation in the foliation gives the direction of maximum stretch (X axis), the orientation of the strain axes at a given outcrop can be inferred. Pairs of longitudinal strain measurements from individual outcrops yield model strain ellipses with X-Z axial ratios ranging from 3:1 to 27:1 with an average of about 9:1. The area change of the model ellipses vary from -22% to +70% with an average of about +12% (Table 1; Fig 6b). The variability in the results reflects a combination of primary heterogeneity in the magnitude and character of strain from one outcrop to another, variable quality of the strain markers, and imperfections in the measurements made on the markers. On average, the strain ellipses show a small positive area-change that may indicate a net flow of material into the X-Z plane as a result of slightly constrictional strain, but the change is not statistically significant due to the variability of the results. Single measurements of longitudinal strain were obtained from boudinage in a number of outcrops (Table 1; Fig 6a), but taken individually, they are insufficient to determine strain ellipses.

Extensional shear zones are another deformational feature observed at outcrop scale in the allochthon (Figure 7). The shear zones are discontinuous, and their displacement is absorbed by the penetrative strain in the adjacent rock mass. They range in size from centimeter-wide zones with a few cm displacement, to meter-wide zones with >10 m of displacement. The shear zones are discordant to the S_2 foliation, but dynamically recrystallized rock within the zones consists of the same kyanite-grade peak

metamorphic mineral assemblage that defines S_2, with no evidence for retrogression. Therefore, the extensional shear zones formed near the metamorphic peak of the allochthon, penecontemporaneously with S_2. The shear zones have geometric and kinematic characteristics similar to large shear-bands or extensional crenulation cleavage (e.g., Platt and Vissers, 1980). Most dip to the ESE and have shear senses which are synthetic to the ESE-transport of the allocthon (Figs 7a-f), but antithetic shear zones that ramp down to the NW are present also (Figs. 7g and h). Whereas the absolute orientations of S_2 foliation and the extensional shear zones vary significantly from location to location due to reorientation by late folding, their relative orientations are more consistent. Field measurements of the acute angle between synthetic extensional shear-bands and S_2 foliation average 30^o- 40^o, and the acute angle between antithetic shear-bands and S_2 foliation average 50^o-60^o (Fig. 8).

KINEMATIC ANALYSIS

Emplacement of the allochthon was accommodated by top-ESE motion along the basal shear zone and was accompanied by substantial penetrative strain distributed heterogeneously in the rock mass at deep levels of the allochthon. The effects of the penetrative deformation, or ductile flow, ultimately depend on the orientation, intensity, and kinematic characteristics of the strain. The characteristics and effects of different types of deformation are reviewed briefly in the next section.

Simple Shear, Pure Shear, and General Shear

Constant-volume deformation has been interpreted commonly in terms of two ideal plane strain regimes — simple shear and pure shear, but these are probably rare in nature. Most strain results from general non-coaxial flow, which may be viewed in two dimensions as a simultaneous combination of simple shear and pure shear (e.g., Ramberg, 1975). Kinematic characteristics and mathematical descriptions of general shear have been examined by a number of workers (e.g. Ramberg, 1975; Means et al., 1980; DePaor, 1983; Bobyarchick, 1986; Simpson and DePaor, 1993; and references therein). Particular aspects of general shear relevant to this discussion are reviewed here. General shear regimes can be resolved into a component of simple shear and a component of pure shear with the principal shortening axis oriented either parallel or perpendicular to the simple-shear plane (Figure 9).

During progressive simple shear, material lines oriented parallel to the shear plane experience no longitudinal strain, and the deforming mass experiences no change in thickness measured perpendicular to the shear plane. However, under conditions of general shear, the pattern of strain becomes more complicated due to the effects of the pure-shear component (Figure 9). If the shortening axis of the pure-shear component is perpendicular to the simple-shear plane, then progressive deformation causes the rock mass to elongate parallel to the simple-shear plane and thin perpendicular the simple-shear plane. Bulk thinning by general shear may be a favorable deformational response when the maximum principal stress (σ_1) driving the deformation is oriented at a high-angle relative to the simple-shear plane. In contrast, if the shortening axis of the pure-shear component is parallel to the simple-shear plane, then progressive deformation

causes the rock mass to shorten parallel to the simple-shear plane and thicken perpendicular to the simple-shear plane. Bulk thickening due to general shear may be a favorable response when the greatest principal stress driving the deformation is oriented at a low-angle relative to the simple-shear plane.

In the context of strain, "vorticity" refers to the rate of rotation of material lines through the infinitesimal stretching axes during non-coaxial progressive deformation (Means et al., 1980; Lister and Williams, 1983). Because general shear is a mixture of coaxial (pure shear) and non-coaxial (simple shear) components, the vorticity of general shear reflects the relative proportions of simple shear and pure shear in the deformation. The kinematic vorticity number (W_n) is a measure of the degree of non-coaxiality of infinitesimal strain (Means et al., 1980; Bobyarchick, 1986; Simpson and DePaor, 1993). It can be defined as the cosine of the angle between the simple shear plane and the inclined eigen vector of strain, measured in the direction of rotation imposed by the simple-shear component (Fig. 9). Defined in this manner, $W_n = 1.0$ (or -1.0) for simple shear, and $W_n = 0.0$ for pure shear. The absolute value of W_n for general shear varies between 0.0 and 1.0, and the sign of W_n indicates whether the rock mass thins (positive W_n) or thickens (negative W_n) perpendicular to the simple-shear plane during progressive deformation.

Deformation at deep levels of the Caledonian Allochthon

Deformational features produced in the Caledonian allochthon during its emplacement include penetrative foliation, lineation, boudinage, folds, and discontinuous shear zones or shear bands (Fig. 10). For purposes of kinematic analysis, the basal shear zone is assumed to approximate the simple-shear plane of penetrative strain in the allochthon because it represents the surface along which the allochthon was thrust during the deformation, and because the relatively undeformed state of the structural basement in the footwall of the basal shear zone provides a kinematic boundary condition. S_2 foliation indicates the X-Y plane of finite strain, an interpretation supported by the elongation of pebbles and cobbles within the plane of S_2 foliation, by the stretching and shortening behavior of dikes relative to the foliation, and by the ubiquitous alignment of strain shadows around garnet porphyroblasts parallel to the foliation. Although penetrative strain in the allochthon is heterogeneous and complex, the deformational features described in this paper can be viewed as a system of kinematically consistent structural elements produced by heterogeneous, progressive general shear (Fig. 10).

The extensional shear bands are an expression of the coaxial component of bulk strain, because they act as small normal faults which produce thinning and transport-parallel elongation of the bulk rock mass (e.g., Platt and Vissers, 1980). The relationship between shear-band orientations and the degree of non-coaxiality of incremental strain is not well known. Bobyarchick (1986) suggested that synthetic shear-bands may form parallel to the inclined eigen vector in general-shear regimes. However, Simpson and

DePaor (1993) noted that such an interpretation does not account for the conjugate orientation of antithetic shear bands found also in sheared rocks. They offered the alternative interpretation that shear bands form at orientations which bisect the angles between the eigen vectors, because these orientations are perpendicular to material lines experiencing the maximum rate of angular strain. Planes bisecting the eigen vectors, therefore, have favorable orientations for localized simple shear. But, even if shear bands form midway between the eigen vectors, they will not preserve that orientation during progressive deformation. Continued strain will progressively rotate the shear bands towards the bulk shear plane. Bearing this caveat in mind, and assuming shear bands bisect the angles between the eigen vectors, shear band orientations can be used to estimate vorticity through the relationship $W_n = \cos 2\alpha$, where W_n is the kinematic vorticity number, and α is the acute angle between synthetic extensional shear-bands and the simple shear plane. Because progressive deformation will rotate shear bands toward the bulk shear plane, it will reduce the apparent angle α between synthetic shear-bands and the bulk shear plane. Therefore, geometric analysis of extensional shear bands which have been reoriented by progressive deformation will yield apparent kinematic vorticity numbers larger than the actual value (i.e., the simple-shear component will be overestimated and the pure-shear component underestimated).

Using the geometric relationships described above, the orientations of the large shear-bands in the allochthon relative to S_2 foliation suggest kinematic vorticity numbers from approximately 0.10 to 0.85 during the interval of strain over which they developed. Several factors probably contribute to this range in values, including: a) variable

reorientation of the shear bands during progressive deformation; b) original spatial heterogeneity in the vorticity of strain; and c) changes in the vorticity during the interval of time in which the shear bands developed. In any case, the orientations of extensional shear bands are consistent with the presence of a pure-shear component in the bulk finite strain.

In addition to the extensional shear bands, the low inclination of S_2 foliation in the allochthon relative to the basal shear zone is consistent with a pure-shear component of D_2 strain. During non-coaxial progressive deformation, the X-Y plane of finite strain rotates progressively towards the shear plane with increasing strain intensity. The initial inclination of the X-Y plane and the amount of rotation toward the shear plane with increasing strain depend on the simple-shear and pure-shear composition of the strain (Figure 11).

Given the interpretation that the orientation of S_2 foliation in the allochthon approximates the X-Y plane of finite strain, extremely high average strain magnitudes would be necessary in order to rotate the foliation into an orientation subparallel to the basal shear zone by simple shear alone. For example, to achieve an average foliation inclination of 5° by simple shear would require strains with an average X:Z axial ratio of approximately 130:1. Simple-shear strains of this intensity may be common in the mylonites of ductile faults, but would be extreme for the average strain in the bulk rock-mass between faults. However, general shear with even a minor component of coaxial strain can produce a low inclination of the foliation at more reasonable finite strain intensities (Figure 11). In the allochthon, the magnitude of penetrative strain accumulated during D_2 is heterogeneous and difficult to determine, but the estimates of

finite strain magnitude at outcrop scale give X:Z strain ratios from about 3:1 to 27:1, with an average of about 9:1. Due to the imperfect nature of the strain markers, these estimates should be viewed with caution. Nonetheless, the apparent magnitude of penetrative deformation at outcrop scale in the allochthon is not sufficient to produce the shallow inclination of S_2 foliation by simple shear alone. However, general non-coaxial flow with a component of pure shear can easily give the observed orientation of the foliation.

Though the preceding analyses suggest a general non-coaxial *finite* strain, the *incremental* strain history is not resolved in detail, and the nature of deformation clearly changed through time. Deformation at deep levels of the allochthon seems to have evolved from early shortening and crustal thickening to later attenuation and transport-parallel elongation, all associated with top-ESE tectonic transport. This evolution may reflect rotation of the maximum principal stress (σ_1) to steeper inclinations during the deformational history.

Subvertical attenuation and transport-parallel elongation of the Caledonian nappe stack during its emplacement has been suggested by a number of studies throughout the orogen. For example, Gee (1975, 1978) recognized westward attenuation of the Caledonian tectonostratigraphy and map-scale pinch-and-swell structures in a transect through the central Caledonides, suggesting transport-parallel elongation of the Caledonian allochthon during its emplacement. More recently, Boyle et al. (1994) inferred that the Sulitjelma nappe in north-central Norway underwent subvertical attenuation during eastward emplacement of the allochthon. Andersen et al. (1994)

suggested vertical thinning and lateral spreading of the nappes in the hinterland of southern Norway while thrusting continued in the foreland. The widespread nature of this general pattern of deformation suggest that it may have played an important role in the structural evolution of the orogen as a whole.

DISCUSSION

General Non-coaxial Flow at Deep Levels of a Nappe Stack

In order to explore the potential tectonic ramifications of general non-coaxial flow at deep levels of a nappe stack, consider the changes in the shape of a rock mass produced as a consequence of such deformation. Figures 12a and 12b illustrate schematically the effects of penetrative strain at deep levels of a block while it was thrust to the right. The geometry in 12a results from simple shear at deep levels of the block; the geometry in 12b results from a general shear of equal magnitude and $W_n = 0.75$.

The cartoons are simplistic due to the block geometry and assumption of homogeneous deformation, but they illustrate some aspects of general non-coaxial flow at deep levels of a nappe stack that are significant tectonically. The volume deformed by general shear differs from that deformed by simple shear in two important ways — it has undergone elongation parallel to the transport direction, and it has thinned perpendicular to the thrust fault at the base of the block. Note that the structural asymmetry, or "sense of shear," throughout the penetratively deformed volume is dextral (thrust sense) even though the material at this structural level has thinned and extended. So, under general shear conditions, "sense of shear" alone is not sufficient to define the significance of

penetrative strain in terms of bulk shortening and thickening versus bulk elongation and thinning.

Due to the transport-parallel elongation produced by general shear, strain compatibility requires the upper portion of the block either to be decoupled from the flow at deeper levels, or to undergo compatible extension. If decoupled, then general non-coaxial flow at depth would produce differential motion across the structural zone that allowed decoupling. Depending on the independent motion of the upper portion of the block, the sense of displacement across the decoupling boundary could be entirely top-right (a thrust), entirely top-left (a low-angle normal fault), or the sense and magnitude of displacement could vary in different locations (Figure 12c). Alternatively, if the upper part of the block were coupled to the deeper portion, then any bulk elongation at depth must be balanced by extension distributed in the upper part of the block (Figure 12d).

Tectonic Framework

Ramburg (1977,1981) and Sanderson (1982) developed kinematic models for the emplacement of thrust nappes that have undergone transport-parallel elongation during thrusting. The tectonic framework favored here builds on their work, and views the deformation within nappes as the result of a dynamic interaction between plate-tectonic convergence and the force of gravity acting on the nappe stack. Ultimately, the structural development and distribution of strain in a collisional orogen is governed by an evolving balance between plate tectonic and gravitational forces, as well as the changing rheologic structure and degree of mechanical coupling between different structural levels in an orogen.

Critically tapered wedge mechanics describes the functional relationships among these variables and their effects on the distribution of deformation within an orogen (Chapple, 1978; Platt 1986; Willett, 1992). The foreland-directed structural transport and internal elongation of the Caledonian allochthon inferred in this study resemble deformation predicted within a supercritically tapered wedge, one in which the combination of internal strength of the wedge and the shear traction across its base are insufficient to support the topographic gradient (Platt, 1986). Under these conditions, the orogenic wedge fails in extension. A stable nappe-stack can become supercritical if its internal strength decreases and/or the shear stress transmitted across its base is reduced. Because rock strength in the ductile regime depends strongly on temperature, prograde metamorphism at deep levels of a nappe stack will progressively reduce the internal strength of the nappe stack, and the rock mass may be weakest during its metamorphic peak. In addition, fluids released via metamorphic dehydration and decarbonation reactions may further reduce the rock strength and basal coupling of the nappes through hydrolytic weakening (Blacic, 1975), and by increasing the pore-fluid pressure (e.g., Hubbert and Rubey, 1959). Thus, several processes operative near the metamorphic peak at deep levels of a nappe stack can lead to its extensional failure while thrusting continues at the base of the nappes.

Tectonic Implications

The preceding kinematic analysis and discussion suggest a two-stage model for the formation and emplacement of the Caledonian allochthon. Stage 1 encompassed early thrusting, folding, and bulk shortening that assembled the composite allochthon

west of its present position. As a consequence of imbrication and crustal thickening in stage 1, the temperature at deep levels of the allochthon increased progressively (Fig. 13 a). In stage 2, as convergence and thrust-emplacement of the allochthon continued, prograde metamorphism caused a decrease in the internal strength and basal coupling of the nappe stack. These changes in the rheologic structure of the orogen resulted in extensional failure of the allochthon while thrusting continued along the basal shear zone and in the foreland of the orogen (Fig. 13 b-c). Heterogeneous non-coaxial flow in the hot, wet, relatively weak rocks at deep levels of the allochthon accommodated foreland-directed transport, sub-vertical thinning, and transport-parallel elongation of the rock mass at depth. In addition, this flow provided a kinematic link between upper-crustal extension and continued thrusting at the base of the nappe stack.

Upper-crustal extension during emplacement of the Caledonian allochthon can not be demonstrated directly because the upper crust of the Caledonian orogen has been removed. However, strain compatibility requires that if shallower levels of the allochthon were coupled to the deep levels examined in this study, then transport-parallel elongation at depth must have been balanced by contemporaneous extension at shallower levels. Alternatively, a low-angle detachment could have decoupled the upper crust from the ductile flow at deeper levels of the nappe stack, and such a detachment could have had either a thrust or a normal sense of relative movement.

Upper-crustal extension during thrust emplacement of the allochthon is supported by studies of the cooling history and structural development in several parts of the orogen. For example, Coker et al. (1995) interpreted the progressive westward younging of $^{40}Ar/^{39}Ar$ cooling ages in the Ofoten-Efjorden region as evidence for regional unroofing

by a low-angle, top-W normal-fault at shallower crustal levels while thrusting continued in the foreland. Gee et al. (1994) presented evidence that the Røragen supra-detachment basin in the central Caledonides developed while thrusting continued at deeper levels. Another example comes from the southern Caledonides, where Andersen et al. (1991) showed that early unroofing of the high-pressure rocks in the Western Gneiss Region of southern Norway occurred while thrusting continued in the foreland.

Comparison with the Himalayan Orogen

The general tectonic model supported by this study — early shortening, imbrication, and crustal thickening of the Caledonian allochthon, followed by syn-metamorphic extensional failure of the nappe stack while thrusting and convergence continued — may be analogous to the tectonic evolution of other collisional orogens. In this regard, the Himalayan system provides a useful example. At high structural levels of the Himalayas, normal-faulting along the South Tibetan Detachment System (STDS) was broadly contemporaneous with continued movement along the Main Central Thrust (MCT) at the base of the Himalayan allochthon (as referenced in Burchfiel et al. 1992). High-grade metamorphism, local anatexis, and strong penetrative deformation occurred in the midcrustal rocks between the STDS and MCT while these fault systems were active (as referenced by Hodges et al. 1988, and Pêcher, 1989).

The geometry of the STDS and MCT in the subsurface of the Himalayas is unconstrained. One possibility is that the normal faults at high structural levels ramp down-section and merge with the thrusts at depth, forming a midcrustal wedge bounded above by the STDS and below by the MCT (e.g., Burchfiel and Royden, 1985).

However, the high-temperature penetrative strain in the midcrustal section of the Himalayas allows another alternative. If ductile flow of the relatively weak midcrustal rocks between the STDS and the MCT included components of both foreland-directed simple-shear and subvertically shortened pure-shear, then the STDS may be analogous to the upper decoupling-zone shown schematically in figures 12 and 13. In this scenario, the STDS served to decouple the foreland-directed flow of weak rocks in the midcrust from the more competent rocks at shallower levels of the orogen. If true, then displacement along the STDS may be due largely to foreland-directed elongation of the midcrustal rock-mass in its footwall, and the STDS may remain sub-parallel to the MCT or even diverge from it at depth.

The comparison between the Caledonian and Himalayan orogens serves to point-out the broadly similar patterns of deformation in these two collisional mountain belts. Furthermore, it underscores the potentially important role of ductile flow in the midcrust as a dynamic link between upper-crustal extension and continued thrusting within collisional orogenic systems.

CONCLUSIONS

A growing number of studies in the Caledonides suggest that contraction and extension were coeval at different locations or crustal levels during Caledonian orogenesis (Andersen et al. 1994; Gee et al. 1994; Coker et al. 1995; this work). Because general non-coaxial flow can produce simultaneous foreland-directed structural transport, penetrative thinning, and transport-parallel elongation at deep levels of the nappe stack, it may have been a common mode of deformation in the midcrust of the Caledonides. In

addition, such flow may represent an important kinematic link between contemporaneous normal faulting at shallow crustal levels and thrusting at deep structural levels, not only in the Caledonides, but in other collisional or contractional orogens as well.

Acknowledgments

Work reported in this paper was supported by the NSF through grant EAR 9304635 to B.C. Burchfiel and through an NSF student fellowship awarded to the author. Informal reviews and/or discussions with J. C. Vannay, D. Hawkins, J. Bartley, K. Hodges, L. Royden, B.C. Burchfiel, O. Svenningsen, and M. Coleman contributed the quality and clarity of this paper — their time and input are much appreciated. Formal reviews and suggestions by M. Steltenpohl, J. Bartley, and K. Burke further improved the focus of the manuscript. J. Bartley, in particular, deserves credit for suggesting the argument that prograde thermal evolution is likely to cause extensional failure of a nappe stack by decreasing the coupling across the basal thrust. Stereographic projection and orientation analysis of field data were aided greatly by use of STEREONET, v. 4.8, by R. W. Allmendinger.

REFERENCES

Andresen, A., and M. G. Steltenpohl, Evidence for ophiolite obduction, terrane accretion and polyorogenic evolution of the north Scandinavian Caledonides, *Tectonophysics, 231,* 59-70, 1994

Andersen, T. B., B. Jamtveit, J. F. Dewey, and E. Swensson, Subduction and eduction of continental crust: Major mechanisms during continent-continent collision and orogenic extensional collapse, a model based on the south Norwegian Caledonides, *Terra Nova, 3,* 303-310, 1991.

Andersen, T. B., P. T. Osmundsen, and L. Jolivet, Deep crustal fabrics and a model for the extensional collapse of the southwest Norwegian Caledonides, *J. Struct. Geol.*, 16, 1191-1203, 1994.

Bartley, J., M., Structural geology, metamorphism, and Rb/Sr geochronology of east Hinnøy, north Norway, Ph.D. thesis, Massachusetts Institute of Technology, Cambridge, MA, 1980.

Bartley, J. M., Limited basement involvement in Caledonian deformation, Hinnøy, north Norway, and tectonic implications, *Tectonophysics, 83*, 185-203, 1982.

Bartley, J., M., Caledonian structural geology and tectonics of east Hinnøy, north Norway, *Bull. Nor. Geol. Unders., 396*, 1-24, 1984.

Blacic, J. D., Plastic deformation mechanisms in quartz: The effects of water, *Tectonophysics, 27*, 271-294, 1975.

Bobyarchick, A. R., The Eigenvalues of steady flow in Mohr space, *Tectonophysics, 122*, 35-51, 1986.

Boyle, A. P., K. W. Burton, and R. K. Westhead, Diachronous burial and exhumation of a single tectonic unit during collisional orogenesis (Sulitjelma, central Scandinavian Caledonides), *Geology, 22*, 1043-1046, 1994.

Burchfiel, B. C., Chen Zhiliang, K. V. Hodges, Liu Yuping, L. H. Royden, Deng Chanrong, and Xu Jiene, The South Tibetan Detachment System, Himalayan Orogen: Extension contemporaneous with and parallel to shortening in a collisional mountain belt, *Geol. Soc. Am. Spec. Paper 269*, 1992.

Burchfiel, B. C., and L. H. Royden, North-south extension within the convergent Himalayan region, *Geology, 13,* 679-682,1985.

Carmignani, L., and R. Kligfield, Crustal extension in the northern Appenines: the transition from compression to extension in the Alpi Apuane core complex, *Tectonics, 9,* 1275-1303, 1990.

Chapple, W. M., Mechanics of thin-skinned fold-and-thrust belts, *Geol. Soc. Am. Bull., 89*, 1189-1198, 1978.

Coker, J. E., M. G. Steltenpohl, A. Andresen, and M. J. Kunk, An $^{40}Ar/^{39}Ar$ thermochronology of the Ofoten-Troms region: Implications for terrane amalgamation and extensional collapse of the northern Scandinavian Caledonides, *Tectonics, 14*, 435-447, 1995.

Depaor, D. G., Orthographic analysis of geological structures - I. Deformation theory, *J. Struct. Geol., 5*, 255-277, 1983.

Foslie, S., Tysfjords geologi, beskrrivelse til det geologiske gradteigskart Tysfjord, *Nor. Geol. Unders., 149*, 298 p., 1941.

Fossen, H., and E. Rykkelid, Postcollisional extension of the Caledonide orogen in Scandinavia: Structural expressions and tectonic significance, *Geology, 20*, 737-740, 1992.

Gee, D. G., A tectonic model for the central part of the Scandinavian Caledonides, *Am. J. Sci., 275-A,* 468-515, 1975

Gee, D. G., Nappe displacements in the Scandinavian Caledonides, *Tectonophysics, 47,* 393-419, 1978

Gee, D. G., M. Lobkowicz, and S. Singh, Late Caledonian extension in the Scandinavian Caledonides - the Røragen Detachment revisited, *Tectonophysics, 231*, 139-155, 1994.

Gee, D.G., R. Kumpulainen, D. Roberts, M. B. Stephens, A. Thon, and E. Zachrisson, Tectonostratigraphic map of the Scandinavian Caledonides: in D. G. Gee and B. A. Sturt, eds., *The Caledonian Orogen - Scandinavia and related areas*, J. Wiley and Sons, Chichester, England, 1985.

Gee, D. G., and M. R. Wilson, The age of orogenic deformation in the Swedish Caledonides, *Am. J. Sci., 274*, 1-9, 1974.

Griffin, W. L., and H. K. Brueckner, Caledonian Sm-Nd ages and a crustal origin for Norwegian Eclogites, *Nature, 285*, 319-321, 1980

Gustavson, M., Narvik, Beskrivelse til det bergrunnsgeologiske gradteigskrat N9 1:250,000, *Nor. Geol. Unders., 308*, 34 p, 1974.

Harland, W. B., and R. A. Gayer, The Arctic Caledonides and earlier oceans, *Geol. Mag., 109*, 289-314, 1972.

Hodges, K. V., Tectonic evolution of the Aefjord-Sitas area, Norway-Sweden, Ph.D. thesis, Massachusetts Institute of Technology, Cambridge, MA, 1982.

Hodges, K., V., Tectonic stratigraphy and structural evolution of the Efjord-Sitasjaure area, Northern Scandinavian Caledonides, *Nor. Geol. Unders., 399*, 41-60, 1985.

Hodges, K. V., and L. Royden, Geologic thermobarometry of retrograded metamorphic rocks: an indication of the uplift trajectory of a portion of the northern Scandinavian Caledonides, *J. Geophys. Res., 89*, 7077-7090, 1984.

Hodges, K. V., and J. D. Walker, Extension in the Cretaceous Sevier orogen, North American Cordillera, *Geol. Soc. Am. Bull., 104*, 560-569, 1992.

Hodges, K. V., J. M. Bartley, and B. C. Burchfiel, Structural evolution of an A-type subduction zone, Lofoten, *Tectonics, 1*, 441-462, 1982.

Hodges, K. V., M. S. Hubbard, and D. S. Silverburg, Metamorphic constraints on the thermal evolution of the central Himalayan Orogen, *Phil. Trans. R. Soc. Lond., A326*, 257-280, 1988.

Hubbert, M. K., and W. W. Rubey, 1959, Role of fluid pressure in mechanics of overthrust faulting, *Geol. Soc. Am. Bull., 70*, 115-166, 1959.

Lister, G. S., and P. F. Williams, The partitioning of deformation in flowing rock masses, *Tectonophysics, 92*, 1-33, 1983.

Means, W. D., B. E. Hobbs, G. S. Lister, and P. F. Williams, Vorticity and non-coaxiality in progressive deformations, *J. Struct. Geol., 2*, 371-378, 1980.

Platt, J. P., Dynamics of orogenic wedges and the uplift of high-pressure metamorphic rocks, *Geol. Soc. Am. Bull., 97*, 1037-1053, 1986.

Platt, J. P., and R. L. M. Vissers, R. L. M., Extensional structures in anisotropic rocks, *J. Struct. Geol., 2*, 397-410, 1980.

Pêcher, A., The metamorphism in the central Himalaya, *J. Metamorphic Geol., 7*, 31-41, 1989.

Ramburg, H., Particle paths, displacement and progressive strain applicable to rocks, *Tectonophysics, 28*, 1-37, 1975.

Ramburg, H., Some remarks on the mechanism of nappe movement, *Geol. Fören. Stock. Förhand., 99,* 110-117, 1977.

Ramburg, H., The role of gravity in orogenic belts: in K. R. McClay and N. J. Price, eds., Thrust and Nappe Tectonics, *Geol. Soc. London Spec. Pub., 9*, 125-140, 1981.

Ramsay, R. G., and M. I. Huber, M. I., The techniques of Modern Structural Geology, Volume 1: Strain Analysis, Academic Press Inc., London. 307 p, 1983.

Roberts, D., and D. G. Gee, An introduction to the structure of the Scandinavian Caledonides, in: D. G. Gee and B. A. Sturt, eds., *The Caledonian Orogen - Scandinavia and Related Areas*, John Wiley & Sons, Ltd., 1985.

Rykkelid, E., and A. Andresen, Late Caledonian extension in the Ofoten area, northern Norway, *Tectonophysics, 231*, 157-169, 1994.

Sanderson, D. J., Models of strain variation in nappes and thrust sheets: a review, *Tectonophysics, 88,* 201-233, 1982.

Simpson, C., and D. G. DePaor, Strain and kinematic analysis in general shear zones, *J. Struct. Geol., 15*, 1-20, 1993.

Steltenpohl, M. G., The structure and stratigraphy of the Ofoten synform, North Norway, M.S. thesis, University of Alabama, University, AL, 1983.

Steltenpohl, M. G., The structural and metamorphic history of Skanland, north Norway, and its significance for tectonics in Scandinavia, Ph.D. thesis, University of North Carolina, Chapel Hill, NC, 1985.

Steltenpohl, M. G., and J. M. Bartley, Thermobarometric profile through the Caledonian nappe stack of western Ofoten, north Norway, *Contrib. Min. Pet., 92*, 93-103, 1987.

Steltenpohl, M. G., and J. M. Bartley, Crossfolds and backfolds in the Ofoten-Tysfjord area, Norway and their significance for Caledonian tectonics, *Geol. Soc. Am. Bull., 100*, 140-151, 1988.

Stephens, M. B., and D. G. Gee, Terranes and polyphase accretionary history in the Scandinavian Caledonides, *Geol. Soc. Am. Spec. Paper, 230*, 17-30, 1989.

Tull, J. F., The geochronology and structure of Vestvagøy in Lofoten, North Norway, Ph.D. thesis, Rice Univ., Houston, 149 p., 1972

Vissers, R. L. M., J. P. Platt, and D. van der Wal, Late orogenic extension of the Betic Cordillera and Alboran Domain: A lithospheric view, *Tectonics, 14,* 786-803, 1995

Willett, S. D., Dynamic and kinematic growth and change of a Coulomb wedge, in: K. R. McClay, ed., *Thrust Tectonics,* Chapman & Hall, 1992.

FIGURE CAPTIONS

Figure 1: Simplified geologic map of the Scandinavian Caledonides, showing the distribution of the erosional remnant of the Caledonian allochthon (modified from Gee et al., 1985). Inset shows a schematic block diagram (not to scale) illustrating emplacement of the Caledonian allochthon onto the margin of Baltica. The white line shows the approximate level of present erosional surface; the white box indicates the general structural position of rocks in the study area during collision.

Figure 2: Simplified geologic map of the Ofoten-Efjorden area, compiled from (Hodges, 1982; Steltenpohl, 1983; and Northrup, unpublished mapping).

Figure 3: Stereographic projections of foliation and lineation orientations in the basal shear zone (a-c) and the allochthon 1 - 4 km structurally above the basal shear zone (d-f). The data are from three sub-areas: a) and d) are from the west limb of the Ofoten synform; b) and e) are from the hinge domain produced by fold interference between the Ofoten synform and the Efjord antiform, where the trend of the basal shear zone turns abruptly from NE to NW; and c) and f) are from the north limb of the Efjord antiform.

Figure 4: Photographs and interpretive sketches of shear-sense indicators in tectonites of the basal shear zone, viewed on surfaces perpendicular to foliation and parallel to lineation. All views look NNE. a) and b) show an asymmetrically boudinaged quartz vein that steps to the right, indicating dextral (top-ESE) shear. c) and d) show mylonitic schist in the basal shear zone containing asymmetric mica 'fish' (darker areas) and shear bands. Sense of asymmetry in all of these features is consistent with dextral (top-ESE) shear.

Figure 5: Photographs and interpretive sketches of foliation boudinage and pinch-and-swell structures in the S_2 foliation, and boudinage in more competent dikes and amphibolite layers in the schists and marbles of the allochthon. All views look to the N or NE at surfaces oriented perpendicular to the foliation and parallel to the lineation. a) and b) show foliation boudinage; note the group of foliation surfaces coming in from the right that terminate near the center of the photo; c) and d) show a similar foliation geometry at larger scale displayed in a road cut. The foliation in a 6-m-thick mass of rock on the right edge of the photo pinches significantly in the center of the outcrop and begins to swell slightly towards the lower-left corner of the photo; e) symmetric boudinage of a 15-cm-thick granitic dike oriented parallel to the foliation in the schist matrix; f) boudinage of a 70-cm-thick amphibolite layer in a marble matrix; g) and h) show an outcrop with dikes in multiple orientations. One dips steeply to the left and shows weak pinch-and-swell geometry; a small dike branching from this one is oriented at a high angle to the foliation and it has been folded and shortened. A third dike dips moderately to the left, slightly oblique to the foliation ramping down through the foliation to the right; this dike has been boudinaged.

Figure 6: Synopsis of longitudinal strain data obtained in the allochthon, listed in Table 1. a) illustration of the stretch magnitudes for material lines in various orientations relative to S_2 foliation; b) model strain ellipses calculated from longitudinal strain pairs listed in Table 1.

Figure 7: Photographs and sketches showing extensional shear zones in the rock mass of the allochthon. All views look NNE at surfaces oriented parallel to lineation and perpendicular to foliation. a) through f) show shear zones that dip to the ESE and have shear senses synthetic to the top-ESE transport direction of the allochthon. g) and h) show an antithetic example. These features are interpreted as large, extensional shear-bands developed during top-ESE general non-coaxial flow of the bulk rock mass.

Figure 8: Rose diagram showing orientations of extensional shear bands relative to the S_2 foliation as viewed in a plane purpendicular to foliation and parallel to the ESE-transport direction of the allochthon.

Figure 9: Material flow-lines and strain geometries produced by various forms of homogeneous dextral shear in a continuum of possible strain regimes. The eigen vector orientations, parallel to lines of no rotational strain, are represented by the darker lines. The plane of the simple-shear component is used as the common reference frame and is horizontal in all cases shown. Finite strains shown result from deformations of equal magnitude, and illustrate the physical significance of the different strain regimes.

Figure 10: A synoptic sketch illustrating the collective geometric relationships among deformational features observed in the allochthon and their inferred orientations relative to the basal shear zone prior to late-Caledonian folding, as viewed on a plane oriented perpendicular to foliation and parallel to the transport direction. Although strain in the allochthon is heterogeneous and complex, the deformational features shown may be viewed as a kinematically consistent system of structural elements produced by top-ESE non-coaxial progressive general shear.

Figure 11: Graph showing the progressive change in orientation of the finite strain ellipse relative to the simple-shear plane as a function of increasing strain for various conditions of dextral general-shear.

Figure 12: Cartoon cross-sections showing finite strain geometries produced by deformation of an originally rectangular area in the lower part of a block as it is thrust to the right. (a) results from simple shear; (b) results from a general non-coaxial strain of equal magnitude and $W_n = 0.75$. Due to shear-parallel elongation produced by general shear, strain compatibility requires that the upper part of the block either be decoupled from the portion undergoing general shear (c), or deform in a compatible manner (d).

Figure 13: Sequential schematic cross-sections illustrating the general model of allochthon formation and emplacement favored in this study: (a) early imbrication and shortening assembled the structurally composite allochthon; (b) as emplacement of the

allochthon continued, prograde metamorphism caused a reduction in the rock strength at deep levels of the nappe stack (darker shade) and decreased the mechanical coupling across the basal shear zone; (c) these changes in the rheological structure of the orogen caused extensional failure of the nappe stack while convergence and thrusting of the allochthon continued. Heterogeneous, non-coaxial flow in the hot, wet, relatively weak rocks at deep levels of the allochthon accommodated concomitant foreland-directed transport, subvertical attenuation, and transport-parallel elongation of the midcrustal rock mass, and it dynamically linked upper crustal extension to continued thrusting at the base of the nappes.

FIGURES FOR CHAPTER 2

Figure 1

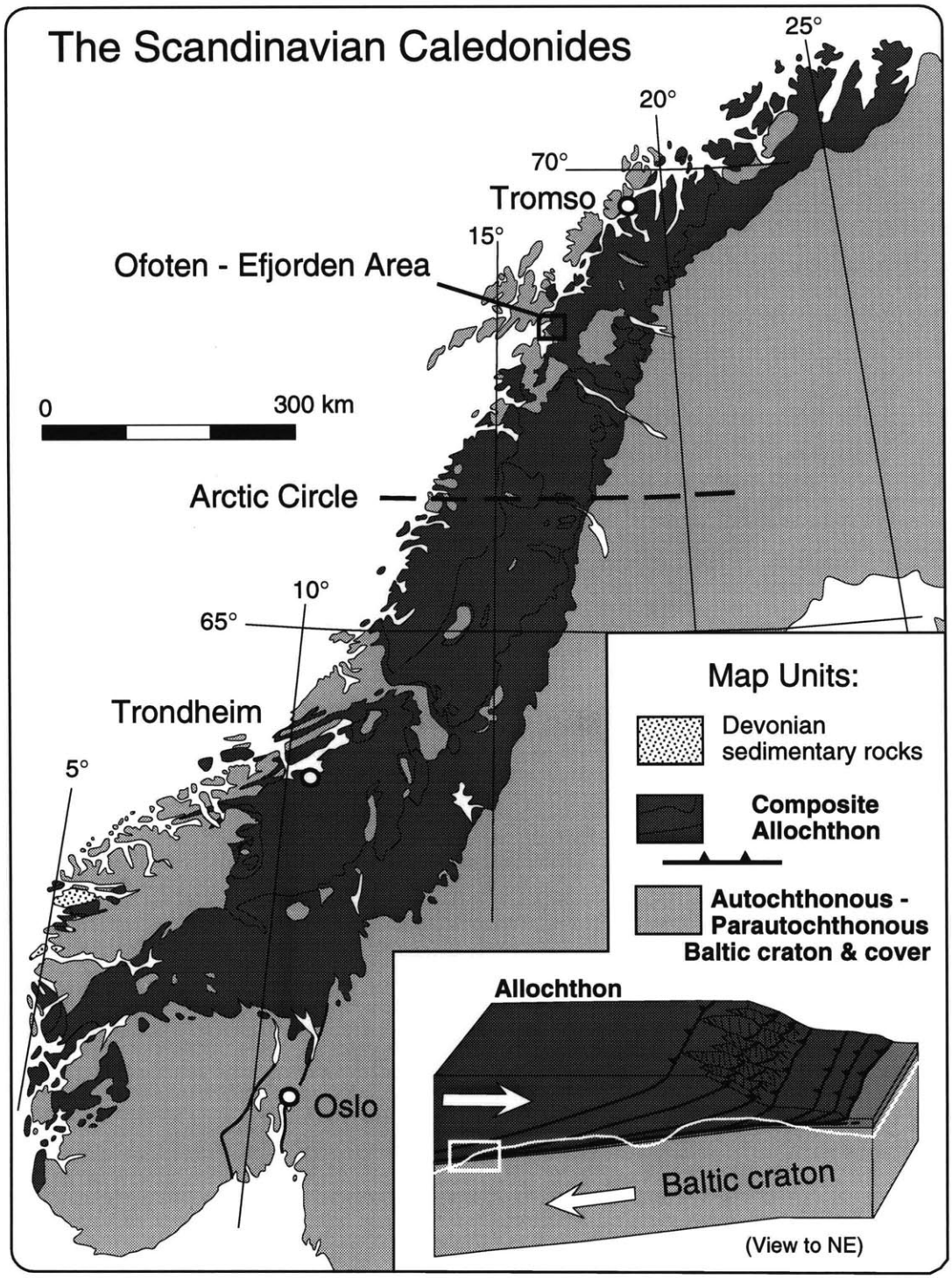
The Scandinavian Caledonides
25°
20°
70°
Tromso
15°
Ofoten - Efjorden Area
0
300 km
Arctic Circle
10°
65°
Trondheim
5°
Oslo
Map Units:
Devonian sedimentary rocks
Composite Allochthon
Autochthonous - Parautochthonous Baltic craton & cover
Allochthon
Baltic craton
(View to NE)

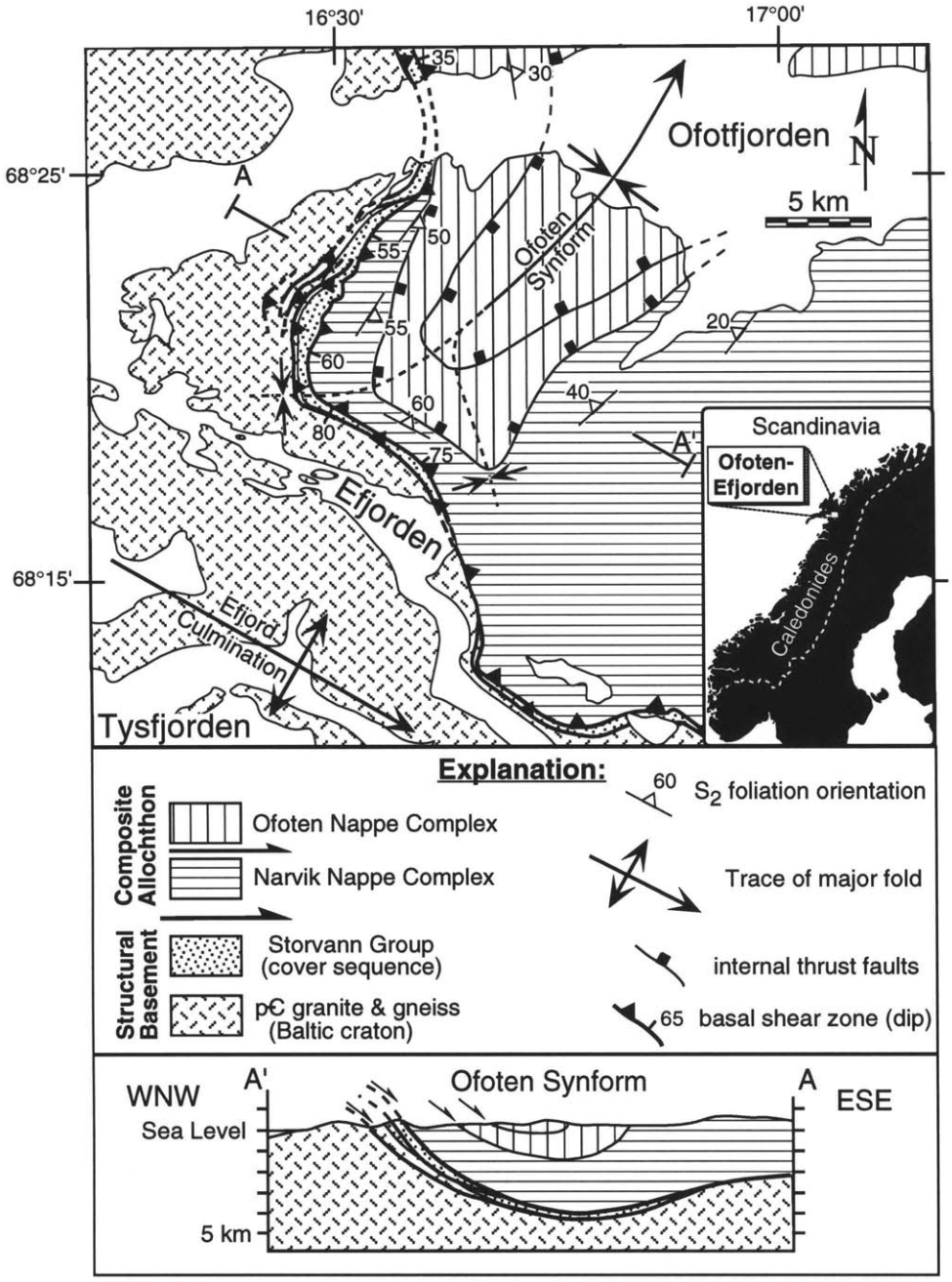
16°30'
17°00'
68°25'
68°15'
Ofotfjorden
N
5 km
Ofoten Synform
Efjorden
Efjord Culmination
Tysfjorden
A
A'
35
30
55
50
55
60
60
80
75
40
20
Scandinavia
Ofoten-Efjorden
Caledonides
Explanation:
Composite Allochthon
Ofoten Nappe Complex
Narvik Nappe Complex
Structural Basement
Storvann Group (cover sequence)
pЄ granite & gneiss (Baltic craton)
60 S2 foliation orientation
Trace of major fold
internal thrust faults
65 basal shear zone (dip)
WNW
ESE
Sea Level
5 km
Ofoten Synform

Figure 2

Figure 3

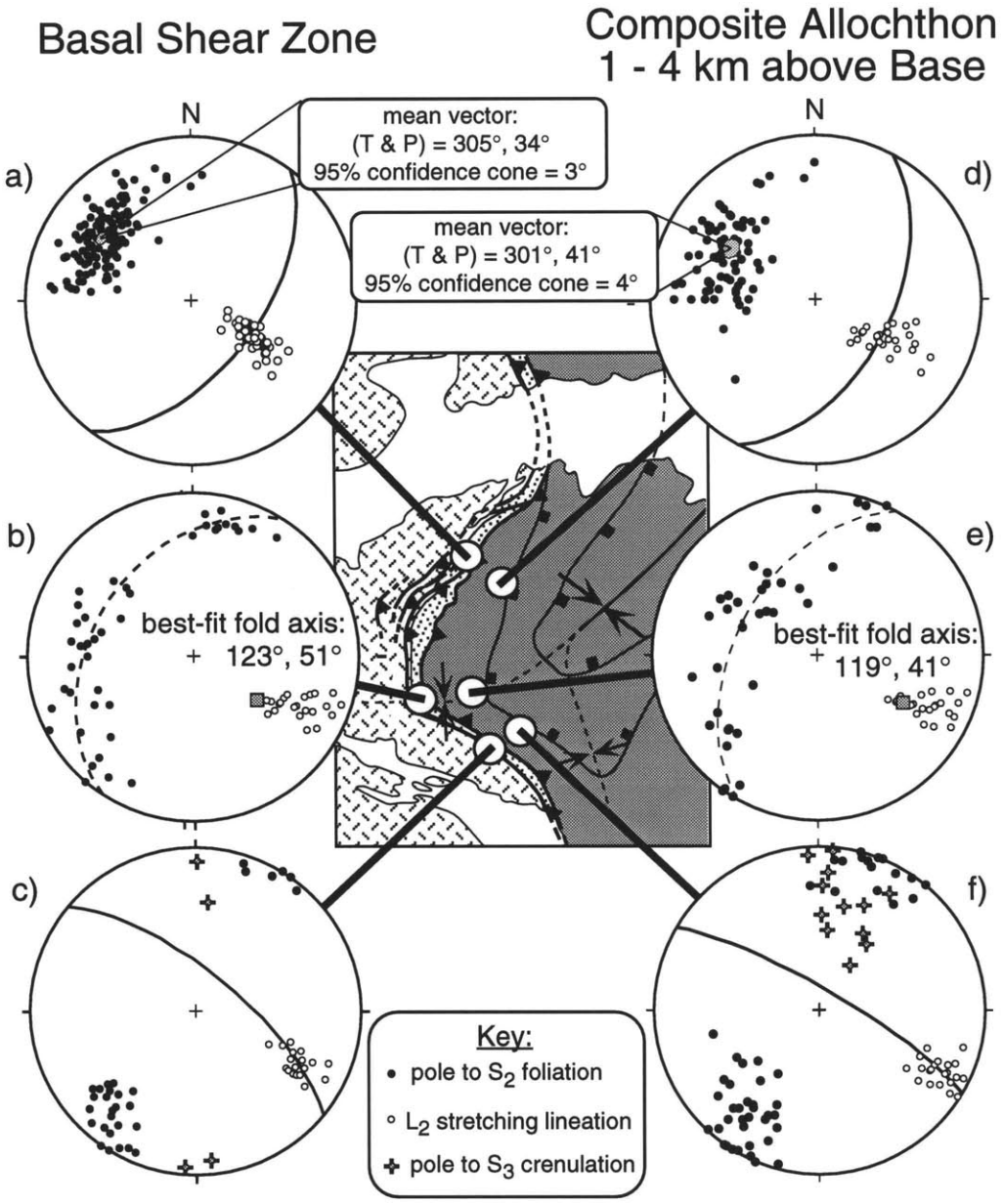
Basal Shear Zone
Composite Allochthon
1 - 4 km above Base
N
N
a)
d)
mean vector:
(T & P) = 305°, 34°
95% confidence cone = 3°
mean vector:
(T & P) = 301°, 41°
95% confidence cone = 4°
b)
e)
best-fit fold axis:
123°, 51°
best-fit fold axis:
119°, 41°
c)
f)
Key:
pole to S_2 foliation
L_2 stretching lineation
pole to S_3 crenulation

Figure4

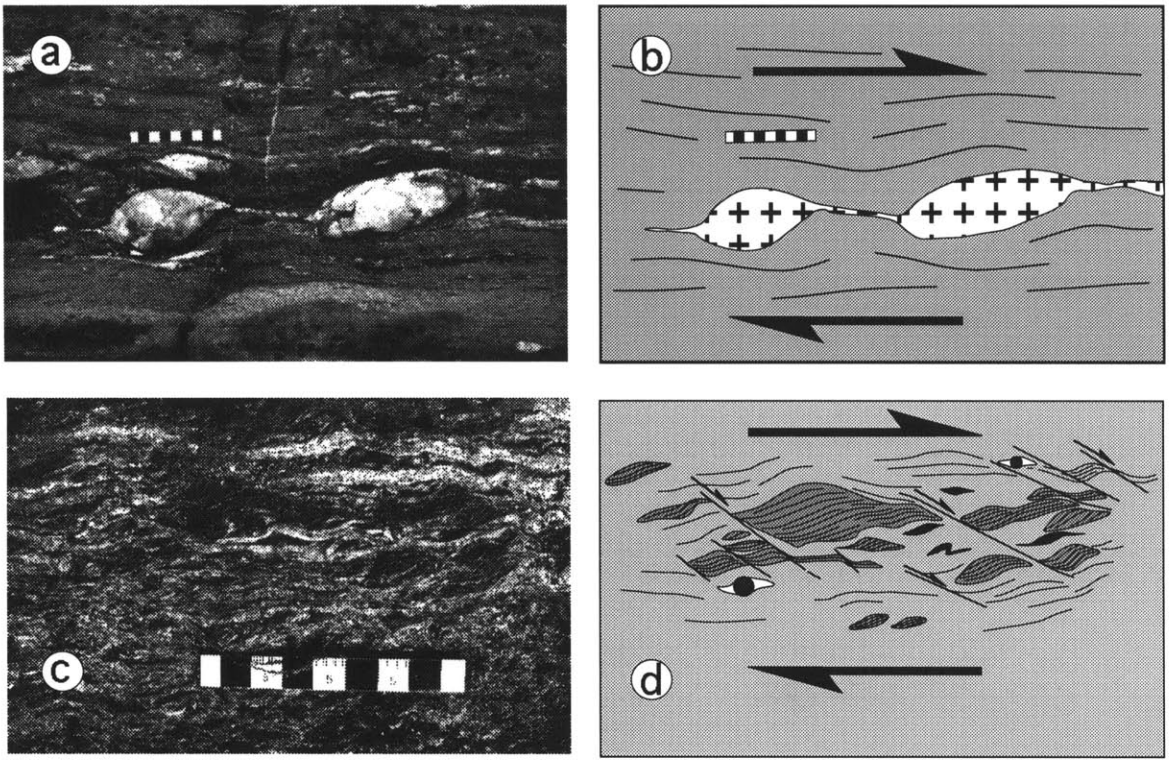

Figure 5

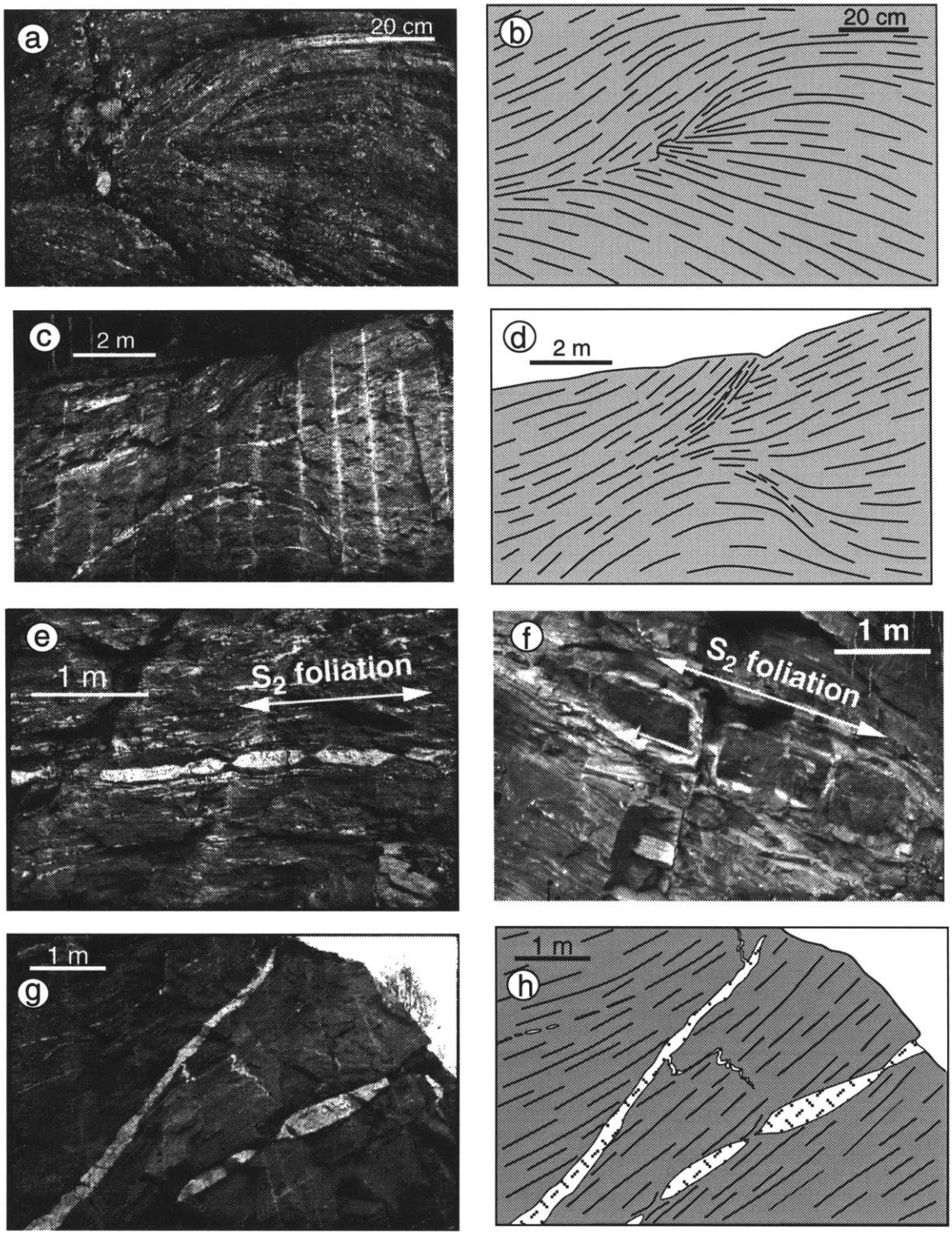
a
20 cm
b
20 cm
c
2 m
d
2 m
e
1 m
S_2 foliation
f
1 m
S_2 foliation
g
1 m
h
1 m

Table 1: Longitudinal Strain Estimates, Ofoten-Efjorden

obs 1		obs 2		Model X-Z Strain Ellipses			
θ	Σ	θ	Σ	Σ_{max}	Σ_{min}	Δ Area (%)	Elipticity
-5	2.12	-71	0.51	2.29	0.48	10	4.7
-2	3.20	10	1.22	3.69	0.22	-17	16.5
7	1.84	75	0.45	2.13	0.44	-7	4.9
-4	1.95	83	0.66	1.99	0.66	30	3.0
-2	3.88	80	0.42	4.10	0.41	70	9.9
-1	2.23	84	0.55	2.24	0.55	22	4.1
-5	2.27	66	0.32	3.07	0.29	-10	10.5
0	5.65	8	1.50	5.65	0.22	22	26.0
-3	3.25	82	0.27	4.21	0.27	12	15.8
1	1.77	90	0.44	1.77	0.44	-22	4.0
0	4.60	-9	1.60	4.60	0.27	23	17.3
-4	2.33	2	2.40	2.42	0.57	38	4.3
4	2.45	-79	0.39	2.73	0.38	5	7.1
-2	2.30	7	1.85	2.36	0.36	-15	6.6
-1	2.1	–	–				
4	1.98	–	–				
0	3.10	–	–				
2	1.67	–	–				
0	4.17	–	–				
7	1.80	–	–				
-3	3.32	–	–				
-6	4.10	–	–				

θ = inclination of material line relative to S_2 foliation, (+ve) inclination is in the direction of tectonic transport; Σ = estimated magnitude of longitudinal strain (L final / L initial); Σ_{max} and Σ_{min}= are calculated maximum and minimum principal strains (L final / L initial); Δ Area and Elipticity are the change in area (relative to a unit circle) and aspect ratio of the model strain ellipses.

Figure 6

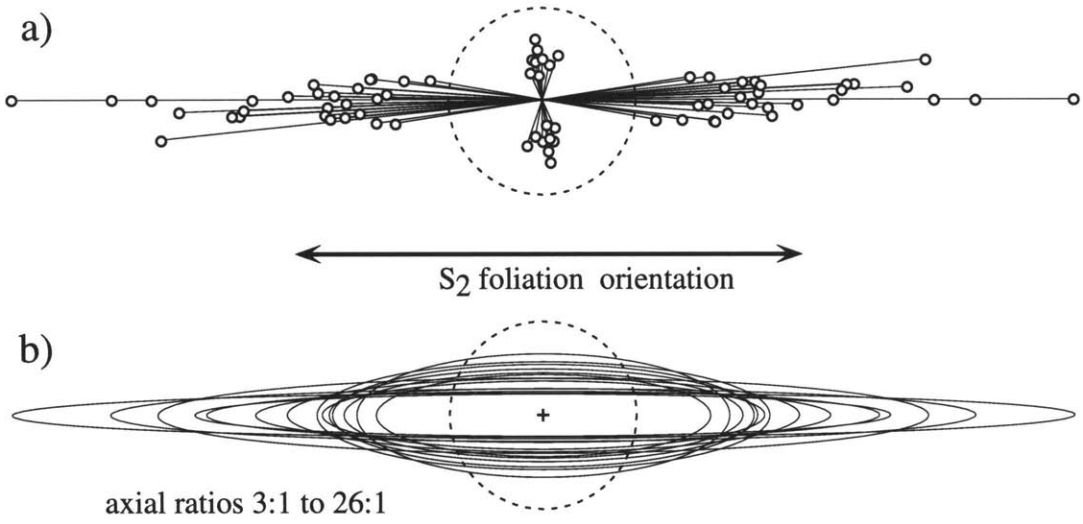

Figure 7

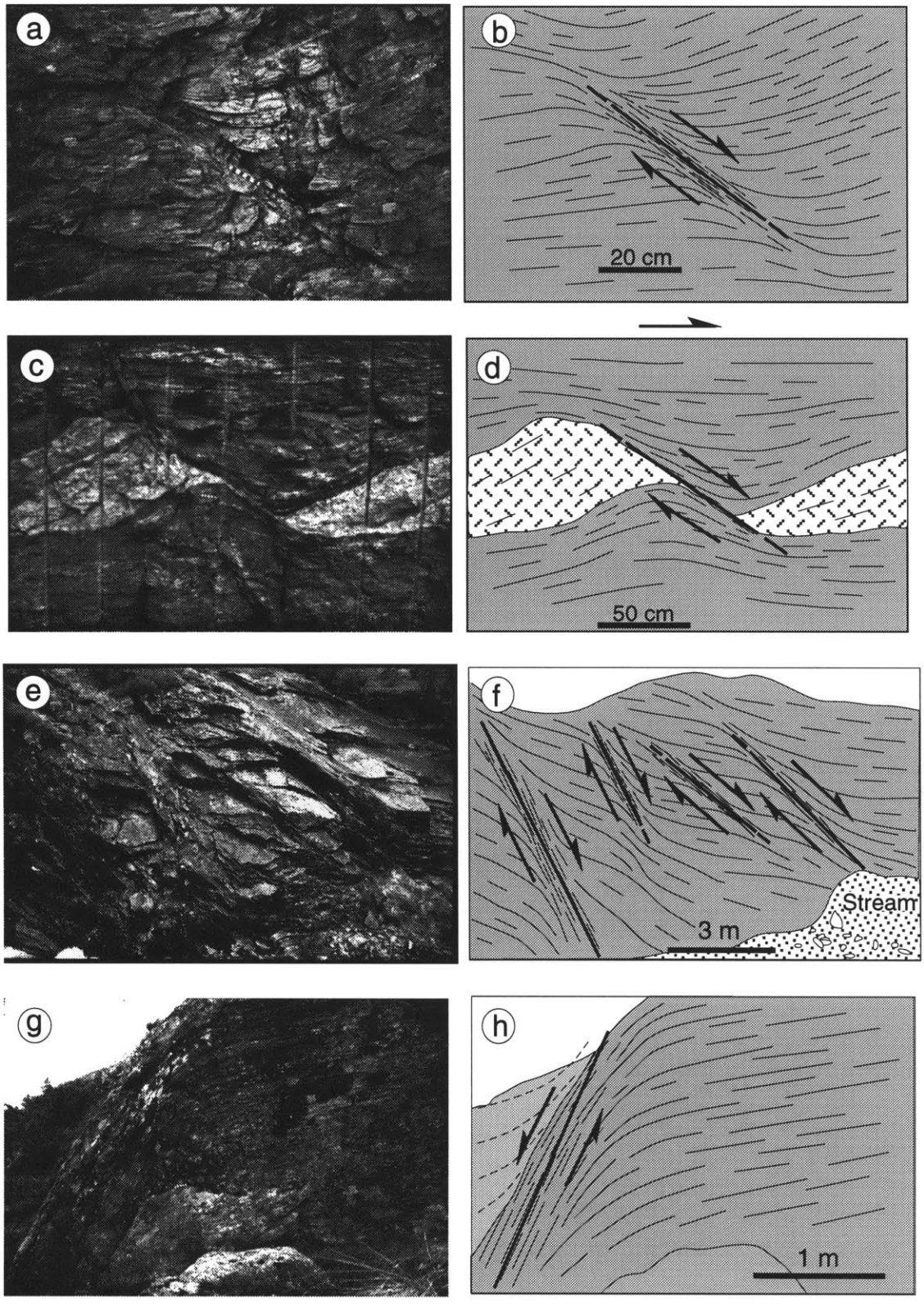

Figure 8

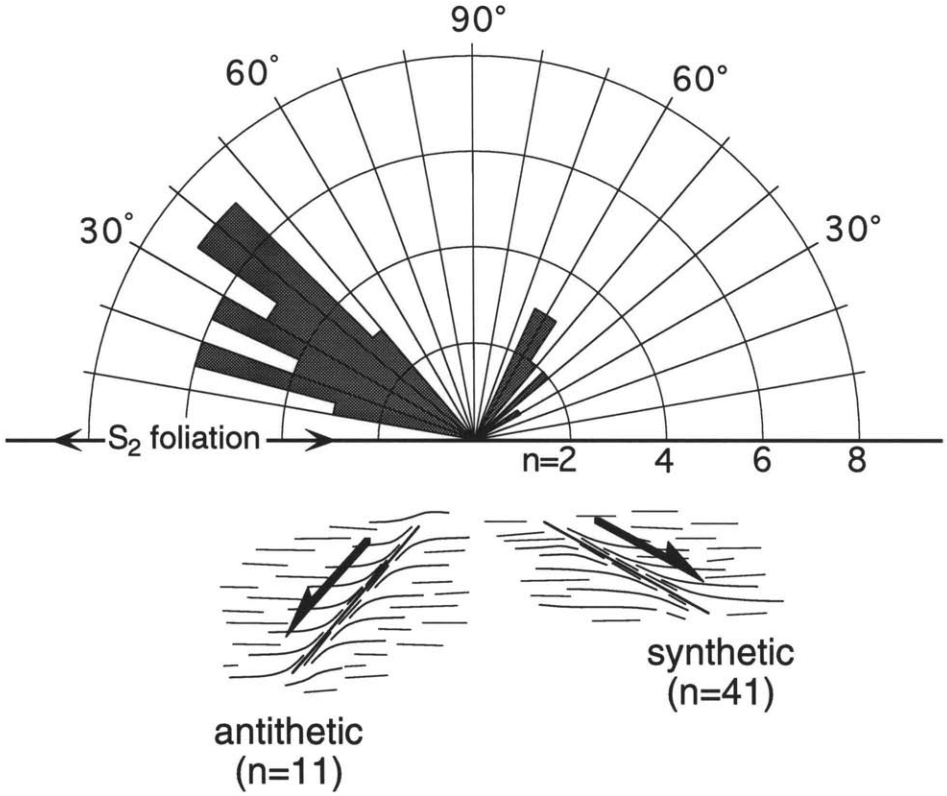
90°
60°
60°
30°
30°
S2 foliation
n=2
4
6
8
antithetic
(n=11)
synthetic
(n=41)

Figure 9

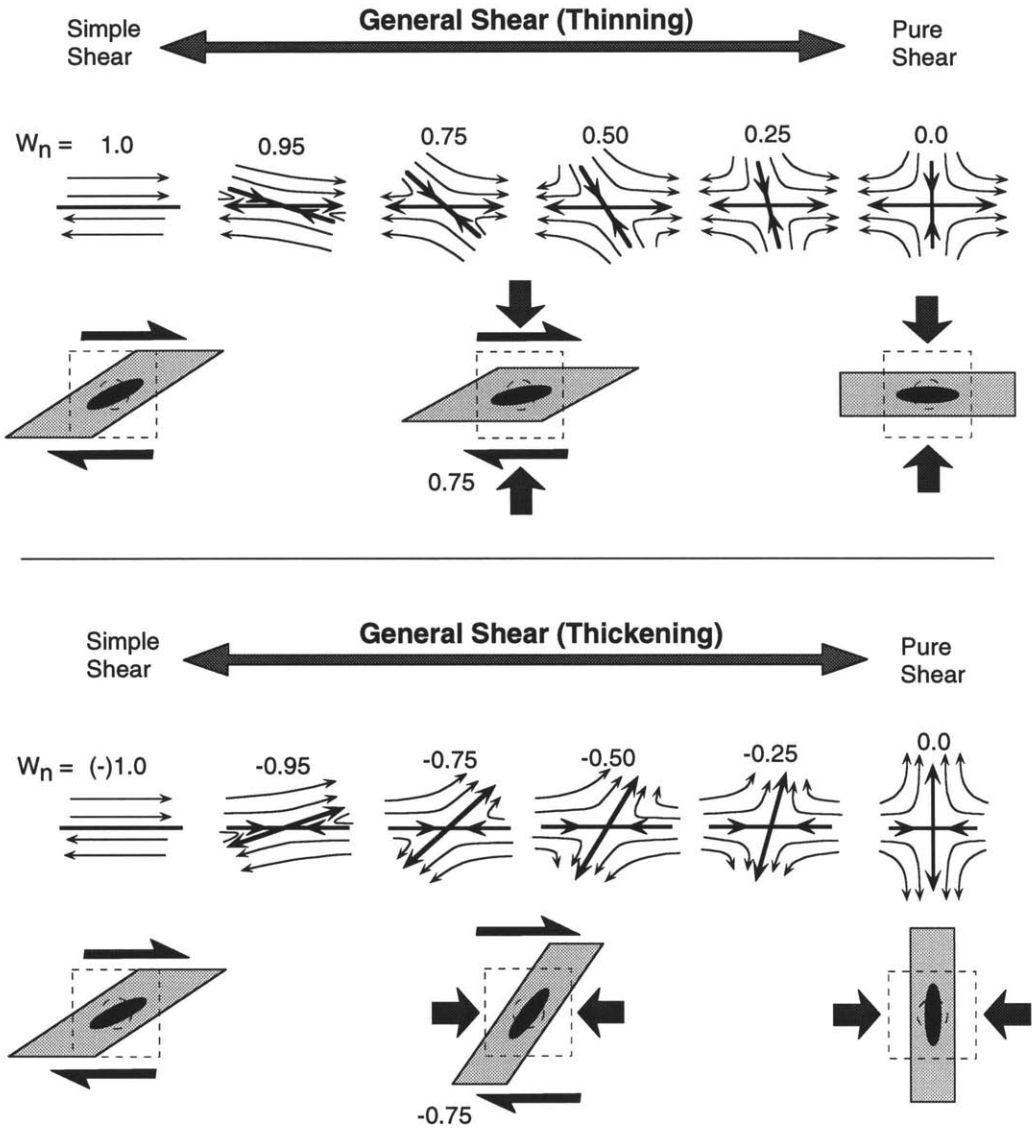
Simple Shear
General Shear (Thinning)
Pure Shear
W_n = 1.0
0.95
0.75
0.50
0.25
0.0
0.75
Simple Shear
General Shear (Thickening)
Pure Shear
W_n = (-)1.0
-0.95
-0.75
-0.50
-0.25
0.0
-0.75

Figure 10

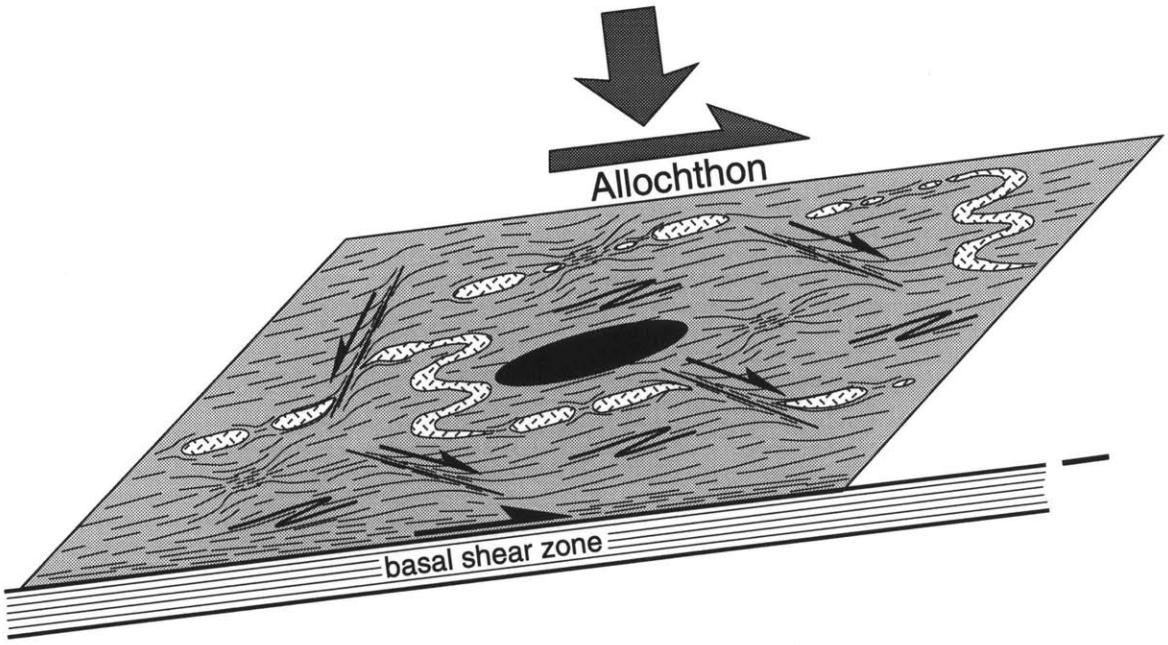

Figure 11

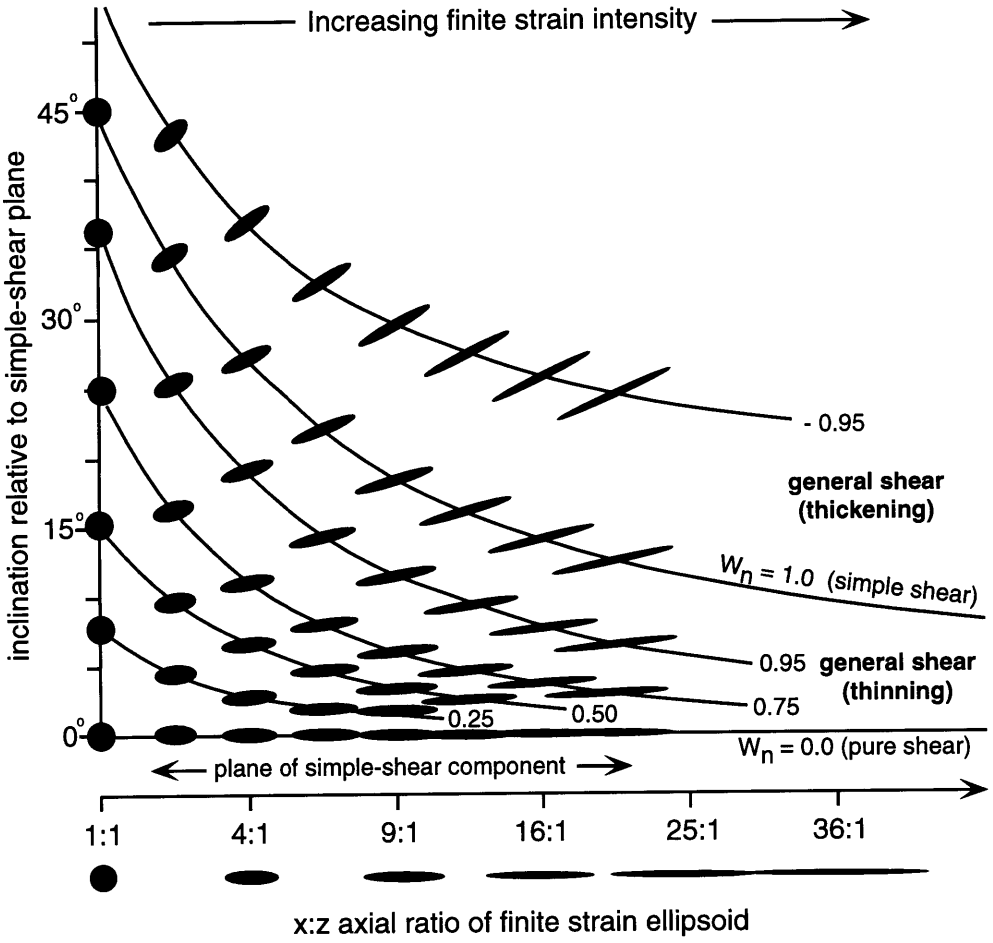
Increasing finite strain intensity
45°
30°
15°
0°
inclination relative to simple-shear plane
- 0.95
general shear
(thickening)
W_n = 1.0 (simple shear)
0.95 general shear
(thinning)
0.75
0.50
0.25
W_n = 0.0 (pure shear)
plane of simple-shear component
1:1
4:1
9:1
16:1
25:1
36:1
x:z axial ratio of finite strain ellipsoid

Figure 12

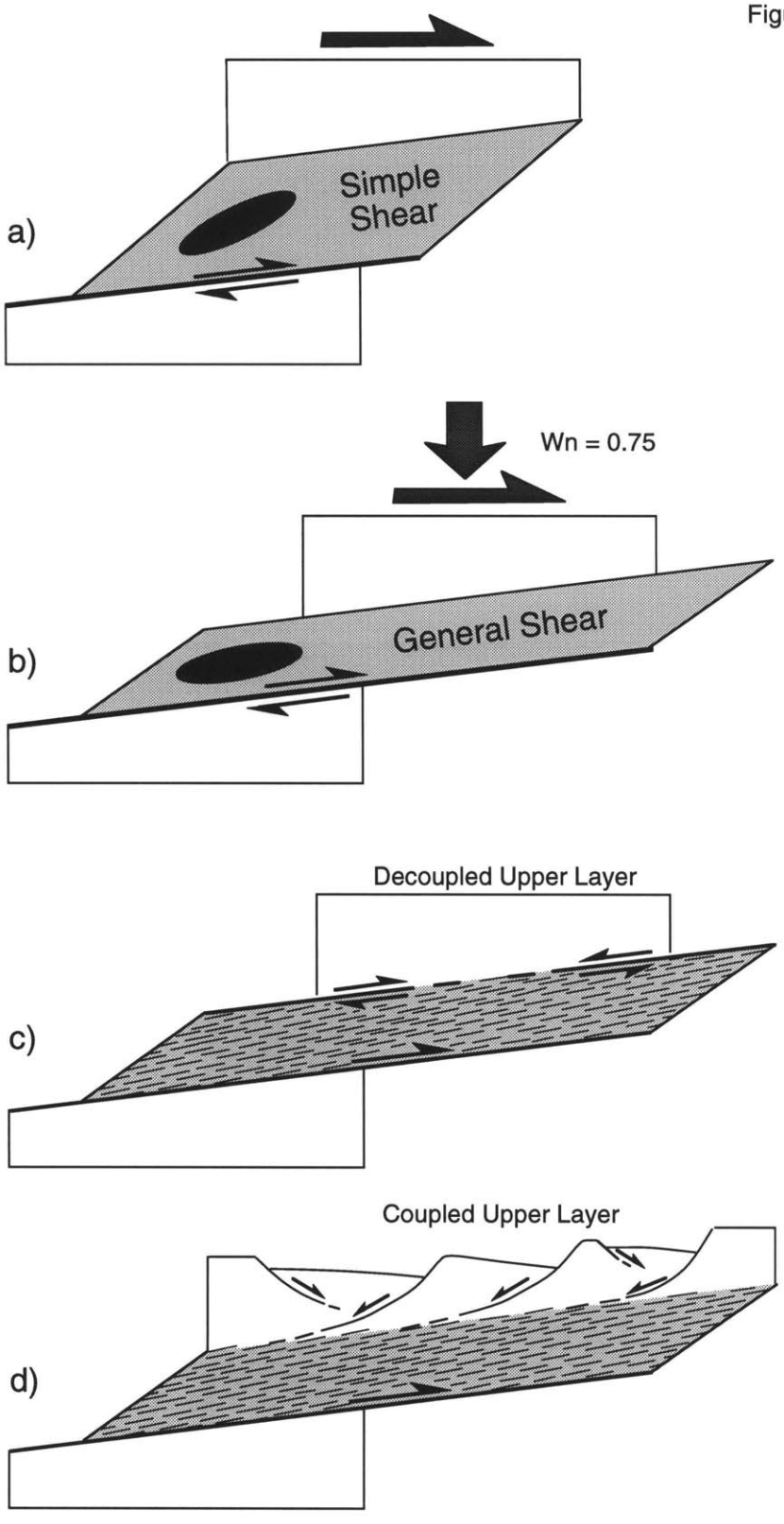
a)
Simple Shear
b)
Wn = 0.75
General Shear
c)
Decoupled Upper Layer
d)
Coupled Upper Layer

Figure 13

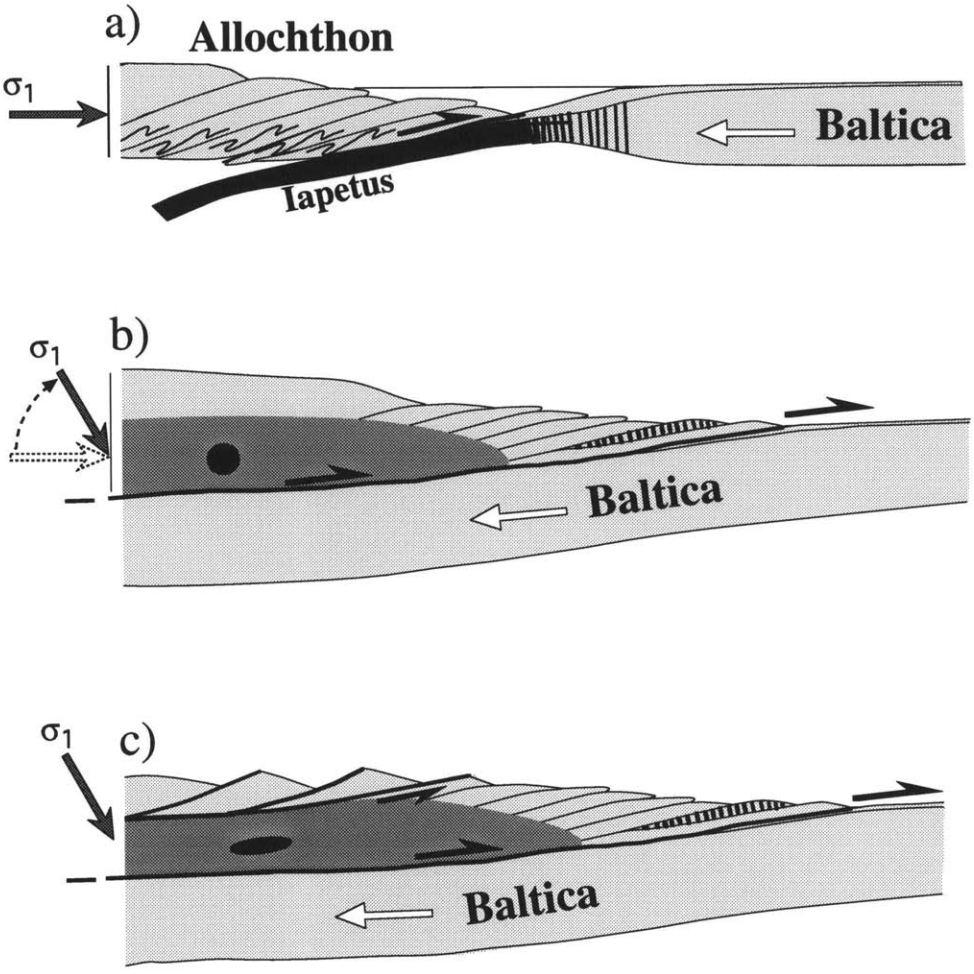

Chapter 3

Orogen-parallel transport and vertical partitioning of strain during oblique collision, Efjorden, north Norway.

ABSTRACT

Thrust sheets in the Caledonian allochthon in northern Scandinavia were emplaced generally toward the ESE, an orientation nearly perpendicular to the trend of the Caledonian orogen. In the Efjord area of north Norway, however, orogenesis also produced top-to-the-SSW motion on N-dipping thrust faults in the cratonal basement beneath the allochthon. The leading edges of some SSW-directed thrust-sheets moved upward into the overlying metasedimentary cover and formed the cores of S-verging recumbent fold-nappes at the base of the Caledonian allochthon. As deformation continued, these fold nappes became entrained in the top-to-the-ESE transport of the overlying allochthon. Mutually cross-cutting relationships suggest contemporaneous SSW-directed thrusting in the cratonal basement and top-to-the-ESE movement of the allochthon. Thus, structures in the Efjord study area reflect vertical partitioning of strain into components with nearly orthogonal displacement directions at different structural levels. Collectively, the top-to-the-SSW (orogen-parallel) and top-to-the-ESE (orogen perpendicular) components of transport are consistent with overall sinistral-oblique, post-collisional convergence between Baltica and Laurentia. Implications include: (1) In some parts of the orogen, recumbent folds with hinges sub-parallel to the transport direction of the allochthon were produced by orogen-parallel transport rather than orogen-

perpendicular sheath-folding; and (2) Orogen-parallel components of structural transport make two-dimensional palinspastic restoration in planes perpendicular to the orogen difficult or inappropriate in some locations.

INTRODUCTION

Geologists often analyze the structural development of mountain belts in two-dimensional cross-sections drawn roughly perpendicular to an orogen, because planes of this orientation are commonly assumed to contain the principal direction of structural transport. Many mountain belts, however, have additional components of structural transport sub-parallel to their trends. Examples include the Alps (Selverstone 1988, Mancktelow 1992), Appalachians (Peterson & Robinson 1993,Vauchez *et al.* 1993), Caledonides (Gilotti & Hull 1991, Holdsworth & Strachan 1991), Caucasus (Jackson 1992), North American Cordillera (Gabrielse 1985, Price & Carmichael 1986), Himalayas (Molnar & Tapponier 1975), and the Tasminides (Glen 1992). Orogen-parallel tectonic transport can occur for a variety of reasons, but it is a particularly common features of mountain belts produced by oblique convergence because a component of the convergence vector can be resolved parallel to an orogen built along the convergent boundary (e.g., Fitch 1972, Dewey 1980). Convergence exactly orthogonal to plate boundaries occurs much less frequently than oblique movement, so most collisional orogens are transpressional and must, in some manner, accommodate an orogen-parallel component of structural transport (e.g. Fossen *et al.* 1994).

At present, the three-dimensional structural architecture and partitioning of deformation within zones of oblique collision or convergence are poorly understood,

particularly at deeper levels of such orogens. Therefore, studies of the geometry, kinematic characteristics, and modes of interaction among structures that have accommodated orogen-parallel and orogen-orthogonal components of deformation within collisional systems are necessary to understand better their tectonic evolution.

The Scandinavian Caledonides provide an opportunity to examine directly the structural development at middle to deep crustal levels of a Paleozoic collisional system. Structural studies and stratigraphic evidence from numerous locations within the Caledonian orogen suggest sinistral-oblique convergence and transpression during the collision of Baltica and Laurentia (e.g. Steltenpohl & Bartley 1988, Soper *et al.* 1992, Fossen 1993). The purpose of this paper is to document the geometry and kinematic characteristics of Caledonian thrust faults and recumbent fold-nappes in the Efjord area of north Norway, and to present a three-dimensional kinematic interpretation for their development within the context of oblique collision.

TECTONIC SETTING

During the Caledonian collision, A-type subduction of the western margin of Baltica resulted in the ESE-directed emplacement of a crustal-scale, composite allochthon onto the Baltic craton (Gee 1975, Hodges *et al.* 1982, Stephens & Gee 1989). Subsequent erosion has removed much of the allochthon and exposed deep levels of the orogen in Scandinavia. The present-day mountain belt consists of a relatively thin veneer of the original allochthonous thrust-stack lying over autochthonous or parautochthonous rocks of the Baltic craton (Figure 1). Because the present erosional surface essentially follows the structural level of the Caledonian A-type subduction zone across the orogen,

the contact between the subducted Baltic craton (lower plate) and the over-riding Caledonian allochthon (upper plate) is well exposed in many structural windows and basement culminations.

A growing number of geologic studies have suggested that the Caledonian orogen resulted from sinistral-oblique convergence. For example, Fossen (1993) interpretted the structural development in part of the Caledonides of SW Norway as the product of orogen-normal thrusting combined with orogen-parallel sinistral shear. Another exmple comes from the Caledonides of east Greenland, where Holdsworth & Strachan (1991) described a system of sinistral strike-slip faulting and orogen-orthogonal thrusting that were interpreted as evidence for a sinistral component to Caledonian orogenesis. Soper *et al.* (1992) inferred sinistral oblique convergence and collision of Baltica and Laurentia to form the Caledonian orogen based on a synthesis of structural, stratigraphic, and paleomagnetic data from various circum-Iapetus continents and continental fragments.

GEOLOGY OF THE EFJORDEN AREA

The Efjorden study area, located near 68°N on the coast of Norway (Figs. 1 & 2), contains exposures of subducted Baltic craton, the far-traveled Caledonian allochthon, and the group of structures which formed the Caledonian A-type subduction zone (Hodges *et al.* 1982, Tull *et al.* 1985). Rocks in the area were metamorphosed and deformed under P-T conditions in the upper-greenschist to epidote-amphibolite facies during Caledonian orogenesis (Hodges 1982, Crowley 1985).

Regional late-Caledonian folds control the first-order pattern of geologic contacts in the study area (Fig. 2, Hodges 1985, Steltenpohl & Bartley 1988). Near the head of

Efjord, the folding produced a gently ESE-plunging antiform. The interaction of the Efjord antiform with the present erosional surface creates an ESE-closing half-window cored by rocks of the Baltic craton and flanked by rocks of the composite Caledonian allochthon. Units dip 25°- 45° N along the north limb of the culmination, 15°- 30° E near its closure, and 20°- 30° S along its southern limb. The radial dips of the structural section around the closure of the Efjord culmination make the geologic map an oblique conical cross-section through the lower portion of the composite allochthon and the upper portion of the Baltic craton. Nearly 1.5 km of local topographic relief yields magnificent three-dimensional exposure of this structural level of the orogen.

Tectonostratigraphy

Rocks in the area can be grouped into four tectonostratigraphic units based on tectonic affinity and magnitude of structural transport (see Roberts & Gee 1985). The *parautochthon*, or structural basement, consists primarily of Precambrian, K-feldspar megacrystic granite (Tysfjord granite, Andresen & Tull 1986), interpreted to be part of the Baltic craton (Hodges 1985, Tull *et al.* 1985). The Precambrian granite intruded older Precambrian schist and gneiss which form a subordinate portion of the cratonal rocks in the Efjord area. Sporadic mafic dikes cut the cratonal basement, and intrusion of these dikes may have been related to rifting along the Baltoscandian margin farther west, as the Iapetus Ocean basin opened. Above the Precambrian rocks, quartzite and garnet-grade psammitic schist represent a strongly deformed and metamorphosed remnant of the early Paleozoic sedimentary cover sequence on Baltica. Although still attached to the craton

locally, the metasedimentary cover commonly is detached and transported to some extent relative to the contiguous cratonal basement (Hodges 1985, Andresen & Rykkelid 1989).

A complex series of thrust sheets, fold nappes, and mylonite zones forms the rock mass structurally above the parautochthon. Thrust sheets and recumbent fold-nappes derived from the Baltic craton and its metasedimentary cover lie directly over the parautochthon and constitute the *lower allochthon.* Total transport distances of these thrust sheets and fold nappes are not known, but lithologic and metamorphic similarity between them and the parautochthon suggests relatively local derivation. Above the lower allochthon is a 50 - 300 m thick *sliver zone* consisting of structurally interleaved mylonitic rocks of uncertain tectonic affinity and heterogeneous lithologic character. The sliver zone forms a fundamental structural and tectonostratigraphic break — it marks the transition between Baltic affinity rocks below and far-traveled oceanic affinity rocks above. Pelitic schist, amphibolite, and impure marbles derived from the Iapetus Ocean basin overlie the sliver zone and form the structurally composite *upper allochthon,* the highest tectonostratigraphic unit in the area (Hodges 1985).

Structure of the Efjorden Area

This paper focuses primarily on the structural evolution of rocks of Baltic affinity (Parautochthon and Lower Allochthon) in the Efjord area. Two important components of the structural architecture of the Baltican rocks can be recognized at map scale: (1) N-dipping thrust faults in the cratonal basement and imbricated sheets of cratonal rocks associated with these thrusts exposed in the northern limb of the Efjord culmination; and

(2) a complex series of S-vergent, E-trending, recumbent fold-nappes cored by cratonal rocks exposed in the southern limb of the Efjord culmination (Figs. 2 - 4).

A series of thrust sheets forms an imbricate stack exposed southeast of Skarvatnet, a lake in the northern part of the area. Thrust sheets in the stack are composed principally of Precambrian granite derived from the Baltic craton. The structurally highest sheet also contains a significant amount of Precambrian gneiss and schist. Granite within the thrust sheets has a moderate fabric (L>S) defined by elongate biotite or feldspar mineral aggregates. Fabric intensity increases notably within a few meters of the mylonitic thrust faults bounding the imbricated sheets (Figs. 5a-b). Strain also increases near the top of the stack and within the leading portions of sheets that ramp up into the overlying schists. In these locations, the cratonal rocks have undergone extensive recrystallization and grain-size reduction. The thrusts dip generally north, and some root locally in the cratonal basement.

Strongly deformed quartzite and garnet schist are present as thin (typically <10 m), discontinuous layers along some of the thrust faults in the imbricate stack near Skarvatnet. Along a given fault, schist and quartzite are thickest in outcrops at the highest elevations and pinch out as the fault is followed to lower elevation. These metasedimentary rocks are interpreted to be remnants of the cover sequence which were overridden or infolded between the granite sheets during imbrication of the stack.

Tectonites within and adjacent to the shear zones contain a well-developed foliation oriented sub-parallel to the thrust contacts (Fig 3). The foliation is defined by mm-scale compositional variations, alignment of mica (001) planes, and flattened mineral aggregates in the mylonitic granite and schists of the metasedimentary cover sequence.

The orientation of the foliation varies somewhat across the study area due to the effects of regional-scale folding. Aside from variations imposed by the broad folding, however, the foliation changes orientation only modestly from one location or structural level to another.

A stretching lineation defined by strain shadows around K-feldspar porphyroclasts and by elongate, polygranular mineral-aggregates lies in the plane of the foliation. In contrast to the relatively consistent orientation of foliation, the orientation of the stretching lineation changes significantly as a function of structural level (Fig. 3). At deeper levels, the lineation trends NNE, and at higher levels it trends ESE. The change in trend from NNE to ESE with increasing level is complex, passing locally through an intermediate zone with variable orientations transitional between the end members.

In zones of significant non-coaxial deformation, the orientation of the stretching lineation is commonly sub-parallel to the orientation of relative structural transport. Strain within the ductile faults of the study area is inferred to have had a high component of simple shear, since deformation within the shear zones clearly accommodated transport of structural blocks past one another (e.g., placing basement granite structurally above the metasedimentary cover). Consequently, the orientations of stretching lineations in the ductile fault zones of the area are interpreted to indicate the directions of relative movement along these structures.

S-C fabric relationships (Lister & Snoke 1984) and/or asymmetric porphyroclasts (Simpson & Schmid 1983) on outcrop surfaces oriented perpendicular to foliation and parallel to the stretching lineation near the mylonitic thrust faults were used to infer the relative-transport direction along the faults (Figs. 3 & 5). The variations in the trend of

lineation indicate that shear displacement was in different directions at different structural levels. At deeper levels where the stretching lineation trends NNE, fabric asymmetry within the shear zones is consistent with top-to-the-SSW transport across the N-dipping thrusts. In contrast, near the top of the thrust stack (as well as in the overlying sliver zone and Upper Allochthon) where the lineation trends generally ESE, fabric asymmetry is consistent with top-to-the-ESE relative transport.

Precambrian cratonal rocks in the hanging walls of the SSW-directed thrusts can be followed to the southeast around the closure of the Efjord culmination into the southern part of the study area, where they form the cores of S-vergent recumbent fold-nappes (Figs. 2 and 3). Hinges of the fold nappes trend E or ESE, sub-parallel to the regional transport direction of the Caledonian allochthon. Quartzite and schist of the metasedimentary cover sequence persist around the limbs and closures of the fold nappes, although they have been highly attenuated in the limbs. Intrafolial isoclinal folds are ubiquitous at outcrop scale, and their orientations mimic those of the larger fold-nappes (Figs. 3 & 6). In detail, numerous mesoscopic to macroscopic parasitic folds add significant complexity to the geometry and internal structure of the fold nappes.

At large scale, the fold nappes are intrafolial with respect to the Baltican affinity rocks in Lower Allochthon. Mesoscopic rootless isoclines are present at all structural levels, including the mylonitic sliver zone and Upper Allochthon, but the sliver zone does not close around the map-scale recumbent folds in the Lower Allochthon. Instead, it forms a continuous zone of mylonitic rocks above the fold-nappe complex and separates the Baltican affinity rocks below from the Oceanic-affinity thrust sheets in the overlying Upper Allochthon.

In many places, W-vergent kink-bands overprint deformational fabrics related to top-to-the-ESE transport of the allochthon and/or top-to-the-SSW movement along thrusts in the cratonal basement. These kink bands are commonly associated with recrystallization to chlorite-bearing retrograde mineral assemblages, and thus clearly post-date the main contractional phase of Caledonian orogenesis in this area. Rykkelid & Andresen (1994) documented top-W extensional reactivation of faults to the NE of Efjorden, and the W-vergent kink-bands at Efjorden provide evidence for some top-to-the-W reactivation in this area as well. However, net structural separations remain thrust-sense, and top-to-the-W reactivation did not produce well-organized, throughgoing detachment zones. Consequently, the magnitude of top-to-the-W reactivation of structures in the Efjord area is inferred to be modest.

DISCUSSION

Sequence of Deformation

Although the structural evolution of the Lower Allochthon at Efjorden was complex, cross-cutting and overprinting relationships broadly constrain the deformation sequence in the area. Individual structures or groups of structures discussed below are indicated by numerical labels (Fig. 2). Cross-cutting relationships indicate that the earliest structures in the area are the southernmost of the N-dipping thrust-faults in the cratonal basement (1). These faults are truncated by a top-to-the-ESE thrust (2), and therefore, predate final movement on the ESE-directed thrust. Farther north, thrust (2) is cut by a top-to-the-SSW thrust (3) which forms the base of a stack of SSW-directed thrust

sheets derived from the cratonal basement. Thrusts (3-5) represent various splays within a complex SSW-directed thrust system. The relative ages of the thrusts are not constrained well by their geometry. Nevertheless, the SSW-directed thrusts farther south (1) are clearly older than those to the north (3-5), suggesting a general S-to-N progression of top-to-the-SSW thrusting in the cratonal basement.

The cratonal rocks in the highest parts of the SSW-directed imbricate stack can be followed southward around the closure of the Efjord culmination into the cores of S-verging, E-trending recumbent fold-nappes (6) near Skarisen. The continuity between the thrust sheets and the fold nappes suggests a genetic relationship in which the top-to-the-SSW thrusts represent the root zones of the S-verging fold-nappes. The N-dipping thrusts and the S-vergent fold-nappes, therefore, formed simultaneously and represent collectively a system of structures which accommodated an orogen-parallel component of structural transport during the Caledonian collision.

At regional scale, the Efjord transverse culmination (7) is one of a series of ESE-trending, basement-involved folds (Foslie 1941, Hodges 1985, Steltenpohl & Bartley 1988). The transverse folds resemble mega-mullions in the upper surface of the Baltic craton. West of the present study area, the structural section in the north limb of the Efjord culmination is overturned locally, and a retrograde cleavage associated with the transverse folds overprints fabric in the top-to-the-ESE shear zone at the base of the Upper Allochthon (Steltenpohl & Bartley 1988). These relationships constrain some of the transverse folding to have developed later than the emplacement of the allochthon, perhaps synchronous with Devonian extension, like transverse folds in southern Norway (e.g. Roberts 1983, Torsvik *et al.* 1986, Norton 1987). However, the relative timing

between the *initiation* of transverse folding and end of ESE-thrusting in the Efjorden area is unknown. Because the axes of the transverse folds are subparallel to the transport direction of the allochthon, the folds are geometrically compatible with simultaneous folding and top-to-the-ESE movement of the allochthon. Thus, early phases of transverse folding may have occurred while ESE-directed thrusting continued. If so, then early transverse folding may represent another structural manifestation of orogen-parallel shortening during the thrust emplacement of the allochthon.

At the latitude of Efjorden, the intensity of transverse folding increases from east to west across the orogen, as does the metamorphic grade achieved by rocks in the structural basement (e.g. Bartley 1980, Hodges 1982, Bjorklund 1989). Bearing the westward increase of paleotemperature in mind, the fact that the top-to-the-SSW thrusts in the cratonal basement at Efjord are located near the eastern termination of a major transverse fold is interesting. Although a clear link can not be demonstrated from field observations, this spatial relationship may reflect a transition in the structural style of orogen-parallel shortening within the basement from ductile folding in the western, high-T regions, to more localized strain along ductile faults in the eastern, low-T regions.

Mutually cross-cutting relationships between top-to-the-SSW thrusts in the cratonal basement and the top-to-the-ESE movement along structures at higher levels may be explained in one of two ways. Such relationships might form by episodic 90° changes in the overall transport direction of the thrust system — from top-to-the-ESE, to top-to-the-SSW, then back to top-to-the-ESE. No evidence exists regionally, however, for repeated changes of this magnitude in the transport direction of the Caledonian

allochthon. A more realistic alternative is that deformation in the area was partitioned vertically, with contemporaneous top-to-the-SSW oblique-thrust movement on N-dipping faults in the cratonal basement and top-to-the-ESE transport of the overlying allochthon. This pattern of deformation may have resulted from local accommodation of mechanical irregularities within the orogenic pile, or it may be part of a more widespread transpressive regime. Consequently, the vertically partitioned system of deformation recognized at Efjorden may provide insight into the nature of strain partitioning at deep levels of oblique collisional orogens.

Strain Partitioning in Oblique Convergent Systems

A number of investigators have examined the potential patterns of strain in transpressional environments (e.g., Fossen *et al.* 1994). Physical modeling and direct observation suggest that deformation in the over-riding plate in zones of oblique convergence evolves commonly into a partitioned system with orogen-parallel strike-slip faults and orogen-orthogonal thrusting (e.g., Fitch 1972, Pinet & Cobbold 1992). Less is known, however, about the distribution of deformation in the lower plate of oblique-convergent zones.

In the Scandinavian Caledonides, the subducted margin of the Baltic craton formed the lower plate of the collisional system, and exposures of Baltic rocks rocks at deep structural levels of the Caledonides allow direct observation of the kinematic characteristics and distribution of strain in the lower plate. Fossen (1993) and Gillotti & Hull (1993) described structural relationships in the Caledonides of southwestern Norway

that suggest vertical partitioning of strain into kinematic domains with different directions of structural transport.

Based on mapping and kinematic analyses in the Efjorden area, we envision a structural system in which orogen-parallel and orogen-orthogonal components of transport were partitioned vertically (Fig. 7). SSW-directed thrusting in the structural basement occurred contemporaneously with continued ESE-directed emplacement of the overriding allochthon. The leading edges of the thrust sheets ramped up into the schists of the cover sequence and formed the cores of E-trending, S-vergent recumbent fold-nappes in the Lower Allochthon. As the fold nappes formed and their mechanical coupling with the basement decreased, the fold nappes became entrained in the top-to-the-ESE transport of the over-riding allochthon.

A kinematic model that includes simultaneous top-to-the-SSW oblique-thrust motion on N-dipping faults in the cratonal basement and top-to-the-ESE transport of the overlying allochthon requires a change in the orientation of the stress field between the cratonal basement and the allochthon. Differences in the mechanical properties of the craton and the allochthon may have allowed such a change. In the Efjorden study area, dry, megacrystic granite formed a relatively strong structural basement (e.g. Bartley 1982). In contrast, the overlying rocks were composed of wet, relatively weak schists. This marked rheologic contrast may have reduced the mechanical coupling between the cratonal basement and the allochthon (Bartley 1982, Northrup in press). Due to the ability of the stronger rocks in the structural basement to transmit stresses over larger distances, the stress field in the basement may have included far-field contributions which were not present in the stress field of the allochthon. Thus, a combination of weak

mechanical coupling across the rheologic boundary at the base of the allochthon and differences in the stress-transmission characteristics through the competent craton versus the weaker allochthon may have resulted in different orientations of the stress field at different structural levels and given rise to vertically partitioned deformation.

An interesting aspect of the structural interpretation at Efjord is that different parts of the same thrust-sheet/fold-nappe are inferred to have moved in different directions at essentially the same time. Top-to-the-SSW movement at deep levels occurred while the leading portions of cratonal thrust sheets were sheared to the ESE by the continued emplacement of the over-riding allochthon (Fig. 7). Within the leading portions of the cratonal thrust sheets, pervasive dynamic recrystallization and the introduction of water from the surrounding metasedimentary rocks would have reduced significantly the strength of the rock mass. From a mechanical perspective, this softening process effectively transferred the weakened leading portions of the cratonal thrust sheets from the kinematic domain of the cratonal basement to the kinematic domain of the weaker overlying rocks. Consequently, the softened portions of the cratonal thrust sheets became entrained in the top-to-the-ESE flow of the weaker rocks, while the more competent parts at depth were thrust to the SSW. Simultaneous movement of different parts of a thrust sheet in different directions requires deformation within the sheet to maintain strain compatibility. In the Efjord area, the zone of transition between the different kinematic domains does contain penetrative deformation, with highly variable lineation orientations and complex mesoscopic folding. However, the heterogeneity and complexity of deformation within the transition zone prevents confident interpretation of its kinematic characteristics.

Relation to Structures in Adjacent Areas

Some of the structural features recognized at Efjorden may have implications for the structural development of allochthonous Baltican rocks in adjacent areas. For example, Björklund (1985,1989) studied thrust sheets of Baltic affinity at the base of the composite allochthon near Akkajaure in Sweden, 40-80 km SE of Efjorden. The Akkajaure area provides excellent WNW-ESE trending exposure in the wall of a broad glacial valley oriented sub-parallel to the regional transport-direction of the main Caledonian allochthon. Björklund's detailed mapping identified several vertical repetitions of strongly deformed granite separated by thin layers of tectonized metasedimentary rocks. Based on two-dimensional palinspastic restoration of the structural section in a WNW-ESE direction, the allochthonous Baltican rocks in the Akkajaure transect have been interpreted to represent imbrication and shortening of at least 350-400 km (Björklund 1989).

Translations of this magnitude are not unreasonable in the Caledonides, and the fabric orientations at Akkajaure indicate clearly that top-to-the-ESE transport was important. However, if some imbrication of Baltican basement and cover occurred via orogen-parallel thrusting and transverse recumbent folding, like that recognized at Efjorden, then accurate structural restoration can be accomplished only by considering the structural development in three-dimensions. Bjorklund (1989) noted that recumbent folds cause vertical repetition of thrust sheets at several locations in the Akkajaure transect, and our reconnaissance in the Akkajaure area confirms the presence of numerous S-vergent, E-trending recumbent-folds at meso- to macroscopic scale. Consequently,

ESE-directed transport distances of the Baltican affinity thrust sheets may be overestimated if an unrecognized component of orogen-parallel imbrication and structural repetition are present.

Comparisons with other Orogens

Nappe translation paths that include nearly 90° changes in directions of relative movement have been described from several orogens. For example, Merle & Brun (1984) studied the incremental strain history of the Parpaillon Nappe in the French Alps and found evidence for initial NW-directed movement of the nappe (D1) followed by SW-directed movement (D2). Likewise, Peterson & Robinson (1993) examined the structural transport directions near the Bronson Hill anticlinorium in the Appalachian orogen, and found a progression from orogen-orthogonal to orogen-parallel transport during the unroofing of rocks in the area.

Changes in the transport direction of nappes through time, like those described in the preceding examples, are not surprising given the complicated evolution of mountain belts. The structural development at Efjord, however, provides an example in which different parts of individual thrust sheets or fold nappes are interpreted to have moved in different directions at essentially the same time — the deep levels of basement-derived thrust sheets moved SSW as the leading portions of the sheets formed recumbent folds and were sheared to the ESE as a consequence of continued emplacement of the overlying allochthon (Fig 7). This pattern of deformation underscores the potential three-dimensional complexity of nappe emplacement kinematics in environments with partitioned deformation and evolving rheologic structure. Interpretation of the

deformational history in such an environment is made difficult by the seemingly contradictory or incompatible kinematic characteristics of contemporaneous deformation at different locations or structural levels. The finite strain produced by a partitioned system of deformation may resemble greatly the results of a series of temporally distinct deformational episodes (D1, D2, D3, etc.), and one might easily assign contemporaneous structures to temporally distinct episodes of deformation because of their apparently disparate kinematic characteristics.

CONCLUSIONS

Structural relationships in the Efjorden study area can be related to vertically partitioned deformation within an obliquely convergent tectonic environment. Oblique convergence resulted in a component of orogen-parallel shortening and transport which were accommodated in the Baltican affinity rocks through a system of thrusts and fold-nappe structures. Within the relatively competent cratonic basement, orogen-parallel shortening was localized along N-dipping oblique thrust faults with top-to-the-SSW relative transport. The leading edges of the SSW-directed thrust sheets cut upward into the schists of the overlying metasedimentary cover sequence and formed the cores of S-verging recumbent fold nappes. These fold nappes became entrained in the ESE-directed transport of the over-riding Caledonian Allochthon.

As is true in any orogen in which deformation becomes partitioned into various components localized in different places or crustal levels, the far-field convergence direction cannot be inferred with precision from the relative-transport directions in the study area. Even if the orientations and relative transport directions of all

contemporaneous faults could be identified, the far-field convergence direction could not be found unless the *rates* of simultaneous movement along each of the faults were known, and the effects of penetrative strain distributed in the rock mass between faults could be resolved. Given that both the far-field convergence direction and the partitioning of deformation within an orogen almost certainly evolve through time, reconstruction of far-field plate-convergence histories from local lineation orientations is unlikely to be accurate. Structures in the Efjord area are consistent with a sinistral component of convergence between Baltica and Laurentia, but the precise convergence direction is unknown.

The presence of top-to-the-SSW thrusts and S-verging recumbent folds with hinges sub-parallel to the transport direction of the allochthon adds potential complexity to the interpretation of structural cross-sections oriented perpendicular to the orogen. Imbrication and vertical repetition of rocks of Baltic affinity may have resulted in part from orogen-parallel thrusting and transverse recumbent folding in addition to the more typical foreland-directed transport and stacking of thrust sheets. Consequently, discerning what combination of structures is present in a given area and unraveling the three-dimensional kinematic history represented by these structures may be difficult in the absence of clear younging-indicators and adequate exposure parallel to orogenic strike.

Acknowledgments

Work reported in this paper was supported by the National Science Foundation through grant EAR-9304635 to BCB and an NSF student fellowship to CJN. The clarity and quality of this paper benefited from formal reviews by H. Fossen and A. Andresen, as well as discussions and informal reviews by J. Bartley, A. Friedrich, M. Coleman, and D. Hawkins. Their comments and suggestions are greatly appreciated. Plotting and analysis

of structural orientation data were facilitated by use of STEREONET v. 4.7, by R. Almendinger.

REFERENCES

Andresen, A. & Tull, J. F. 1986. Age and tectonic setting of the Tysfjord gneiss granite, Efjord, North Norway. *Norsk Geologisk Tidsskrift,* **66,** 69-80.

Andresen, A. & Rykkelid, E. 1989. Basement shortening across the Caledonides in the Tornetrask-Ofoten area. *Geologiska Föreningens i Stockholm Förhandlingar* **111**, 381-383.

Bartley, J. M. 1980. Structural geology, metamorphism, and Rb/Sr geochronology of east Hinnøy, north Norway. Ph.D. thesis, Massachusetts Institute of Technology, Cambridge, MA.

Bartley, J. M. 1982. Limited basement involvement in Caledonian deformation Hinnøy, north Norway. *Tectonophysics* **83,** 185-203

Bartley, J. M. 1984. Caledonian structural geology and tectonics of east Hinnøy, north Norway. *Nor. Geol. Unders.*, **396,** 1-24.

Berthé, D., Choukroune, P., & Jegouzo, P. 1979. Orthogneiss, mylonite and non-coaxial deformation of granites: the example of the South Amoricain shear zone. *J. Struc. Geol.* **1,** 31-42.

Björklund, L. 1985. The Middle and Lower Allochthons in the Akkajaure area, northern Scandinavian Caledonides. In: *The Caledonian Orogen - Scandinavia and Related Areas* (edited by D. G. Gee and B. A. Sturt), John Wiley & Sons, Ltd.

Björklund, L. 1989. Geology of the Akkajaure-Tysfjord-Lofoten traverse, N. Scandinavian Caledonides. Ph.D. thesis, Geologiska Institutionen, Gothenburg, Sweden, Publ. A 59, 214 pp.

Crowley, P. D. 1985. The structural and metamorphic evolution of the Sitas area, northern Norway and Sweden. Ph.D. thesis, Massachusetts Institute of technology, Cambridge, MA. U.S.A. 253 pp.

Dewey, J. F. 1980. Episodicity, sequence, and style at convergent plate boundaries. In: The continental crust and its mineral deposits (edited by D. W., Strangway). *Geol. Assoc. Can. Spec. Paper **20**,* 553-573.

Foslie, S., 1941, Tysfjords Geologi. *Norges Geol. Unders.* 149, 298 pp.

Fossen, H. 1993. Linear fabrics in the Bergsdalen Nappes, southwest Norway: implications for deformation history and fold development. *Nor Geol. Tidsskr.* **73**, 95-108.

Fossen, H., Tikoff, T. B. & Teyssier, C. T. 1994. Strain modeling of transpressional and transtensional deformation. *Nor. Geol. Tidsskr.* **74**, 134-145.

Fitch, T. J. 1972. Plate convergence, transcurrent faults, and internal deformation adjacent to Southeast Asia and the Western Pacific. *J. Geophys. Res.,* **77,** 4432-4461.

Gabrielse, H. 1985. Major dextral transcurrent displacements along the Northern Rocky Mountain Trench and related lineaments in north-central British Columbia. *Geol. Soc. Am. Bull.* **96,** 1-14.

Gee, D. G. 1975. A tectonic model for the central part of the Scandinavian Caledonides. *Am. J. Sci., **275-A,*** 468-515.

Gee, D. G. & Wilson, M. R. 1974. The age of orogenic deformation in the Swedish Caledonides. *Am. J. Sci.* **274,** 1-9.

Gilotti, J. A. & Hull, J. M. 1991. A new tectonic model for the central Scandinavian Caledonides. *Terra Nova* **3**, 18

Gilotti, J. A. & Hull, J. M. 1993. Kinematic stratification in the hinterland of the central Scandinavian Caledonides. *J. Struc. Geol.* **15**, 629-646.

Glenn, R.A. 1992. Thrust, extensional and strike-slip tectonics in an evolving Paleozoic orogen — a structural synthesis of the Lachlan Orogen of southeastern Australia. *Tectonoph.,* **214,** 341-380.

Hodges, K. V. 1982. Tectonic evolution of the Aefjord-Sitas area, Norway-Sweden. Ph.D. thesis, Massachusetts Institute of Technology, Cambridge, MA.

Hodges, K., V. 1985. Tectonic stratigraphy and structural evolution of the Efjord-Sitasjaure area, Northern Scandinavian Caledonides. *Nor. Geol. Unders.* **399,** 41-60.

Hodges, K. V., Bartley, J. M. & Burchfiel, B. C.1982. Structural evolution of an A-type subduction zone, Lofoten. *Tectonics* **1,** 441-462.

Holdsworth, R. E. & Strachan, R. A. 1991. Interlinked system of ductile strike slip and thrusting formed by Caledonian sinistral transpression in northeastern Greenland. *Geology* **19,** 510-513.

Jackson, J. 1992. Partitioning of strike-slip and convergent motion between Eurasia and Arabia in Eastern Turkey and the Caucasus. *J. Geophys Res.* **97,** 12,471-12,479.

Lister, G. S. & Snoke, A. W. 1984. S-C mylonites. *J. Struct. Geol.* **6,** 617-638

Lister, G. S. & Williams, P. F. 1983. The partitioning of deformation in flowing rock masses. *Tectonoph.* **92,** 1-33.

Mancktelow, N. S. 1992. Neogene lateral extension during convergence in the Central Alps: Evidence from interrelated faulting and backfolding around the Simplonpass (Switzerland). *Tectonoph.* **215,** 295-317.

Molnar, P. & Tapponnier, P. 1975. Cenozoic tectonics of Asia: Effects of a continental collision. *Science* **189,** 419-426.

Norton, M. G. 1987. The Nordfjord-Sogn Detachment, W. Norway. *Nor.Geol. Tidssk.* **67**, 93-106.

Peterson, V. L. & Robinson, P. 1993. Progressive evolution from uplift to orogen-parallel transport in a late-Acadian upper amphibolite- to granulite-facies shear zone, south-central Massachusetts. *Tectonics* **12,** 550-567.

Price, R. A. & Carmichael, D. M. 1986. Geometric test for Late Cretaceous - Paleogene intracontinental transform faulting in the Canadian Cordillera. *Geology* **14,** 469-471.

Roberts, D. 1983. Devonian tectonic deformation in the Norwgian Caledonides and its regional perspectives. *Nor. Geol. Unders.* **380**, 85-96.

Roberts, D. & Gee, D. G. 1985. An introduction to the structure of the Scandinavian Caledonides. In: *The Caledonian Orogen - Scandinavia and Related Areas* (edited by D. G. Gee and B. A. Sturt), John Wiley & Sons, Ltd.

Rykkelid, E. & Andresen, A. 1994. Late Caledonian extension in the Ofoten area, northern Norway. *Tectonoph.* **231,** 157-169.

Selverstone, J. 1988. Evidence for east-west crustal extension in the Eastern Alps: implications for the unroofing history of the Tauern Window. *Tectonics* **7,** 87-105.

Simpson, C. & Schmid, S. M. 1983. An evaluation of criteria to deduce the sense of movement in sheared rocks. *Geol. Soc. Am. Bull.* **94,** 1281-1288.

Soper, N. J., Strachan, R. A., Holdsworth, R. E., Gayer, R. A. & Greiling, R. O. 1992. Sinistral transpression and the Silurian closure of Iapetus. *J. Geol. Soc. Lond.* **149,** 871-880.

Steltenpohl, M. G. & Bartley, J. M. 1988. Crossfolds and backfolds in the Ofoten-Tysfjord area, Norway and their significance for Caledonian tectonics. *Geol. Soc. Am. Bull.* **100,** 140-151.

Stephens, M. B. & Gee, D. G. 1989. Terranes and polyphase accretionary history in the Scandinavian Caledonides. *Geol. Soc. Am. Spec. Paper* **230,** 17-30.

Strachan, R. A., Holdsworth, R. E., Friderichsen, J. D., & Jepsen, H. F. 1992. Regional Caledonian structure within an oblique convergence zone, Dronning Louise Land, NE Greenland. *J. Geol. Soc. Lond.* **149,** 359-371.

Torsvik, T. H., Sturt, B. A., Ramsay, D. M., Kisch, H. J. & Bering, D. 1986. The tectonic implications of Solundian (Upper Devonian) magnetization of the Devonian rocks of Kvamshesten, western Norway. *Earth Planet. Sci Lett.* **80**, 337-347.

Tull, J. F., Bartley, J. M., Hodges, K. V., Andresen, A., Steltenpohl, M. G., and White, J. M. 1985. The Caledonides in the Ofoten region (68°-69°N), north Norway: key aspects of tectonic evolution. In: *The Caledonian Orogen - Scandinavia and Related Areas* (edited by D. G. Gee and B. A. Sturt), John Wiley & Sons, Ltd.

Vauchez, A., Babaie, H. A., and Babaei, A. 1993. Orogen-parallel tangential motion in the Late Devonian - Early carboniferous southern Appalachians internides. *Can. J. Earth Sci.* **30,** 1297-1305.

FIGURE CAPTIONS

Figure 1: Simplified geologic map of the Scandinavian Caledonides (modified from Gee *et al.* 1985)

Figure 2: Geologic map of the Efjord study area showing topography and the distribution of rock types. Numbers refer to locations mentioned in the text.

Figure 3: Geologic map of the Efjord study area showing structural orientations and kinematic information.

Figure 4: An oblique aerial photograph of outcrops E of Skarvatnet showing the structurally highest of the imbricated thrust sheets derived from the Baltic craton, overlain by the mylonitic sliver zone (heterogeneous mylonites of uncertain affinity), and the far-traveled Upper-Allochthon (oceanic affinity).

Figure 5: Outcrop photographs and sketches of tectonites in the Efjord area. Surfaces shown are parallel to the stretching lineation and perpendicular to foliation in each outcrop. Figs. 5(a) - (b): Strain gradient adjacent to mylonitic thrust in the Skarvatnet duplex. The thrust places tectonized Precambrian granite (hanging wall) over schist and quartzite of the metasedimentary cratonal cover (footwall). Figs. 5(c) - (f): Views looking ESE at tectonized granite adjacent to thrust contacts at deep levels of the Skarvatnet duplex. Porphyroclast asymmetry (c.f. Simpson & Schmid, 1983) and S-C fabric relations (c.f., Berthe et al., 1979; Lister and Snoke, 1984) indicate dextral (top-to-the-SSW) transport. Figs. 5(g)-(h): Views looking NNE at mylonitic schist at the top of the Skarvatnet duplex, just below the Sliver Zone. The inclination of mica "fish" and S-C fabric relationships in the schist are consistent with dextral (top-to-the-ESE) transport of the over-lying allochthon.

Figure 6: Photograph - sketch pairs showing meso- to macroscopic examples of S-vergent, recumbent folds. All views look E, subparallel to the fold axes. Figs 6(a)-(b): dm-scale rootless S-verging folds of quartzite and garnet-schist of the metasedimentary cover sequence just below the Sliver Zone. Figs. 6(c)-(d): S-verging, recumbent anticline cored by Precambrian cratonal basement; this anticline is a parasitic fold on the lower limb of a larger, S-verging fold-nappe cored by the Precambrian rocks at the top of the view.

Figure 7: Schematic block diagram illustrating the formation of structures in the Efjorden area within the context of sinistral-oblique Caledonian collision.

FIGURES FOR CHAPTER 3

Figure 1

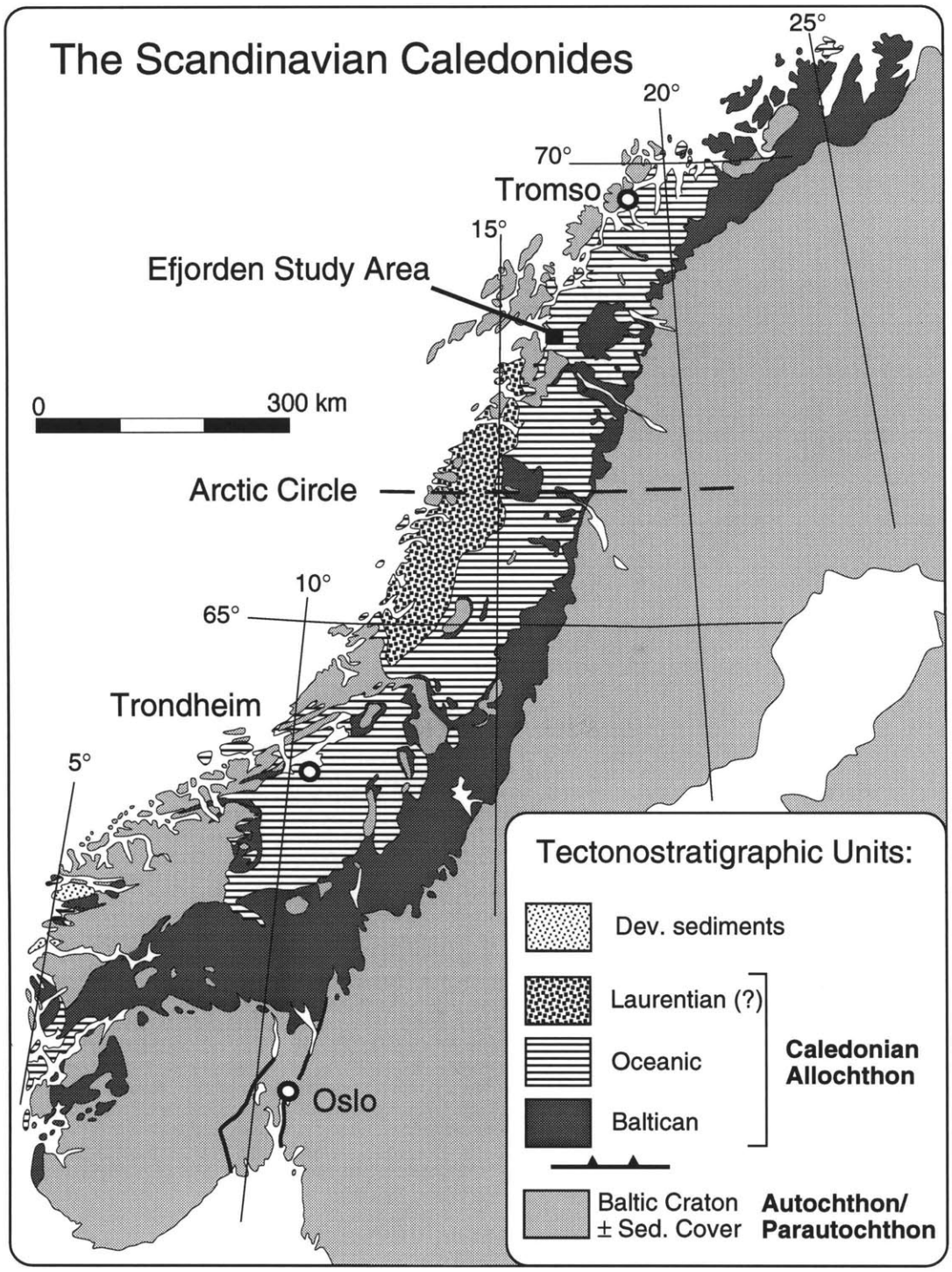
The Scandinavian Caledonides
25°
20°
70°
Tromso
15°
Efjorden Study Area
0
300 km
Arctic Circle
10°
65°
Trondheim
5°
Oslo
Tectonostratigraphic Units:
Dev. sediments
Laurentian (?)
Oceanic
Baltican
Caledonian Allochthon
Baltic Craton ± Sed. Cover
Autochthon/ Parautochthon

Figure 2

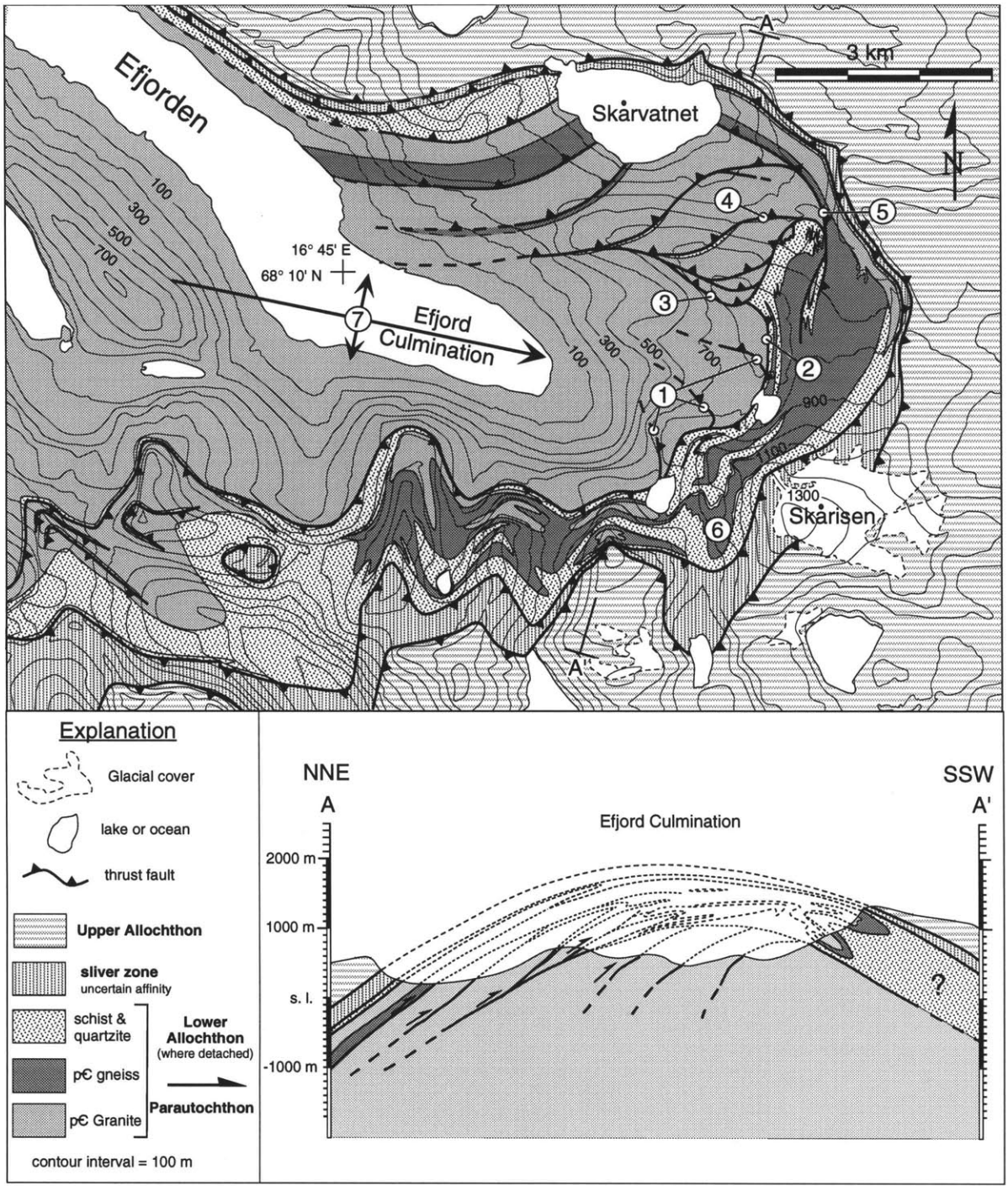
Efjorden
Skårvatnet
A
3 km
N
100
300
500
700
16° 45' E
68° 10' N
7
Efjord
Culmination
1
2
3
4
5
6
900
1300
Skårisen
A'
Explanation
Glacial cover
lake or ocean
thrust fault
Upper Allochthon
sliver zone
uncertain affinity
schist & quartzite
pЄ gneiss
pЄ Granite
Lower Allochthon
(where detached)
Parautochthon
contour interval = 100 m
NNE
A
SSW
A'
Efjord Culmination
2000 m
1000 m
s. l.
-1000 m
?

Figure 3

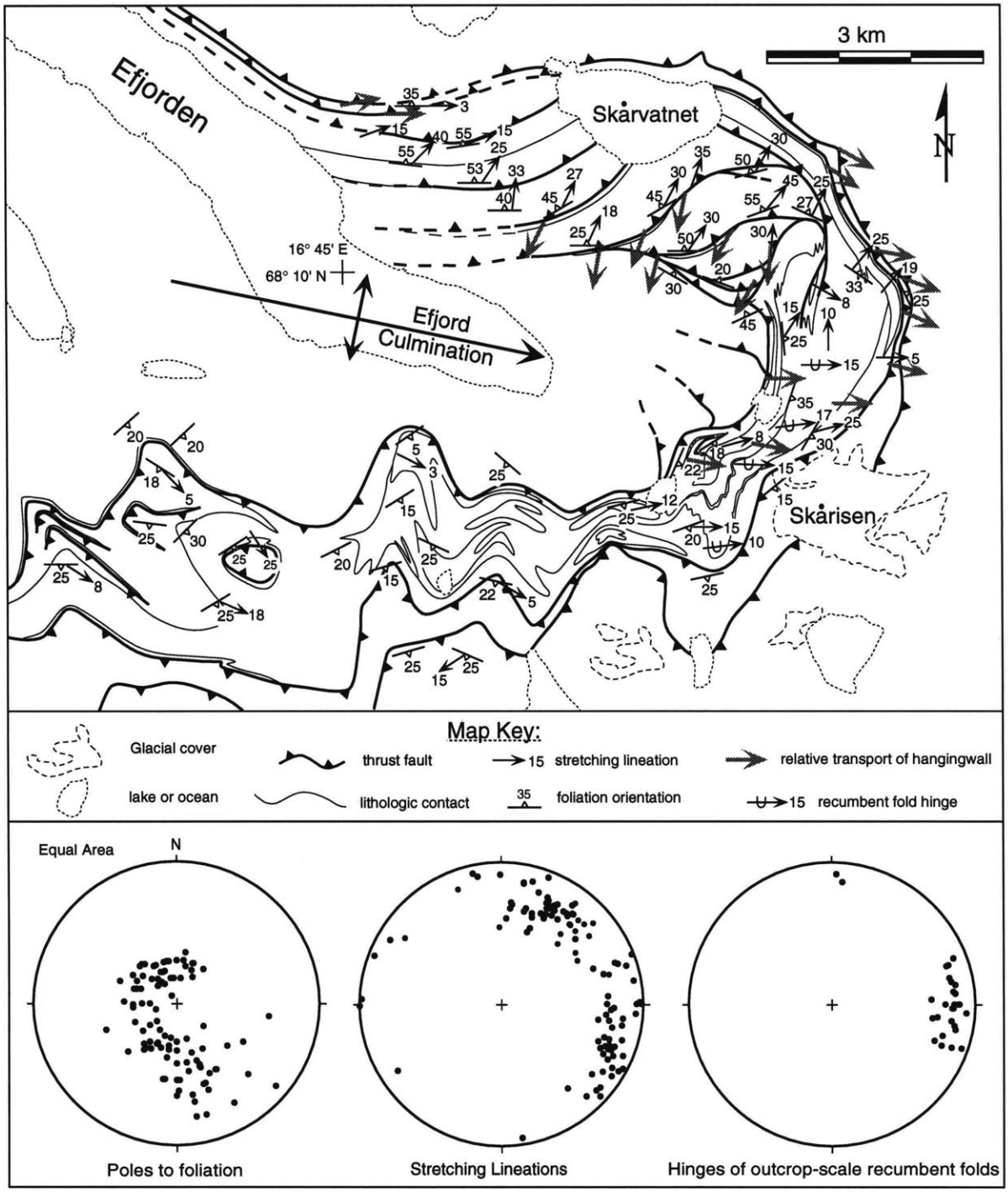
3 km
Efjorden
Skårvatnet
Skårisen
N
16° 45' E
68° 10' N
Efjord
Culmination
Map Key:
Glacial cover
lake or ocean
thrust fault
lithologic contact
15 stretching lineation
35 foliation orientation
relative transport of hangingwall
15 recumbent fold hinge
Equal Area
N
Poles to foliation
Stretching Lineations
Hinges of outcrop-scale recumbent folds

Figure 4

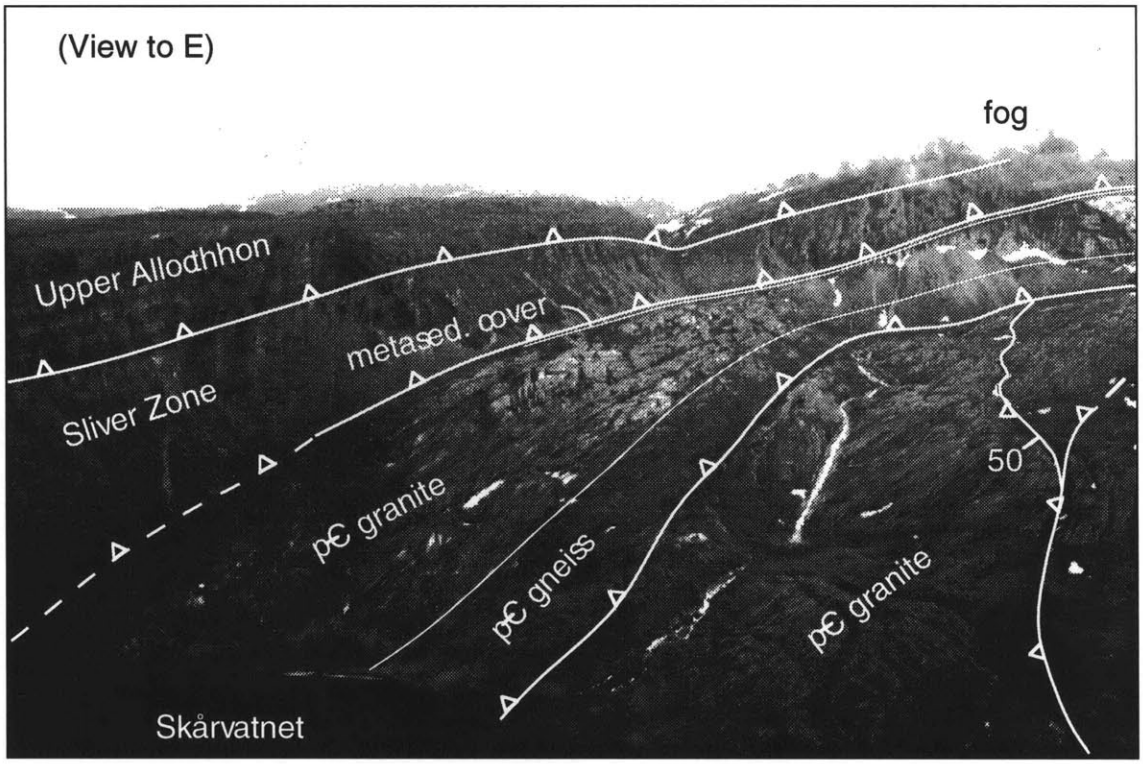
(View to E)
fog
Upper Allodhhon
metased. cover
Sliver Zone
50
pЄ granite
pЄ gneiss
pЄ granite
Skårvatnet

Figure 5

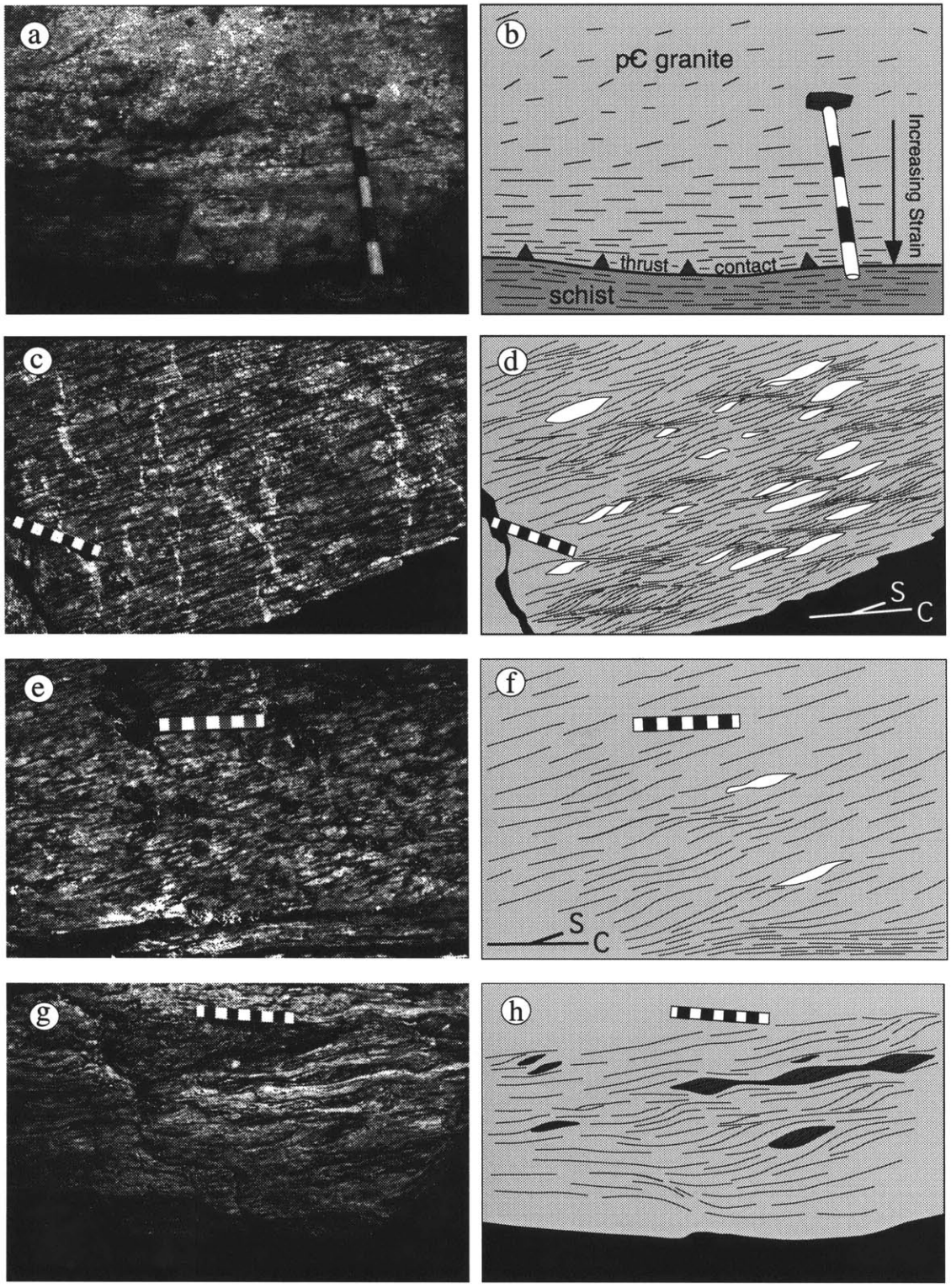
a
b
pC granite
Increasing Strain
thrust
contact
schist
c
d
S
C
e
f
S
C
g
h

Figure 6

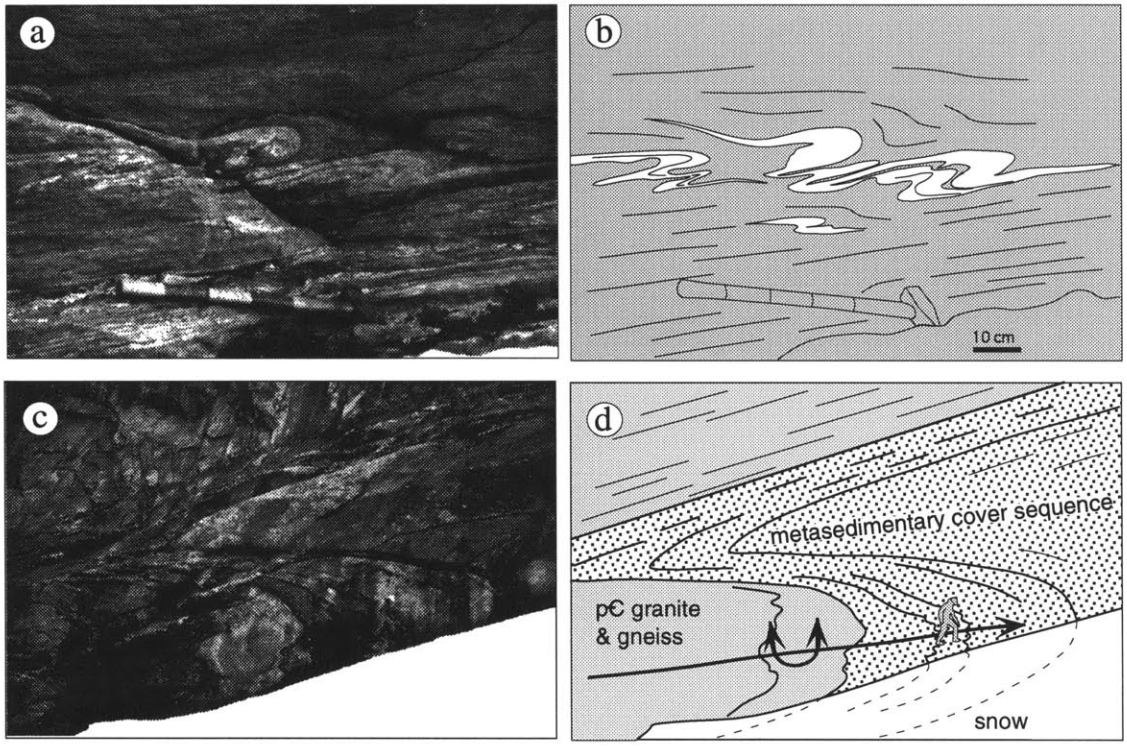
a
b
10 cm
c
d
metasedimentary cover sequence
pC granite
& gneiss
snow

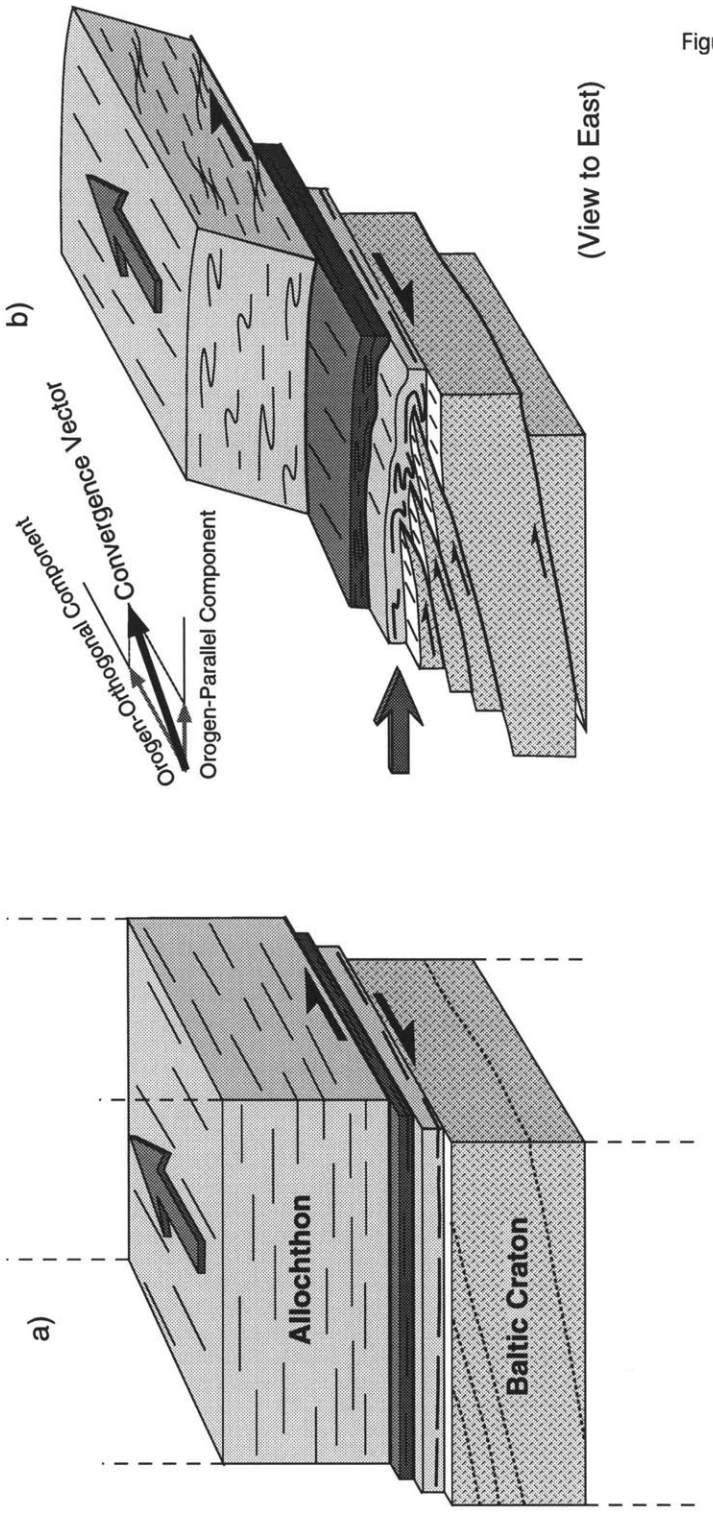
a)
Allochthon
Baltic Craton
b)
(View to East)
Convergence Vector
Orogen-Parallel Component
Orogen-Orthogonal Component

Figure 7

Chapter 4

U-Pb and $^{40}Ar/^{39}Ar$ constraints on the assembly, metamorphism, and cooling history of the Caledonian allochthon, Ofoten-Efjorden, north Norway

INTRODUCTION

The Caledonian orogen in Scandinavia resulted from the collision of Baltica and Laurentia during the final stages of closure of the Iapetus Ocean basin in Suluro-Devonian time (Fig. 1; Harland and Gayer, 1972; Gee, 1975; Stephens and Gee, 1989). An important and often challenging goal of tectonic studies in ancient mountain belts like the Caledonides is to reconstruct the evolution of these orogenic systems through time. Commonly, *relative* timing relations among phases of deformation, metamorphism, and igneous activity can be established from careful field observations. However, relative timing relations alone provide little information concerning the absolute ages of these events or the rates of the geologic processes involved. Our ability to develop a clear understanding of Caledonian tectonic history, therefore, depends critically on building a framework of absolute-age information that delineates the evolution of the system through time.

This paper presents the results of U-Pb and $^{40}Ar/^{39}Ar$ geochronologic analyses of samples from the Ofoten-Efjorden region of north Norway, in the northern Scandinavian Caledonides (Figure 1). These data, together with previously determined isotopic ages from the region, illuminate several aspects of Caledonian tectonic development,

including: (1) the timing of thrust assembly of deep levels of the Caledonian allochthon; (2) the age of epidote-amphibolite facies metamorphism; and (3) the cooling history of rocks at this structural level, from peak metamorphic conditions of approximately 700°C to about 350°C. By combining the T-t history derived from these data with published information about the local P-T history, the time-integrated rates of tectonic burial and early unroofing can be estimated for this portion of the orogen.

TECTONIC SETTING

Subduction and final closure of the Iapetus Ocean basin led to the assembly of a composite nappe stack composed of rocks derived from the eastern margin of Laurentia, igneous and sedimentary rocks of oceanic affinity, and thrust slices of the westernmost margin of Baltica (Roberts and Gee 1985; Stephens and Gee 1989). During the culmination of the Caledonian collision in Silurian time, this nappe stack was thrust eastward over the western portion of the Baltic craton, and rocks at deep levels of the system underwent high-grade metamorphism (Gee and Wilson 1974). Extensional modification of the orogen began locally during late stages of the emplacement of the Caledonian allochthon (chapter 2; Gee et al. 1994; Coker et al. 1995), and became the dominant mode of tectonism in much of the orogen by early to middle Devonian time (Norton 1986; Andersen et al. 1991).

Late Caledonian extensional unroofing and subsequent erosion have removed shallow crustal levels of the collisional system, allowing direct observation of relatively deep parts of the orogen. The present erosional surface cuts the nappe stack close to the structural level of the basal thrust across the orogen, from the foreland in the east to

progressively deeper and hotter crustal levels of the hinterland farther west (Figure 1). Consequently, the tectonic evolution of rocks that formed the basal portion of the Caledonian allochthon at a variety of crustal levels can be studied in different parts of the orogen.

The Ofoten-Efjorden Region

Rocks examined in this paper come from the Ofoten-Efjorden region, located approximately 68° 30' N on the west coast of Norway (Figures 1 and 2). This area contains some of the westernmost and, therefore, deepest exposures of the Caledonian allochthon at this latitude on the Norwegian mainland. Late Caledonian NE-trending folds and SE-trending cross-folds affected both the allochthon and the structural basement, and these folds control the general pattern of lithologic contacts in the region (Steltenpohl and Bartley, 1988). Much of the area considered in this study occupies the western limb of the Ofoten synform, a gently NNE-plunging fold of regional significance. Due to the effects of the Ofoten synform, the structural section dips moderately or steeply to the east in most places, and the geologic map represents an oblique cross section through the lower few km of the allochthon and the upper portion of the underthrust Baltic craton (Figure 2).

Rocks of oceanic affinity that make up the allochthon in this area can be divided into two first-order tectonostratigraphic packages: the Narvik Nappe Complex and the Ofoten Nappe Complex (Figures 2 and 3; nomenclature after Steltenpohl et al. 1990). The Narvik Nappe Complex (NNC) contains the structurally lowest thrust sheets and consists chiefly of kyanite grade schist and amphibolite, with minor quartzite and

sporadic lenses of ultramafic cumulates and pillow basalt (Hodges, 1982; Crowley, 1985). The lithologic assemblage and complex internal structure of the NNC suggest that it may represent a subduction-related accretionary complex that became incorporated into the Caledonian nappe stack during closure of the Iapetus basin. Strongly deformed granite and tonalite dikes are common in rocks of the NNC, and their presence is characteristic of this tectonostratigraphic package.

Structurally above the NNC lies the Ofoten Nappe Complex (ONC). The lower portion of the ONC is dominated by marble, with lesser amounts of calcareous schist and amphibolite (Steltenpohl, 1983). A basal unit composed of amphibolite ± tonalite overlain by a conglomerate containing clasts similar in lithologic character to the amphibolite and tonalite on which it sits, is present discontinuously at the bottom of the ONC. This basal unit has been interpreted by some workers as the remains of an early Paleozoic ophiolite beneath an erosional unconformity related to Cambro-Ordovician "Finnmarkian" tectonism (Boyd, 1983; Steltenpohl et al. 1990). Granite and tonalite dikes like those in the Narvik Nappe Complex are rare or absent in the marbles and schists that makeup the lower portion of the Ofoten Nappe Complex, but lithologically similar dikes can be found in thrust sheets higher in the ONC. The ubiquitous presence of felsic dikes in some thrust sheets but not others indicates that intrusion of such dikes predated final thrust assembly at deep levels of the nappe stack.

Because the Ofoten-Efjorden region contains some of the deepest exposures of the Caledonian allochthon at this latitude, it offers an opportunity to examine the timing and duration of tectonic processes at deep levels of the allochthon as the collisional system evolved.

Previous Age Constraints

Geologists working in the region have long recognized the potential importance of absolute age information, and a number of studies have contributed to the existing state of knowledge. Table 1 summarizes the existing geochronologic data from rocks at deep levels of the allochthon. Most of the previous work employed the Rb-Sr and K-Ar (including $^{40}Ar/^{39}Ar$) isotopic systems and analyzed minerals with nominal closure temperatures for these systems in the range of ca. 350 to 500°C. Given that rocks at deep levels of the allochthon achieved peak metamorphic temperatures of at least 650°C (e.g., Hodges and Royden, 1984; Steltenpohl and Bartley, 1987), most of these ages have been interpreted as cooling ages that delineate the moderate temperature portion of the regional cooling history.

Only a few U-Pb ages have been reported for rocks in the region. However, even though such data are sparse, they provide important information about the history of the allochthon. In particular, the age of the Råna layered mafic intrusion (437 ± 2 Ma, Tucker et al., 1990) is significant, because it provides a maximum age of metamorphism and high-T deformation in the Narvik Nappe Complex. Furthermore, it indicates that these rocks probably remained in the Iapetus Ocean basin west of the Baltic margin until at least 437 Ma.

SAMPLE SELECTION

U-Pb and $^{40}Ar/^{39}Ar$ geochronologic studies presented here focused on three questions regarding the tectonic evolution of the Ofoten-Efjorden region: (1) what was the age of thrust assembly at deep levels of the nappe stack? (2) When did rocks at this structural

level undergo amphibolite facies metamorphism? and (3) after the metamorphic peak, what was the T-t path followed by these rocks? Sample selection was geared toward addressing these issues. Figure 2 shows the locations of samples collected for U-Pb and $^{40}Ar/^{39}Ar$ analyses, and figure 3 illustrates their relative structural positions within the nappe stack.

Intrusion of the numerous felsic dikes in the Narvik Nappe Complex predated the assembly, metamorphism, penetrative deformation, and final emplacement of the nappe stack. Therefore, crystallization ages of these dikes would provide a maximum age of these tectonic events. I sampled two of dikes for U-Pb zircon analyses: (1) a strongly deformed granite dike with coarse to locally pegmatitic grain size (sample 93SC-77); and a deformed tonalite dike with modest grain-size and an equigranular texture (sample 93SC-78). Pre-tectonic felsic dikes also are found in mafic rocks (fragmented ophiolite?) present intermittently at the base of the Ofoten Nappe complex, and I collected a sample of the Ruggevik tonalite gneiss for U-Pb zircon analysis, because it is one of the larger felsic igneous bodies at this structural level (sample 93SC-13). To constrain more directly the age of peak metamorphism, I collected samples of garnet-kyanite schist (93SC-30) and an anatectic segregation from a migmatitic portion of the Narvik Nappe Complex (93SC-31) for U-Pb analyses of metamorphic monazite and/or zircon.

One way to delineate the cooling history of rocks in the region is to date a series of minerals with different closure temperatures for the isotopic systems of interest (e.g. Hodges, 1991). Minerals potentially amenable to U-Pb or $^{40}Ar/^{39}Ar$ thermochronology with nominal closure temperatures at or below the conditions of peak metamorphism include hornblende (Harrison, 1981), muscovite (Robbins, 1972) and rutile (Mezger,

1989). Sphene may also be useful in this regard, but the characteristics of Pb diffusion in sphene and, therefore, its isotopic retentivity at high temperatures are controversial at present (e.g., Mezger, et al. 1993; Cherniak, 1993; Shärer, 1996). Many of the samples described previously, which were collected primarily for zircon and monazite analyses, also contained minerals of interest for thermochronology, and some of these samples were used as sources of rutile, sphene, and muscovite for U-Pb and $^{40}Ar/^{39}Ar$ analyses. Additional samples of amphibolite (93SC-17, 93SC-49) and schist (93SC-37, 93SC-52) were collected to provide hornblende, sphene, and muscovite.

An original goal of this study was to compare the tectonothermal evolution of the allochthon to that of the structural basement on which it sits. Toward that end, I collected a suite of samples from the metasedimentary cover of Baltica hoping to find minerals such as sphene or monazite that might constrain the age of metamorphism at this structural level. I found zircon and sphene in a sample of mylonitic Precambrian granite from the footwall of the basal thrust (93SC-117), but none of the other samples yielded sphene or monazite. Many of the rocks at this structural level do, however, contain minerals amenable to $^{40}Ar/^{39}Ar$ thermochronology, and I separated muscovite (samples 92SC-114 & 93SC-26) and hornblende (93SC-31) for such analyses.

U-PB ANALYSES

Analytical Methods

Standard crushing, sieving, Wilfley table, heavy liquid, and magnetic separation techniques were used to extract zircon, monazite, rutile, and sphene from the samples.

Zircon grains were air abraded for 24 to 48 hours to diminish the effects of surface-correlated Pb-loss (e.g., Krogh, 1982), and washed in warm 30% HNO_3 prior to dissolution. Monazite grains were washed in dilute HNO_3 and warm H_2O. Sphene and rutile were washed in 15% HNO_3 and warm H_2O. All samples were placed in teflon microcapsules and spiked with ^{205}Pb-^{233}U-^{235}U tracer prior to dissolution. Zircon, sphene, and rutile, were dissolved in concentrated HF at 220°C for 48 to 96 hours; monazite was dissolved in 10-11 N HCl at 180°C for 60-72 hours. Separation of Pb and U from zircon and monazite fractions was accomplished using HCl-based ion chromatography procedures modified after Krogh (1973). Separation of Pb and U for sphene and rutile employed two-stage HBr and HCl cation-exchange column chemistry modified after Parrish et al. (1987). Isotopic compositions of Pb and U were analyzed using conventional thermal ionization mass spectrometry. Lead analyses were conducted either: 1) in static mode, using Faraday detectors for all isotopes except ^{204}Pb, which was measured with a Daly detector; or 2) by peak jumping, using a Daly detector in ion counting mode. U was measured in static mode using Faraday collectors.

Results

Data obtained from U-Pb analyses are presented in Table 2 and illustrated graphically in figures 4-10. Isotopic ages and uncertainties have been calculated using two statistical methods described by Ludwig (1989; 1990). Most of the zircon data form discordant linear arrays, and an upper intercept age for each set of data was calculated by linear regression assuming that most of the scatter about the best fit line results from analytical uncertainty (York, 1969). Due to the small degree of discordance of the zircon data, lower intercepts are poorly determined; none differs from zero, however, within the uncertainties of the regressions and, therefore, the discordances is interpreted to reflect recent Pb-loss. Because the lower intercepts are zero and the degree of discordance is low, the weighted mean of the $^{207}Pb/^{206}Pb$ ages of individual analyses provides another reasonable indication of the age for a given sample. For each set of zircon data, the upper intercept age and weighted mean $^{207}Pb/^{206}Pb$ age are statistically indistinguishable, but the weighted mean age commonly has a smaller uncertainty. Both the upper intercept and weighted mean ages have been evaluated using the mean square of the weighted deviates (MSWD; e.g.,Wendt and Carl 1991).

93SC-13: Ruggevik tonalite gneiss

The Ruggevik tonalite gneiss sample contained clear, euhedral zircon grains with aspect ratios of about 3:1 and no visible cores. Five multi-grain fractions of zircon were

analyzed, and they define a normally discordant (<3%) linear array with an upper intercept age of 477 ± 2 Ma and a weighted mean $^{207}Pb/^{206}Pb$ age of 479 ± 1 Ma (Fig. 4).

93SC-78: deformed tonalite dike, Narvik Nappe Complex

This sample contained clear, euhedral, pale brown zircon grains with aspect ratios varying from about 3:1 to 5:1. Some grains had optical cores defined by darker colored zircon, and such grains were avoided during sample selection. Five multi-grained zircon fractions were analyzed (Figure 5). All are normally discordant, and four of the analyses (Z1, Z4, Z5, and Z6; <2% discordant) form a linear array with an upper intercept age of 436 Ma (+22 Ma, -2 Ma; MSWD = 0.85) and a weighted mean age of 437±1 Ma (MSWD = 0.66). The other zircon fraction (Z2) has significantly older $^{206}Pb/^{238}U$ and $^{207}Pb/^{235}U$ ages, consistent with an inherited component of older zircon in this fraction.

93SC-77: deformed granite dike in the Narvik Nappe Complex

This sample contained euhedral, pale to dark brown zircon grains with a nominal aspect ratio of about 3:1. Four multi-grain fractions (Z2, Z5, Z6, and Z7) and two single grains (Z1 and Z8) were analyzed (figure 6). The data define a normally discordant linear array with an upper intercept age of 436 ± 2 Ma (MSWD = 0.66) and a weighted mean age of 436.5 ± 0.4 Ma (MSWD = 0.42). Fraction Z2 was excluded from the regression and weighted-mean age calculations because it has an anomalously old $^{206}Pb/^{207}Pb$ age, possibly due to a small component of inherited zircon. Inclusion of this fraction in the

regression and weighted mean age calculations does not change the results significantly, but increases the uncertainties and MSWD values associated with the ages (inclusion of Z2: upper intercept 436 ± 6 Ma, MSWD = 2.12; weighted mean 437 ± 1 Ma, MSWD = 1.90).

Dark red to nearly opaque rutile grains in this sample have subhedral prismatic morphologies. Four rutile fractions were analyzed. The Pb_{rad}/Pb_{com} ratios in the rutile were low (0.2 to 1.3), making standard age calculations sensitive to the isotopic composition chosen for the initial common lead component. However, in a plot of $^{206}Pb/^{204}Pb$ versus $^{238}U/^{204}Pb$, the data define an isochron with an age of 382 ± 11 Ma (MSWD = 0.41) and an initial $^{206}Pb/^{204}Pb$ ratio of 17.504 ± 0.428 (Figure 7).

94SC-31: anatectic segregation in gar-ky schist, Narvik Nappe Complex

This sample contained very large (>500μ) zircon grains with clear to pale brown rims and dark brown cores. During air abrasion, several large grains broke into numerous fragments, and these fragments were separated into dark brown and pale populations. Five fractions were analyzed: Z1, Z3, and Z5 contained dark brown fragments; Z2 and Z4 contained pale fragments (Figure 8). Collectively, the analyses form a linear array of concordant to slightly discordant points which yield an upper intercept age of 432 ± 1 Ma (MSWD = 1.36) and a weighted mean age of 432 ± 1 Ma (MSWD of 1.75).

94SC-30: garnet-kyanite schist, Narvik Nappe Complex

This sample of aluminous schist contained abundant, bright yellow monazite grains with subhedral to euhedral morphologies. Five fractions were analyzed, and the data yield concordant to slightly reversely discordant (<3%) ages (Figure 9). Reverse discordance like that observed in this sample might result either from: 1) a disproportionate gain or loss of U and radiogenic Pb, causing a net decrease in the U/Pb_{rad} ratio; or 2) incorporation of significant ^{230}Th at the time of crystallization which subsequently decayed to ^{206}Pb not derived from the original ^{238}U contents of the crystal (Th disequilibrium; Shärer, 1984; Parrish, 1990). Extra ^{206}Pb formed in this manner causes a small increase the $^{206}Pb/^{238}U$ ratio relative to the $^{207}Pb/^{235}U$ ratio, and moves the analysis upward off concordia. Assuming that the reverse discordance resulted from Th disequilibrium, the $^{207}Pb/^{235}U$ ratios provide the most reliable estimate of the "true" monazite ages. Four of the monazite grains analyzed (M3, M8, M11, and M12) have $^{207}Pb/^{235}U$ ages in the range of 430 to 433 Ma, and collectively give a weighted mean age of 432 ± 2 Ma (MSWD = 2.8). The relatively high MSWD for the weighted mean age indicates that the range in ages obtained is larger than the amount a variability attributable to analytical uncertainties alone, consistent with diachronous growth of monazite over this interval of time. Monazite grain M9 yielded an anomalously old $^{207}Pb/^{235}U$ age (438 ±1 Ma), and may provide evidence for either an inherited component of monazite, or a somewhat older episode of monazite growth. Although possibly fortuitous, it is interesting that the age determined for M9 is essentially the same as the age obtained for granitic dikes nearby (samples 93SC-77 and 93SC-78).

93SC-76: garnet amphibolite, basal unit of the Ofoten Nappe Complex

This sample contained euhedral to subhedral lentil-shaped sphene grains ranging in size from 70 to 300μ in diameter. Grains were separated into coarse (ca. 300μ x 300μ x 130μ) and fine (ca. 120μ x 100μ x 40μ) varieties. One fraction of coarse sphene and four fractions of fine sphene were analyzed. The radiogenic Pb contents of all sphene fractions was extremely low ($^{206}Pb/^{204}Pb$ ratios of 25 to 27; Pb_{rad}/Pb_{com} ratios of 0.1), making age calculations very sensitive to the isotopic composition chosen for the initial common Pb component. Using the isotopic composition of galena from a strata-bound massive sulfide deposit in the Narvik Nappe Complex 10 km east of the sample location (Bjørkasen deposit, Bjørlykke et al., 1993) for the common Pb correction, the fine sphene fractions give a weighted mean $^{206}Pb/^{238}U$ age of 415 ± 2 Ma (MSWD = 1.76) and the coarse fraction gives an age of 429 ± 2 Ma. However, these ages should be viewed with a great deal of skepticism given the poor Pb_{rad}/Pb_{com} ratios of the sphene. In a plot of $^{206}Pb/^{204}Pb$ versus $^{238}U/^{204}Pb$, data from the fine-grained sphene fractions define an isochron with an age of 419 ± 58 Ma (MSWD = 0.74), but the $^{238}U/^{204}Pb$ ratios do not vary enough to yield a precise isochron age.

93SC-117: mylonitic granite in the footwall of the basal shear zone.

This sample contained euhedral, brown, cloudy zircon grains, and euhedral to subhedral sphene grains of variable sizes. Grains were separated into coarse (ca. 230μ x 200μ x

75μ), medium (ca. 140μ x 120μ x 50μ) and fine (ca. 80μ x 70μ x 25μ) varieties. Two single grains of zircon and 9 fractions of sphene (4 coarse, 1 medium, and 3 fine) were analyzed. The data are variably discordant and scatter about a best-fit line with intercepts at 1862 and 407 Ma (Figure 10). The two zircon analyses plot much closer to the upper intercept, an age consistent with the 1700 - 1900 Ma ages of Proterozoic granites in this portion of the Baltic craton (e.g. Skiöld, 1988). The sphene data cluster near the lower intercept, but are not colinear (MSWD of best fit line: 131). In general, this pattern of data might be consistent with either or both of the following: (1) variable amounts of diffusional Pb-loss from original Proterozoic sphene during the Caledonian thermal event (partial thermal resetting); or (2) physical mixtures of new sphene crystallized during the Caledonian event and older Proterozoic sphene. Distinguishing between these possibilities is not straightforward, nor are they mutually exclusive. If the sphene systematics in this sample were controlled chiefly by diffusional loss of Pb, one might expect to see a systematic relationship between the degree of discordance and the grain size of the sphene (assuming that the characteristic dimension for diffusion of Pb in sphene is equivalent to the physical grain size). Neither the positions of the sphene analyses along the discordia nor their dispersion away from the best fit line vary systematically with grain size. Consequently, I tentatively favor the interpretation that the sphene fractions analyzed represent physical mixtures of Caledonian and Proterozoic sphene, with the caveat that diffusional modification of the sphene may have occurred as well. Projection of the sphene data from the best-fit upper intercept (1862 Ma) down to concordia yields a range in ages from 391 to 426 Ma. Given the complexity and

uncertainty of the sphene systematics in this sample, it is difficult to assign geologic significance to these ages. One nearly concordant sphene analysis (S6) indicates that some of sphene in this sample may have an age of about 425 Ma. Projection of other analyses to younger ages may reflect continuous or episodic sphene growth to about 390 Ma, or it may reflect variable amounts of younger Pb-loss. It is interesting to note that the ages in the range of 390-400 Ma are identical within uncertainty to concordant ages of fine-grained sphene determined by Gromet and Andresen (1993) from a sample of mylonitic Proterozoic granite collected near Efjorden, 40 km south of this sample location. Nevertheless, the sphene data from this sample do not yield results that can be interpreted with confidence.

$^{40}Ar/^{39}Ar$ THERMOCHRONOLOGY

Analytical Methods

Virtually all previous $^{40}Ar/^{39}Ar$ analyses from the area have utilized the incremental-heating technique to release Ar from samples. Given that a significant body of incremental-heating data already exist for the region, I elected to use laser total fusion and Ar laser microprobe analyses to explore grain-scale variability in the Ar-isotopic system. Total fusion and laser microprobe analyses have the advantage of relatively small spatial resolution, but these techniques have a diminished ability to resolve the effects of unsupported ^{40}Ar in a given analysis because fusion data result in a total gas age.

Ar isotopic analyses were conducted at MIT in the Cambridge Laboratory for Argon Isotopic Research (CLAIR). Standard crushing, sieving, heavy liquid and

magnetic separation techniques were employed to generate concentrates of hornblende and muscovite. Mineral fractions for analysis were picked by hand from the concentrates to assure > 99.9% purity. In addition, several large muscovite grains (1.5 to 4.0mm in diameter) were extracted by hand from intact rock samples for Ar laser microprobe analysis. All mineral grains were washed in ethanol, distilled H_2O, and acetone, and then were enclosed in aluminum foil packets prior to irradiation. Samples were included in irradiation package CLAIR23, which was irradiated for 14.5 hours in the core of the research reactor at McMaster University in Hamilton, Ontario. Cadmium shielding was used to moderate the thermal neutron flux, and the fast neutron flux was monitored using Mmhb-1 hornblende (520.4 Ma; Samson and Alexander, 1987).

Samples were analyzed using a MAP 215-50 mass spectrometer. Extraction of Ar from the samples was done with a Coherent 10 W argon-ion laser. Total fusion analyses were accomplished by exposing 1 to 3 grains of muscovite or 5 to 7 grains of hornblende to continuous emission of the laser for 10 seconds at approximately 4 W output. For each sample analyzed in this manner, 8 to 10 individual total fusion analyses were done.

Ar laser microprobe analyses of larger muscovite grains consisted of 10 to 24 spot analyses per grain. Ar extraction at each location was accomplished by firing multiple pulses from the laser until a visible melt pit was produced in the muscovite at the site of analysis. The laser was operated at 15 to 20 W, and the duration of individual pulses ranged from 50 to 200 milliseconds. Fusion of muscovite occurred in an area approximately 50μ in diameter, but the zone of dehydration and structural disruption of

the muscovite lattice included a larger region, typically 100 to 300μ in diameter (e.g. Hames and Hodges 1993).

Results

Ar isotopic data and ages are presented in Table 3 and illustrated graphically in figures 11-19. Model ages for laser spot fusion or total fusion analyses have been calculated assuming that all non-radiogenic Ar in the sample had the isotopic composition of modern atmosphere ($^{40}Ar/^{36}Ar$ = 295.5). This is clearly not a valid assumption for some analyses, and the effects of unsupported ^{40}Ar are evident in a number of the apparent ages. However, the high radiogenic yield obtained from most analyses precluded meaningful resolution of the nonradiogenic component.

A ^{39}Ar-weighted mean age has been determined from all the analyses conducted on a given sample, and it provides as an estimate of the volume-averaged total-gas age for the mineral. Another way to view the data from a given set of fusion analyses is to assume that the calculated age and 1-sigma uncertainty for each analysis represent the mean and standard deviation of a probability distribution function. These age probability distributions can then be weighted by their yield of ^{39}Ar, summed together, and normalized to give an apparent-age distribution for a given data set. Some of the graphs shown in figures 11 through 19 depict the data in this manner, assuming a standard Gausian probability distribution for individual fusion analyses.

$^{40}Ar/^{39}Ar$ Laser Microprobe Analyses

Ar laser microprobe analyses of muscovite grains indicate significant variability in the apparent age of muscovite at sub-grain scale (Figures 11 through 14). Model ages of spot analyses within a given grain varied by as much as 80 Ma, but I found no clear or consistent systematic relationship between age and location within the grains. Although muscovite exhibited heterogeneity in apparent age at sub-grain scale, the ^{39}Ar-weighted mean age of all the spot analyses on a given grain was remarkably consistent from one muscovite grain to another, ranging from 392 ± 2 Ma to 397 ± 2 Ma. The normalized apparent-age distributions calculated for each of the muscovite grains yielded a dominant mode in the range of 396 to 398 Ma, in good agreement with the weighted mean ages. Consequently, these data are interpreted to indicate a nominal cooling-age for muscovite of about 395 to 400 Ma. Some of the apparent-age distributions contain a secondary mode in the range of 370 to 380 Ma, but this mode is defined by a relatively small number of analyses in each sample, and it may not have geologic significance.

$^{40}Ar/^{39}Ar$ Laser Total Fusion Analyses

In contrast to the results of the Ar laser microprobe experiments, the laser total fusion analyses yielded results that are more problematic. Model ages of hornblende total fusion analyses spanned a range from 350 Ma to nearly 650 Ma, indicating complex Ar systematics (Figures 15-17). Given the abundant evidence for mid-Silurian amphibolite facies metamorphism of these rocks, $^{40}Ar/^{39}Ar$ hornblende ages older than about 425 Ma are not likely to represent well-resolved cooling ages; such ages probably result from

variable quantities of unsupported ^{40}Ar in the samples. Because of the heterogeneity of the results and evidence of problems with unsupported ^{40}Ar, these data can not be used to infer a geologically meaningful cooling age for hornblende.

Like the hornblende total fusion experiments, the two samples of muscovite analyzed this manner produced results that are difficult to interpret (Figures 18 and 19). Sample 93SC-26 yielded a weighted mean age of 423 Ma and its normalized apparent-age distribution contains a principal mode at ca. 432 Ma. Sample 93SC-37 produced a weighted mean age of 432 Ma and its age distribution has a principal mode at ca. 435 Ma. Viewed within the context of other thermochronologic data from the region, these ages are too old to represent geologically realistic cooling ages for muscovite. The simplest explanation of these data is that many of the individual fusion analyses contained a component of unsupported ^{40}Ar which increased the apparent age determined for muscovite. Muscovite in the total fusion analyses had a relatively fine grain size (ca. 300μ) and, therefore, a relatively high surface-area-to-volume ratio compared to the coarse muscovite analyzed by laser mapping. Thus, one explanation of the disparity between the total fusion and laser mapping results is that unsupported ^{40}Ar corrolates with surface area. The normalized apparent-age distributions for the muscovite total fusion analyses contain a secondary mode at ca. 400 Ma (particularly 93SC-26), similar to the cooling age determined for muscovite grains using the laser microprobe technique. Although defined by only a few of the total fusion analyses, this secondary mode may represent a weak signal of the uncontaminated age for the muscovite in these samples.

However, the presence of unsupported ^{40}Ar in most of the analyses precludes confident interpretation of these data.

Summary

Laser microprobe and total fusion Ar isotopic analyses indicate: (1) resolvable heterogeneity in the apparent age of muscovite and hornblende at small spatial scales; and (2) variable contamination by a component enriched in ^{40}Ar. Hornblende and muscovite total fusion analyses contained variable but significant quantities of unsupported ^{40}Ar, which prevented determination of meaningful $^{40}Ar/^{39}Ar$ ages for these mineral by this technique. The best resolved $^{40}Ar/^{39}Ar$ ages come from laser microprobe analyses of coarse-grained muscovite. Four muscovite grains examined in this manner yielded weighted mean ages between 392-397 Ma, and the normalized apparent-age spectra of these grains contained principal modes at 396-398 Ma. Based on these data, muscovite at this structural level is interpreted to have a nominal cooling-age of 395 to 400 Ma.

DISCUSSION

Crystallization ages of felsic intrusive rocks

The U-Pb zircon age of the Ruggevik tonalite gneiss (479 ± 1 Ma) is the oldest age determined for rocks in the allochthon in this study, and it is interpreted as the time of intrusion and crystallization of the tonalite body. Tonalite-trondhjemite igneous activity ranging in age from ca. 470 - 500 Ma has been found at a variety of locations along the Caledonian Orogen, and it is commonly associated with rocks of ophiolitic affinity in these areas (e.g., Claesson et al. 1987; Dunning and Pedersen, 1988; Stephens et al.

1993). Therefore, the age of 479 ± 1 Ma determined for the Ruggevik tonalite gneiss is consistent with interpretation of the mafic rocks present locally at the base of the Ofoten Nappe Complex as the fragmented remains of an early Paleozoic ophiolite (Boyd, 1983; Steltenpohl et al. 1990). If this tonalite represents the source of tonalitic cobbles in the conglomerate at the base of the overlying sedimentary section, then this age may also provide an upper bound on the depositional age of these sediments. Dating the cobbles in the conglomerate would be a straightforward test of this hypothesis.

Even if these mafic rocks ± tonalite overlain by coarse clastic sediments represent a fragmented early Paleozic ophiolite capped by an erosional unconformity, however, they probably do not represent the "Finnmarkian phase" of Caledonian orogenesis in the strict sense. Finnmarkian tectonism, by definition, was located along the Baltoscandian margin (e.g. Stephens et al., 1993). Rocks within the Ofoten Nappe Complex are of marine affinity (broadly correlative with the upper Köli nappes in the central Caledonides), and originated in the ocean basin well outboard of the of Baltoscandian margin. Consequently, these rocks may record tectonic activity within the Iapetus Ocean basin that is contemporaneous with Finnmarkian orogenesis along Baltoscandia, but their Cambro-Ordovician history probably should not be termed Finnmarkian.

The U-Pb zircon analyses of granite and tonalite dikes in the Narvik Nappe Complex yielded precise crystallization ages of 437 ± 1 Ma, an age indistinguishable from that obtained for zircon in the Råna layered mafic intrusion by Tucker et al. (1990). These data are significant in two regards: 1) they indicate that widespread igneous activity in rocks of the NNC at this time included granitic as well as mafic components;

and 2) they place an upper bound of 437 ± 1 Ma on the age of assembly, high-grade metamorphism and concomitant penetrative deformation in the Narvik Nappe Complex.

Metamorphism and cooling of the Narvik Nappe Complex

The most robust constraints on the timing of peak metamorphism in the Narvik Nappe Complex comes from the ages of metamorphic monazite (432 ± 2 Ma) and zircon (432 ±1 Ma) from schist and migmatite in the NNC. Due to the highly retentive nature of these minerals (particularly zircon), their isotopic ages are interpreted to record the time of crystal growth during the high-T prograde to earliest retrograde segments of the metamorphic event. The zircon in the anatectic segregation probably grew as the local melt crystallized immediately following the metamorphic peak and, therefore, the crystallization age of this zircon may indicate the time of transition from peak metamorphism to post-metamorphic cooling at this structural level.

Cooling continued through Siluro-Devonian time, and the T-t path followed by rocks at this structural level is relatively well delineated by the cooling ages determined from several minerals with different closure temperatures (Figure 20). Given nominal values of the closure temperatures for the K-Ar, Rb-Sr or U-Pb isotopic systems in hornblende (500°C), muscovite, (410°C), rutile (400°C), and biotite (360°C), data from this study together with previously determined ages from the region constrain the cooling history of rocks at deep levels of the allochthon from about 700°C down to 325°C over the time interval from 432 Ma to 360 Ma. The time-integrated cooling rate during the early, high-temperature part of the history was ca. 8-10°C/My, but cooling slowed during the later, moderate-temperature part of the history to a time-integrated rate of 2-3°C/My.

Combining the T-t path determined for these rocks with information about their Pressure-Temperature evolution (Figure 21), and estimates of the age and depth of emplacement of the Råna layered mafic intrusion (Tucker et al. 1990; Barnes et al. 1988), we can reconstruct a crude depth-time history for rocks in the Narvik Nappe Complex (Figure 22). Following emplacement of the Råna pluton at 437 Ma at relatively shallow crustal depths, rocks in the NNC were tectonically buried to depths of ca. 40-50 km by about 432 Ma, consistent with a time-integrated tectonic burial rate of ca. 7 mm/yr. Following the metamorphic peak, these rocks were unroofed to 20-25 km depth by about 410-405 Ma, indicating a time-integrated unroofing rate of ca. 1 mm/yr.

Relatively slow, steady cooling of the Narvik Nappe Complex between 400 and 360 Ma is consistent with slow unroofing of the region during early to middle Devonian time. This cooling history suggests that the tectonic development of the Ofoten-Efjorden region in Siluro-Devonian time was significantly different than in the central and southern Scandinavian Caledonides where active tectonic exhumation of midcrustal rocks was widespread. Thus, the late Caledonian history in the northern part of the orogen may be markedly different than farther south.

Rocks in the structural basement beneath the nappes contain textural evidence of high-temperature decompression, and such decompression may be related to extensional modification of the nappe stack during late stages of its emplacement (see chapters 2 and 5). If so, then this decompression probably occurred in Silurian time prior to ca. 410 to 405 Ma. If decompression occurred as a response to ductile thinning of the nappe stack, then it must have occurred while the rocks in the nappes were hot and flowing (e.g.,

greater than ca. 500°C). Hornblende $^{40}Ar/^{39}Ar$ cooling ages suggest that the rock mass cooled through about 500°C by 410-405 Ma. Furthermore, the slow, steady cooling of the NNC between ca 400-360 Ma suggests that significant extensional denudation at higher structural levels is unlikely to have occured in the Ofoten-Efjorden area during early to middle Devonian time. Consequently, significant high-temperature decompression of the footwall probably occurred before the Devonian.

CONCLUSION

U-Pb and 40Ar/39Ar geochronology of samples from the Ofoten-Efjorden region of the northern Scandinavian Caledonides illuminate several aspects of the tectonic development in this part of the orogen. Two phases of igneous activity within Oceanic affinity rocks of the allochthon have been established: (1) the crystallization age of the Ruggevik tonalite gneiss (479 ±1 Ma) provides evidence for felsic magmatism within a possible fragment of Ordovician ophiolite in the region; and (2) granite and tonalite dikes were emplaced in the Narvik Nappe complex at 437 ± 1 Ma. The age of the younger suite of dikes also provides an upper bound on the age of assembly, metamorphism and strong penetrative deformation within the allochthon. Metamorphic monazite and zircon within the Narvik Nappe Complex indicate that amphibolite facies peak metamorphism occurred at ca. 432 ± 2 Ma, followed by protracted cooling history spanning more than 70 million years. Time-integrated cooling rates of ca. 8-10 °C/My followed the metamorphic culmination for ca. 30 million years, and then diminished to about 2-3 °C/My over the next 40 million years. Combining the T-t history with metamorphic data and other age constraints from the region suggests that the Narvik

Nappe Complex underwent tectonic burial at a time-integrated rate of ca. 7 mm/yr between 437 and 432 Ma, followed by unroofing at a time integrated rate of ca. 1 mm/yr until ca. 405 Ma.

REFERENCES

Andersen, T. B., Jamtveit, B., Dewey, J. F., and Swensson, E., 1991, Subduction and eduction of continental crust: Major mechanisms during continent-continent collision and orogenic extensional collapse, a model based on the south Norwegian Caledonides. *Terra Nova*, **3**, 303-310.

Barnes, S.-J., Sawyer, E. W., Boyd, R., and Tucker, R. D., 1988, The tectonic setting of the Råna layered intrusion (abstr.) *Geological Association of Canada, Mineralogical Association of Canada, Canadian Geophysical Union Program with Abstracts 13*, A5.

Bartley, J., M., 1981, Structural geology, metamorphism, and Rb/Sr geochronology of east Hinnøy, north Norway, Ph.D. thesis, Massachusetts Institute of Technology, Cambridge, MA.

Bjørlykke, A., Vokes, F. M., Birkeland, A., and Thorpe, R. I., 1993, Lead isotope systematics of strata-bound sulfide deposits in the Caledonides of Norway. *Econ. Geol.*, **88**, 397-417.

Boyd, R., 1983, The Lillevik dyke complex, Narvik:geochemistry and tectonic implications of a probable ophiolite fragment in the Caledonides of the Ofoten region, North Norway. *Norsk Geologisk Tidsskrift*, **63**, 39-54.

Cherniak, D. J., 1993, Lead diffusion in titanite and preliminary results on the effects of radiation damage on Pb transport. *Chem. Geol.*, **110**, 177-194.

Claesson, S., Stephens, M. B., and Klingspor, I., 1987, U-Pb zircon dating of felsic intrusions, Middle Köli Nappes, central Scandinavian Caledonides. *Norsk Geol. Tidsskr.* **67**, 89-97.

Coker, J. E., Steltenpohl, M. G., Andresen, A., and Kunk, M. J., 1995, An $^{40}Ar/^{39}Ar$ thermochronology of the Ofoten-Troms region: Implications for terrane amalgamation and extensional collapse of the northern Scandinavian Caledonides. *Tectonics,* **14**, 435-447.

Crowley, P. D., 1985, The structural and metamorphic evolution of the Sitas area, northern Norway and Sweden, Ph.D. thesis, M.I.T., Cambridge, MA, 253pp.

Gee, D. G., 1975, A tectonic model for the central part of the Scandinavian Caledonides, *Am. J. Sci.,* **275-A**, 468-515.

Gee, D.G., R. Kumpulainen, D. Roberts, M. B. Stephens, A. Thon, and E. Zachrisson, 1985, Tectonostratigraphic map of the Scandinavian Caledonides: in D. G. Gee and B. A. Sturt, eds., *The Caledonian Orogen - Scandinavia and related areas*, J. Wiley and Sons, Chichester, England.

Gee, D. G., Lobkowicz, M., and Singh, S., 1994, Late Caledonian extension in the Scandinavian Caledonides - the Roragen Detachment revisited. *Tectonophysics,* **231**, 139-155.

Gee, D. G., and M. R. Wilson, 1974, The age of orogenic deformation in the Swedish Caledonides, *Am. J. Sci.,* **274**, 1-9.

Gromet, P. and Andresen, A., 1993, U-Pb Constraints on Caledonian shear strain developed at the Basement-Allochthon contact, Ofoten region, Noeway. abstr., EOS, Transactions of the American Geophysical Union, 74, no 16, 123.

Gustavson, M., 1974, Narvik, Beskrivelse til det bergrunnsgeologiske gradteigskrat N9 1:250,000, *Nor. Geol. Unders.,* **308,** 34 p.

Hames, W. E., and Hodges, K. V., 1993, Laser 40Ar/39Ar evaluation of slow cooling and episodic loss of 40Ar from a sample of polymetamorphic muscovite. *Science* **261**, 1721-1723.

Harland, W. B., and R. A. Gayer, 1972, The Arctic Caledonides and earlier oceans, *Geol. Mag.,* **109,** 289-314.

Harrison, T. M., 1981, Diffusion of 40Ar in hornblende. *Contrib. Mineral. Petrol.* **78**, 324-331.

Hodges, K. V., 1982, Tectonic evolution of the Aefjord-Sitas area, Norway-Sweden, Ph.D. thesis, Massachusetts Institute of Technology, Cambridge, MA.

Hodges, K. V., 1991, Pressure-Temperature-Time paths. *Ann. Rev. Earth Planet. Sci.* **19**, 207-236.

Hodges, K. V., and L. Royden, 1984, Geologic thermobarometry of retrograded metamorphic rocks: an indication of the uplift trajectory of a portion of the northern Scandinavian Caledonides, *J. Geophys. Res.,* **89,** 7077-7090.

Krogh, T. E., 1973, A low contamination method for hydrothermal decomposition of zircon and extraction of U and Pb for isotopic age determination. *Geochemica et Cosmochemica Acta* **37**, 485-494.

Krogh, T. E., 1982, Improved accuracy of U-Pb zircon ages by the creation of more concordant systems using an air abrasion technique. *Geochemica et Cosmochemica Acta* **46**, 637-649.

Ludwig, K. R.,1989, Pb.dat: A computer program for processing raw Pb-U-Th isotope data: U.S. Geological Survey Open-File report 88-557.

Ludwig, K. R., 1990, Isoplot: A plotting and regression program for radiometric-isotope data: U. S. Geological Survey Open-File Report 90-91.

Mezger, K., 1989, Dating the P-T evolution of granulites. Ph.D thesis. State Univ. N. Y., Stony Brook. 172 pp.

Mezger, K., Essene, E. J., van der Plujim, B. A., and Halliday, A. N., 1993, U-Pb geochronology of the Grenville Orogen of Ontario and Hew York: Constraints on ancient crustal tectonics. *Contrib. Mineral. Petrol.*, **114**, 13-26.

Norton, M. G., 1986, Late Caledonian extension in western Norway: A response to extreme crustal thickening. *Tectonics*, **5**, 195-204.

Parrish, R. R., 1990, U-Pb dating of monazite and its application to geologic problems. *Canadian Journal of Earth Sciences,* **27**, 1435-1450.

Parrish, R. R., Roddick, J. C., Loveridge, W. A., and Sullivan, R. W., 1987, Uranium-lead analytical techniques at the geochronology laboratory, Geological Survey of Canada. in: *Radiogenic Age and Isotopic Studies: Report 1,* Geological Survey of Canada Paper 87-2, p. 3-7.

Roberts, D., and Gee, D. G., 1985, An introduction to the structure of the Scandinavian Caledonides, in: D.G. Gee and B. A. Sturt, eds., *The Caledonian Orogen - Scandinavia and Related Areas*, John Wiley, New York, p. 55-68.

Robbins, G. A., 1972, Radiogenic argon diffusion in muscovite under hydrothermal conditions. MS thesis. Brown Univ., Providence, RI.

Sampson, S. D., and Alexander, E. C., 1987, Calibration of the interlaboratory 40Ar/39Ar dating standard, Mmhb-1. *Chemical Geology,* **66**, 27-34.

Schärer, U., 1984, The effect of initial ^{230}Th disequilibrium on young U-Pb ages: the Makalu case, Himalaya. *Earth and Planetary Science Letters*, **67**, 191-204.

Sharer, 1996, EPSL sphene inheritance paper.

Skiöld, T., 1988, Implications of new U-Pb zircon chronology to early Proterozoic crustal accretion in northern Sweden. *Precambrian Research*, **38**, 147-164.

Stacey, J. S., and Kramers, J. D., 1975, Approximation of terrestrial lead isotopes evolution by a two-stage model. *Earth and Planetary Science Letters*, **26**, 207-221.

Steltenpohl, M. G., 1983, The structure and stratigraphy of the Ofoten synform, North Norway, M.S. thesis, University of Alabama, University, AL.

Steltenpohl, M. G., 1985, The structural and metamorphic history of Skanland, north Norway, and its significance for tectonics in Scandinavia, Ph.D. thesis, University of North Carolina, Chapel Hill, NC.

Steltenpohl, M. G., and J. M. Bartley, 1987, Thermobarometric profile through the Caledonian nappe stack of western Ofoten, north Norway, *Contrib. Min. Pet.*, **92**, 93-103.

Steltenpohl, M. G., and J. M. Bartley, 1988, Crossfolds and backfolds in the Ofoten-Tysfjord area, Norway and their significance for Caledonian tectonics, *Geol. Soc. Am. Bull.*, **100,** 140-151.

Steltenpohl, M. G., Andresen, A., and Tull, J. F., 1990, Lithostratigraphic correlation of the Salangen (Ofoten) and Balsfjord (Troms) Groups: evidence for the post-Finmarkian unconformity, North Norwegian Caledonides. *Nor. Geol. Unders.*, **418**, 61-77.

Stephens, M. B., and D. G. Gee, 1989, Terranes and polyphase accretionary history in the Scandinavian Caledonides, *Geol. Soc. Am. Spec. Paper,* **230,** 17-30.

Stephens, M. B., Kullerud, K., and Claesson, S., 1993, Early Caledonian tectonothermal evolution in outboard terranes, central Scandinavian Caledonides: new constraints from U-Pb zircon dates. *J. Geol. Soc. Lond.*, **150**, 51-56.

Tilke, P. G., 1986, Caledonian structure, metamorphism geochronology, and tectonics of the Sitas-Singas area, Sweden. Ph.D. thesis, M.I.T., Cambridege, MA, 295 pp.

Tucker, R. D., Boyd, R., and Barnes, S-J., 1990, A U-Pb age for the Råna intrusion, N. Norway: New evidence of basic magmatism in the Scandinavian Caledonides in Early Silurian time. *Norsk. Geol. Tidsskr.*, **70**, 229-239.

York, D.,1969, Least-squares fitting of a straight line with correlated errors. *Earth Planet. Sci. Lett.*, **5**, 320-324.

Wendt, I., and Carl, C., 1991, The statistical distribution of the mean squared weighted deviation. *Chemical Geology*, **86**, 275-285.

APENDIX 1: DATA TABLES

Table 2: U-Pb data

		Weight	Concentrations U	Pb	206 Pb*	208 Pb	206 Pb	Errors 2-sigma (%) 207 Pb		207 Pb		Age (Ma) 206 Pb	207 Pb	207 Pb		com. Pb	est. Blank
Mineral	Frac.	(µg)	(ppm)	(ppm)	204 Pb	206 Pb	238 U	% err	235 U	% err	206 Pb	% err	238 U	235 U	206 Pb	error	(pg)	(pg)
93SC-77: deformed granite dike in the Narvik Nappe Complex																		
zircon	Z1	5.0	22881.31	1452.24	30579.65	0.008	0.06935	(.14)	0.53149	(.15)	0.05559	(.06)	**432.2**	**432.8**	**435.9**	± 1.4	16.4	5.0
zircon	Z2	4.0	48449.09	3074.66	47234 62	0.011	0.06919	(.14)	0.53082	(.15)	0.05565	(.05)	**431.2**	**432.4**	**438.2**	± 1.1	17.9	5.0
zircon	Z5	2.0	53018.48	3396.92	39409 34	0.014	0.06960	(.06)	0.53350	(.08)	0.05560	(.04)	**433.7**	**434.1**	**436.3**	± 0.9	11.8	3.5
zircon	Z6	2.1	46020.19	2934.75	60550 98	0.014	0.06932	(.09)	0.53152	(.10)	0.05561	(.04)	**432.1**	**432.8**	**436.8**	± 0 9	7.0	3.5
zircon	Z7	1.2	39018.70	2528.80	2856.22	0.012	0.06908	(.07)	0.52960	(.09)	0.05560	(.05)	**430.6**	**431.5**	**436.5**	± 1.0	71.5	3.5
zircon	Z8	1.5	27680.14	1766.94	10986.69	0.009	0.06945	(.09)	0.53256	(.10)	0.05561	(04)	**432.9**	**433.5**	**436.9**	± 1.0	16.0	3.5
rutile	R1	275	7.74	2.79	29.96	0.054	0.05847	(.50)	0.42872	(6.35)	0.05318	(5.96)	**366.3**	**362.3**	**336.3**	± 135.1	653.8	5.0
rutile	R2	340	5.64	0.54	107.98	0.010	0.06140	(.55)	0.44326	(.87)	0.05236	(.65)	**384.2**	**372.6**	**301.0**	± 14.8	82.1	5.0
rutile	R3	322	5.97	0.74	68.85	-0.005	0.05951	(.48)	0 37883	(4.58)	0.04617	(4.33)	**372.6**	**326.2**	**6.4**	± 104.2	141.1	3.5
rutile	R4	327	5 27	0.94	47.81	-0.008	0.06124	(.66)	0 36666	(7.31)	0.04343	(7.02)	**383.1**	**317.2**	**-143.1**	± 173.9	216.9	5 0
93SC-117: mylonitized granite in the footwall of the basal shear zone																		
zircon	Z1	9	227.09	75.73	5901.45	0.248	0.28378	(12)	4.37326	(.15)	0.11177	(.09)	**1610.4**	**1707.3**	**1828.4**	± 1.7	5 8	3.5
zircon	Z2	10	257.20	63.90	13068.08	0.220	0.21757	(.11)	3.18139	(.13)	0.10605	(.06)	**1269.0**	**1452.7**	**1732.6**	± 1.1	2.8	2.8
sphene	S1	330	26.42	3.38	170.61	0.155	0.08769	(.09)	0.89320	(.21)	0.07387	(.18)	**541.9**	**648.1**	**1038.0**	± 3.7	311.5	3.5
sphene	S2	521	27.97	3.94	143.10	0.182	0.08956	(.08)	0.90257	(.29)	0.07309	(.27)	**553.0**	**653.1**	**1016.4**	± 5.4	648.3	3.5
sphene	S3	109	25.61	3.51	80.56	0.197	0.06642	(.24)	0.53802	(.89)	0.05875	(.81)	**414.5**	**437.1**	**557.9**	± 17 8	184.9	3.5
sphene	S4	150	26.05	2.95	115.29	0.166	0.06736	(.22)	0.52522	(.97)	0.05655	(.90)	**420.2**	**428.6**	**473.9**	± 19.9	169.2	3.5
sphene	S6	180	23.19	2.92	99.62	0.188	0.06900	(.18)	0.53127	(.76)	0.05585	(.70)	**430.1**	**432.7**	**446.3**	± 15.6	219.9	3.5
sphene	S7	284	26.31	2.67	140 93	-0.099	0.07617	(.12)	0.68664	(.32)	0.06538	(28)	**473.2**	**530.8**	**786.5**	± 6.0	288.8	3.5
sphene	S8	363	21.26	2.09	148.91	0.114	0.06668	(.11)	0.53151	(.31)	0.05781	(27)	**416.1**	**432.8**	**522.7**	± 6.0	245.3	3.5
sphene	S9	555	28.26	3.16	211.13	0.116	0.08341	(.09)	0.81344	(.17)	0.07073	(.14)	**516.5**	**604.4**	**949.6**	± 2.8	423.4	3.5
93SC-13: Rugvik tonalite gneiss																		
zircon	Z1	15	710.42	54.39	16790.94	0.120	0.07564	(.10)	0.59121	(12)	0.05669	(.07)	**470.1**	**471.6**	**479.3**	± 1.5	3.1	3.1
zircon	Z2	15	673.97	51 14	26943.06	0.103	0.07612	(.13)	0.59461	(.13)	0.05666	(.05)	**472.9**	**473.8**	**478.2**	± 1.0	1.8	1.8
zircon	Z3	20	546.58	40.80	37867.18	0.098	0.07515	(.07)	0.58743	(.08)	0.05669	(.05)	**467.1**	**469.2**	**479.7**	± 1.0	1.4	1 4
zircon	Z4	17	623.02	47.20	12211.59	0.106	0.07569	(.10)	0.59134	(.12)	0.05666	(.06)	**470.3**	**471.7**	**478.5**	± 1.3	4.2	3.5
zircon	Z5	10	704.83	58 34	4455 87	0.205	0.07569	(.13)	0.59132	(.15)	0.05666	(08)	**470.3**	**471.7**	**478.5**	± 1.7	7.6	3.5
93SC-78: deformed tonalite dike in Narvik Nappe Complex																		
zircon	Z1	15	521.69	34.82	6892.98	0.061	0.06931	(.17)	0.53129	(.18)	0.05559	(.07)	**432.0**	**432.7**	**436.1**	± 1.6	5.0	3.5
zircon	Z2	13	544.59	36.75	14420.13	0.053	0.07075	(.10)	0.55196	(.12)	0.05658	(.07)	**440.7**	**446.3**	**475.3**	± 1.6	2.2	2.2
zircon	Z4	20	105.82	7.45	2074.93	0.113	0.06949	(.37)	0.53307	(.39)	0.05564	(.13)	**433.1**	**433.8**	**438.0**	± 2.8	4.6	3.5
zircon	Z5	10	344.25	22.75	2241.15	0.045	0.06888	(.24)	0.52836	(.28)	0.05563	(.14)	**429.4**	**430.7**	**437.8**	± 3 1	6.8	3.5
zircon	Z6	10	534 47	35.40	2259.71	0.040	0.06896	(.19)	0.52881	(.22)	0.05562	(.10)	**429.9**	**431.0**	**437.2**	± 2.3	10.4	3.5
94SC-30: garnet+kyanite+biotite schist in Narvik Nappe Complex																		
monazite	M3	1.4	20365.15	3680.50	7772 86	1.942	0.06958	(.12)	0.53016	(.15)	0.05527	(.09)	**433.6**	**431.9**	**423.0**	± 1.9	15.9	3.5
monazite	M8	5.8	16127.58	2290.42	11892.83	1.315	0.06920	(.11)	0.52941	(.12)	0.05548	(.04)	**431.4**	**431.4**	**431.7**	± 0.9	34.3	3.5
monazite	M9	1.0	12797.42	2039.88	5555.64	1.550	0.07056	(14)	0 53927	(.16)	0.05543	(.09)	**439.5**	**437.9**	**429.5**	± 1.9	9.8	3.5
monazite	M11	1.1	18148.91	2917.97	5146 47	1.611	0.06948	(.12)	0.53039	(.15)	0.05537	(.09)	**433.0**	**432.1**	**427.0**	± 2.0	17.1	3 5
monazite	M12	1.8	25121.58	3508.27	10367 01	1.276	0 06919	(.18)	0.52817	(.20)	0.05537	(.10)	**431.3**	**430.6**	**427.0**	± 2.1	19.0	3.5
94SC-31: anatectic segregation in garnet+kyanite+biotite schist, Narvik Nappe Complex																		
zircon	Z1	45	3732.78	232.59	107528 11	0.017	0.06761	(.26)	0.51749	(.26)	0.05552	(04)	**421.7**	**423.5**	**433.0**	± 1 0	6.7	3.5
zircon	Z2	42	655.10	41.43	36826.94	0.008	0.06923	(.23)	0.52967	(.23)	0.05549	(.05)	**431.5**	**431.6**	**431.9**	± 1.0	3 3	3.3
zircon	Z3	27	4254.22	271.30	17209.51	0 017	0 06893	(.32)	0.52717	(.32)	0.05547	(.05)	**429.7**	**429.9**	**431.0**	± 1.1	28.9	3.5
zircon	Z4	22	1298.81	82.15	22685.16	0 008	0.06912	(.18)	0.52892	(.19)	0.05550	(.05)	**430.8**	**431.1**	**432.4**	± 1.0	5.5	3.5
zircon	Z5	17	2734.88	172.58	79787.47	0.013	0.06875	(.26)	0.52604	(26)	0.05549	(.05)	**428.6**	**429.2**	**432.2**	± 1.1	2.6	2.6
93SC-76: amphibolite, basal portion of Ofoten Nappe Complex																		
sphene	S1	251	5.85	4.16	24.94	0.107	0.06884	(.41)	0.57568	(5.11)	0.06065	(4.78)	**429.2**	**461.7**	**626.8**	± 103.0	946.8	5 0
sphene	S2	343	9 29	4.87	27.30	0.082	0.06646	(.41)	0.59073	(4.65)	0.06447	(4.35)	**414.8**	**471.3**	**757.0**	± 91.8	1467.4	5 0
sphene	S3	525	8.29	4.96	26.05	0.075	0.06648	(.37)	0.50711	(5.55)	0.05532	(5.22)	**414.9**	**416.5**	**425.2**	± 116.4	2326.0	5.0
sphene	S5	155	10.55	6.36	26.01	0.194	0.06627	(.44)	0.45221	(5.83)	0.04949	(5.52)	**413.6**	**378.8**	**171.3**	± 128.9	874.9	5.0
sphene	S6	245	8.11	4.79	26.17	0.080	0.06671	(.37)	0.50849	(5.25)	0.05528	(4.96)	**416.3**	**417.4**	**423.6**	± 110.7	1049.2	5.0

Ar data table

Sample: 93SC-52 muscovite
J Value: 3.74E-03 ± 7.48E-05

	36/40	(36/40)err	39/40	(39/40)err	39ArK moles	40Ar*%	Age (Ma)		err	w/o J
1	4.51E-05	6.59E-06	1.48E-02	4.52E-05	7.16E-16	98.6	401	±	7.3	1.3
2	-2.21E-06	7.10E-06	1.51E-02	4.60E-05	6.78E-16	100.0	400	±	7.3	1.3
3	-2.91E-06	4.28E-06	1.48E-02	4.20E-05	1.11E-15	100.0	406	±	7.4	1.1
4	2.41E-05	2.39E-06	1.47E-02	3.89E-05	1.97E-15	99.2	405	±	7.3	1.0
5	4.56E-06	2.38E-06	1.52E-02	4.04E-05	2.04E-15	99.8	396	±	7.2	1.0
6	1.56E-05	4.71E-06	1.53E-02	4.19E-05	1.04E-15	99.5	393	±	7.2	1.1
7	1.47E-06	5.95E-06	1.53E-02	4.41E-05	8.21E-16	99.9	393	±	7.2	1.2
8	1.31E-04	4.89E-06	1.53E-02	4.26E-05	9.98E-16	96.1	382	±	7.0	1.1
9	1.03E-04	1.19E-05	1.49E-02	5.13E-05	4.00E-16	96.9	393	±	7.3	1.8
10	5.49E-05	4.68E-06	1.50E-02	4.23E-05	1.02E-15	98.3	396	±	7.2	1.1
11	3.35E-04	1.42E-05	1.40E-02	5.49E-05	3.17E-16	90.1	388	±	7.3	2.2
12	3.99E-04	6.94E-06	1.29E-02	3.99E-05	6.08E-16	88.2	410	±	7.5	1.5
13	1.80E-06	1.13E-05	1.49E-02	5.00E-05	4.19E-16	99.9	405	±	7.5	1.7
14	1.42E-03	8.02E-06	9.69E-03	3.17E-05	4.45E-16	57.9	364	±	6.9	1.9
15	1.82E-05	2.61E-06	1.50E-02	3.97E-05	1.86E-15	99.4	399	±	7.2	1.0
16	3.57E-05	6.80E-06	1.49E-02	4.49E-05	7.00E-16	98.9	400	±	7.3	1.3
17	-3.24E-06	8.35E-06	1.52E-02	4.78E-05	5.81E-16	100.0	397	±	7.3	1.4
						Error Wtd. Mean Age:	395	±	1.8	
						39Ar Wtd. Mean Age:	397	±	1.8	

Sample: 92SC-114 muscovite
J Value: 3.74E-03 ± 7.48E-05

	36/40	(36/40)err	39/40	(39/40)err	39ArK moles	40Ar*%	Age (Ma)		err	w/o J
1	2.60E-03	4.47E-04	5.83E-03	3.71E-04	3.13E-17	23.2	250	±	134.0	134.0
2	1.10E-03	1.65E-04	1.03E-02	1.42E-04	1.50E-16	67.5	394	±	27.1	26.1
3	5.91E-06	3.45E-05	1.44E-02	4.31E-05	1.00E-15	99.8	417	±	8.4	4.0
4	5.74E-05	1.28E-05	1.52E-02	3.72E-05	2.85E-15	98.2	391	±	7.2	1.6
5	1.45E-04	1.70E-04	1.61E-02	1.47E-04	2.27E-16	95.7	363	±	18.7	17.5
6	1.18E-04	8.16E-05	1.52E-02	7.68E-05	4.46E-16	96.5	385	±	11.3	8.9
7	4.60E-05	1.55E-05	1.60E-02	4.30E-05	2.48E-15	98.6	374	±	7.0	1.8
8	1.07E-04	4.34E-05	1.44E-02	4.89E-05	7.96E-16	96.8	405	±	8.8	5.0
9	3.16E-05	1.66E-04	1.40E-02	1.42E-04	2.03E-16	99.0	423	±	20.4	19.0
10	3.37E-05	9.61E-06	1.48E-02	3.90E-05	3.71E-15	99.0	402	±	7.3	1.4
11	1.15E-04	1.65E-05	1.54E-02	3.88E-05	2.25E-15	96.6	380	±	7.1	1.9
12	5.59E-05	3.80E-05	1.53E-02	4.77E-05	9.69E-16	98.3	388	±	8.1	4.1
13	8.89E-05	7.62E-06	1.48E-02	3.77E-05	4.69E-15	97.3	396	±	7.2	1.2
14	-2.89E-06	2.65E-05	1.48E-02	3.94E-05	1.34E-15	100.0	407	±	7.9	3.0
15	1.71E-04	8.42E-05	1.66E-02	8.01E-05	4.74E-16	94.9	349	±	10.6	8.5
16	9.77E-05	1.41E-04	1.55E-02	1.23E-04	2.64E-16	97.1	380	±	16.5	15.0
17	2.73E-04	7.74E-05	1.46E-02	7.23E-05	4.52E-16	91.9	383	±	11.1	8.8
18	7.20E-05	8.60E-05	1.50E-02	7.93E-05	4.20E-16	97.8	393	±	11.7	9.4
19	-2.83E-06	6.67E-05	1.52E-02	6.51E-05	5.47E-16	100.0	398	±	10.1	7.2
20	9.99E-04	1.17E-03	1.53E-02	9.70E-04	3.16E-17	70.4	286	±	130.6	130.5
21	3.36E-05	4.35E-05	1.53E-02	4.81E-05	8.44E-16	99.0	391	±	8.5	4.7
22	5.24E-06	2.41E-04	1.40E-02	2.04E-04	1.39E-16	99.8	427	±	28.7	27.7
23	4.08E-05	5.78E-05	1.51E-02	5.81E-05	6.26E-16	98.7	396	±	9.5	6.3
24	2.51E-04	1.90E-04	1.44E-02	1.62E-04	1.83E-16	92.5	388	±	22.6	21.5
						Error Wtd. Mean Age:	392	±	1.9	
						39Ar Wtd. Mean Age:	392	±	1.8	

Ar data table

Sample: 93SC-78 muscovite 1
J Value: 3.72E-03 ± 7.44E-05

	36/40	(36/40)err	39/40	(39/40)err	39ArK moles	40Ar*%	Age (Ma)		err	w/o J
1	9.11E-05	1.80E-06	1.42E-02	3.92E-05	1.79E-15	97.3	411	±	7.4	1.1
2	5.24E-06	1.63E-06	1.47E-02	3.98E-05	2.07E-15	99.8	406	±	7.3	1.0
3	6.26E-06	2.93E-06	1.44E-02	4.14E-05	1.09E-15	99.8	415	±	7.5	1.1
4	5.17E-07	1.30E-06	1.51E-02	4.20E-05	2.56E-15	99.9	397	±	7.2	1.0
5	3.57E-05	3.93E-06	1.48E-02	4.32E-05	8.38E-16	98.9	400	±	7.3	1.1
6	1.45E-04	1.18E-05	1.55E-02	5.24E-05	4.71E-16	95.7	374	±	7.0	1.7
7	9.14E-05	8.90E-06	1.45E-02	4.77E-05	5.85E-16	97.2	402	±	7.4	1.5
8	4.19E-05	3.32E-06	1.51E-02	4.11E-05	1.62E-15	98.7	394	±	7.2	1.0
9	3.84E-05	6.31E-06	1.48E-02	4.43E-05	8.42E-16	98.8	400	±	7.3	1.3
10	1.37E-04	1.32E-05	1.67E-02	5.73E-05	4.51E-16	95.9	350	±	6.6	1.7
11	6.01E-05	4.61E-06	1.53E-02	4.29E-05	1.19E-15	98.2	386	±	7.0	1.1
12	8.85E-05	4.44E-06	1.49E-02	4.20E-05	1.20E-15	97.3	393	±	7.2	1.1
13	1.79E-05	3.25E-06	1.50E-02	4.05E-05	1.65E-15	99.4	399	±	7.2	1.0
14	6.77E-05	3.86E-06	1.52E-02	4.08E-05	1.41E-15	97.9	388	±	7.1	1.0
						Error Wtd. Mean Age:	393	±	1.9	
						39Ar Wtd. Mean Age:	397	±	1.9	

Sample: 93SC-78 muscovite 2
J Value: 3.72E-03 ± 7.44E-05

	36/40	(36/40)err	39/40	(39/40)err	39ArK moles	40Ar*%	Age (Ma)		err	w/o J
1	2.91E-04	4.23E-05	1.20E-02	6.39E-05	2.89E-16	91.4	450	±	9.9	5.9
2	1.34E-06	1.42E-05	1.49E-02	4.45E-05	1.07E-15	99.9	402	±	7.4	1.9
3	1.13E-06	1.20E-05	1.52E-02	4.34E-05	1.29E-15	99.9	396	±	7.3	1.6
4	3.11E-06	3.19E-05	1.47E-02	5.86E-05	4.67E-16	99.9	407	±	8.2	3.7
5	1.95E-06	2.06E-05	1.50E-02	4.91E-05	7.36E-16	99.9	400	±	7.6	2.5
6	1.21E-06	1.28E-05	1.52E-02	4.34E-05	1.20E-15	99.9	395	±	7.3	1.7
7	8.55E-07	2.39E-05	1.54E-02	5.19E-05	6.54E-16	99.9	391	±	7.6	2.8
8	1.62E-06	1.71E-05	1.61E-02	4.80E-05	9.53E-16	99.9	375	±	7.1	2.0
9	1.96E-06	2.07E-05	1.58E-02	4.97E-05	7.72E-16	99.9	382	±	7.3	2.4
10	2.21E-06	2.34E-05	1.50E-02	5.04E-05	6.51E-16	99.9	399	±	7.7	2.8
						Error Wtd. Mean Age:	397	±	2.4	
						39Ar Wtd. Mean Age:	396	±	2.4	

Sample: 93SC-26 muscovite
J Value: 3.72E-03 ± 7.44E-05

	36/40	(36/40)err	39/40	(39/40)err	39ArK moles	40Ar*%	Age (Ma)		err	w/o J
1	3.49E-05	5.17E-06	1.37E-02	3.32E-05	4.38E-15	98.9	430	±	7.7	1.1
2	6.06E-05	1.64E-05	1.33E-02	3.28E-05	1.35E-15	98.2	438	±	8.1	2.1
3	4.77E-05	6.21E-06	1.37E-02	3.40E-05	3.66E-15	98.5	428	±	7.7	1.2
4	5.10E-05	8.60E-06	1.37E-02	3.73E-05	2.64E-15	98.4	429	±	7.8	1.4
5	5.72E-05	5.90E-06	1.36E-02	3.43E-05	3.83E-15	98.3	429	±	7.7	1.2
6	7.44E-05	1.35E-05	1.42E-02	3.49E-05	1.74E-15	97.8	413	±	7.6	1.8
7	2.49E-05	9.28E-06	1.49E-02	3.69E-05	2.66E-15	99.2	399	±	7.3	1.3
8	8.42E-05	1.69E-05	1.45E-02	3.74E-05	1.42E-15	97.5	403	±	7.5	2.1
						Error Wtd. Mean Age:	420	±	2.7	
						39Ar Wtd. Mean Age:	423	±	2.7	

Ar data table

Sample: 93SC-37 muscovite
J Value: 3.72E-03 ± 7.44E-05

	36/40	(36/40)err	39/40	(39/40)err	39ArK moles	40Ar*%	Age (Ma)		err	w/o J
1	1.12E-04	3.57E-06	1.45E-02	3.21E-05	2.47E-15	96.6	400	±	7.2	0.9
2	3.19E-05	2.60E-06	1.34E-02	3.23E-05	3.11E-15	99.0	439	±	7.9	1.0
3	4.50E-05	2.51E-06	1.37E-02	3.28E-05	3.30E-15	98.6	430	±	7.7	1.0
4	2.46E-06	2.88E-06	1.38E-02	3.25E-05	2.88E-15	99.9	432	±	7.7	1.0
5	2.61E-05	2.11E-06	1.37E-02	3.26E-05	3.93E-15	99.2	432	±	7.7	1.0
6	2.79E-05	3.48E-06	1.35E-02	3.52E-05	2.35E-15	99.1	436	±	7.8	1.1
7	3.84E-05	3.99E-06	1.42E-02	3.39E-05	2.15E-15	98.8	417	±	7.5	1.0
8	6.03E-05	1.75E-06	1.35E-02	3.14E-05	4.67E-15	98.2	434	±	7.8	0.9
9	6.33E-05	1.75E-06	1.31E-02	3.14E-05	4.57E-15	98.1	442	±	7.9	1.0
10	2.73E-05	1.50E-06	1.34E-02	3.29E-05	5.42E-15	99.1	438	±	7.8	1.0
						Error Wtd. Mean Age:	429	±	2.4	
						39Ar Wtd. Mean Age:	432	±	2.5	

Sample: 93SC-17 hornblende
J Value: 3.72E-03 ± 7.44E-05

	36/40	(36/40)err	39/40	(39/40)err	39ArK moles	40Ar*%	Age (Ma)		err	w/o J
1	1.49E-04	6.60E-06	1.12E-02	2.89E-05	1.75E-15	95.5	498	±	8.8	1.5
2	1.88E-04	8.70E-06	9.67E-03	2.60E-05	1.07E-15	94.4	560	±	9.8	1.9
3	1.39E-04	1.09E-05	1.05E-02	3.00E-05	9.02E-16	95.9	527	±	9.4	2.0
4	1.34E-04	8.11E-06	1.05E-02	2.77E-05	1.24E-15	96.0	529	±	9.3	1.7
5	1.98E-04	8.46E-06	9.86E-03	2.72E-05	1.14E-15	94.1	548	±	9.6	1.8
6	1.87E-04	9.10E-06	1.09E-02	2.95E-05	1.18E-15	94.4	504	±	9.0	1.7
7	1.69E-04	1.96E-05	8.71E-03	3.02E-05	4.09E-16	95.0	615	±	11.0	3.7
8	-1.34E-05	1.79E-05	1.03E-02	3.21E-05	5.25E-16	100.4	560	±	10.1	3.0
9	1.61E-04	1.46E-05	9.68E-03	2.87E-05	6.11E-16	95.2	563	±	10.0	2.6
10	1.62E-04	1.32E-05	1.05E-02	3.04E-05	7.43E-16	95.2	526	±	9.4	2.3
						Error Wtd. Mean Age:	539	±	3.0	
						39Ar Wtd. Mean Age:	533	±	3.0	

Sample: 93SC-31 hornblende
J Value: 3.72E-03 ± 7.44E-05

	36/40	(36/40)err	39/40	(39/40)err	39ArK moles	40Ar*%	Age (Ma)		err	w/o J
1	3.95E-05	7.31E-06	9.31E-03	3.55E-05	6.16E-16	98.8	601	±	10.5	2.3
2	1.88E-04	6.76E-06	1.08E-02	3.66E-05	8.20E-16	94.4	507	±	9.0	1.8
3	1.28E-04	1.32E-05	1.09E-02	5.83E-05	3.54E-16	96.2	514	±	9.4	3.0
4	2.11E-04	8.90E-06	1.01E-02	4.16E-05	5.78E-16	93.7	536	±	9.6	2.3
5	1.10E-04	1.21E-05	1.04E-02	5.41E-05	3.76E-16	96.7	537	±	9.8	3.0
6	1.09E-04	1.05E-05	1.08E-02	4.84E-05	4.79E-16	96.7	517	±	9.3	2.5
7	1.47E-04	1.20E-05	8.40E-03	5.07E-05	3.15E-16	95.6	638	±	11.4	3.8
8	1.12E-04	1.47E-05	1.18E-02	6.38E-05	3.62E-16	96.7	482	±	9.0	3.0
9	1.86E-04	8.32E-06	1.04E-02	4.02E-05	6.90E-16	94.5	526	±	9.4	2.2
						Error Wtd. Mean Age:	534	±	3.2	
						39Ar Wtd. Mean Age:	537	±	3.2	

Ar data table

Sample: 93SC-49 hornblende
J Value: 3.72E-03 ± 7.44E-05

	36/40	(36/40)err	39/40	(39/40)err	39ArK moles	40Ar*%	Age (Ma)		err	w/o J
1	3.05E-04	7.64E-06	1.36E-02	3.57E-05	1.09E-15	91.0	401	±	7.3	1.3
2	4.84E-04	7.44E-06	1.21E-02	3.25E-05	1.10E-15	85.7	424	±	7.7	1.5
3	2.78E-04	1.06E-05	1.26E-02	3.43E-05	7.28E-16	91.8	432	±	7.9	1.7
4	1.71E-04	9.03E-06	1.25E-02	3.49E-05	8.96E-16	94.9	451	±	8.1	1.6
5	9.25E-04	3.53E-05	1.21E-02	5.18E-05	1.96E-16	72.6	365	±	8.3	5.0
6	5.30E-04	2.79E-05	1.21E-02	4.75E-05	2.52E-16	84.3	417	±	8.4	3.9
7	3.18E-04	1.92E-05	1.40E-02	4.20E-05	4.28E-16	90.6	388	±	7.4	2.4
8	1.79E-04	9.70E-06	1.25E-02	3.46E-05	8.04E-16	94.7	450	±	8.1	1.7
9	2.77E-04	1.23E-05	1.26E-02	3.42E-05	5.95E-16	91.8	433	±	7.9	1.9
10	5.43E-04	2.74E-05	1.13E-02	4.52E-05	2.40E-16	83.9	442	±	8.9	4.1
						Error Wtd. Mean Age:	419	±	2.5	
						39Ar Wtd. Mean Age:	425	±	2.5	

FIGURES FOR CHAPTER 4

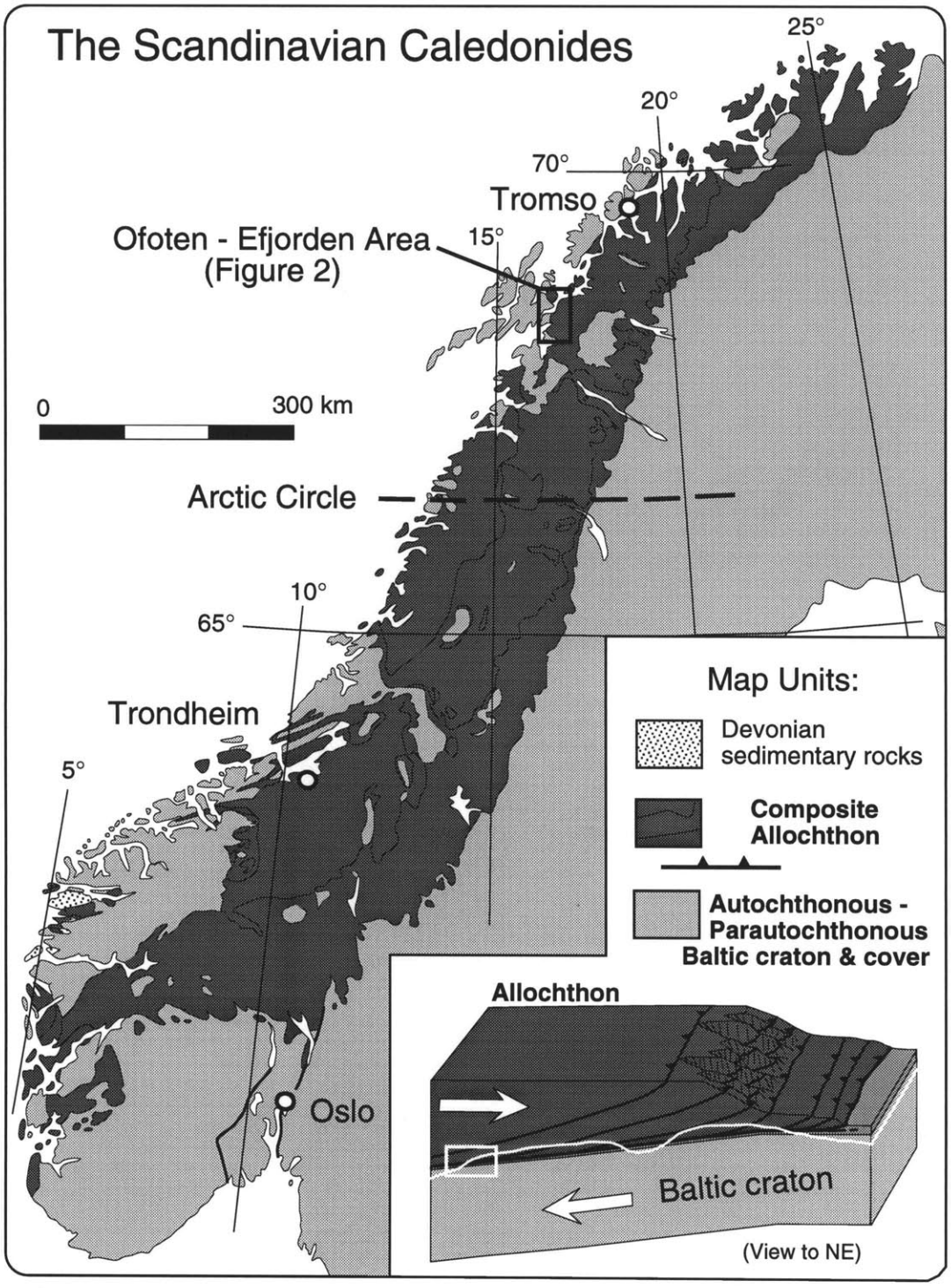

Figure 1: Simplified geologic map of the Scandinavian Caledonides, showing the distribution of the erosional remnant of the Caledonian allochthon (modified from Gee et al., 1985). Inset shows a schematic block diagram (not to scale) illustrating A-type subduction of the Baltic craton beneath the composite allochthon during the Caledonian collision. The white line shows the approximate level of exposure today, and the white box indicates the general structural position inferred for rocks in the study area during the collision.

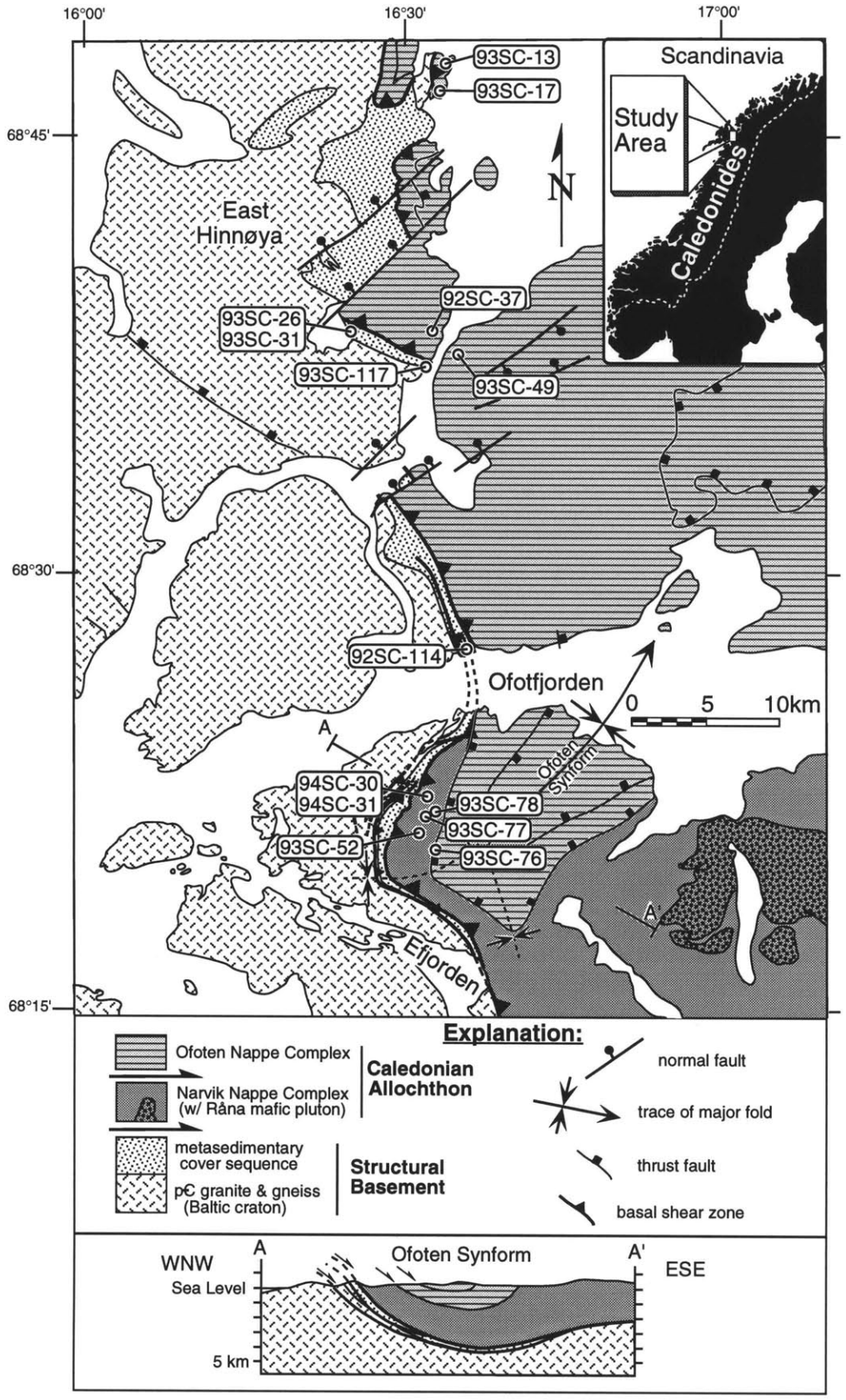

Figure 2: Simplified geologic map of the Ofoten-Efjorden area. (compiled from Gustavson, 1974; Bartley, 1980; Hodges, 1982; Steltenpohl, 1983, 1985; and Northrup, unpublished mapping). Lables indicate locations of samples used for U-Pb and 40Ar/39Ar geochronology.

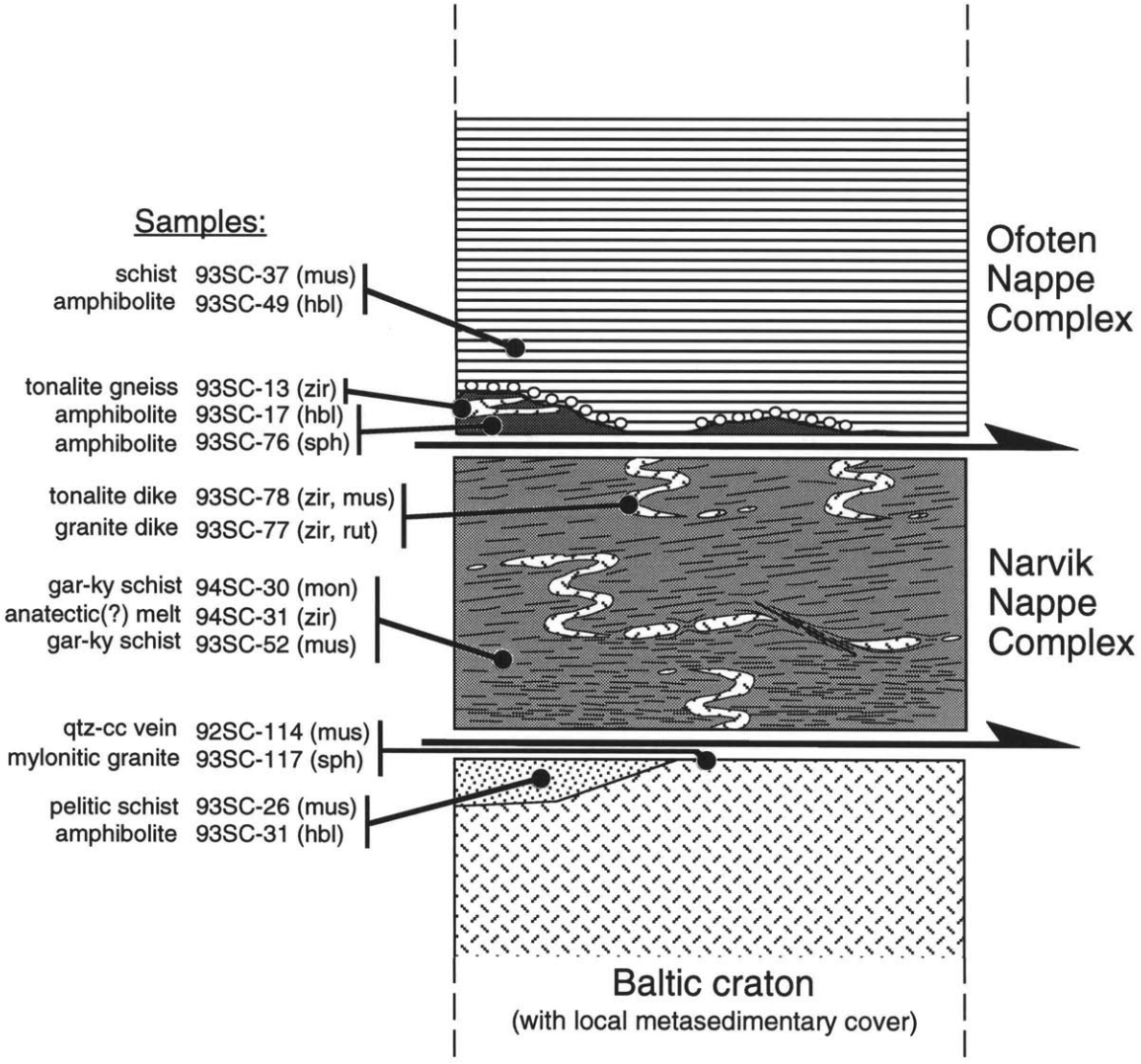

Figure 3: Schematic tectonostratigraphic column showing the relative structural positions of samples analyzed for U-Pb and 40Ar/39Ar geochronology.

Table 1: Previous age constraints from deep levels of the allochthon in the region

source	mineral	method	age (Ma)	interpretation
1	hornblende	40Ar/39Ar	< 425	cooling age
1	hornblende	40Ar/39Ar	387 ± 4	dynamic recrystallization, basal thrust
2	hornblende	40Ar/39Ar	ca. 405	cooling age
2	hornblende	40Ar/39Ar	ca. 405	cooling age
2	hornblende	40Ar/39Ar	ca. 411	cooling age
1	muscovite	40Ar/39Ar	370 ± 3	cooling age
2	muscovite	40Ar/39Ar	395 ± 2	cooling age
2	muscovite	40Ar/39Ar	387 ± 2	cooling age
2	muscovite	40Ar/39Ar	ca. 400	cooling age
1	biotite	40Ar/39Ar	358 ± 3	cooling age
6	biotite	K-Ar	377 ± 16	cooling age
6	biotite	K-Ar	369 ± 16	cooling age
3	biotite	Rb-Sr	358 ± 4	cooling age
3	biotite	Rb-Sr	361 ± 3	cooling age
5	sphene	U-Pb	395 ± 5	dynamic recrystallization, basal thrust
4	zircon	U-Pb	437 ± 2	crystallization age, Råna mafic complex

sources of previous ages: (1) Tilke, 1986; (2) Coker et al. 1995; (3) Bartley, 1981; (4) Tucker et al. 1990; (5) Gromet and Andresen, 1993; (6) Hodges, 1982

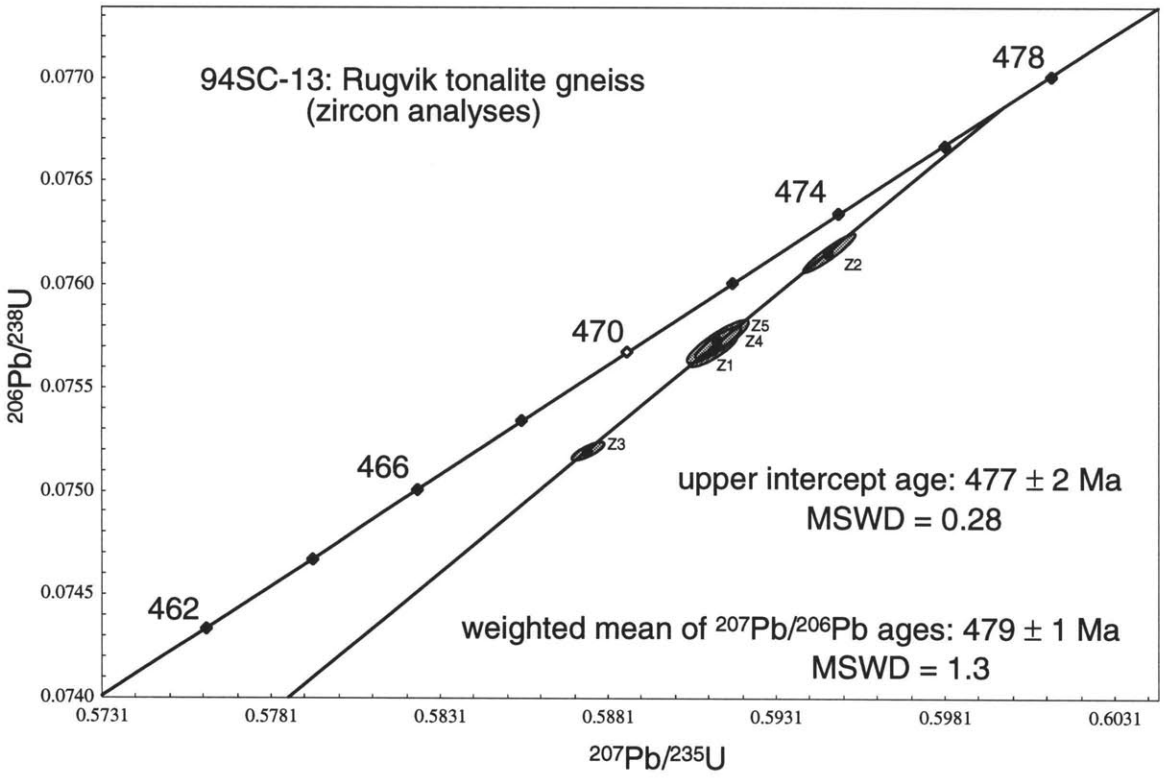

Figure 4: Concordia plot of zircon analyses from the Rugvik tonalite gneiss (sample 93SC-13).

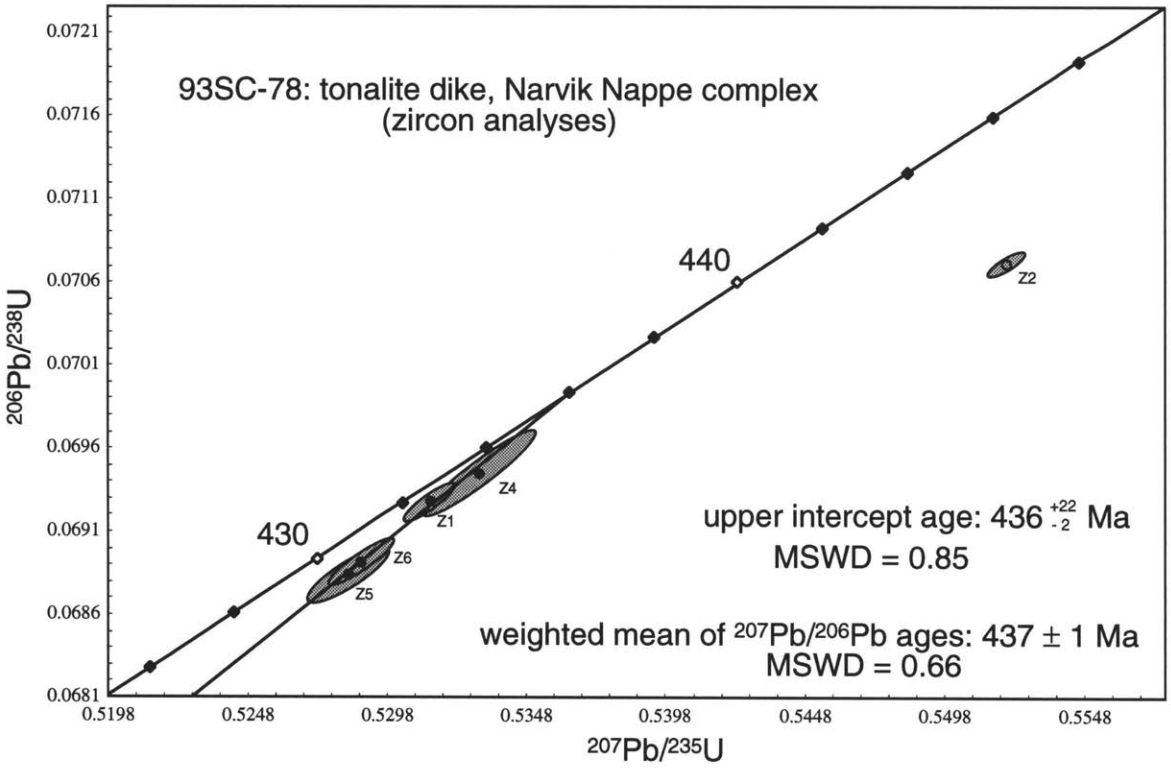

Figure 5: Concordia plot of zircon analyses from a deformed tonalite dike in the Narvik Nappe Complex (sample 93SC-78). Ages calculated exclude point Z2 which is inferred to contain an inherited component of older zircon.

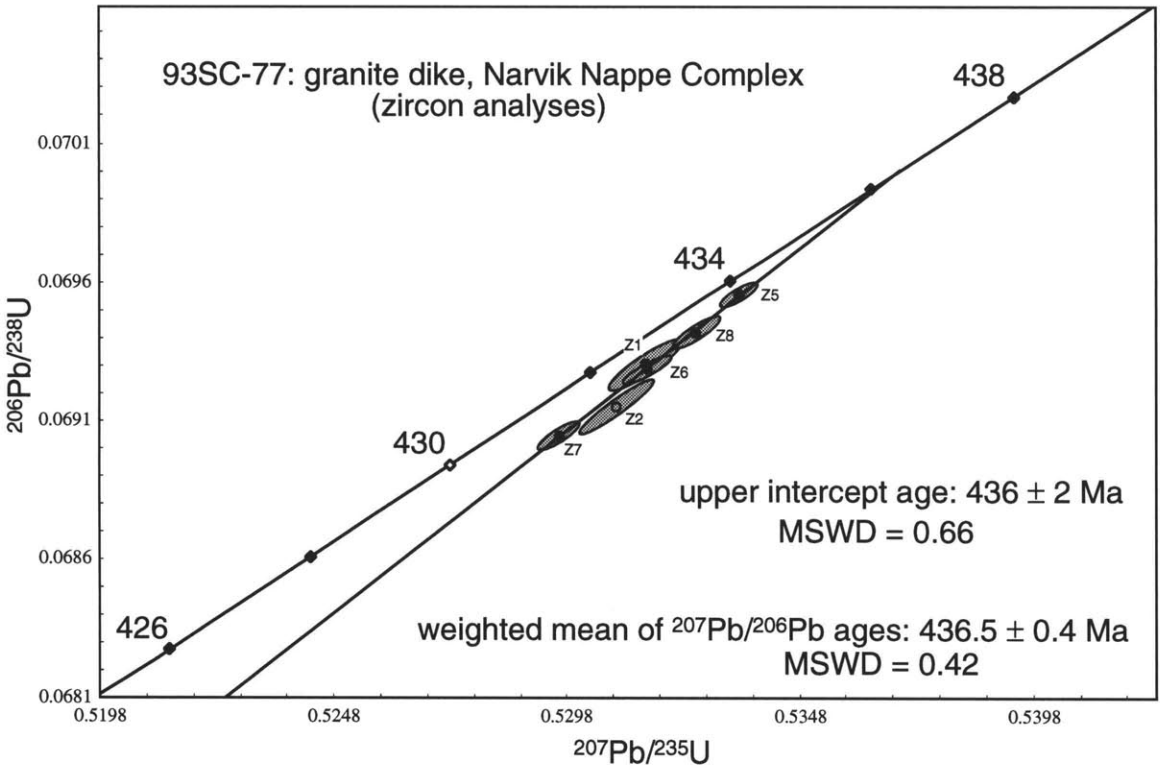

Figure 6: Concordia plot of zircon analyses from a deformed granite dike in the Narvik Nappe Complex (sample 93SC-77).

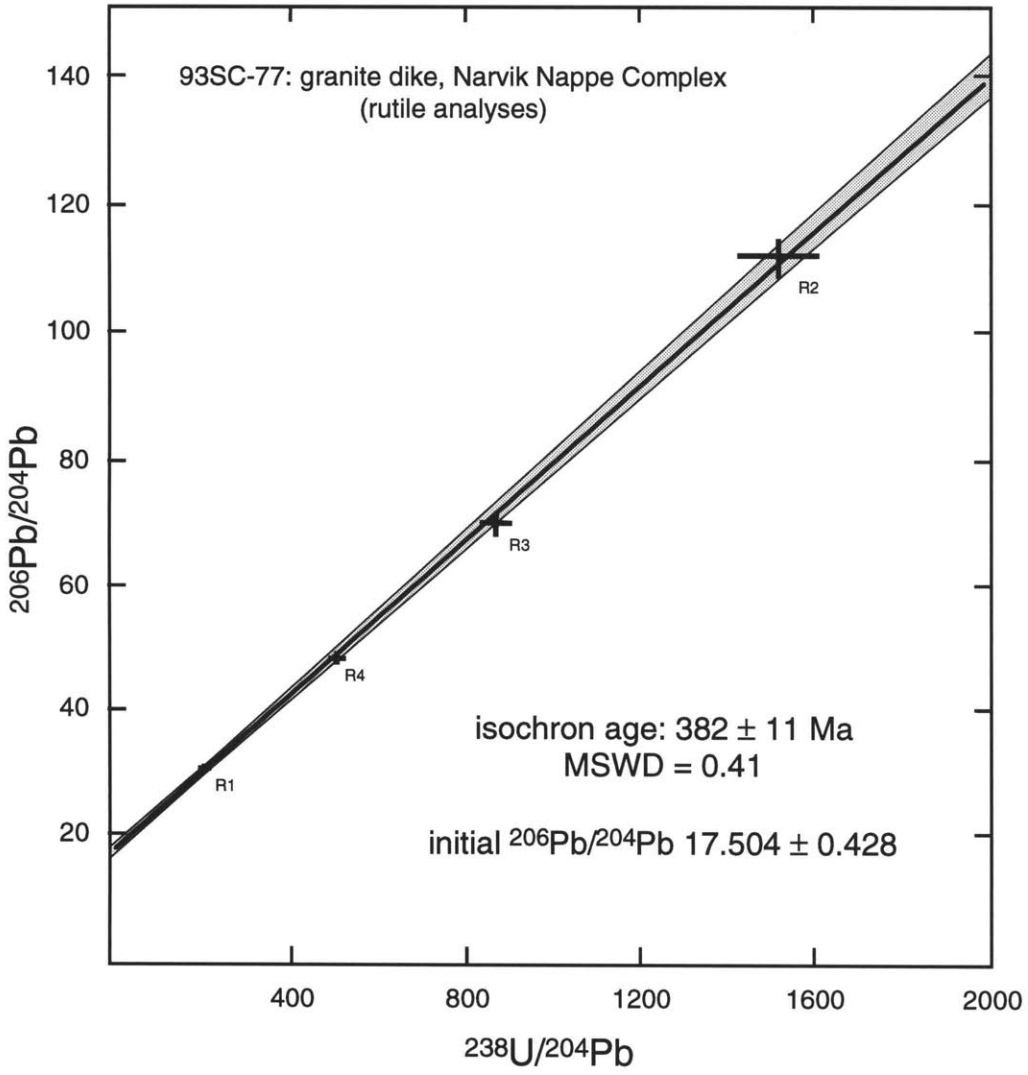

Figure 7: isochron plot of U-Pb analyses of rutile from a granite dike in the Narvik Nappe Complex.

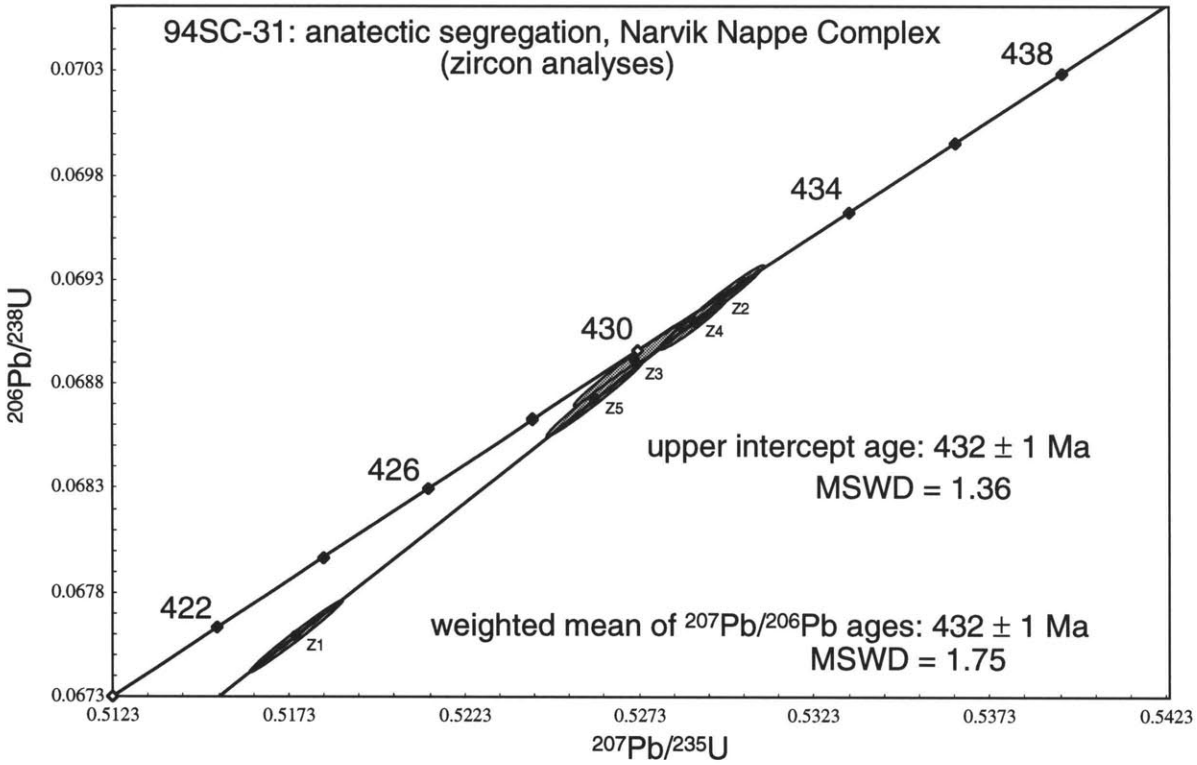

Figure 8: Concordia plot of zircon analyses from a granitic segregation interpreted as the product of local anatexis in garnet-kyanite schist of the Narvik Nappe Complex.

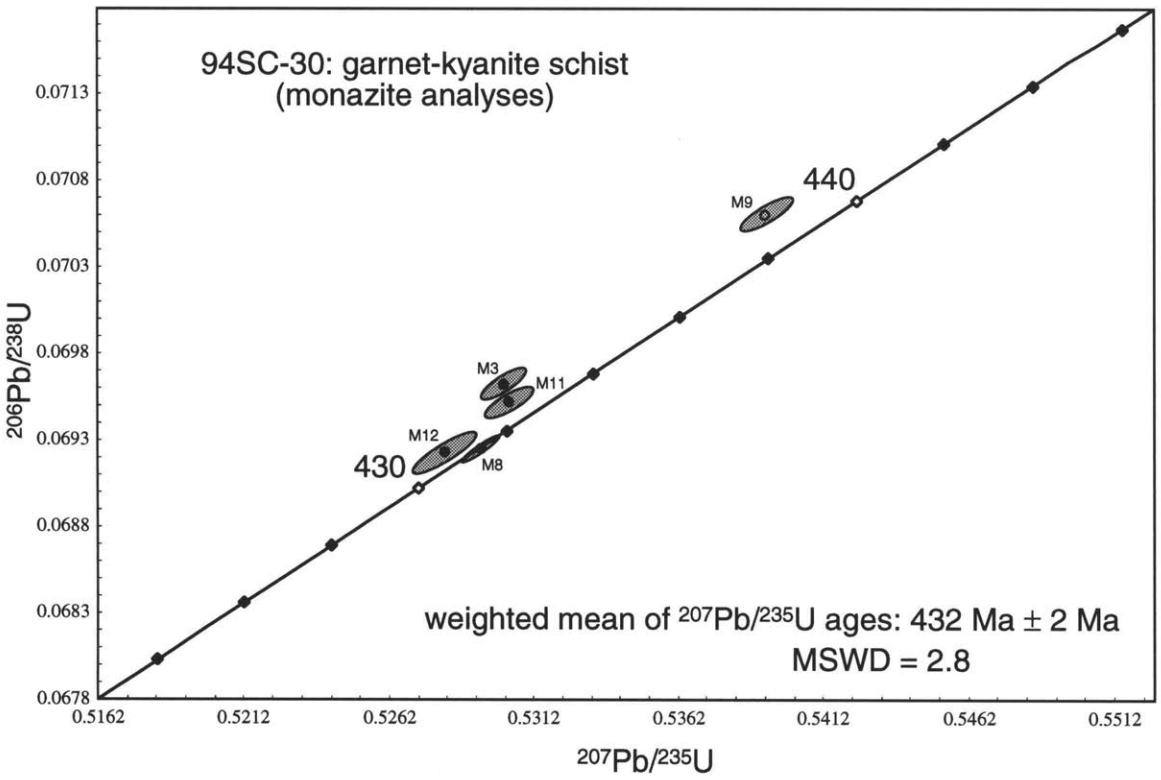

Figure 9: Concordia plot of monazite from garnet-kyanite schist in the Narvik Nappe Complex (sample 94SC-30). The weighted mean age shown excludes point M9 which may contain an inherited(?) component. Inclusion of M9 in the weghted mean yields and age of 433 ± 4 Ma, with and MSWD of 68.

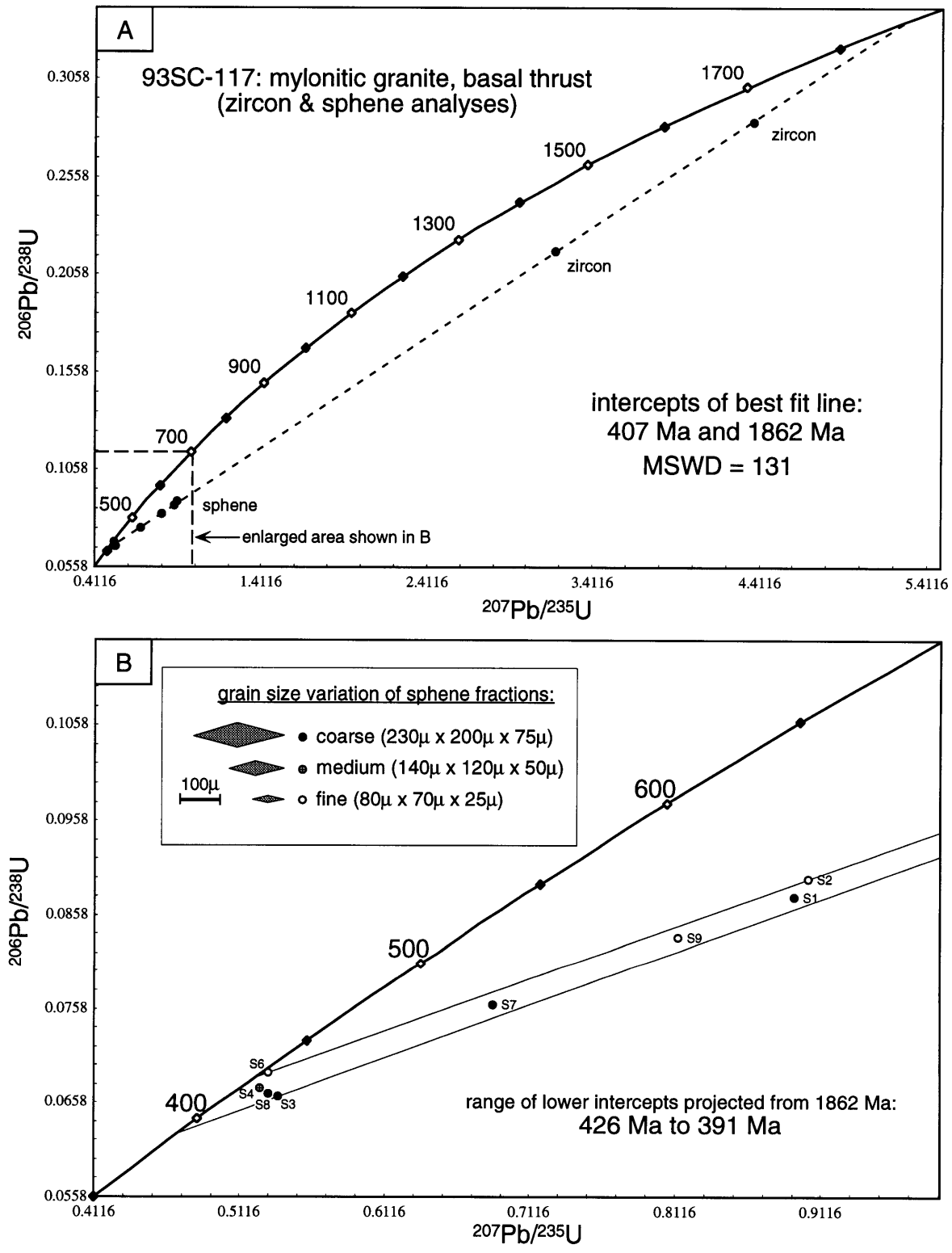

Figure 10: Concordia plot of sphene and zircon analyses from mylonitic Proterozoic granite in the basal shear zone of the Caledonian allochthon. Analytical uncertainties are smaller than the dots used for symbols. Figure A) shows all the data; figure B) shows an enlarged view of the sphene data which all plot near the lower intercept. See text for discussion and possible interpretation.

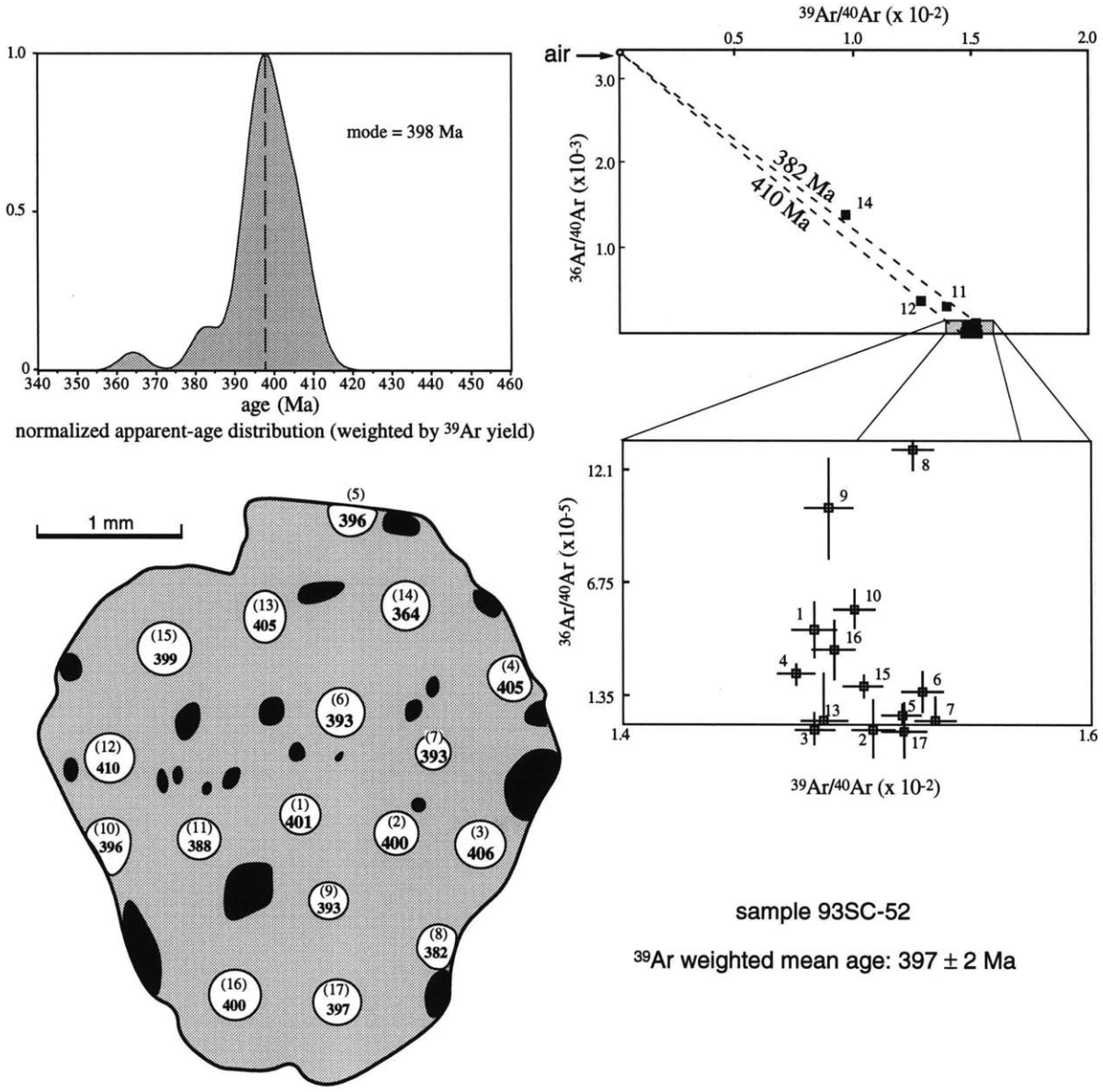

Figure 11: Results of 40Ar/39Ar laser microprobe analyses of a muscovite grain from garnet-kyanite schist of the Narvik Nappe Complex. The circular areas in the sketch of the grain show the regions fused and/or significantly disrupted by the analyses; the numbers in parentheses correspond to the analysis number, and those in bold correspond to the age (Ma) determined from the isotopic composition of Ar released from each spot. Black areas indicate locations of biotite inclusions within the muscovite.

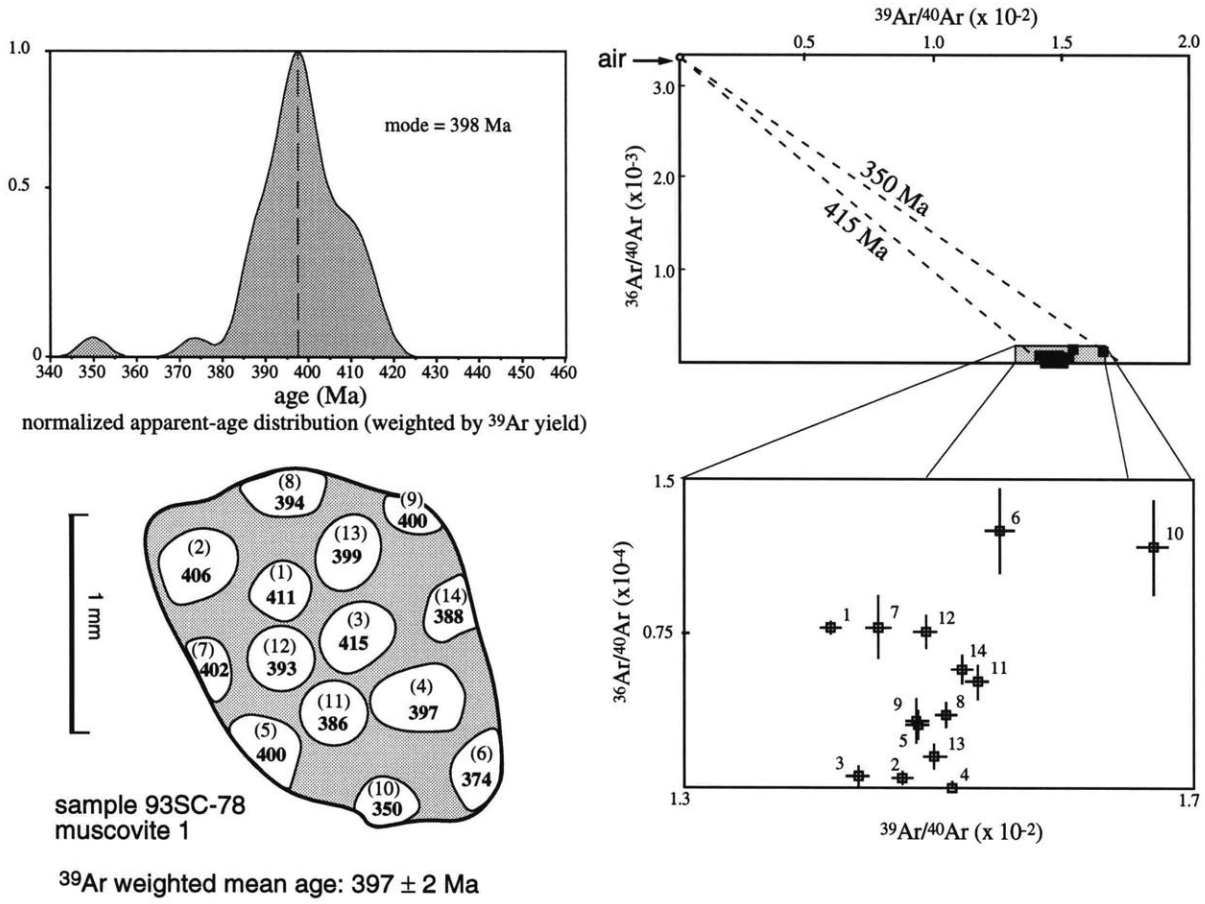

Figure 12: Results of Ar laser microprobe analysis of a muscovite grain from a felsic dike in the Narvik Nappe Complex (sample 93SC-78, muscovite 1). The circular areas in the grain sketch show the regions fused and/or significantly disrupted by the analyses; the numbers in parentheses indicate the analysis number, and those in bold give the age (Ma) determined from the isotopic composition of Ar released from each spot.

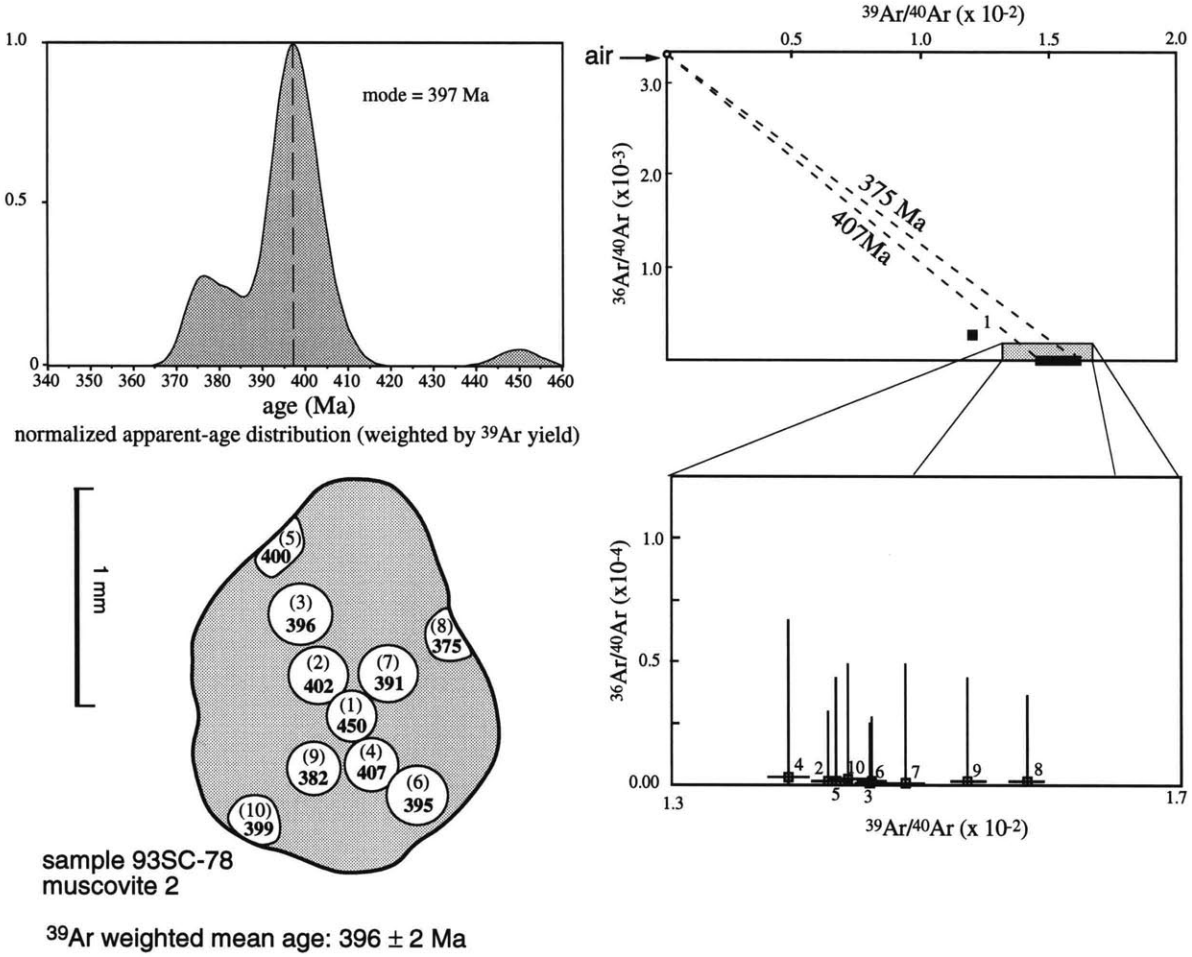

Figure 13: Results of Ar laser microprobe analysis of a muscovite grain from a felsic dike in the Narvik Nappe Complex (sample 93SC-78, muscovite 2). The circular areas in the grain sketch show the regions fused and/or significantly disrupted by the analyses; the numbers in parentheses indicate the analysis number, and those in bold give the age (Ma) determined from the isotopic composition of Ar released from each spot.

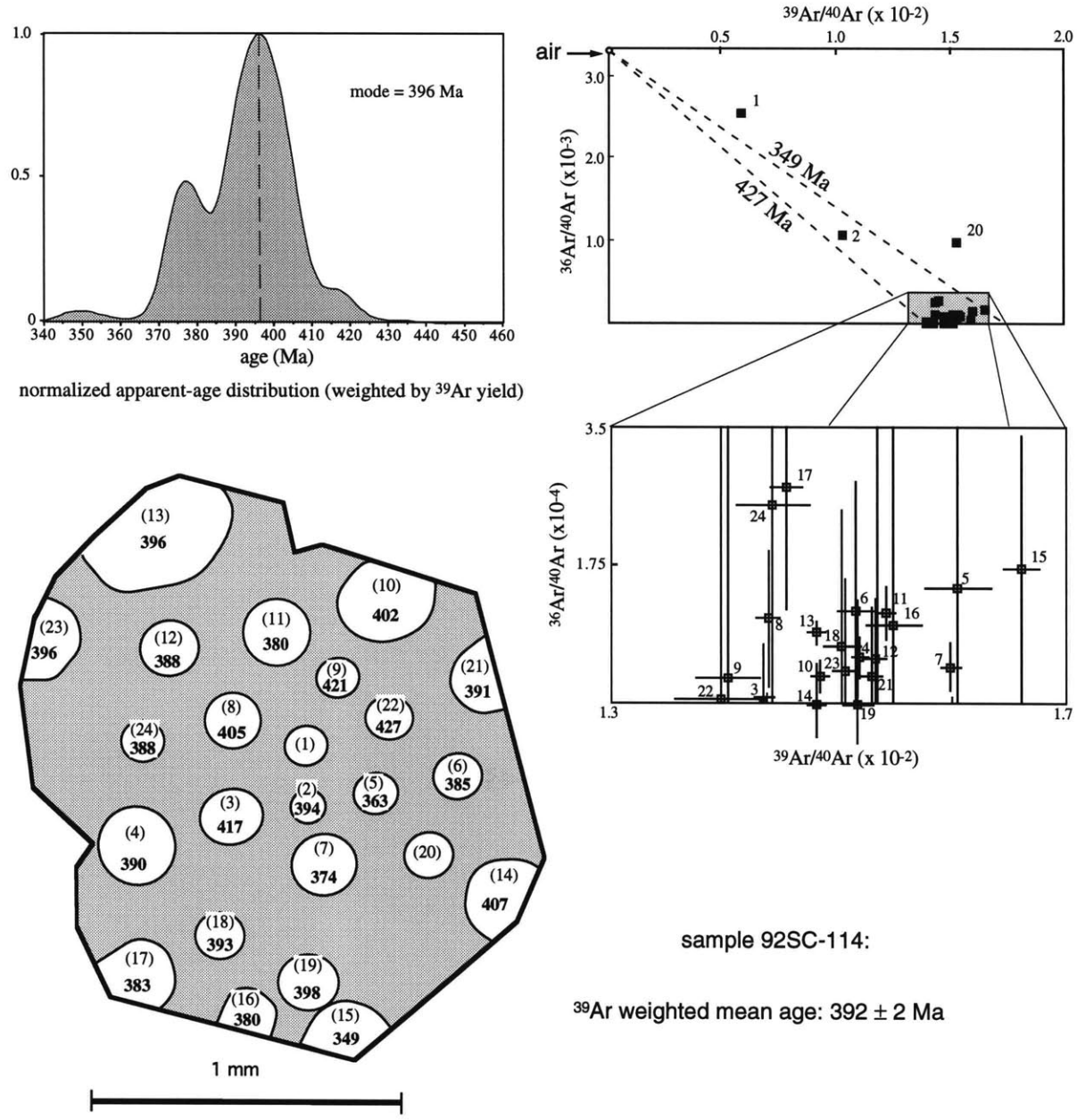

Figure 14: Results of 40Ar/39Ar laser microprobe analyses of a muscovite grain from a quartz-calcite-plagioclase-muscovite vein in the metasedimentary cover of Baltica, in the footwall of the basal shear zone. The circular areas in the sketch of the grain show the regions fused and/or significantly disrupted by the analyses; the numbers in parentheses designate the analysis number, and those in bold give the age (Ma) determined from the isotopic composition of Ar released from each spot.

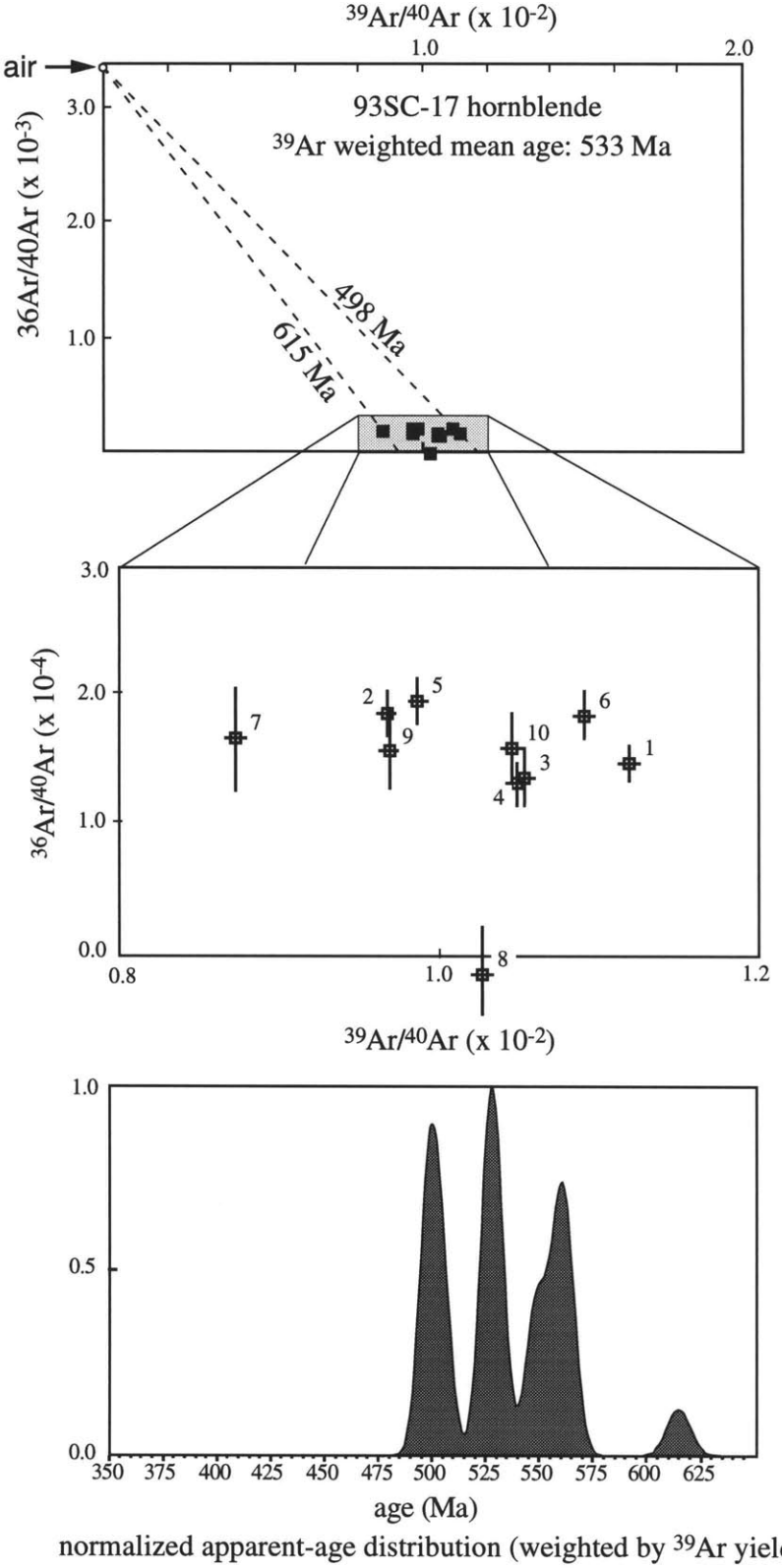

Figure 15: Results of hornblende total fusion analyses, sample 93SC-17.

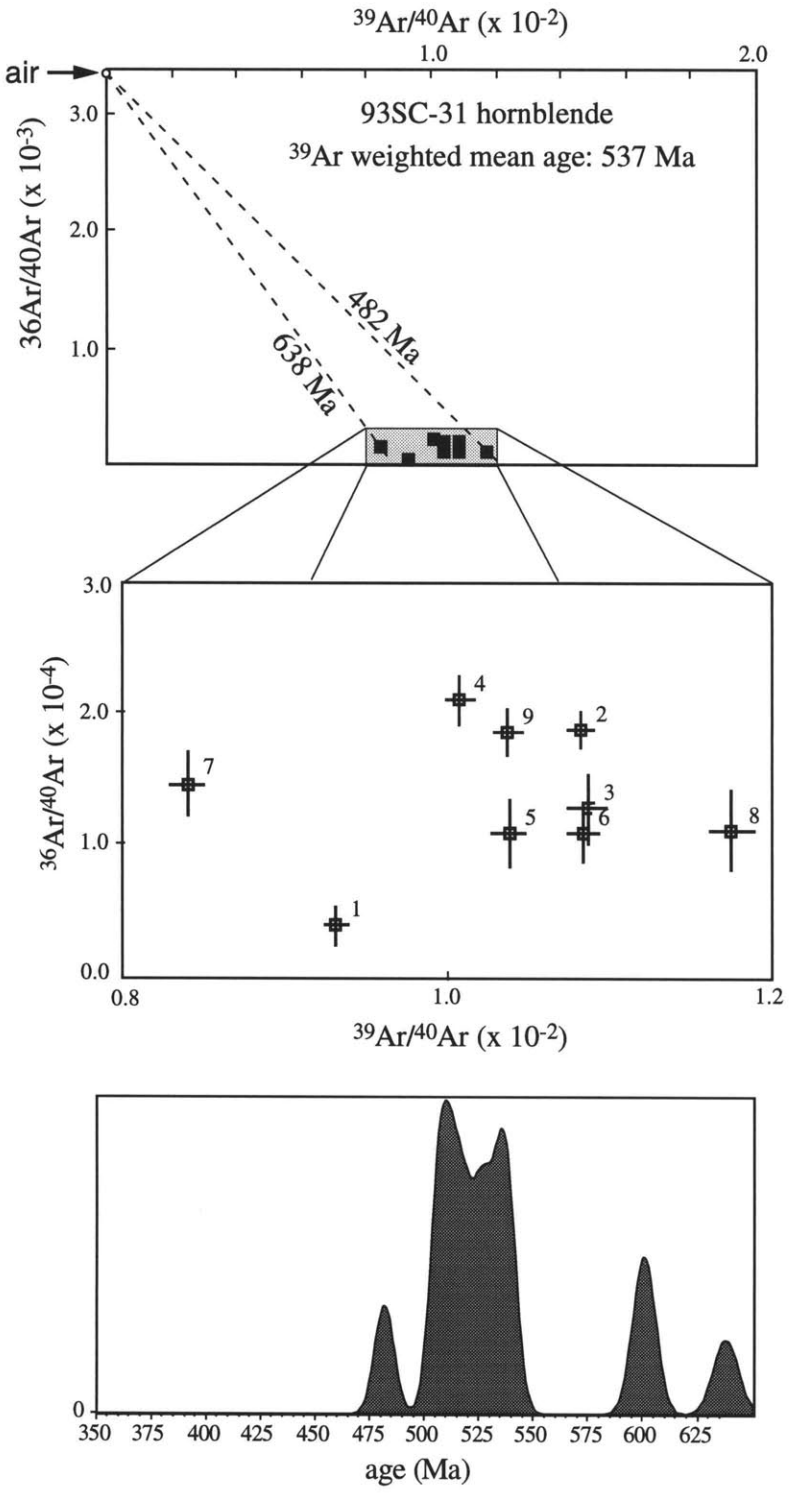

Figure 16: Results of hornblende total fusion analyses, sample 93SC-31.

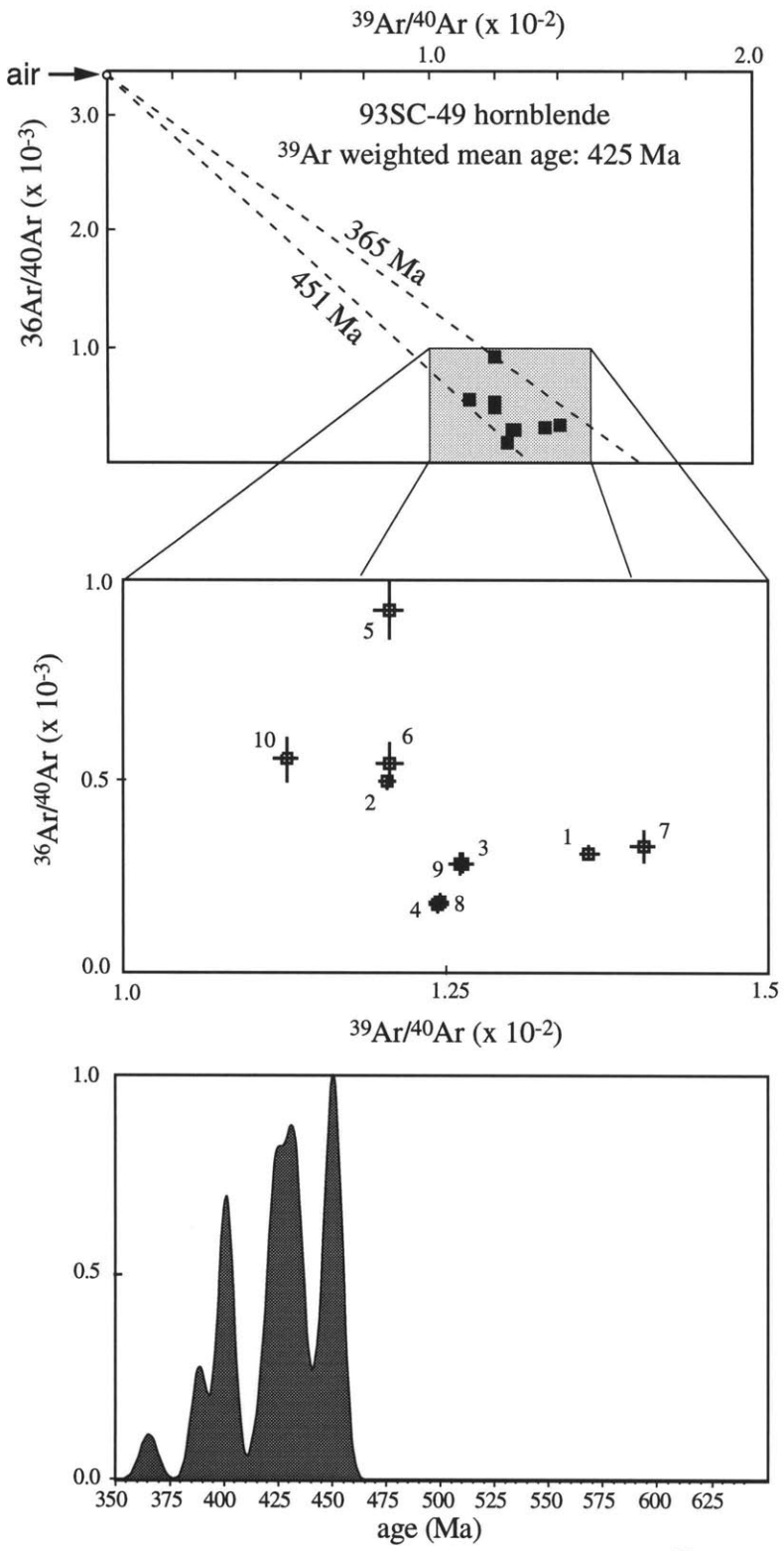

Figure 17: Results of hornblende total fusion analyses, sample 93SC-49.

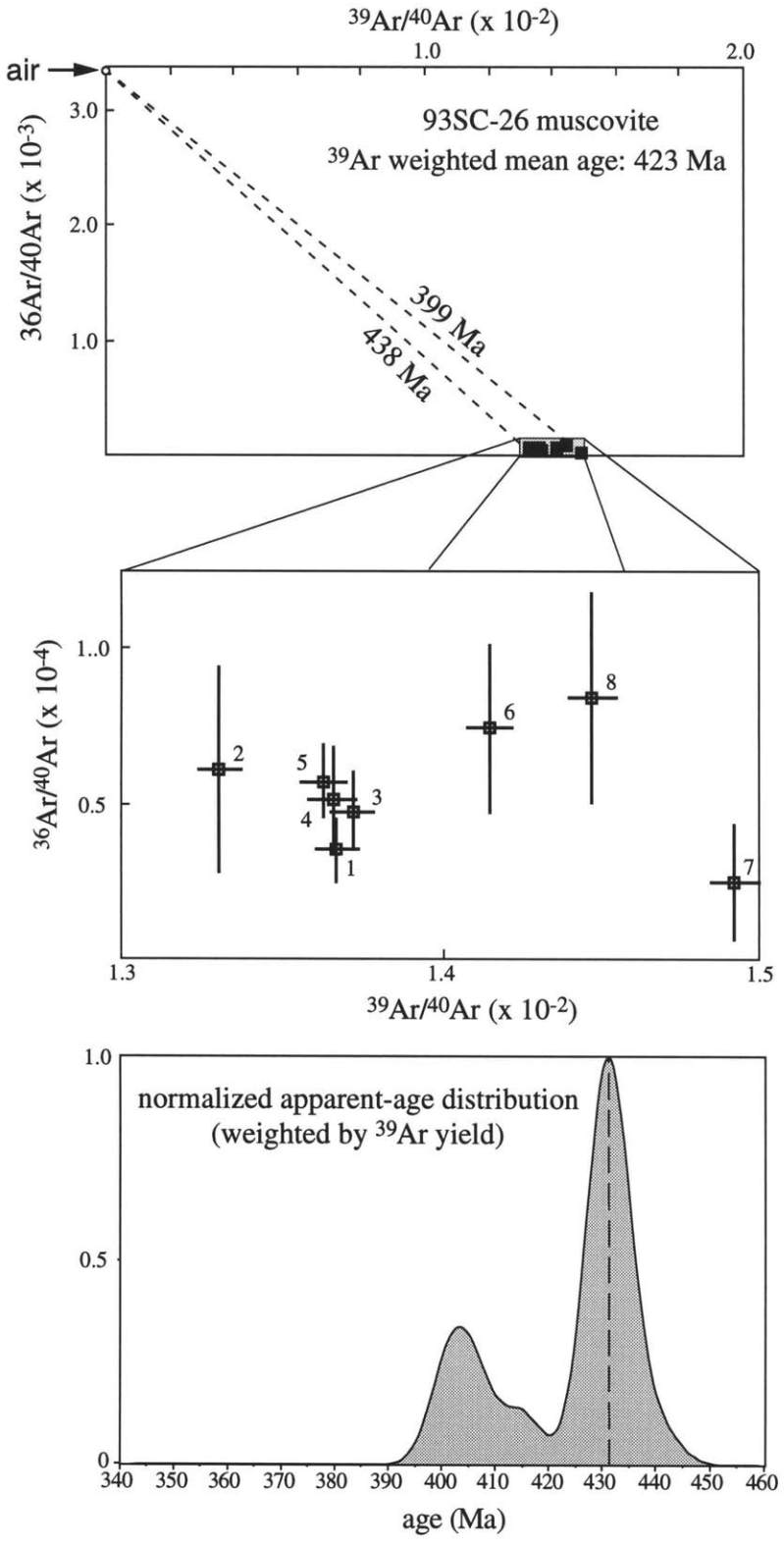

Figure 18: Results of muscovite total fusion analyses, sample 93SC-26.

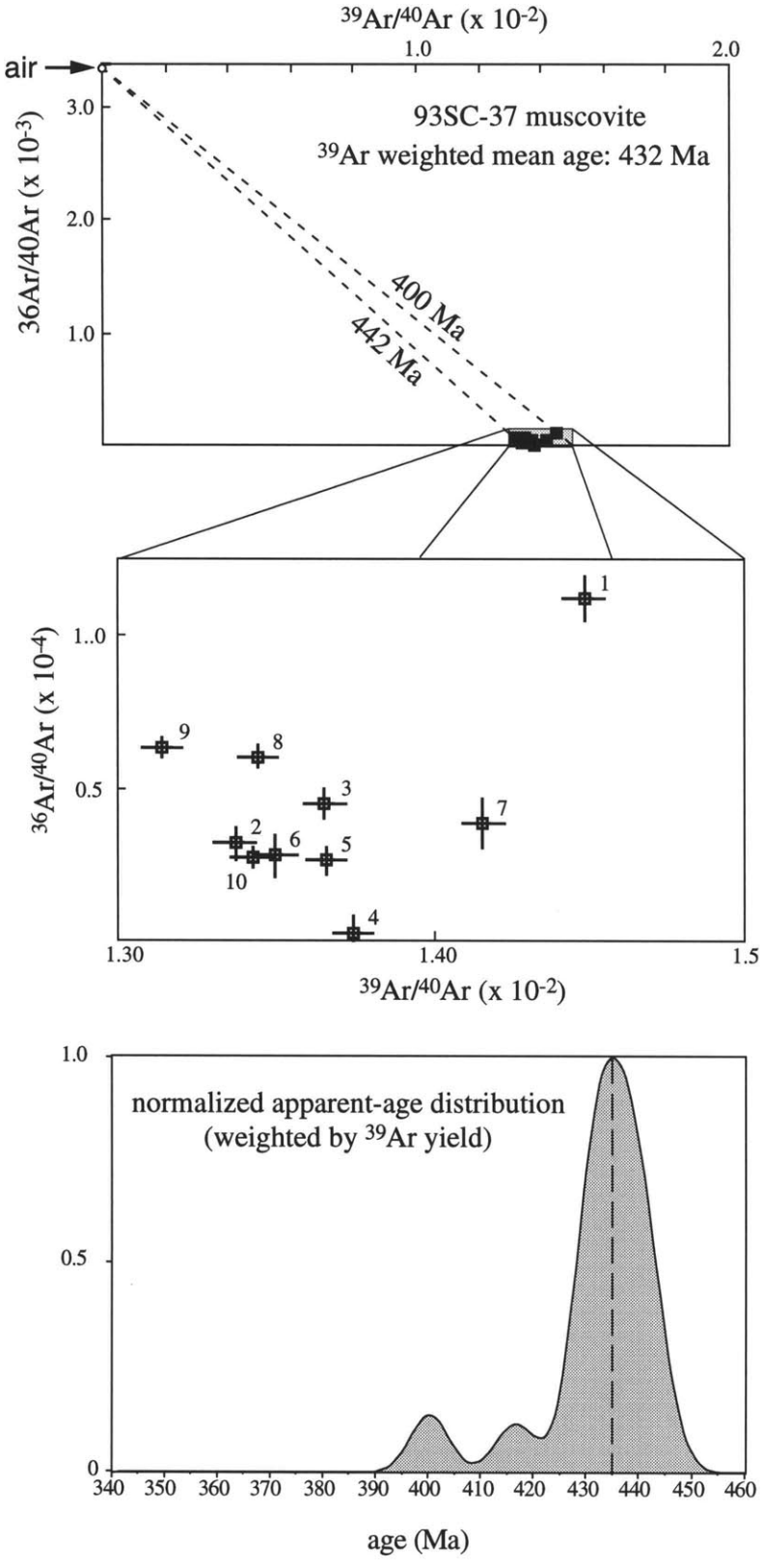

Figure 19: Results of muscovite total fusion analyses, sample 93SC-37.

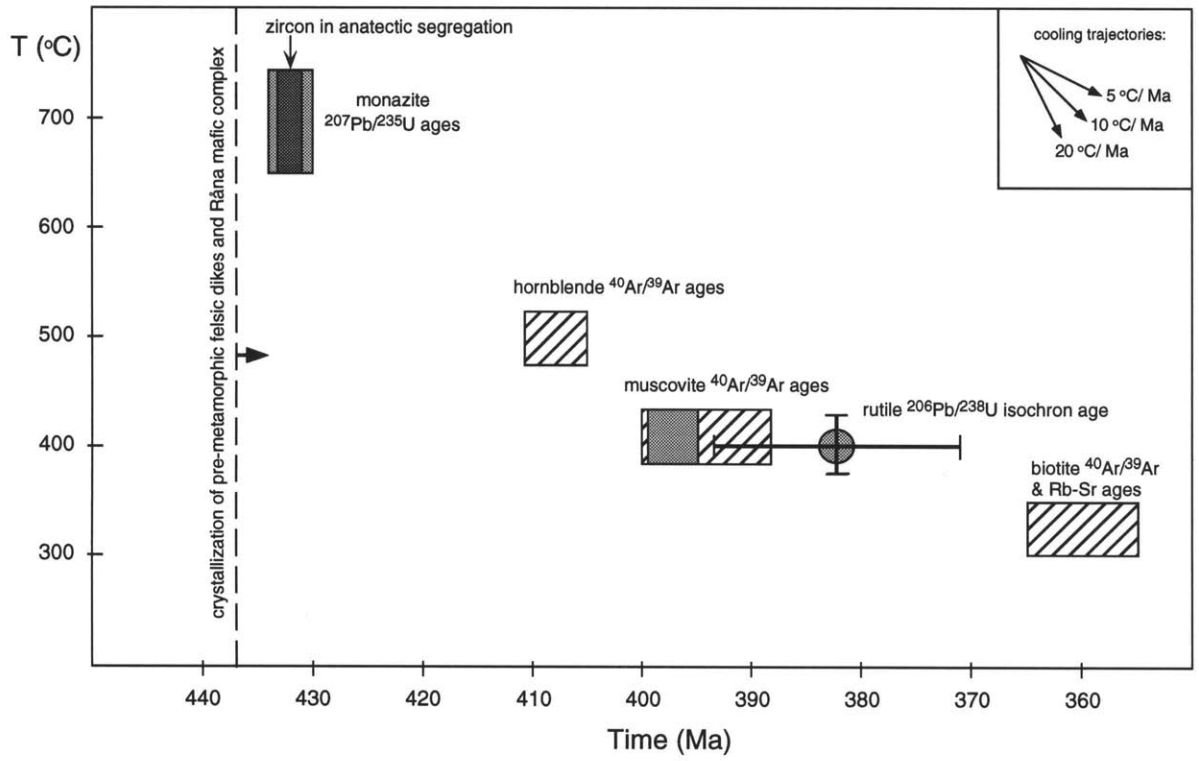

Figure 20: Synthesis of constraints on the age of metamorphism and cooling of rocks at deep levels of the Caledonian allochthon in the western Ofoten region. Shaded boxes indicate constraints from this study; hatchered boxes show the range of ages previously determined for samples collected at the same general structural level within the region. Previously determined 40Ar/39Ar ages are from Coker et al. (1995) and Tilke (1986); Rb-Sr biotite ages are from Bartley (1981). Nominal closure temperatures for the K-Ar isotopic system in hornblende, muscovite and biotite, the U-Pb system in rutile, and the Rb-Sr system in biotite are from Hodges (1991) and references therein. The temperature ranges given for hornblende, muscovite, rutile, and biotite reflect an arbitrary uncertainty of ±25 °C about the nominal value. The temperature range shown for monazite and zircon indicates the range in estimates for peak metamorphic conditions achieved by rocks within the allochthon from petrogenetic constraints and quantitative thermobarometry (Hodges and Royden, 1984; Steltenpohl and Bartley, 1987). Crystallization ages of pre-metamorphic felsic dikes are from this study and the crystallization age of the Råna mafic complex is from Tucker et al. (1990).

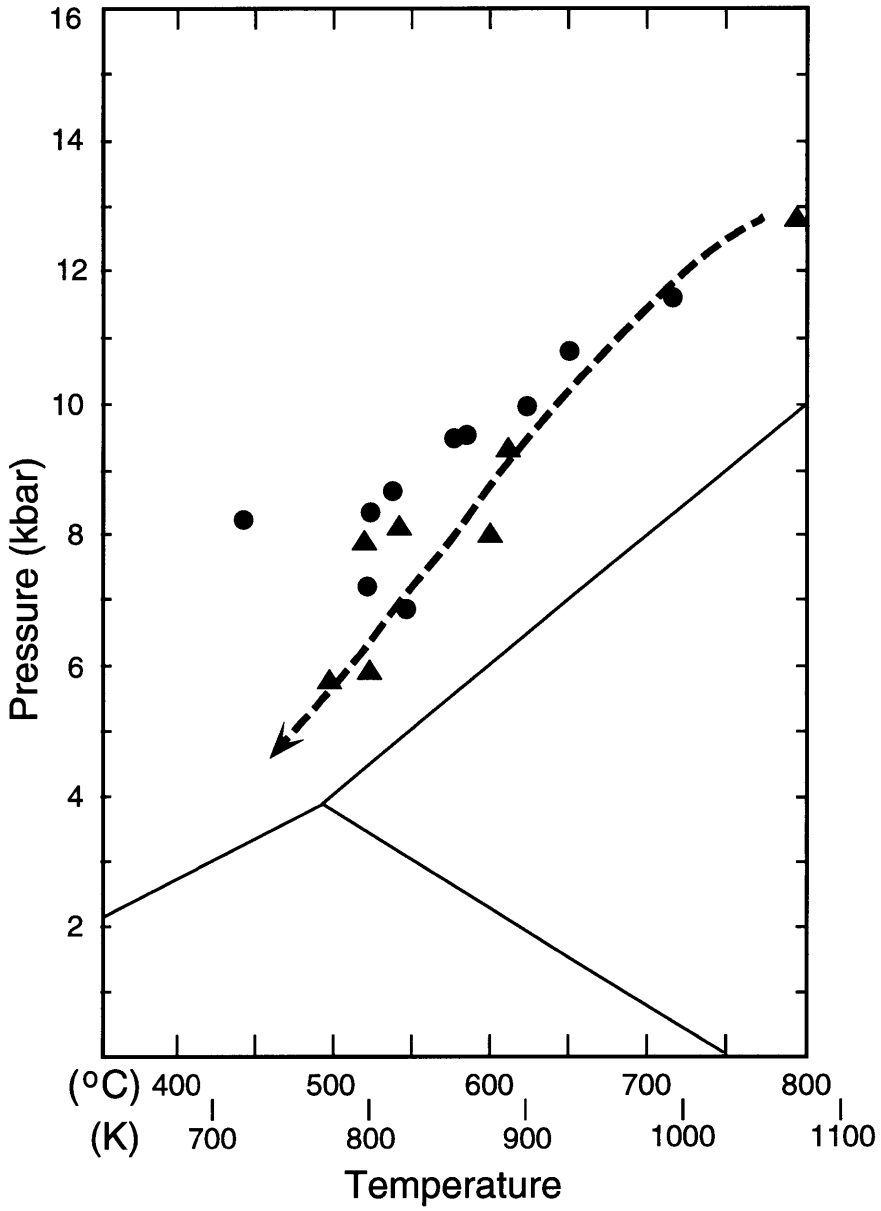

Figure 21: P-T data from the Caledonian allochthon in the western Ofoten region. Circles show P-T estimates recalculated from the data of Steltenpohl and Bartley (1987); triangles show P-T estimates recalculated from the data of Hodges and Royden (1984). Dashed arrow illustrates a general P-T path for rocks within the allochthon consistent with the data.

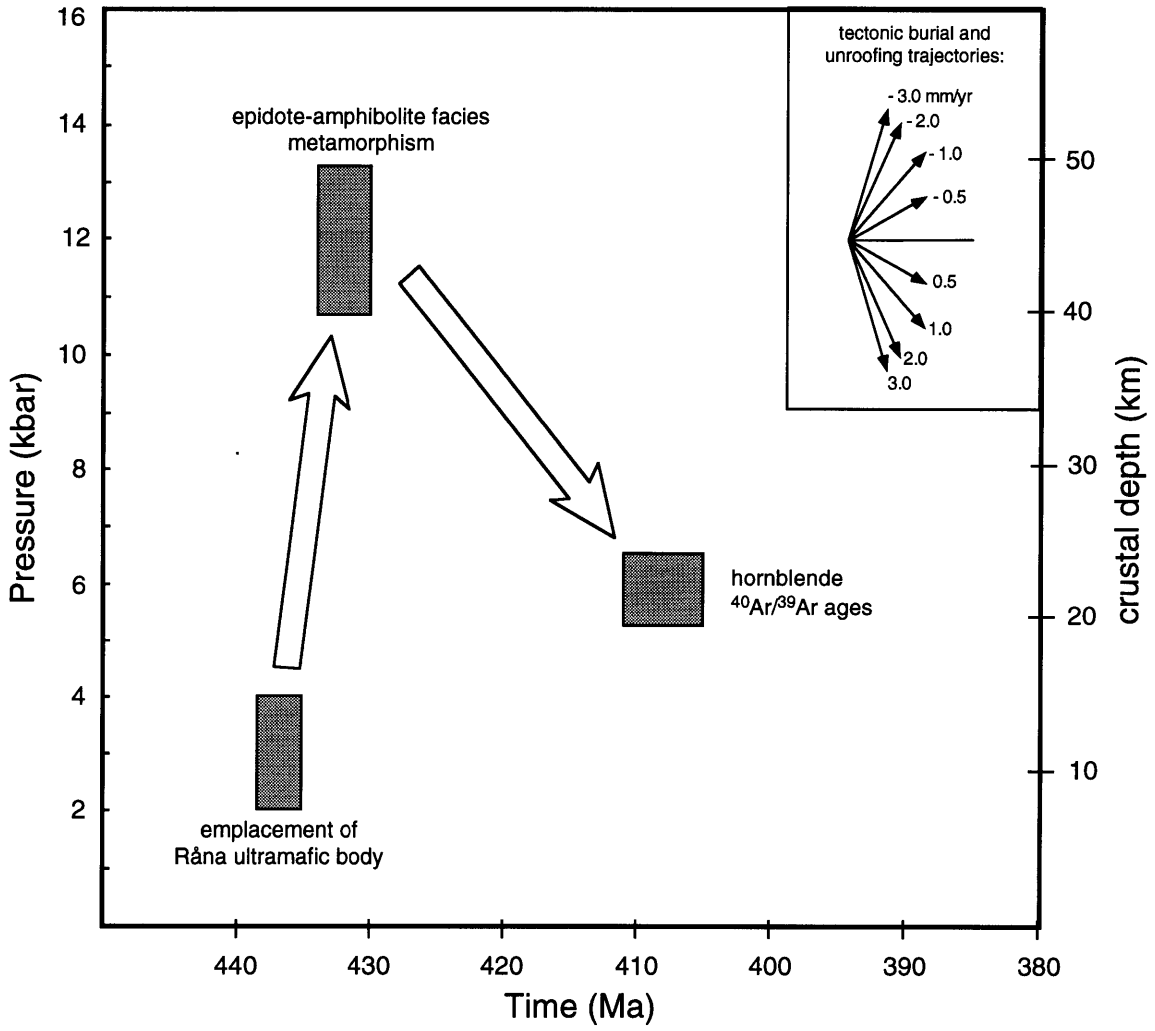

Figure 22: Depth-time path followed by rocks in the Narvik Nappe Complex based on: 1) the age and estimated depth of emplacement of the Råna ultra mafic body (Tucker et al. 1990); 2) the T-t information shown in figure 21; and 3) the general P-T path inferred for rocks in the Narvik Nappe Complex shown in figure 21. Crustal depths assume an average density of 2.75g/cc for the crustal column, corresponding to a depth change of c.a. 3.7 km / kbar.

Chapter 5

P-T-Deformation history of the footwall of the Caledonian A-type subduction zone, Ofoten-Efjorden, north Norway

INTRODUCTION

The Caledonian orogen in Scandinavia is an outstanding example of a deeply eroded collisional mountain belt, and it provides an opportunity to examine directly the geologic record of tectonic processes characteristic of middle to deep crustal levels of a continent-continent collision zone (Fig. 1). Mid-Paleozoic closure of the Iapetus Ocean basin culminated with the collision of Baltica and Laurentia and, as a consequence of the collision, a crustal-scale allochthon was thrust eastward onto the western margin of Baltica (Harland and Gayer, 1972; Gee and Wilson, 1974; Stephens and Gee, 1989). The overall structural geometry of the collision may be viewed as a continental (or A-type) subduction zone, in which the Caledonian allochthon formed the upper plate and the Baltic margin formed the lower plate (Gee, 1975; Hodges et al., 1982). As the margin of the Baltic craton was subducted, most of its early Paleozoic sedimentary cover was accreted to the leading edge of the allochthon. Local remnants of the cover, however, remained attached to the craton and were carried with the lower plate to significant crustal depths. The metamorphism and deformation of these metasedimentary remnants provides a record of the movement of the lower plate through the Caledonian A-type subduction system.

The Ofoten-Efjorden region of north Norway contains exposures of the basal portion of the Caledonian allochthon and the upper portion of the subducted Baltic craton with part of its parautochthonous metasedimentary cover (Figures 1 & 2). This paper describes the metamorphic and deformational characteristics of the metasedimentary cover in the footwall of the Caledonian A-type subduction zone in the Ofoten-Efjorden area, and uses this information to interpret aspects of the tectonic evolution of the orogen at this latitude.

GEOLOGY OF OFOTEN-EFJORDEN

Ofoten-Efjorden is located along the west coast of Norway, approximately 200 km north of the Arctic circle (Figures 1 & 2). Rocks in the region comprise two fundamental tectonostratigraphic packages: (1) the composite Caledonian allochthon, and (2) the parautochthonous structural basement. Far-traveled thrust sheets of schist, marble, and amphibolite compose the allochthon. The Precambrian Baltic craton and part of its early Paleozoic metasedimentary cover form the structural basement onto which the Caledonian allochthon was emplaced.

Late- to post-Caledonian NE-trending folds and NW-trending cross-folds control the general pattern of lithologic contacts in the area (Hodges, 1985; Steltenpohl and Bartley, 1988). One of the most significant folds in the region is the Ofoten Synform, a broad, gently NE-plunging structure cored by rocks of the Caledonian allochthon and flanked by exposures of the structural basement. In the western limb of the Ofoten synform, the structural section has been rotated into a moderately E-dipping orientation, such that the geologic map of this part of the region provides an oblique cross-sectional

view through the lower part of the allochthon and the upper part of the structural basement. The metamorphosed cover of Baltica forms a persistent sequence of outcrops in the footwall of the basal thrust of the allochthon in this portion of the fold.

Caledonian Metamorphism

Several studies have examined the metamorphic characteristics of rocks in the Caledonian allochthon in the Ofoten-Efjorden region. For example, Hodges and Royden (1984) used quantitative thermobarometric analyses of variably retrograded samples from the allochthon near Efjorden to reconstruct part of the unroofing and cooling path followed by rocks at this structural level. Their data define a trend in P-T space from peak conditions of ca. 750-800°C, 13 kbar down to retrograde conditions of near 500°C, 6 kbar. Steltenpohl and Bartley (1987) generated an array of P-T estimates from samples collected along a profile through the nappe stack north of Ofotfjord. Thermobarometric estimates from their samples plot as a trend overlapping that of Hodges and Royden (1984) from ca. 700°C and 11-12 kbar, to about 500°C and 7 kbar, with no clear correlation between P-T estimate and structural level within the nappe stack. Steltenpohl and Bartley (1987) interpreted the variability in their P-T estimates as the result of several factors, including correlated effects of uncertainties in mineral compositions and potential polymetamorphism of rocks in part of the nappe complex. Although some aspects of the metamorphic history in the allochthon remain controversial (e.g., the possibility of earlier metamorphism in some nappes), all workers agree that deep levels of the allochthon attained conditions of at least 625°C, 9 kbar during the culmination of the Caledonian collision in mid-to-late Silurian time.

In contrast to the metamorphism in the allochthon, the Caledonian P-T evolution of the parautochthonous structural basement has received comparatively little quantitative study. Evaluation of Caledonian metamorphism in the basement is hampered by the presence of mineral assemblages inherited from Precambrian amphibolite to granulite facies metamorphism in some rocks of the Baltic craton (e.g., Griffin and Heier, 1969). Consequently, distinguishing the products of Caledonian metamorphism from Precambrian metamorphism can be difficult in the cratonal portion of the structural basement. This problem may be circumvented by examining rocks that post-date the Precambrian tectonism in the craton and, therefore, record only the Caledonian event. Bartley (1980) identified a laterally persistent sequence of quartzite, impure marbles, psammitic and pelitic schists above the cratonal basement of Baltica and structurally beneath the thrust sheets in the Caledonian allochthon on east Hinnøya. He interpreted these metasedimentary rocks as remnants of the early-Paleozoic sedimentary cover on Baltica and estimated Caledonian metamorphic condition in the amphibolite facies (ca. 550-700°C, 5-9 kbar) based on mineral assemblages. However, Björklund (1987) re-examined locally the basement-cover relations on East Hinnøya and interpreted differently the structure, tectonostratigraphy, and grade of metamorphism. Björklund regarded most of Bartley's metasedimentary cover as far-traveled oceanic affinity rocks within the Caledonian allochthon, and interpreted quartzite, "greenschist facies" mica schists, and amphibolite at deeper structural levels as the early Paleozoic cover on Baltica. The present study explores in more detail the metamorphic and deformational history of the metasedimentary cover on the deeply subducted Baltic craton.

FIELD RELATIONSHIPS

This section first gives lithologic descriptions of the metasedimentary rocks inferred to be early Paleozoic cover on Baltica, and then presents observations bearing on the viability of Björklund's (1987) alternative interpretation of basement-cover relations on East Hinnøya.

Stratigraphy of the Metasedimentary Cover

Rocks interpreted as the cover of Baltica in the Ofoten-Efjorden area are strongly deformed, but contain a fairly consistent and recognizable sequence of lithologic units (Figs 3, 4, and 5). The shoreline exposures along the northeast shore of Storvann on East Hinnøya display one of the thickest and most complete sections, and these exposures were designated by Bartley (1980) as the type locality. Consequently, the quartzite, schist, and marble that constitute the cover sequence in this region are known collectively as the Storvann group. Stratigraphic and lithologic descriptions of the Storvann group in its type area were provided by Bartley (1980, 1981). Only a brief summary of the sequence is given here, noting variations in the characteristics of the section in exposures from Storvann southward to Efjorden (Figs 3, 4, and 5).

The base of the Storvann group consists of a heterogeneous quartzite that varies in thickness from a few cm up to more than 200 m and ranges in character from vitreous quartzite, to sugary arkosic quartzite, to quartzofeldspathic schist. South of Ofotfjorden, much of the quartzite is arkosic, with sporadic layers of white vitreous quartzite or quartzofeldspathic schist up to 10 m thick. Banded white vitreous quartzite is the most

distinctive manifestation of this unit, and it allows easy recognition of the basal quartzite even where it has been thinned to only a few cm by intense deformation.

The basal quartzite is overlain intermittently by up to 10 m of impure calcite marble, but this lower marble becomes progressively more rare and eventually absent in exposures south of the type location. Psammitic schist overlies the quartzite and/or lower marble, and it represents the most widespread and volumetrically significant rock type within the cover sequence. Garnet is present as 1-10 mm porphyroblasts within a quartz-plagioclase-muscovite-biotite matrix. Mica commonly forms lenticular segregations within the quartzofeldspathic schist, lending a distinctive appearance to outcrops of this unit. In places, the psammitic schist becomes calcarious near its top and is overlain by an impure marble up to 100 m in thickness. This upper marble unit is typically banded gray and buff, and the color banding records strong internal deformation in the form of intrafolial isoclinal folds.

The stratigraphically highest rock type recognized in the metasedimentary cover is rusty-weathering calc-pelitic schist. This unit is more aluminous than the psammitic schist, and contains kyanite and abundant garnet porphyroblasts up to 3 cm in diameter in a muscovite-rich matrix. The thickness of the calc-pelitic schist is highly variable and commonly difficult to estimate with certainty due to poor exposure and complex internal deformation. Near the type location, the calc-pelitic schist is perhaps 250 m thick; however, south of Ofotfjorden, it is present only as discontinuous outcrops or lenses up to 50 m in thickness directly beneath the Caledonian allochthon.

Metasedimentary rocks correlative with the Storvann group of Bartley (1980) can be found structurally beneath the Caledonian allochthon from East Hinnøya southward

for approximately 45 km to Efjorden. However, most locations do not contain all of the units recognized in the type locality. In part, the variability within the sequence along strike may reflect original lateral changes in sedimentary facies. However, because the metasedimentary cover has been strongly deformed, much of the lateral variability is probably due to structural complications within the section. Along most of the exposure (particularly south of Ofotfjorden), only the basal quartzite and psammitic schist can be found consistently. Structurally dismembered portions of the impure marble and calc-pelitic schist units are present sporadically, but they rarely exhibit lateral continuity for more than 100-200 m.

Björklund (1987) examined local basement-cover relationships near Storvann on Hinnøya and argued that rocks within the Storvann Group of Bartley (1980, 1981) above the basal quartzite were allochthonous and correlative with the oceanic affinity Köli nappes exposed farther east in Sweden. In his view, the metasedimentary cover of Baltica consisted of quartzite, "greenschist facies" mica schists, and amphibolite found structurally beneath this level in a series of "thrust-repeated" basement-cover slices. Björklund's interpretation raises three important questions regarding basement-cover relations on East Hinnøya: (1) which rocks represent early Paleozoic cover? (2) what is the degree of structural transport of the cover? and (3) were the conditions of Caledonian metamorphism of the cover limited to the greenschist facies?

Björklund's map (figure 2 of Björklund 1987) contains no orientation data, but shows that he interpreted the structural section near Storvann to be monotonically north dipping (e.g., the hanging walls of all inferred thrusts are shown consistently on the north side of the fault contacts and are not indicated to be overturned). However, mapping of

the area during the present study suggests that much of the apparent repetition of basement and cover described by Björklund is the result of late-Caledonian transverse folding and the fact that some of the rocks interpreted by Björklund as early Paleozoic cover are demonstrably Proterozoic in age. The importance of the transverse folds in controlling the location, geometry, and apparent repetition of some contacts is evident in Figure 4. Relatively continuous exposure along the northeast shore of Storvann allows unambiguous recognition of NW-trending folds of variable amplitudes and wavelengths. The contact between cratonal basement and metasedimentary cover is repeated at least three times by the folds, and the local orientation of the section clearly rotates through subhorizontal in the intervening crests and troughs. The geometry of the folds tightens from south to north, and some fold limbs become overturned.

In addition to complications due to fold-related repetition of basement-cover contacts, some of the rocks interpreted by Björklund as part of the metasedimentary cover are intruded by Proterozoic granite and, therefore, are part of the Precambrian cratonal basement rather than the early Paleozoic cover. Intrusive relations with amphibolite are well exposed along the shore of Storvann (location A in figure 4; relationship shown in figure 6). Though more poorly exposed, intrusive relationships were also found with biotite-muscovite schist in the Storvann area (stream bed exposures at location B in figure 4). Screens and xenoliths of amphibolite, epidote-amphibolite schist, and mica schists can be found sporadically in the cratonal rocks throughout the region (e.g., location C in figure 5; relationship shown in figure 6), and in some places thay have localized zones of increased strain near their magins. However, these high strain zones are discontinuous along strike and do not indicate significant detachment or tectonic transport.

Consistency of the stratigraphy of the Storvann Group and its relationship to cratonal basement, not only on East Hinnoya as described by Bartley (1980, 1981), but also southward as far as Efjorden argues strongly that Bartley's original interpretation was correct: the Storvann Group represents a parautochthonous to locally transported remnant of the early Paleozoic cover on Baltica. Supracrustal rocks occur at deeper structural levels, but these are part of the Precambrian cratonal basement.

STRUCTURAL AND KINEMATIC CHARACTERISTICS

Remnants of the metasedimentary cover of Baltica formed the immediate footwall of the Caledonian A-type subduction zone and, as a result, these rocks were strongly tectonized during Caledonian orogenesis. Tectonic fabric is well developed in all parts of the section. The most prominent fabric element is a penetrative composite foliation (S_2) defined by anastomosing schistosity in the mica-rich rocks and compositional banding in the marbles and basal quartzite. The fabric contains intrafolial isoclinal folds at the cm to m scale, and these folds may contain an earlier tectonic foliation (S_1?) that has now been transposed into S_2. However, many of the intrafolial isoclines probably resulted from polycyclic fabric development in which S_2 was continuously refolded and transposed during heterogeneous progressive deformation in the footwall of the subduction zone. S_2 foliation is generally subparallel to the thrust contact at the base of the Caledonian allochthon but has been reoriented locally by NE- and NW-trending folds of variable wavelengths and amplitudes. The Caledonian S_2 tectonic fabric can be followed continuously from the metasedimentary cover structurally downward into the cratonal

rocks, but the fabric intensity decreases significantly with depth in the Baltic craton (Bartley 1980, 1982).

The S_2 foliation contains a mineral alignment and stretching lineation (L_2) defined by strain shadows on garnet porphyroblasts, an alignment of the long axes of inequant mineral grains, and elongate polycrystalline aggregates of mica, feldspar, or quartz. This stretching lineation trends consistently to the ESE, although its plunge varies considerably as a consequence of reorientation by late folding. Outcrop surfaces oriented perpendicular to S_2 and parallel to L_2 contain a variety of kinematic indicators that yield a consistent top-to-the-ESE sense of structural transport across the shear zone at the base of the Caledonian allochthon (Fig 7).

The strongly tectonized schists and marbles of the metasedimentary cover contain veins that occupy sites of syntectonic dilatancy, including tension-gash fractures and the necks of foliation boudinage (Fig 8). These veins are composed of quartz, calcite, and plagioclase ± muscovite and graphite. Progressive deformation during and after vein formation resulted in complex geometries in the S_2 foliation surrounding the veins. Some of the complex foliation patterns resulted from pinching inward at the ends of foliation boudins, generating 'fish mouth' geometry (cf. Ramsay and Huber, 1983). In many cases, progressive non-coaxial deformation rotated the veins in a manner consistent with continued top-to-the-ESE shear during formation of the veins. Fracture tips on the gash veins propagated at a steep inclination (ca. 75-80°) relative to S_2 foliation and the basal shear zone of the allochthon.

The S_2 composite foliation is folded by NE- and NW-trending folds of variable wavelengths and amplitudes. Mesoscopic examples of the NW-SE trending folds are particularly well developed where the effects of map-scale folds of similar orientation are strong. For example, the exposures of the metasedimentary cover near Storvann and farther south at Efjorden both occupy the limbs of large, WNW-ESE trending folds. In both cases, the structural section dips steeply or is overturned locally due to the folding. In these areas, mesoscopic WNW-ESE trending folds are ubiquitous. The folds have relatively tight geometries, and are associated with a retrograde crenulation cleavage (S_3) which is subparallel to the axial surfaces of the folds. In contrast, the NNE-trending exposures along the west limb of the Ofoten synform contain only gentle WNW-ESE folds and S_3 crenulation cleavage is weak or absent.

Ubiquitous internal deformation of the metasedimentary cover during the emplacement of the Caledonian allochthon indicates that, in many places, it has been detached and transported somewhat relative to the adjacent cratonal basement. South of Ofotfjorden, evidence of such detachment is clear where thrusts have structurally interleaved slivers of granite and the metasedimentary cover rocks in several places. Although the magnitude of transport at any given location is difficult to determine, total transport is inferred to be modest due to the lithologic similarity between clearly detached sections of cover and more autochthonous cover, and to the lateral continuity of the metasedimentary section as a whole.

PETROGRAPHY

Petrographic analysis focused on identification of the mineral assemblages and textural relationships in the psammitic and calc-pelitic schists of the metasedimentary cover sequence. Thin sections were made in two orientations relative to deformational fabric: some were cut perpendicular to S_2 and parallel to L_2; others were cut perpendicular to both S_2 and L_2. The second orientation is also essentially perpendicular to the S_3 crenulation in samples containing that fabric element.

The psammitic schist has a relatively simple mineralogy, consisting of quartz, plagioclase, biotite, muscovite, and garnet. Minor and accessory phases include calcite, alanite, apatite, rutile, ilmenite, tourmaline, pyrite, and graphite. Anastomosing films of muscovite and biotite define the foliation, and these films envelop well annealed polygranular aggregates of quartz and plagioclase. The color of the biotite in thin section varies from dark green to reddish brown, the latter being more common.

Garnet porphyroblasts in the psammitic schist vary in morphology from equant, subhedral, idiomorphic grains to heavily embayed and resorbed grains (Figs. 9, 10 and 11). Where present, resorption of garnet is commonly more prominent on the sides of garnets adjacent to strain shadows. Typically, plagioclase and biotite (± quartz and calcite) fill the strain shadows, and muscovite is concentrated on the high-pressure sectors of some garnets. In other examples, plagioclase ± biotite envelop the entire garnet. In some samples, graphite occurs preferentially around the margins of garnet, producing an opaque rim, and this rim marks the original location of the grain boundary of some resorbed garnets (e.g., Figure 11). These textural relationships suggest variable but locally significant progress of the reaction:

garnet + muscovite = plagioclase + biotite.

In contrast to the relatively simple mineralogy of the psammitic schist, the calc-pelitic schist contains a more diverse group of minerals, including quartz, muscovite, biotite, plagioclase, calcite, garnet, kyanite, staurolite, chlorite, margarite, zoisite, and clinozoisite, with accessory alanite, apatite, rutile, ilmenite, pyrite, tourmaline, and graphite. Although these minerals are all found together in the schist (and commonly in the same thin section), the large number of phases present suggests that these minerals probably do not represent a single, well-equilibrated assemblage. Instead, they are interpreted as an accumulation of minerals produced during progressive metamorphism. The rock contains abundant textural evidence of reaction relationships among several of the minerals, as noted below.

The matrix of the rock consists chiefly of muscovite, biotite, and quartz with minor calcite. S_2 foliation in the schist is defined by films of muscovite and biotite that anastomose around polygranular aggregates of well-annealed, polygonalized quartz.

Garnet porphyroblasts in the calc-pelitic schist are large (1-3 cm), subhedral, and contain numerous inclusions. Trails of inclusions within the garnets form an internal foliation that is planar in the core regions, but becomes curved near the rim. In some examples, the internal foliation is semicontinuous with the S_2 foliation in the matrix; in other instances, it is truncated by the matrix foliation, possibly due to resorption of garnet along the interface. Some garnet porphyroblasts contain inclusions that preserve relics of mineral assemblages present during garnet growth (Fig 12). Petrogenetically significant

mineral associations preserved as inclusions consist of the following: chloritoid-chlorite, chloritoid-staurolite-chlorite, and staurolite-chlorite (± quartz, muscovite, margarite, paragonite, rutile, and ilmenite). Chloritoid and chlorite are absent from the matrix, except for local growth of retrograde chlorite adjacent to Fe-Mg bearing minerals.

Biotite is present in three manifestations: (1) small disseminated grains aligned with the S_2 foliation; (2) relatively large porphyroblasts up to 7 mm in diameter aligned with S_2; and (3) texturally late biotite grains that are distinctly discordant to S_2 and parallel to the S_3 crenulation. Biotite porphyroblasts contains inclusions of quartz, rutile, and allanite.

Staurolite is found both as inclusions within some garnets and as small porphyroblasts in the matrix of some (but not all) samples. Schist containing staurolite is interlayered at the m scale with schist barren of staurolite and, therefore, factors other than differences in peak metamorphic conditions control the local presence or absence of staurolite. Where present, staurolite porphyroblasts are highly embayed and resorbed. The corroded appearance of staurolite combined with the absence of prograde chlorite and the presence of garnet, biotite, and kyanite in the schist is consistent with at least partial progress of prograde, staurolite-consuming reactions like:

str + chl + mus = ky + bio

str +mus = gar + bio + ky

In addition, staurolite locally participated in retrograde reactions to produce late chlorite, particularly in rocks with well-developed S_3 crenulation cleavage.

Kyanite is nearly ubiquitous in samples of the calc-pelitic schist and is present as highly embayed, anhedral porphyroblasts up to 5 mm in length. Commonly poikiloblastic, the kyanite contains inclusions of quartz, rutile, micas, and more rarely of zoisite and clinozoisite (Figure 13). The coexistence of kyanite and zoisite provides evidence for the reaction: margarite + quartz = kyanite + zoisite + H_2O during part of the growth history of the kyanite porphyroblasts. Kyanite is strongly resorbed and commonly replaced or overgrown by plagioclase. These textures suggest the progress of reactions that yield plagioclase at the expense of kyanite, such as:

$ky + cc + qtz = plag_{(an)} + CO_2$

$ky + qtz + zo = plag_{(an)} + H_2O$

$ky + gar_{(grs)} + qtz = plag_{(an)}$

Plagioclase porphyroblasts are anhedral, up to 1.5 cm in diameter, and contain numerous inclusions of a wide variety of minerals (Figure 14). Plagioclase envelops peak metamorphic minerals such as garnet, kyanite, biotite, and staurolite. S_2 foliation in the matrix is usually continuous with foliation defined by inclusions in the plagioclase. S_3 crenulation of S_2 is absent or weakly present within some porphyroblasts, but is more strongly developed in the surrounding matrix.

Retrograde micas including margarite and chlorite are common in some samples, particularly those with strong S_3 crenulation. Fine-grained aggregates of margarite are intimately intergrown with pre-existing muscovite and biotite porphyroblasts in some

samples. Neoblastic margarite and chlorite are sometimes aligned with the S_3 crenulation, and also locally form radiating sprays nucleated on pre-existing minerals.

In summary, both the psammitic and calc pelitic schists of the cover sequence exhibit textural evidence of the evolution of their mineral assemblages during progressive metamorphism. Reaction textures and relict mineral grains from various parts of their metamorphic history are relatively well preserved, particularly in the calc-pelitic schist. Peak metamorphic mineral parageneses include gar-bio-mus-ky-plag ± str in the calc pelitic schist, and gar-bio-mus-plag in the psammitic schist. Prograde chlorite is notably absent from all the samples examined. Although different in bulk chemistry and mineralogy, both the psammitic and calc-pelitic schists exhibit significant growth of plagioclase during the peak metamorphic to early-retrograde segment of their evolution.

MINERAL CHEMISTRY & QUANTITATIVE THERMOBAROMETRY

Microchemical analyses were performed on samples from the metasedimentary cover in order to characterize the compositions of phases and to estimate the conditions of metamorphism using quantitative thermobarometry.

Analytical Methods

Polished thin sections were carbon coated and analyzed on a JEOL 733 electron microprobe in the analytical facilities at MIT. The microprobe was operated with a 15 Kev accelerating potential and a 10 nA beam current. Beam diameter was maintained at about 1 micron, although the size of the interaction volume was larger and dependent on the mineral analyzed. A variety of synthetic and natural materials were used as primary

and secondary standards to calibrate the microprobe for analysis of MgO, Al_2O_3, SiO_2, CaO, TiO_2, MnO, FeO, Na_2O, K_2O, and ZnO. Data reduction followed the scheme of Bence and Albee (1968). All measured Fe is reported as Fe^{2+}. The mineral compositions given represent the mean of three to five point analyses per mineral in each of three to five different locations on a thin section (i.e., a total of 9 to 25 point analyses). Standard deviations of the point analyses are reported to provide a statistical measure of the compositional heterogeneity observed. Except for analytical traverses across porphyroblasts to examine zoning characteristics, all compositions were measured at grain boundaries. Garnet, plagioclase, biotite, and muscovite compositions used for thermobarometry were obtained from the rims of minerals coexisting within 500 microns of each other at each of the locations analyzed on a thin section.

Mineral Compositions

Mineral chemical data are presented in Appendix I, and figures 15 thru 18; sample locations are given in figures 4 and 5. Garnet porphyroblasts are concentrically zoned (Figs. 15-17). Spessartine is enriched in garnet cores (up to Xsps = 0.20), and decreases progressively outward, except for a zone of variable thickness adjacent to garnet rims in which spessartine is locally more concentrated. In general, grossular and pyrope components both increase steadily from core to rim. Some samples, however, exhibit local enrichment of grossular in the cores, and some have a thin (<200 micron) zone of anomalously high or low concentration of grossular at the rim. Although some garnets are more enriched in almandine than others, the shape of almandine zonation is consistent. Xalm is moderate in the center of garnets and increases outward, reaching a

maximum in the outer core and then decreasing steadily to minimum values near the grain boundaries. However, the Fe/(Fe+Mg) ratio decreases consistently from core to rim except for a local increase adjacent to the rim of some samples.

Staurolite porphyroblasts are enriched in the Fe-endmember (XFestr = 0.70-0.73). All staurolites analyzed contain Zn, and the concentration varies from one porphyroblast to another (0.25 - 4.46 wt % ZnO). Zn is enriched locally at the margins of some irregularly-shaped and embayed staurolite grains, possibly due to inward diffusion of Zn during resorption of the rims.

Biotite in the calc-pelitic schist (Xann = 0.25) has a lower Fe/(Fe+Mg) ratio compared to biotite in the psammitic schist (Xann = 0.40). Individual biotite grains are relatively homogeneous, but the FeO and MgO concentrations vary somewhat (5 to 10 relative %) over the scale of a thin section. All biotite analyzed contained 1 to 3 wt % TiO_2, and those samples with dark reddish-brown biotite consistently contained the highest TiO_2 concentrations ($\geq$ 1.8 wt %).

Muscovite in all samples exhibits solid solution with paragonite and phengite components. A typical muscovite from the calc-pelitic schist contains 12-15 mole % paragonite and 5-7 mole % phengite. Muscovite in the psammitic schist contains 4-8 mole % paragonite and 7-10 mole % phengite.

Some garnet porphyroblasts contain inclusions of staurolite, chlorite, chloritoid, ilmenite, margarite, and paragonite, and analysis of such inclusions can provide information about the chemical evolution of minerals during prograde metamorphism. The locations and mineral associations found within inclusions in a garnet porphyroblast

from sample 93SC-24 are shown in figure 17 and table 1. Staurolite inclusions are found everywhere in the garnet, including the core region. All are Fe-rich and contain a moderate amount of Zn (typically 0.25 to 1.0 wt %). Chloritoid is found everywhere in the garnet except the outer 1-2 mm, and like staurolite, is more enriched in the Fe-endmember. Chlorite inclusions are found everywhere except within about 1 mm of rim. Among all the ferromagnesian minerals at a given location within the porphyroblast, the Fe/(Fe+Mg) ratio decreases in the order: garnet > staurolite > chloritoid >> chlorite (figure 18). Inclusions of chloritoid and chlorite become more magnesian from the core toward the rim of the garnet porphyroblast. In contrast, staurolite seems to decrease and then increase somewhat in Fe/(Fe+Mg) from core to rim. The composition of garnet adjacent to inclusions of ferromagnesian minerals, particularly staurolite, shows local enrichment in Fe (note the local compositional anomalies adjacent to staurolite-bearing inclusions 1, 5, and 12 in the analytical traverse shown in figure 17). The local change in garnet composition adjacent to inclusions indicates some post-entrapment diffusional exchange between the garnet and Fe-Mg minerals in the inclusions.

Thermobarometry

Quantitative thermobarometry represents a potentially powerful tool for investigation of the P-T history of metamorphic rocks. The mineralogy of the psammitic and calc-pelitic schists allows application of two relatively well-calibrated thermobarometric reactions:

GARB: $gar_{(alm)} + bio_{(phl)} = gar_{(pyr)} + bio_{(ann)}$ (Ferry and Spear, 1978)

GMAP: $gar_{(alm)} + gar_{(grs)} + mu = bio_{(ann)} + plag_{(an)}$ (Ghent and Stout, 1981)

P-T estimates presented in this study were determined by simultaneous solution of the GARB and GMAP thermobarometers using the Hodges and McKenna (1987) calibration of GARB and thermodynamic constants for GMAP calculated from the thermodynamic data of Berman (1988, 1990). Because all of the minerals involved in these reactions exhibit solid solution behavior, solid solution models are required to convert mineral composition data into the component activities used in the pressure-temperature calculations. Following the recommendations of Applegate and Hodges (1994), thermobarometric calculations in this study relied on the solution models of Berman (1990), Patiño-Douce et al. (1993), and Elkins and Grove (1990) for garnet, biotite, and plagioclase respectively.

P-T estimates derived for rock in the metasedimentary cover sequence are presented in figure 19. Uncertainty ellipses were calculated using Monte Carlo analysis in the manner of Hodges and McKenna (1987). The ellipses reflect 2-sigma uncertainty in the pressure and temperature determined for a sample due to propagation of the variability in mineral compositions through the P-T calculations; they do not include uncertainties in the counting statistics of individual microprobe spot analyses, nor do they account for uncertainties in the calibrations of the GARB and GMAP reactions. P-T determinations for samples from the metasedimentary cover of Baltica plot as a broad array in P-T space, ranging from about 10 kbar, 625 °C, down to about 5 kbar, 475 °C.

DISCUSSION

Thermobarometry

Interpretation of the thermobarometric results is not straight forward due to the large uncertainties in individual P-T estimates and the relatively broad range of values encompassed by all of the estimates collectively. The variability observed may be explained by one or more of the following: (1) chemical disequilibrium; (2) final equilibration of the GARB and GMAP reactions in a given sample independently at different times in the P-T history; and (3) final equilibration of GARB and GMAP in a given sample simultaneously, but at different times in the P-T history for different samples.

The relatively large uncertainties for each P-T estimate arise from variability in the rim compositions of coexisting garnet, plagioclase, biotite, and muscovite within each sample. This variability suggests that the spatial scale of equilibrium is small in many of the samples. Such an interpretation is consistent with the petrographic observation that the degree of resorption and replacement of garnet by plagioclase + biotite varies significantly at the scale of a given thin section. On the positive side, these textures also provide clear evidence for progress of the GMAP barometer reaction during the peak to early retrograde portion of the metamorphic history. Consequently, the series of GMAP equilibria determined from the suite of samples may point to the range in pressures over which the peak to early retrograde segment of the P-T path occurred (Fig 20).

Within the uncertainties, all but two of the P-T estimates can be fit by a single position of the GARB geothermometer in the range of 525 to 540°C at 8 kbar, and the

resolvable difference between the highest and lowest temperatures determined is only about 18°C. The fact that most of the temperatures calculated from the samples are statistically indistinguishable while the pressures vary significantly is consistent with either: (1) A P-T path involving isothermal decompression; or (2) diffusional re-equilibration and final closure of the GARB Fe-Mg exchange thermometer on the retrograde path after closure of the GMAP net-transfer barometer. Given that evidence of high-temperature extensional processes can be found within the overlying nappe complex (see Chapter 2), the possibility of isothermal decompression of the structural basement is provocative. Further support for an interpretation of high-temperature decompression comes from the resorption of garnet and growth of plagioclase during the peak to early retrograde segment of the metamorphic evolution of footwall rocks. These textures are consistent with progress of reactions that consume garnet and yield plagioclase, and such reactions are typical of decompression.

The textural evidence supporting decompression notwithstanding, disequilibrium between GARB and GMAP remains a posibility, and the two are not mutually exclusive. In fact, the highly variable progress of reactions involved in the resorption of garnet and growth of plagioclase at the scale of an individual thin section indicates that the assumption of equilibrium necessary for quantitative thermobarometry is dubious for these rocks. Furthermore, petrogenetic evidence for peak metamorphic temperatures higher than those indicated by the exchange thermometer can be found for many of the samples (as discussed below). Consequently many of the P-T estimates generated may not represent conditions of simultaneous equilibrium of GARB and GMAP. However,

assuming a clock-wise P-T path and closure of GMAP prior to GARB due to the kinetic differences between the net-transfer barometer and exchange thermometer, the intersection points of GARB and GMAP equilibria may provide a lower bound on the peak metamorphic conditions (Figure 20).

constraints from mineral parageneses

The complex mineral assemblages and reaction textures in the calc-pelitic schist place general but important constraints on the P-T evolution of the metasedimentary cover. Phase relationships in the K-Fe-Mg-Al-Si-H (KFMASH) and Ca-Na-Al-Si-H-C (CNASHC) compositional subsystems provide a useful framework in which to evaluate the petrogenesis of these rocks.

The presence of staurolite in pelitic schists has been used often to infer peak metamorphic temperatures greater than about 550 °C (e.g., Bickle and Archibald, 1984). Unfortunately, a host of potential complications arise when staurolite stability relations are considered in detail. The incorporation of minor components (notably Zn and Fe^{3+}) into staurolite can increase its stability, causing staurolite to come into an assemblage at lower temperatures and remain at higher temperatures than predicted by ideal phase relations (Giaramita and Day, 1991; many others). In addition, because staurolite is a hydrous phase, many reactions involving this mineral are sensitive to the ambient fluid composition. The fact that staurolite in samples from the metasedimentary cover sequence contains variable amounts of Zn and the composition of the metamorphic fluid is not easly constrained makes the petrogenetic significance of staurolite in these rocks difficult to assess.

The complexities of staurolite notwithstanding, a minimum temperature of ca. 575-600°C is consistent with other petrogenetic considerations. In particular, the absence of prograde chlorite or chloritoid in the matrix of any of the garnet-bearing samples examined argues for amphibolite-facies conditions. Chloritoid and/or chlorite were clearly present during prograde metamorphism because these minerals are preserved as inclusions within some garnet porphyroblasts (fig. 12). Therefore, peak metamorphic conditions must have exceeded the terminal stability of either chloritoid or chlorite + garnet parageneses.

Estimates of the upper stability limit of mineral assemblages containing chloritoid or garnet + chlorite vary due to several factors, including: (1) the choice of thermodynamic data used to calculate petrogenetic relationships; (2) the chemical system chosen to depict phase relationships; and (3) the specific compositions of the phases involved in the reactions. The petrogenetic grid of Powell and Holland (1990) indicates stability of Fe-Mg chloritoid in the KFMASH system to 560 - 600°C, and garnet + chlorite to 600 - 640°C, for pressures in the range of 5 to 12 kbar (Fig 21). In contrast, the grid of Spear and Cheney (1989) shows chloritoid-out increasing from 550°C to 580°C over the pressure range 5 to 9.5 kbar, and restricts garnet + chlorite parageneses to a narrow sliver of P-T space spanning only 540-560°C at 5 kbar and disappearing into an invariant point at about 580°C, 9.5 kbar (Fig 22). Spear and Cheney (1989) indicated that although garnet + chlorite assemblages in the end-member KFMASH system may be restricted to an unrealistically narrow range in temperature, the presence of additional components, notably Mn and Ca in garnet, expands the stability field of garnet + chlorite

for rocks of more realistic bulk composition. Garnets analyzed in the present study contain about 10 mole % spessartine on average, which may increase the stability field up to 575-600°C (Figure 22; Spear and Cheney, 1989; Wang and Spear, 1991).

An important caveat is that reactions involving the breakdown of chlorite and chloritoid are commonly sensitive to fluid composition and fO_2 (e.g., Vidal et al., 1994), and these two variables are difficult to determine. Bearing all of the potential complexities in mind, the fact that the general petrogenetic constraints from staurolite, chloritoid, and garnet + chlorite are consistent strengthens the interpretation that peak metamorphic temperatures attained by the metasedimentary cover were greater than about 575-600°C.

The calc-pelitic schist contains a variety minerals and reaction textures that may be evaluated in terms of phase relations in the CNASHC composition system. Relevant minerals found either in the matrix of samples or preserved as inclusions in porphyroblasts include: quartz, kyanite, margarite, paragonite, zoisite, clinozoisite, $plagioclase_{(an)}$, $garnet_{(grs)}$ and calcite. Textural relationships can be used to infer a sequence of parageneses and reactions among these minerals, and the reaction history can then be related in a general way to the temperature-pressure evolution of the area. Figure 23 illustrates some of reactions which are inferred or indicated texturally to have occurred in the calc-pelitic schist. Note that the positions of all of these reactions are fluid sensitive. Because the metasedimentary cover on Baltica underwent a series of dehydration and decarbonation reactions during progressive metamorphism, the composition of the metamorphic fluid almost certainly varied through time.

Consequently, the reaction boundaries shown illustrate the general reaction topology rather than rigorously define stability fields in P-T space.

Margarite and paragonite inclusions within garnet porphyroblasts provide evidence that these white micas (accompanied by calcite and quartz) may represent part of the early CNASHC mineral assemblage in the rock. Zoisite inclusions in kyanite porphyroblasts record a change in the paragenesis in which margarite reacted to form kyanite and zoisite through the relationship:

$$\text{margarite} + \text{quartz} = \text{kyanite} + \text{zoisite} + H_2O$$

In thin sections of the calc-pelitic schist, kyanite porphyroblasts are commonly resorbed and replaced by plagioclase, and these textures are consistent with the progress of several reactions in the CNASHC system which yield plagioclase at the expense of kyanite:

$$\text{kyanite} + \text{quartz} + \text{calcite} = \text{plagioclase}_{(an)} + CO_2$$

$$\text{kyanite} + \text{quartz} + \text{zoisite} = \text{plagioclase}_{(an)} + H_2O$$

$$\text{kyanite} + \text{garnet}_{(grs)} + \text{quartz} = \text{plagioclase}_{(an)}$$

Production of significant plagioclase at the expense of kyanite and/or garnet seems to have occurred during the peak to early retrograde segment of the pressure-temperature path followed by rocks at this structural level. This devolatilization coupled with

production of plagioclase may have been related to the widespread occurrence of syntectonic to post-tectonic veins of quartz, calcite, and plagioclase (fig. 7).

The texturally latest CNASHC paragenesis observed in the calc-pelitic schist is the growth of late margarite during formation of S_3 crenulation. The common association of this margarite with retrograde chlorite confirms its formation late in the overall metamorphic and deformational history, perhaps via the rehydration reaction:

kyanite + plagioclase $_{(an)}$ + H_2O = margarite + quartz

In summary, quantitative thermobarometry and petrogenetic considerations are consistent with prograde metamorphism of the metasedimentary cover on Baltica to conditions of at least 575-600°C and 9-10 kbars (Figure 24). Temperatures must have been greater than about 575-600°C based on three petrogenetic arguments: (1) presence of the mineral assemblage: gar-bio-ky ± str in the aluminous schists; (2) removal of all chloritoid from the aluminous schists; and (3) the absence of prograde chlorite in any of the garnet-bearing samples examined. These reactions involved in the petrogenetic constraints have relatively steep Clapeyron slopes and, therefore, they provide little information about peak metamorphic pressures. The best pressure constraints come from the positions of GMAP equilibria calculated for the samples examined. The rocks contain abundant textural evidence for progress of the GMAP reaction during the peak to early retrograde segment of the metamorphic history. Consequently, these equilibria may point to the general range in pressure over which the peak to early retrograde portion of

the metamorphism occurred. Collectively, the petrogenetic considerations and thermobarometric calculations indicate minimum peak metamorphic conditions of ca. 575-600°C, 9-10 kbar. Resoption of garnet and production of appreciable amounts of plagioclase during the peak to early retrograde portion of the metamorphic evolution suggests significant high-temperature decompression during this interval.

Relation of Deformation to Progressive Metamorphism

Textural relationships between metamorphic minerals and deformational fabric elements can be used to link parts of the deformational history to parts of the progressive metamorphic history. For example, formation of the dominant foliation (S_2) is related kinematically to the ESE-directed thrust emplacement of the Caledonian allochthon. In thin section, S_2 is defined in part by an alignment of biotite porphyroblasts, and is continuous with locally curved inclusion trails in garnet and kyanite porphyroblasts. The foliation wraps around some garnets, especially those near the thrust contact, and asymmetric pressure shadows on garnets indicate top-to-the-ESE transport on the thrust (figure 9). These observations suggest that S_2 fabric formed initially during prograde metamorphism and continued to develop at least locally during peak to early retograde metamorphism. By inference, ESE-directed emplacement of the allochthon occurred during prograde to peak metamorphism, perhaps with some movement continuing into the high-temperature retrograde history. Such an interpretation is not surprising, given that tectonic burial beneath the allochthon is considered to have caused the metamorphism of the tectonized sedimentary cover.

The genesis of plagioclase-bearing veins in sites of local syntectonic dilatancy can be related to devolatilization reactions that yielded plagioclase and are interpreted to have occurred during the peak to early retrograde portion of the metamorphic history (Figs. 7 and 23). Fracture tips of tension gash veins are steeply inclined relative to the S_2 foliation, and the veins exhibit varying amounts of rotation by top-to-the-ESE noncoaxial deformation. Collectively, these observation are consistent with formation of the veins during the waning stages of ESE-directed thrusting of the allochthon, synchronous with peak to early-retrograde metamorphism. The steep inclination of the fracture tip propagation direction suggests that the greatest principal stress (σ_1) was inclined steeply late in the emplacement history of the allochthon at the time of vein formation. Such an orientation of the stress field is consistent with the pattern of deformation recognized in the overlying allochthon, which includes foreland-directed elongation and subvertical attenuation of the Caledonian nappe stack during late stages of its thrust emplacement (see Chapter 2). Furthermore, attenuation of the overlying nappe stack may have produced decompression of the footwall rocks, enhancing devolatilization, resorption of garnet, and production of plagioclase.

S_3 crenulation is related to the development of NW-SE trending transverse folds, and is defined in part by lower-temperature retrograde minerals such as chlorite and late margarite. Consequently, the crenulation and associated folding developed relatively late in the metamorphic evolution of the area. In southwestern Norway, transverse folds like those recognized in the Ofoten-Efjorden area have been linked with late-to-post-Caledonian extension. However, little evidence of such extension has been recognized as

yet in this area. Still, the transverse folding may have developed during the late, lower temperature part of the regional cooling history (see chapter 4).

CONCLUSIONS

The preceding observations and discussion form the basis for several conclusions regarding the tectonic evolution of the Caledonian collision-subduction system at this lattitude. First, because the metasedimentary cover sequence on Baltica in the Ofoten-Efjorden region achieved minimum temperatures and pressures of ca. 575-600°C, 9-10 kbar during Caledonian orogenesis, the portion of Baltic craton now exposed in the Ofoten region must have undergone A-type subduction to depths equivalent to at least 9 kbars of lithostatic pressure — approximately 35 km. Because an additional 35-40 km of continental crust remain beneath the present erosion surface, A-type subduction of the Baltic craton may have produced a composite crustal thickness of 70 to 80 km in this area, assuming that all of the modern crustal section was present during the collision.

P-T estimates for deep levels of the Caledonian allochthon by Hodges and Royden (1984) and Steltenpohl and Bartley (1987) may delineate the cooling and unroofing path followed by the allochthon in the area (figure 24). If so, then the retrograde P-T path inferred for the allochthon converges with minimum P-T estimates for peak metamorphism in the metasedimentary cover at about 9-10 kbar, 625°C. Such convergence may indicate that final juxtaposition of the allochthon and structural basement occurred under these conditions followed by movement in unison along a retrograde P-T trajectory to conditions of about 6 kbar, 500°C. Reaction textures observed in the footwall rocks are consistent with high-temperature decompression

following the metamorphic peak,and this decompression may have resulted from extensional failure of the overlying nappe stack between ca. 430 and 410 Ma (see chapters 2 and 4).

REFERENCES

Applegate, J. D. R., and Hodges, K. V., 1994, Empirical evaluation of solution models for pelitic minerals and their application to thermobarometry. *Contrib. Mineral. Petrol. 117,* 56-65.

Bartley, J., M., 1980, Structural geology, metamorphism, and Rb/Sr geochronology of east Hinnøy, north Norway, Ph.D. thesis, Massachusetts Institute of Technology, Cambridge, MA.

Bartley, J. M., 1981, Lithostratigraphy of the Storvann Group, east Hinnøy, north Norway, and its regional implications. *Nor. Geol. Unders. 370*, 11-24.

Bartley, J. M., 1982, Limited basement involvement in Caledonian deformation, Hinnøy, north Norway, and tectonic implications, *Tectonophysics, 83*, 185-203.

Bartley, J., M., 1984, Caledonian structural geology and tectonics of east Hinnøy, north Norway, *Bull. Nor. Geol. Unders., 396*, 1-24.

Berman, R. G., 1988, Internally-consistent thermodynamic data for stoichiometric minerals in the system Na2O-K2O-CaO-MgO-FeO-Fe2O3-Al2O3-SiO2-TiO2-H2O-CO2. *J. Petrol. 29,* 445-522.

Berman, R. G., 1990, Mixing properties of Ca-Mg-Fe-Mn garnets. *Am. Mineral., 75,* 328-344.

Bickle, M. J., and Archibald, N. J., 1984, Chloritoid and staurolite stability: implications for metamorphism in the Archean Yilgarn Block, Western Australia. *J. Metamorphic Geol., 2,* 179-203.

Björklund, L. J. O., 1987, Basement-cover relationships and regional correlations of the Caledonian nappes, eastern Hinnøy, N. Norway. *Norsk Geologisk Tidsskrift, 67*, 3-14.

Coker, J. E., M. G. Steltenpohl, A. Andresen, and M. J. Kunk, 1995, An $^{40}Ar/^{39}Ar$ thermochronology of the Ofoten-Troms region: Implications for terrane amalgamation and extensional collapse of the northern Scandinavian Caledonides, *Tectonics, 14*, 435-447.

Elkins, L. T., and Grove, T. L., 1990, Ternary feldspar experiments and thermodynamic models. *Am Mineral. 75,* 544-559.

Ferry, J. M., and Spear, F. S., 1978, Experimental calibration of the partitioning of Fe and Mg between biotite and garnet. *Contrib Min. Petrol. 66,* 113-117.

Gee, D. G., 1975, A tectonic model for the central part of the Scandinavian Caledonides, *Am. J. Sci., 275-A,* 468-515.

Gee, D.G., R. Kumpulainen, D. Roberts, M. B. Stephens, A. Thon, and E. Zachrisson, 1985, Tectonostratigraphic map of the Scandinavian Caledonides: in D. G. Gee and B. A. Sturt, eds., *The Caledonian Orogen - Scandinavia and related areas*, J. Wiley and Sons, Chichester, England.

Gee, D. G., and M. R. Wilson, 1974, The age of orogenic deformation in the Swedish Caledonides, *Am. J. Sci., 274*, 1-9.

Ghent, E. D., and Stout, M Z., 1981, Geobarometry and geothermometry of plagioclase-biotite-garnet-muscovite assemblages. *Contrib. Mineral. Petrol. 76,* 92-97.

Giaramita, M. J., and day, H. W., 1991, The four-phase AFM assemblage staurolite-aluminum silicate-biotite-garnet: Extra components and implications for staurolite-out isograds. *J. Petrol. 32,* 1203-1229.

Griffin, W. L., and Heier, K. S., 1969, Paragneisses of garnet in granulite facies rocks, Lofoten-Vesteraalen, Norway, *Contributions to Mineralogy and Petrology, 23*, 89-116.

Gustavson, M., 1974, Narvik, Beskrivelse til det bergrunnsgeologiske gradteigskrat N9 1:250,000, *Nor. Geol. Unders., 308*, 34 p.

Harland, W. B., and R. A. Gayer, 1972, The Arctic Caledonides and earlier oceans, *Geol. Mag., 109*, 289-314.

Hodges, K. V., 1982, Tectonic evolution of the Aefjord-Sitas area, Norway-Sweden, Ph.D. thesis, Massachusetts Institute of Technology, Cambridge, MA.

Hodges, K., V., 1985, Tectonic stratigraphy and structural evolution of the Efjord-Sitasjaure area, Northern Scandinavian Caledonides, *Nor. Geol. Unders., 399*, 41-60.

Hodges, K. V., J. M. Bartley, and B. C. Burchfiel, 1982, Structural evolution of an A-type subduction zone, Lofoten, *Tectonics, 1*, 441-462.

Hodges, K. V., and McKenna, L. W., 1987, Realistic propagation of uncertainties in geologic thermobarometry. *Am. Mineral. 72,* 671-680.

Hodges, K. V., and L. Royden, 1984, Geologic thermobarometry of retrograded metamorphic rocks: an indication of the uplift trajectory of a portion of the northern Scandinavian Caledonides, *J. Geophys. Res., 89*, 7077-7090.

Patiño-Douce, A. E., Johnston, A. D., and Rice, J. M., 1993, Octahedral excess mixing properties in biotite: a working model with applications to geobarometry and geothermometry. *Am Mineral. 78,* 113-131.

Powell, R., and Holland, T., 1990, Calculated mineral equilibria in the pelite system, KFMASH (K2O-FeO-MgO-Al2O3-SiO2-H2O). *Am. Mineralogist 75,* 367-380.

Spear, F. S., and Cheney, J. T., 1989, A petrogenetic grid for pelitic schsits in the system Si)2-Al2O3-FeO-MgO-K2O-H2O. *Contrib. Mineral. Petrol. 101,* 149-164.

Steltenpohl, M. G., 1983, The structure and stratigraphy of the Ofoten synform, North Norway, M.S. thesis, University of Alabama, University, AL.

Steltenpohl, M. G., 1985, The structural and metamorphic history of Skanland, north Norway, and its significance for tectonics in Scandinavia, Ph.D. thesis, University of North Carolina, Chapel Hill, NC.

Steltenpohl, M. G., and J. M. Bartley, 1987, Thermobarometric profile through the Caledonian nappe stack of western Ofoten, north Norway, *Contrib. Min. Pet., 92*, 93-103.

Steltenpohl, M. G., and J. M. Bartley, 1988, Crossfolds and backfolds in the Ofoten-Tysfjord area, Norway and their significance for Caledonian tectonics, *Geol. Soc. Am. Bull., 100*, 140-151.

Stephens, M. B., and D. G. Gee, 1989, Terranes and polyphase accretionary history in the Scandinavian Caledonides, *Geol. Soc. Am. Spec. Paper, 230*, 17-30.

Vidal, O., Theye, T., and Chopin, C., 1994, Experimental study of chloritoid stability at high pressure and various fO_2 conditions. *Contrib Mineral. Petrol. 118,* 256-270.

Wang, P. and Spear, F. S., 1991, A field and theoretical analysis of garnet+chlorite+chloritoid+biotite assemblages from the tri-state (MA, CT, NY) area, USA. *Contrib. Mineral. Petrol. 106,* 217-235.

APPENDIX 1: MINERAL COMPOSITIONS

92SC-50, psammitic schist

	garnet		biotite		plagioclase		muscovite	
	wt% (1σ)	stoich.	wt% (1σ)	stoich.	wt% (1σ)	stoich.	wt% (1σ)	stoich.
SiO_2	37.11 (0.48)	3.02	36.70 (0.21)	2.87	59.36 (0.88)	2.62	49.48 (0.35)	3.21
TiO_2	0.09 (0.02)	0.01	1.87 (0.24)	0.11	— —	—	0.94 (0.45)	0.05
Al_2O_3	21.41 (0.19)	2.05	18.47 (0.14)	1.65	26.59 (0.67)	1.38	33.51 (0.61)	2.57
FeO	28.17 (0.44)	1.92	17.68 (0.36)	1.12	0.38 (0.06)	0.01	1.63 (0.10)	0.09
MgO	1.73 (0.14)	0.21	10.26 (0.08)	1.16	0.03 (0.01)	0.00	1.16 (0.06)	0.11
MnO	6.30 (0.35)	0.43	0.10 (0.03)	0.01	— —	—	0.05 (0.03)	0.00
CaO	3.45 (0.31)	0.30	0.06 (0.02)	0.01	7.91 (0.59)	0.37	0.03 (0.02)	0.00
Na_2O	— —	—	0.11 (0.02)	0.02	6.77 (0.17)	0.58	0.49 (0.04)	0.06
K_2O	— —	—	9.32 (0.11)	0.90	0.05 (0.01)	0.00	9.45 (0.30)	0.78
Total:	98.27	7.95	94.57	7.75	101.08	4.98	96.76	6.88

Xalm	0.670	Xann 0.397	Xan 0.390	Xkmu 0.924
Xpyr	0.073	Xphl 0.410	Xab 0.607	Xnamu 0.073
Xsps	0.152			Xalmu 0.877
Xgrs	0.105	Al_2SiO_5 polymorph: none		

92SC-55, calc-pelitic schist

	garnet		biotite		plagioclase		muscovite	
	wt% (1σ)	stoich.	wt% (1σ)	stoich.	wt% (1σ)	stoich.	wt% (1σ)	stoich.
SiO_2	38.51 (0.29)	2.97	39.47 (0.37)	2.82	60.87 (1.37)	2.67	48.75 (1.12)	2.99
TiO_2	0.07 (0.04)	0.00	1.05 (0.08)	0.06	— —	—	0.46 (0.08)	0.03
Al_2O_3	21.67 (0.17)	1.97	18.47 (0.31)	1.55	25.73 (1.25)	1.33	34.95 (1.17)	2.81
FeO	31.08 (0.87)	2.00	13.10 (0.82)	0.78	0.23 (0.15)	0.01	0.92 (0.12)	0.07
MgO	4.32 (0.12)	0.50	16.24 (0.18)	1.73	0.06 (0.04)	0.00	1.27 (0.39)	0.16
MnO	1.58 (0.25)	0.10	0.04 (0.06)	0.00	— —	—	0.05 (0.03)	0.00
CaO	6.06 (0.18)	0.50	0.02 (0.04)	0.00	6.56 (1.10)	0.31	0.01 (0.02)	0.00
Na_2O	— —	—	0.28 (0.02)	0.04	7.86 (0.89)	0.67	0.96 (0.10)	0.11
K_2O	— —	—	8.47 (0.21)	0.77	0.11 (0.02)	0.01	8.84 (0.51)	0.93
Total:	103.28	8.04	97.15	7.75	101.41	5.00	96.22	7.10

Xalm	0.646	Xann 0.266	Xan 0.313	Xkmu 0.857
Xpyr	0.160	Xphl 0.588	Xab 0.681	Xnamu 0.142
Xsps	0.033			Xalmu 0.903
Xgrs	0.161	Al_2SiO_5 polymorph: kyanite		

92SC-75, psammitic schist

	garnet		biotite		plagioclase		muscovite	
	wt% (1σ)	stoich.	wt% (1σ)	stoich.	wt% (1σ)	stoich.	wt% (1σ)	stoich.
SiO_2	36.81 (0.29)	2.99	36.88 (0.26)	2.77	59.92 (0.66)	2.68	48.39 (0.88)	3.17
TiO_2	0.14 (0.03)	0.01	1.89 (0.23)	0.11	— —	—	0.79 (0.13)	0.04
Al_2O_3	21.12 (0.17)	2.02	18.72 (0.33)	1.65	25.09 (0.57)	1.32	34.19 (0.32)	2.64
FeO	29.95 (0.41)	2.03	17.84 (0.20)	1.12	0.36 (0.06)	0.01	1.65 (0.09)	0.09
MgO	2.25 (0.12)	0.27	10.55 (0.22)	1.18	0.03 (0.02)	0.00	1.03 (0.15)	0.10
MnO	1.36 (0.39)	0.09	0.16 (0.06)	0.01	— —	—	0.03 (0.03)	0.00
CaO	6.53 (0.50)	0.57	0.06 (0.03)	0.00	6.48 (0.37)	0.31	0.05 (0.02)	0.00
Na_2O	— —	—	0.14 (0.05)	0.02	7.78 (0.40)	0.68	0.47 (0.09)	0.06
K_2O	— —	—	9.36 (0.11)	0.90	0.14 (0.11)	0.01	9.19 (0.54)	0.77
Total:	98.16	7.99	95.60	7.76	99.80	5.01	95.79	6.88

Xalm 0.685
Xpyr 0.092
Xsps 0.032
Xgrs 0.191

Xann 0.394
Xphl 0.416

Xan 0.312
Xab 0.680

Xkmu 0.924
Xnamu 0.072
Xalmu 0.887

Al_2SiO_5 polymorph: none

92SC-87, psammitic schist

	garnet		biotite		plagioclase		muscovite	
	wt% (1σ)	stoich.	wt% (1σ)	stoich.	wt% (1σ)	stoich.	wt% (1σ)	stoich.
SiO_2	36.92 (0.28)	2.99	36.43 (0.39)	2.75	55.80 (1.47)	2.54	49.75 (0.92)	3.26
TiO_2	0.11 (0.04)	0.01	3.32 (0.15)	0.19	— —	—	1.42 (0.13)	0.07
Al_2O_3	21.45 (0.16)	2.04	17.96 (0.25)	1.60	27.10 (1.40)	1.45	31.17 (1.05)	2.41
FeO	26.16 (1.19)	1.77	18.58 (0.85)	1.17	0.55 (0.22)	0.02	2.07 (0.18)	0.11
MgO	1.80 (0.07)	0.22	9.60 (0.17)	1.08	0.04 (0.02)	0.00	1.70 (0.33)	0.17
MnO	3.80 (1.43)	0.26	0.10 (0.08)	0.01	— —	—	0.05 (0.03)	0.00
CaO	8.11 (0.17)	0.70	0.10 (0.07)	0.01	9.32 (1.39)	0.45	0.07 (0.06)	0.00
Na_2O	— —	—	0.08 (0.02)	0.01	6.16 (0.88)	0.54	0.25 (0.03)	0.03
K_2O	— —	—	9.18 (0.17)	0.88	0.05 (0.02)	0.00	9.82 (0.26)	0.82
Total:	98.35	7.99	95.34	7.71	99.01	5.01	96.31	6.89

Xalm 0.600
Xpyr 0.074
Xsps 0.088
Xgrs 0.238

Xann 0.419
Xphl 0.386

Xan 0.453
Xab 0.544

Xkmu 0.957
Xnamu 0.038
Xalmu 0.826

Al_2SiO_5 polymorph: none

92SC-91a, psammitic schist

	garnet		biotite		plagioclase		muscovite	
	wt% (1σ)	stoich.	wt% (1σ)	stoich.	wt% (1σ)	stoich.	wt% (1σ)	stoich.
SiO_2	37.51 (0.25)	3.01	36.77 (0.30)	2.77	56.02 (1.37)	2.50	1.37 (0.14)	3.18
TiO_2	0.09 (0.02)	0.01	2.29 (0.04)	0.13	— —	—	0.99 (0.21)	0.05
Al_2O_3	21.75 (0.17)	2.06	18.45 (0.11)	1.64	28.40 (1.00)	1.50	33.50 (0.56)	2.60
FeO	25.07 (0.87)	1.68	17.90 (0.41)	1.13	0.58 (0.21)	0.02	2.01 (0.41)	0.11
MgO	1.65 (0.09)	0.20	10.42 (0.39)	1.17	0.08 (0.11)	0.01	1.06 (0.14)	0.10
MnO	6.12 (0.61)	0.42	0.13 (0.03)	0.01	— —	—	0.05 (0.03)	0.00
CaO	6.94 (1.24)	0.60	0.10 (0.03)	0.00	9.91 (0.87)	0.48	0.06 (0.04)	0.00
Na_2O	— —	—	0.10 (0.02)	0.01	5.59 (0.65)	0.49	0.42 (0.03)	0.05
K_2O	— —	—	9.24 (0.06)	0.89	0.08 (0.09)	0.00	9.51 (0.21)	0.80
Total:	99.14	7.96	95.40	7.74	100.65	4.99	95.78	6.90

Xalm 0.581
Xpyr 0.068
Xsps 0.144
Xgrs 0.206

Xann 0.398
Xphl 0.413

Xan 0.492
Xab 0.504

Xkmu 0.933
Xnamu 0.062
Xalmu 0.870

Al_2SiO_5 polymorph: none

92SC-91b, psammitic schist

	garnet		biotite		plagioclase		muscovite	
	wt% (1σ)	stoich.	wt% (1σ)	stoich.	wt% (1σ)	stoich.	wt% (1σ)	stoich.
SiO_2	36.94 (0.46)	3.02	36.72 (0.22)	2.78	59.57 (0.83)	2.64	49.27 (0.62)	3.21
TiO_2	0.10 (0.03)	0.01	1.81 (0.23)	0.10	— —	—	0.86 (0.38)	0.04
Al_2O_3	21.25 (0.28)	2.05	18.49 (0.14)	1.65	25.95 (1.08)	1.36	33.72 (0.60)	2.59
FeO	28.77 (0.99)	1.97	17.75 (0.32)	1.12	0.37 (0.06)	0.01	1.62 (0.09)	0.09
MgO	1.84 (0.19)	0.22	10.25 (0.10)	1.16	0.03 (0.02)	0.00	1.08 (0.13)	0.10
MnO	4.77 (2.26)	0.33	0.10 (0.03)	0.01	— —	—	0.05 (0.03)	0.00
CaO	4.17 (1.12)	0.37	0.07 (0.02)	0.01	7.37 (0.91)	0.35	0.04 (0.02)	0.00
Na_2O	— —	—	0.13 (0.04)	0.02	7.12 (0.56)	0.61	0.51 (0.05)	0.06
K_2O	— —	—	9.32 (0.48)	0.90	0.10 (0.10)	0.01	9.32 (0.48)	0.77
Total:	97.85	7.95	94.65	7.75	100.51	4.99	96.47	6.87

Xalm 0.681
Xpyr 0.078
Xsps 0.114
Xgrs 0.127

Xann 0.398
Xphl 0.410

Xan 0.361
Xab 0.633

Xkmu 0.920
Xnamu 0.076
Xalmu 0.883

Al_2SiO_5 polymorph: none

92SC-102, psammitic schist

	garnet		biotite		plagioclase		muscovite	
	wt% (1σ)	stoich.	wt% (1σ)	stoich.	wt% (1σ)	stoich.	wt% (1σ)	stoich.
SiO_2	37.38 (0.28)	2.99	36.70 (0.53)	2.73	56.95 (1.21)	2.55	48.76 (0.83)	3.17
TiO_2	0.09 (0.02)	0.01	2.53 (0.13)	0.14	— —	—	1.03 (0.40)	0.05
Al_2O_3	21.55 (0.19)	2.03	19.19 (0.52)	1.68	27.54 (0.64)	1.45	34.22 (0.95)	2.62
FeO	25.37 (0.55)	1.70	18.35 (0.51)	1.14	0.39 (0.08)	0.01	1.93 (0.42)	0.11
MgO	1.56 (0.15)	0.19	10.16 (0.35)	1.13	0.02 (0.01)	0.00	1.13 (0.12)	0.11
MnO	8.74 (0.45)	0.59	0.20 (0.07)	0.01	— —	—	0.03 (0.03)	0.00
CaO	5.83 (0.63)	0.50	0.08 (0.05)	0.01	8.87 (0.78)	0.43	0.04 (0.05)	0.00
Na_2O	— —	—	0.28 (0.13)	0.04	6.39 (0.46)	0.56	0.45 (0.06)	0.06
K_2O	— —	—	9.27 (0.14)	0.88	0.06 (0.01)	0.00	9.03 (0.71)	0.75
Total:	100.53	7.99	96.77	7.75	100.21	5.00	96.61	6.87

Xalm 0.570
Xpyr 0.062
Xsps 0.199
Xgrs 0.168

Xann 0.403
Xphl 0.398

Xan 0.432
Xab 0.565

Xkmu 0.926
Xnamu 0.071
Xalmu 0.871

Al_2SiO_5 polymorph: none

93SC-22, calc-pelitic schist

	garnet		biotite		plagioclase		muscovite	
	wt% (1σ)	stoich.	wt% (1σ)	stoich.	wt% (1σ)	stoich.	wt% (1σ)	stoich.
SiO_2	37.92 (0.28)	3.00	36.96 (0.78)	2.76	61.11 (1.59)	2.70	47.12 (0.39)	3.15
TiO_2	0.04 (0.04)	0.00	1.56 (0.15)	0.09	— —	—	0.55 (0.06)	0.03
Al_2O_3	21.27 (0.21)	1.99	18.06 (0.37)	1.59	25.10 (0.81)	1.31	33.51 (0.61)	2.64
FeO	30.74 (0.93)	2.04	15.97 (0.82)	1.00	0.15 (0.12)	0.01	1.31 (0.15)	0.07
MgO	2.95 (0.33)	0.35	13.07 (0.47)	1.46	0.01 (0.03)	0.00	1.41 (0.19)	0.14
MnO	2.77 (0.23)	0.19	0.06 (0.03)	0.00	— —	—	0.03 (0.02)	0.00
CaO	5.15 (1.14)	0.44	0.02 (0.01)	0.00	5.92 (1.11)	0.28	0.01 (0.01)	0.00
Na_2O	— —	—	0.22 (0.06)	0.03	8.27 (0.61)	0.71	0.95 (0.08)	0.12
K_2O	— —	—	9.01 (0.36)	0.86	0.14 (0.21)	0.01	9.83 (0.11)	0.84
Total:	100.83	8.00	94.93	7.80	100.70	5.01	94.71	6.99

Xalm 0.677
Xpyr 0.116
Xsps 0.062
Xgrs 0.145

Xann 0.344
Xphl 0.502

Xan 0.281
Xab 0.712

Xkmu 0.871
Xnamu 0.128
Xalmu 0.880

Al_2SiO_5 polymorph: none

93SC-24, calc-pelitic schist

	garnet		biotite		plagioclase		muscovite	
	wt% (1σ)	stoich.	wt% (1σ)	stoich.	wt% (1σ)	stoich.	wt% (1σ)	stoich.
SiO_2	38.68 (0.18)	3.01	38.86 (0.18)	2.80	60.05 (0.87)	2.64	49.44 (0.38)	3.20
TiO_2	0.11 (0.05)	0.01	1.38 (0.04)	0.07	— —	—	0.44 (0.06)	0.02
Al_2O_3	21.29 (0.15)	1.96	18.39 (0.18)	1.56	26.54 (0.65)	1.38	34.73 (0.38)	2.65
FeO	29.65 (0.31)	1.93	12.88 (0.28)	0.78	0.06 (0.02)	0.00	1.01 (0.25)	0.05
MgO	4.24 (0.21)	0.49	15.94 (0.31)	1.72	0.02 (0.05)	0.00	1.25 (0.08)	0.12
MnO	2.81 (0.28)	0.19	0.09 (0.04)	0.01	— —	—	0.01 (0.02)	0.00
CaO	4.95 (0.11)	0.41	0.01 (0.01)	0.00	7.53 (0.95)	0.35	0.04 (0.02)	0.00
Na_2O	— —	—	0.25 (0.04)	0.04	6.87 (0.23)	0.59	0.97 (0.06)	0.12
K_2O	— —	—	8.20 (0.14)	0.76	0.09 (0.39)	0.01	8.41 (0.11)	0.69
Total:	101.74	8.00	96.00	7.73	101.16	4.97	96.30	6.86
	Xalm 0.639		Xann 0.264		Xan 0.374		Xkmu 0.848	
	Xpyr 0.163		Xphl 0.583		Xab 0.620		Xnamu 0.149	
	Xsps 0.061						Xalmu 0.904	
	Xgrs 0.137		Al_2SiO_5 polymorph: kyanite					

93SC-25, calc-pelitic schist

	garnet		biotite		plagioclase		muscovite	
	wt% (1σ)	stoich.	wt% (1σ)	stoich.	wt% (1σ)	stoich.	wt% (1σ)	stoich.
SiO_2	38.86 (0.59)	2.98	39.25 (0.31)	2.81	59.17 (1.48)	2.60	49.25 (0.94)	3.17
TiO_2	0.07 (0.02)	0.00	1.19 (0.21)	0.06	— —	—	0.40 (0.15)	0.02
Al_2O_3	21.87 (0.33)	1.98	18.59 (0.28)	1.57	27.14 (1.24)	1.41	35.27 (0.79)	2.68
FeO	30.93 (0.74)	1.98	13.17 (0.27)	0.79	0.17 (0.10)	0.01	1.04 (0.12)	0.06
MgO	4.24 (0.17)	0.50	16.03 (0.49)	1.71	0.03 (0.07)	0.00	1.23 (0.26)	0.12
MnO	1.48 (0.57)	0.10	0.02 (0.03)	0.00	— —	—	0.07 (0.05)	0.00
CaO	6.08 (0.22)	0.50	0.04 (0.02)	0.00	8.17 (1.34)	0.38	0.01 (0.01)	0.00
Na_2O	— —	—	0.28 (0.03)	0.04	6.82 (0.86)	0.58	0.92 (0.07)	0.12
K_2O	— —	—	8.51 (0.10)	0.78	0.08 (0.07)	0.00	8.80 (0.33)	0.72
Total:	103.53	8.03	97.07	7.75	101.57	4.99	97.00	6.89
	Xalm 0.647		Xann 0.268		Xan 0.396		Xkmu 0.862	
	Xpyr 0.158		Xphl 0.582		Xab 0.600		Xnamu 0.137	
	Xsps 0.031						Xalmu 0.904	
	Xgrs 0.163		Al_2SiO_5 polymorph: kyanite					

93SC-26, calc-pelitic schist

	garnet		biotite		plagioclase		muscovite	
	wt% (1σ)	stoich.	wt% (1σ)	stoich.	wt% (1σ)	stoich.	wt% (1σ)	stoich.
SiO_2	38.18 (0.14)	3.01	39.22 (0.09)	2.85	60.81 (0.93)	2.67	47.35 (0.36)	3.15
TiO_2	0.11 (0.05)	0.01	1.42 (0.03)	0.08	— —	—	0.33 (0.05)	0.02
Al_2O_3	21.39 (0.13)	1.99	18.17 (0.18)	1.56	26.21 (0.72)	1.36	34.15 (0.39)	2.68
FeO	26.47 (0.34)	1.75	12.23 (0.29)	0.74	0.06 (0.02)	0.00	0.94 (0.22)	0.05
MgO	3.69 (0.22)	0.43	15.07 (0.34)	1.63	0.05 (0.06)	0.00	1.28 (0.06)	0.13
MnO	4.79 (0.31)	0.32	0.09 (0.04)	0.01	— —	—	0.04 (0.02)	0.00
CaO	5.60 (0.09)	0.47	0.04 (0.02)	0.00	6.62 (1.09)	0.31	0.04 (0.02)	0.00
Na_2O	— —	—	0.24 (0.04)	0.03	7.14 (0.22)	0.61	1.06 (0.05)	0.14
K_2O	— —	—	8.77 (0.13)	0.81	0.25 (0.38)	0.01	9.19 (0.10)	0.78
Total:	100.23	7.99	95.25	7.72	101.14	4.96	94.37	6.95
	Xalm 0.587		Xann 0.259		Xan 0.333		Xkmu 0.848	
	Xpyr 0.146		Xphl 0.570		Xab 0.652		Xnamu 0.149	
	Xsps 0.108						Xalmu 0.902	
	Xgrs 0.159		Al_2SiO_5 polymorph: kyanite					

93SC-33, psammitic schist

	garnet		biotite		plagioclase		muscovite	
	wt% (1σ)	stoich.	wt% (1σ)	stoich.	wt% (1σ)	stoich.	wt% (1σ)	stoich.
SiO_2	37.48 (0.25)	3.01	36.84 (0.26)	2.77	56.37 (1.08)	2.52	48.18 (0.39)	3.18
TiO_2	0.09 (0.02)	0.01	2.29 (0.04)	0.13	— —	—	1.01 (0.20)	0.05
Al_2O_3	21.76 (0.18)	2.06	18.44 (0.11)	1.63	28.15 (0.81)	1.48	33.46 (0.57)	2.60
FeO	24.97 (0.87)	1.67	17.85 (0.42)	1.12	0.57 (0.20)	0.02	2.02 (0.44)	0.11
MgO	1.64 (0.08)	0.20	10.50 (0.36)	1.17	0.07 (0.11)	0.00	1.05 (0.14)	0.10
MnO	6.09 (0.64)	0.41	0.12 (0.04)	0.01	— —	—	0.06 (0.03)	0.00
CaO	7.11 (1.21)	0.61	0.09 (0.02)	0.01	9.73 (0.84)	0.47	0.06 (0.04)	0.00
Na_2O	— —	—	0.10 (0.02)	0.01	5.72 (0.53)	0.50	0.42 (0.03)	0.05
K_2O	— —	—	9.24 (0.07)	0.88	0.08 (0.10)	0.00	9.58 (0.14)	0.81
Total:	99.13	7.96	95.47	7.74	100.67	4.99	95.84	6.91
	Xalm 0.578		Xann 0.396		Xan 0.481		Xkmu 0.933	
	Xpyr 0.068		Xphl 0.415		Xab 0.514		Xnamu 0.062	
	Xsps 0.143						Xalmu 0.869	
	Xgrs 0.211		Al_2SiO_5 polymorph: none					

inclusion compositions, inner core of garnet, 93SC-24

(average of analyses from locations 1, 4, and 5 shown in figure 16)

	local garnet	staurolite	chloritoid	chlorite	margarite	paragonite	ilmenite
SiO_2	37.46	28.93	24.93	24.93	33.19	47.72	0.11
TiO_2	0.12	0.59	0.50	0.12	0.11	0.12	53.70
Al_2O_3	21.16	56.21	38.16	24.40	48.88	41.12	0.03
FeO	29.59	12.65	21.45	25.20	0.78	0.44	46.03
MgO	2.01	1.44	3.92	14.23	0.21	0.06	0.07
MnO	7.90	0.36	0.93	0.26	0.00	0.01	2.17
CaO	2.92	0.02	0.00	0.06	9.95	1.33	0.05
Na_2O	—	(ZnO=0.68)	—	—	2.11	5.12	—
K_2O	—	—	—	—	0.04	0.09	—
Total:	101.17	100.87	89.39	89.21	95.27	96.01	102.16
fomula basis:	(12)	(48)	(12)	(28)	(11)	(11)	(3)
Si	3.00	8.09	2.11	5.14	2.19	3.00	0.00
Ti	0.01	0.12	0.00	0.02	0.01	0.01	1.00
Al	1.99	18.52	3.80	5.93	3.80	3.04	0.00
Fe	1.98	2.96	1.52	4.35	0.04	0.02	0.95
Mg	0.24	0.60	0.49	4.38	0.02	0.01	0.00
Mn	0.54	0.08	0.08	0.05	0.00	0.00	0.05
Ca	0.25	0.01	0.01	0.01	0.70	0.09	0.00
Na	—	(Zn=0.28)	—	—	0.27	0.62	—
K	—	—	—	—	0.00	0.01	—
cation total:	8.00	30.67	7.99	19.87	7.04	6.79	2.00

inclusion compositions, intermediate core of garnet, 93SC-24

(average of analyses from locations 2, 6, 12, 13, and 14 shown in figure 16)

	local garnet	staurolite	chloritoid	chlorite	margarite	paragonite	ilmenite
SiO_2	37.96	28.59	25.12	24.80	33.71	48.55	not analyzed
TiO_2	0.07	0.57	0.00	0.10	0.13	0.13	
Al_2O_3	21.00	53.80	41.56	23.64	48.83	41.70	
FeO	30.54	12.42	21.97	23.97	0.92	0.61	
MgO	2.54	2.22	4.10	16.88	0.38	0.07	
MnO	5.55	0.20	0.62	0.20	0.00	0.00	
CaO	3.67	0.02	0.00	0.06	9.67	1.36	
Na_2O	—	(ZnO=1.08)	—	—	2.08	4.83	
K_2O	—	—	—	—	0.06	0.51	
Total:	101.33	98.90	93.37	89.64	95.78	97.76	
fomula basis:	(12)	(48)	(12)	(28)	(11)	(11)	
Si	3.01	8.12	2.03	5.07	2.21	3.00	
Ti	0.00	0.12	0.00	0.02	0.01	0.01	
Al	1.97	18.13	3.95	5.70	3.78	3.04	
Fe	2.03	2.97	1.48	4.10	0.05	0.03	
Mg	0.30	0.95	0.49	5.14	0.04	0.01	
Mn	0.37	0.05	0.04	0.04	0.00	0.00	
Ca	0.31	0.01	0.00	0.01	0.68	0.09	
Na	—	(Zn=0.46)	—	—	0.27	0.58	
K	—	—	—	—	0.00	0.04	
cation total:	8.00	30.86	8.00	20.07	7.03	6.79	

inclusion compositions, outer core of garnet, 93SC-24

(average of analyses from locations 7, 8, 15, and 18 shown in figure 16)

	local garnet	staurolite	chloritoid	chlorite	margarite	paragonite	ilmenite
SiO_2	38.28	28.58	25.30	25.61	34.14	48.84	0.11
TiO_2	0.06	0.53	0.00	0.09	0.44	0.19	54.24
Al_2O_3	21.27	53.65	42.27	23.86	48.79	40.39	0.03
FeO	32.02	13.02	21.31	20.30	0.98	0.36	47.01
MgO	2.92	2.16	4.98	18.67	0.38	0.04	0.39
MnO	3.19	0.11	0.19	0.12	0.04	0.00	0.71
CaO	4.23	0.02	0.03	0.04	9.15	0.68	0.03
Na_2O	—	(ZnO=0.82)	—	—	2.40	5.14	—
K_2O	—	—	—	—	0.09	0.22	—
Total:	101.96	98.88	94.07	88.70	96.43	95.85	102.51
fomula basis:	(12)	(48)	(12)	(28)	(11)	(11)	(3)
Si	3.01	8.18	2.01	5.18	2.23	3.06	0.00
Ti	0.00	0.11	0.00	0.01	0.02	0.01	1.00
Al	1.97	18.11	3.97	5.69	3.75	2.98	0.00
Fe	2.11	3.12	1.42	3.43	0.05	0.02	0.96
Mg	0.34	0.92	0.59	5.63	0.04	0.00	0.01
Mn	0.21	0.03	0.01	0.02	0.00	0.00	0.02
Ca	0.36	0.01	0.00	0.01	0.64	0.05	0.00
Na	—	(Zn=0.35)	—	—	0.31	0.63	—
K	—	—	—	—	0.01	0.02	—
cation total:	8.00	30.82	8.00	19.97	7.04	6.76	2.00

FIGURES FOR CHAPTER 5

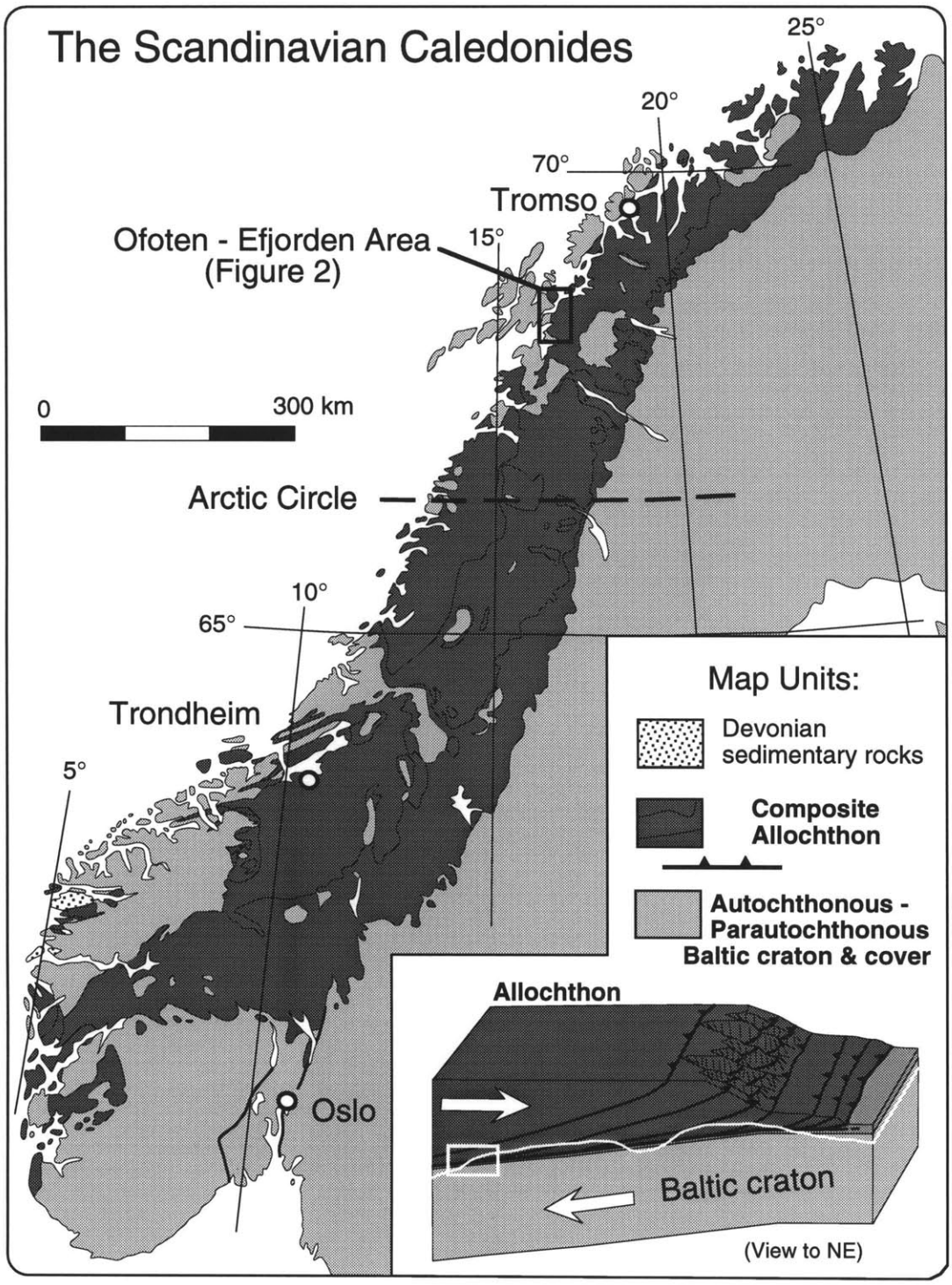

Figure 1: Simplified geologic map of the Scandinavian Caledonides, showing the distribution of the erosional remnant of the Caledonian allochthon (modified from Gee et al., 1985). Inset shows a schematic block diagram (not to scale) illustrating A-type subduction of the Baltic craton beneath the composite allochthon during the Caledonian collision. The white line shows the approximate level of exposure today, and the white box indicates the general structural position inferred for rocks in the study area during the collision.

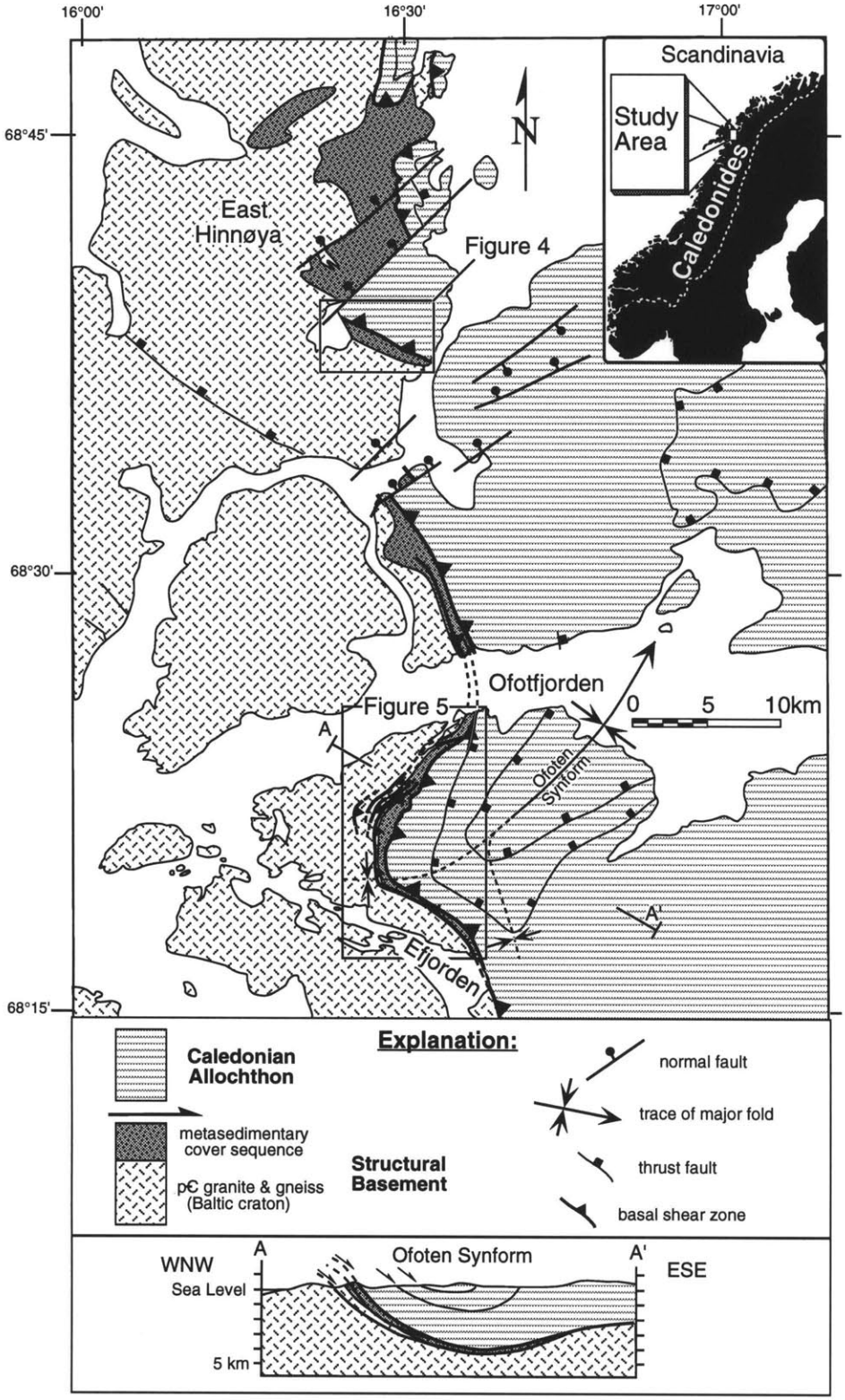

Figure 2: Simplified geologic map of the Ofoten-Efjorden area. (compiled from Gustavson, 1974; Bartley, 1981; Hodges, 1982; Steltenpohl, 1983, 1985; and Northrup, unpublished mapping)

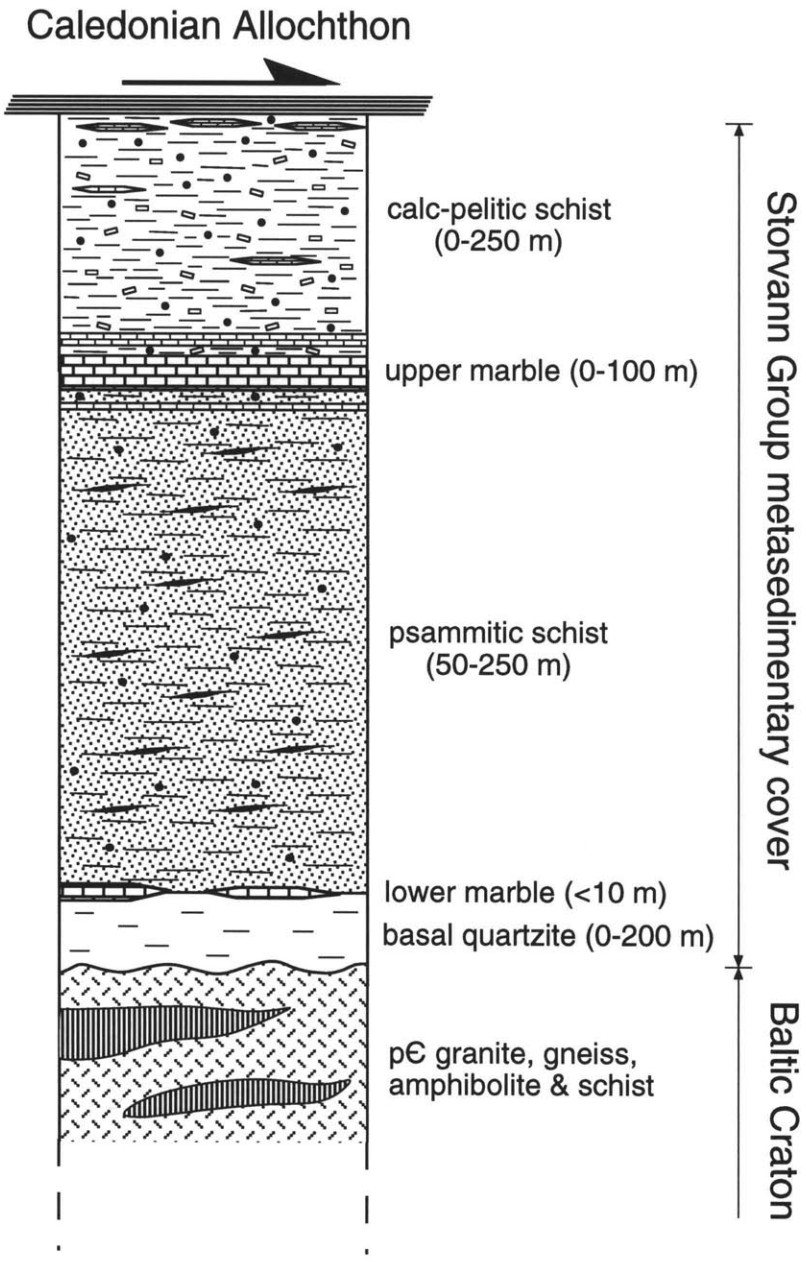

Figure 3: Stratigraphy of the Storvann Group metasedimentary rocks interpreted as a strongly tectonized remnant of the early Paleozoic cover sequence on Baltica (after Bartley 1981).

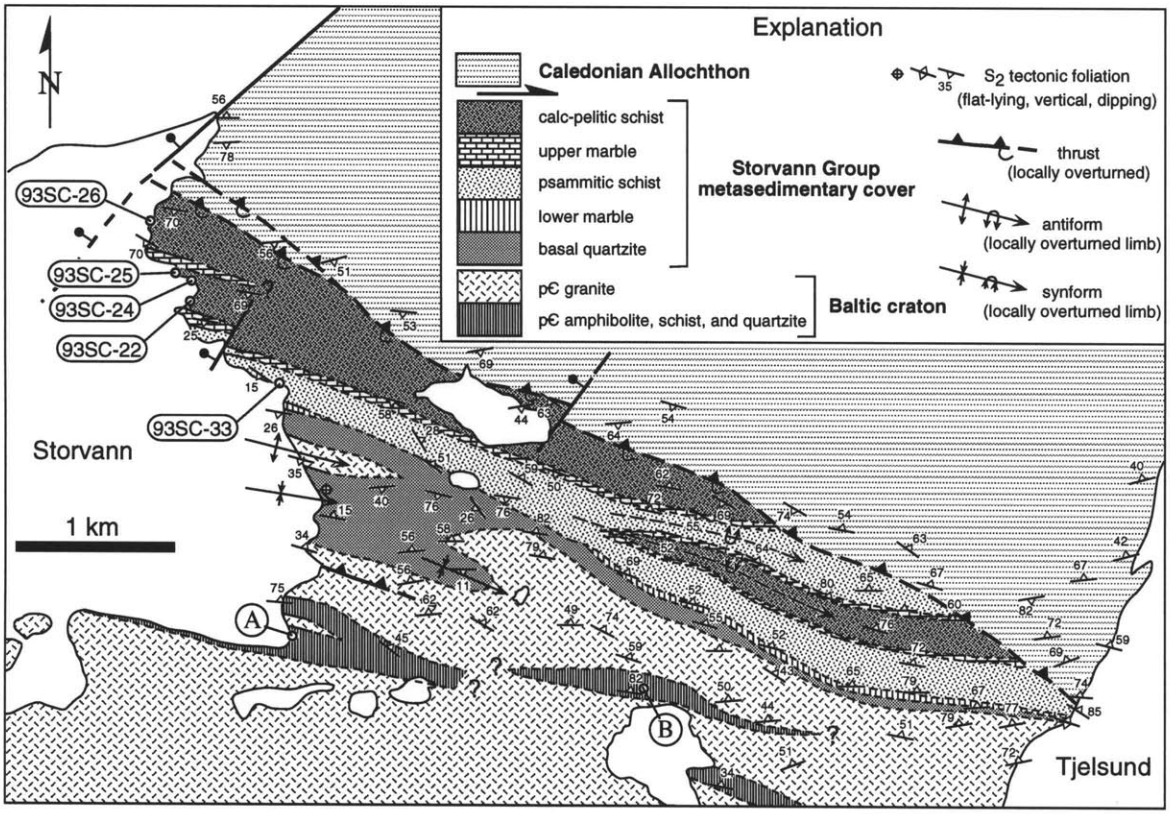

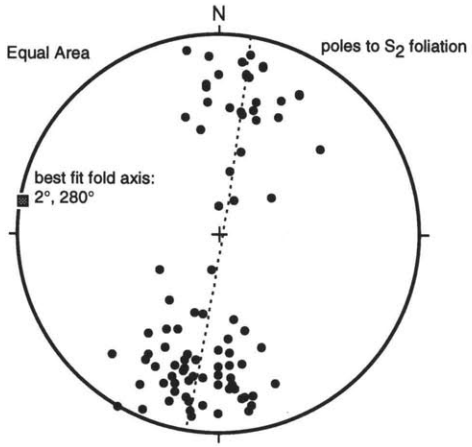

Figure 4: Simplified geologic map of the metasedimentary cover rocks on E. Hinnøya from Storvann to Tjelsund. Exposures along the eastern shore of Storvann were designated as the type locality by Bartley (1980, 1981). Elongate lables refer to sample locations; circled letters refer to locations where intrusive relations between Proterozoic granite and Precambrian supracrustal rocks were observed.

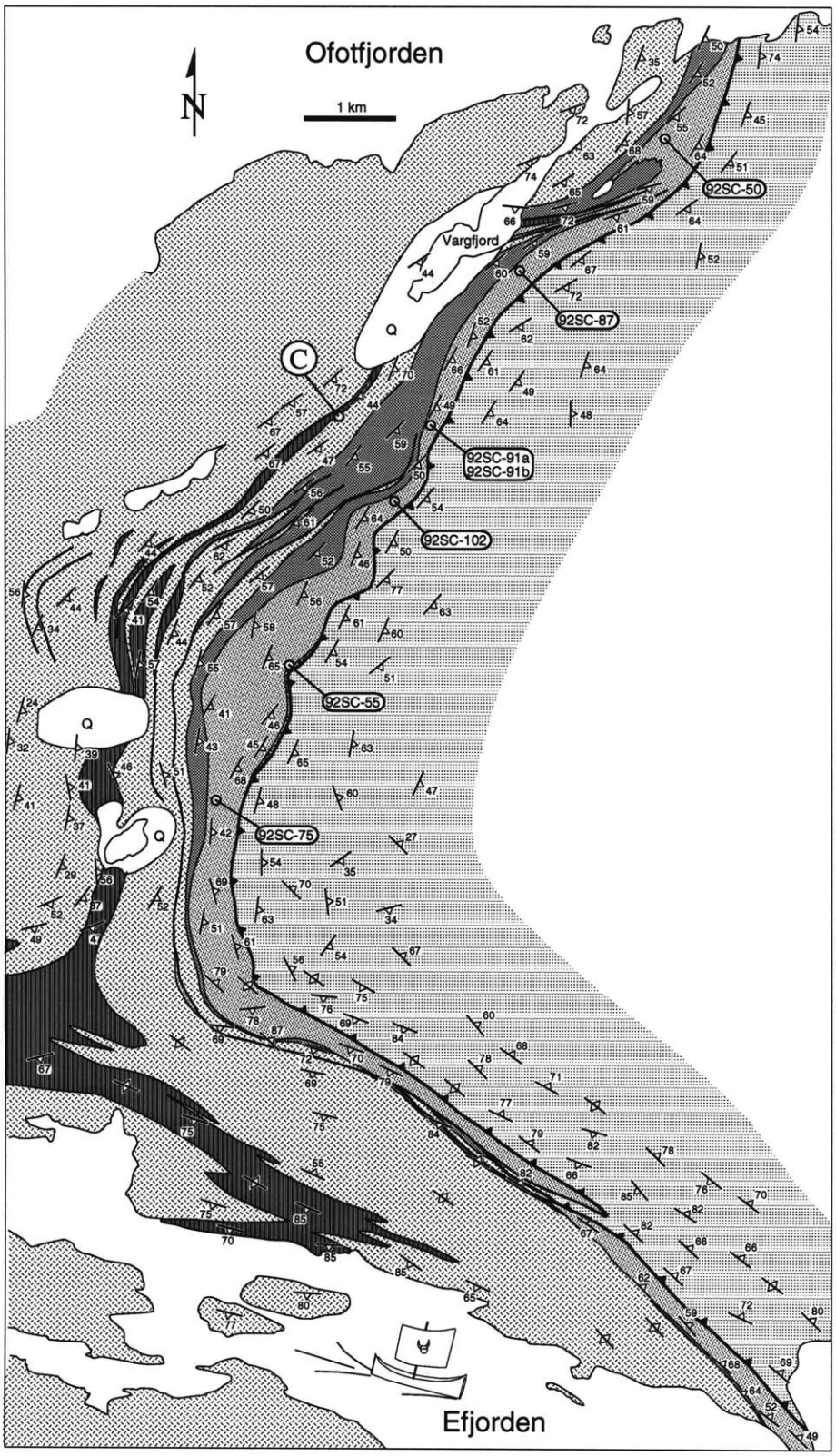

Figure 5: Simplified Geologic map illustrating the distribution of Storvann Group metasedimentary rocks beneath the Caledonian aloochthon from Ofotfjorden southward to Efjorden. Elongate lables show sample locations; circled letter shows location of clear intrusive relationship between Proterozoic granite and older Precambrian supracrustal rocks.

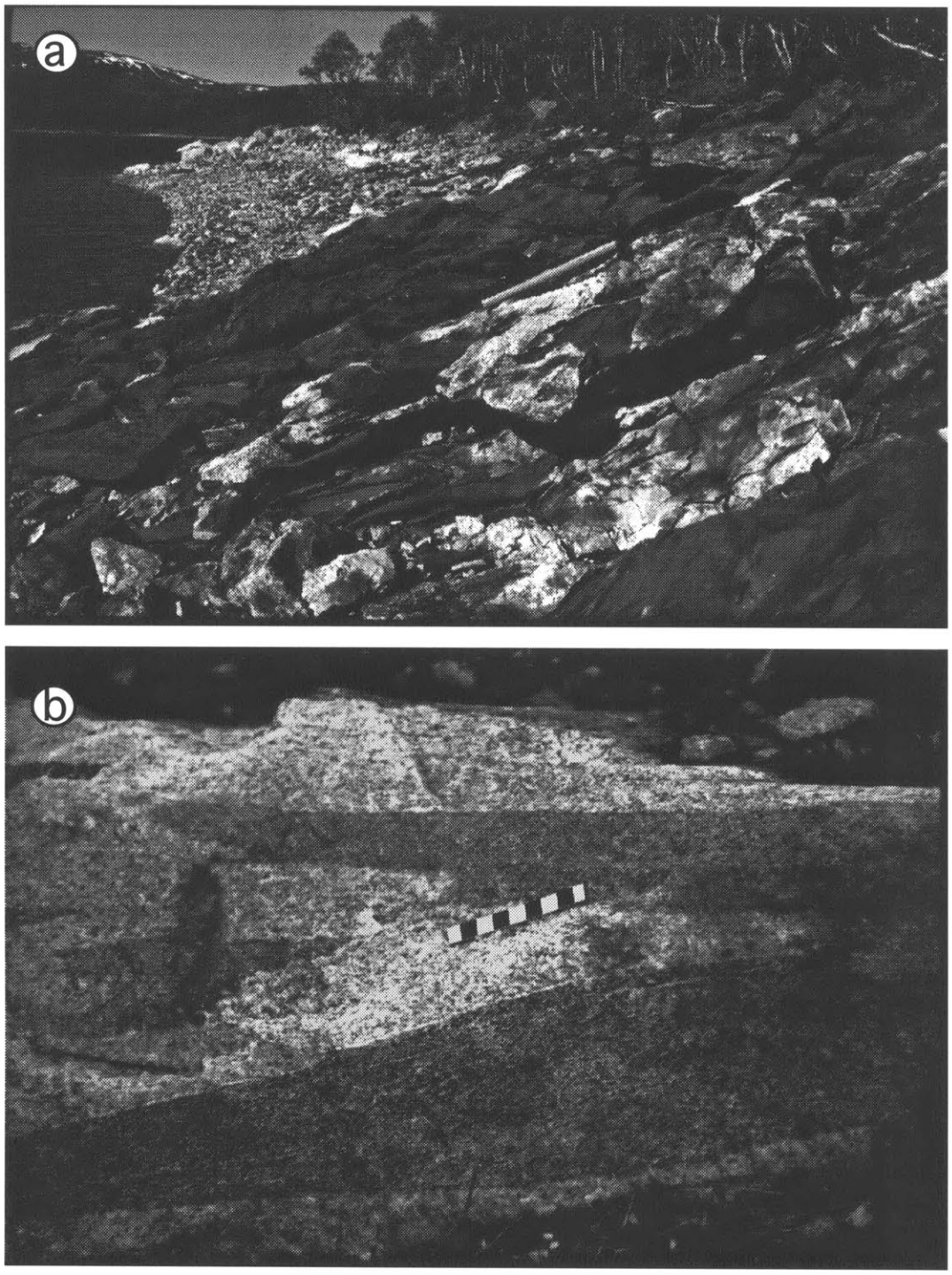

Figure 6: Photographs of intrusive relationship between Proterozoic granite and supracrustal rocks within the Baltic craton. a) granite intruding amphibolite along the shore of Storvann on East Hinnøya (location A, Figure 4). b) Xenoliths of epidote-amphibolite and quartz-biotite schist surrounded by Proterozoic granite on Vargfjellet, south of Ofotfjorden (location C, figure 5).

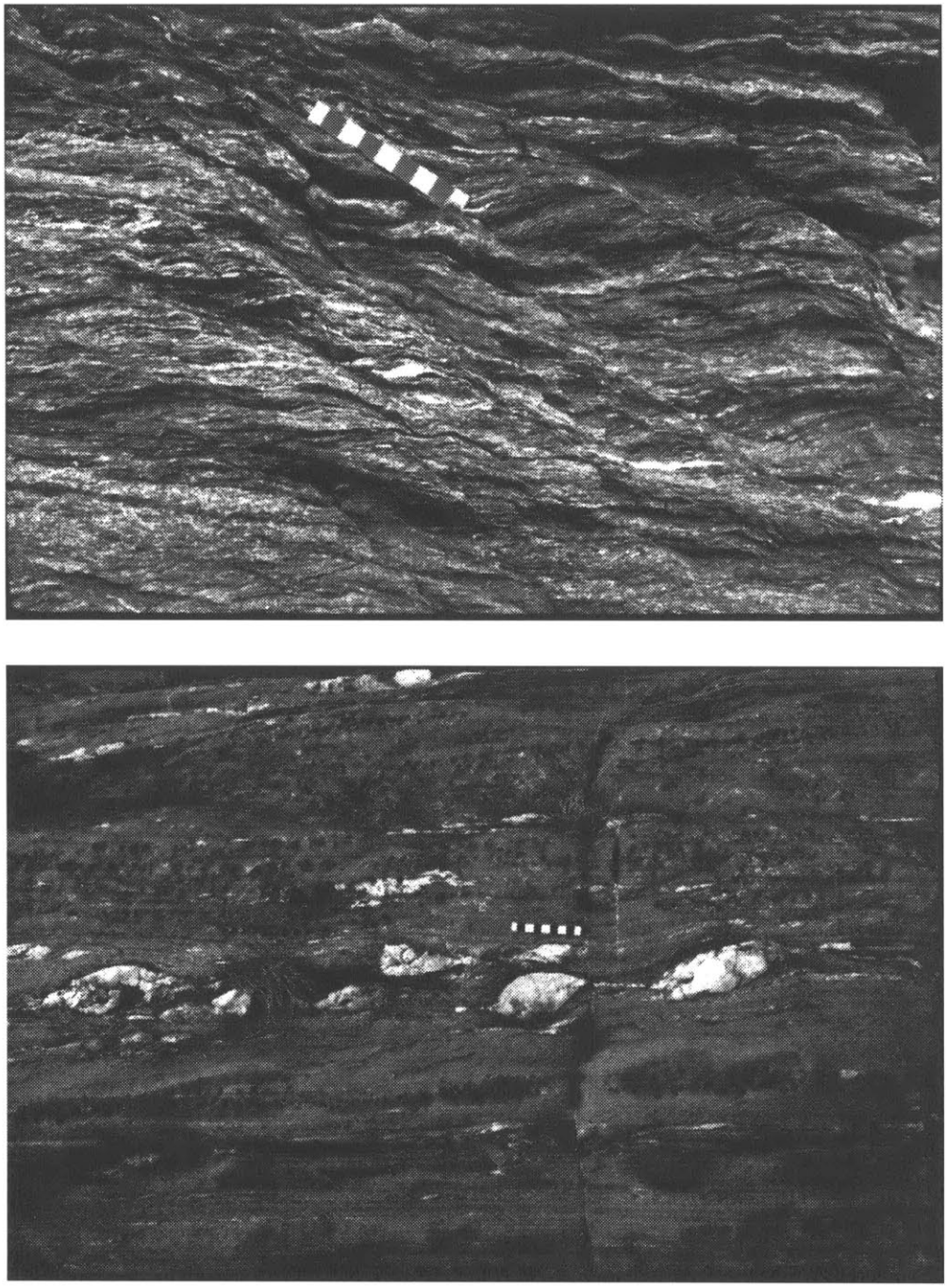

Figure 7: Outcrop photographs showing features used to infer sense of shear across the basal thrust of the Caledonian allochthon. Outcrop surfaces are oriented purpendicular to foliation (S2) and parallel to the strethching lineation (L2). All views look NNE. a) asymetric shear bands or extensional crenulation cleavage. b) asymmetrically boudinaged veins yielding porphyroclasts that step to the right. All are consistent with dextral (top-to-the-ESE) shear.

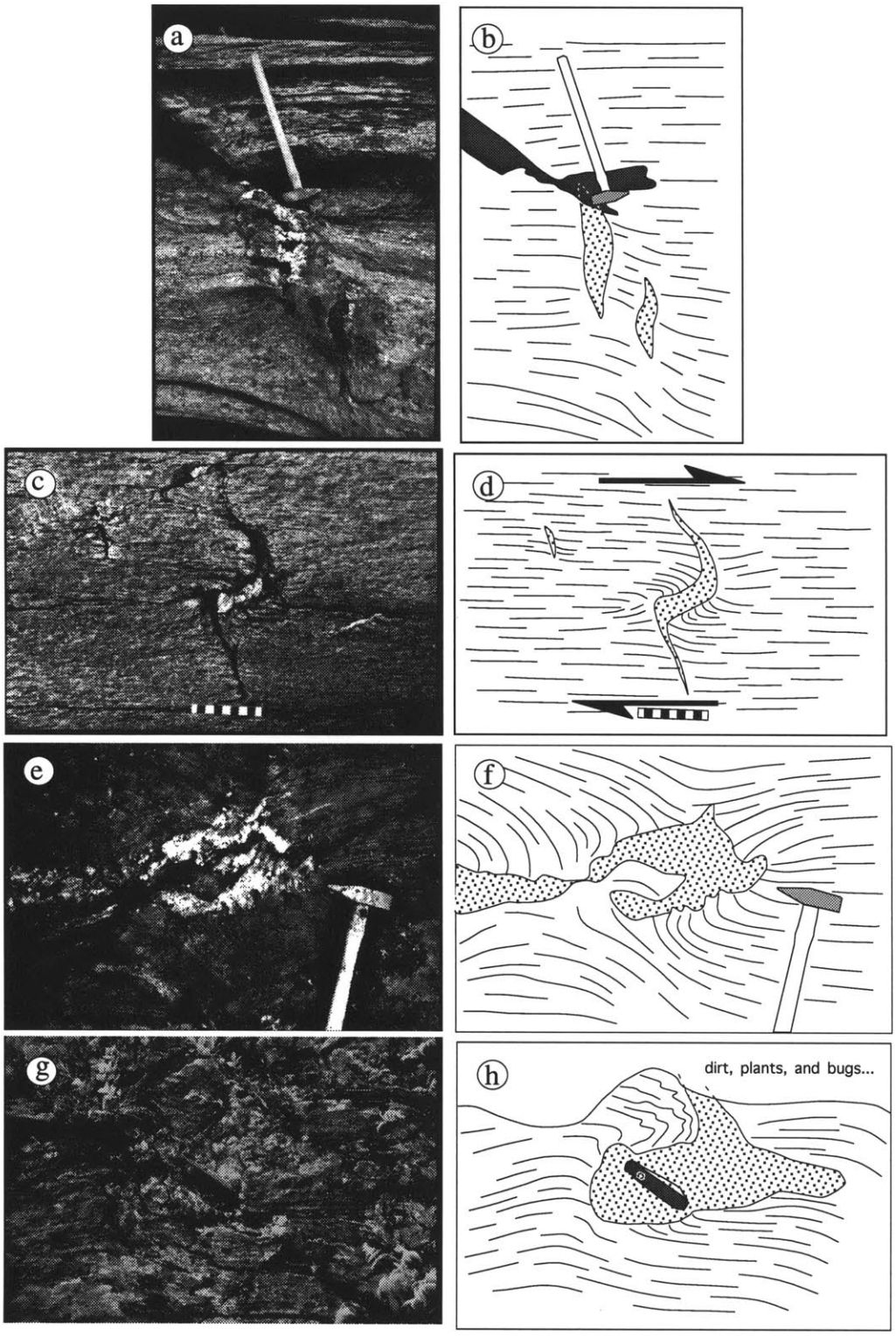

Figure 8: Outcrop photograph & sketch pairs showing vaious manifestations of quartz-calcite-plagioclase veins filling sites of local syntectonic dilatancy. All outcrop surfaces are oriented purpendicular to foliation (S2) and parallel to stretching lineation (L2), and the view is to the NNE. a-b) tension gash veins with slightly sigmoidal geometry; c-d) tension gash veins with stronger sigmoidal geometry due to rotation of the central section of the vein; e-f) vein filling the neck region of foliation boudinage. Note complex foliation geometry in surrounding schist; g-h) vein filling the neck of foliation boudinage. The vein and adjacent schist exhibit clockwise rotation, consistent with dextral (top-to-the ESE) progressive shear.

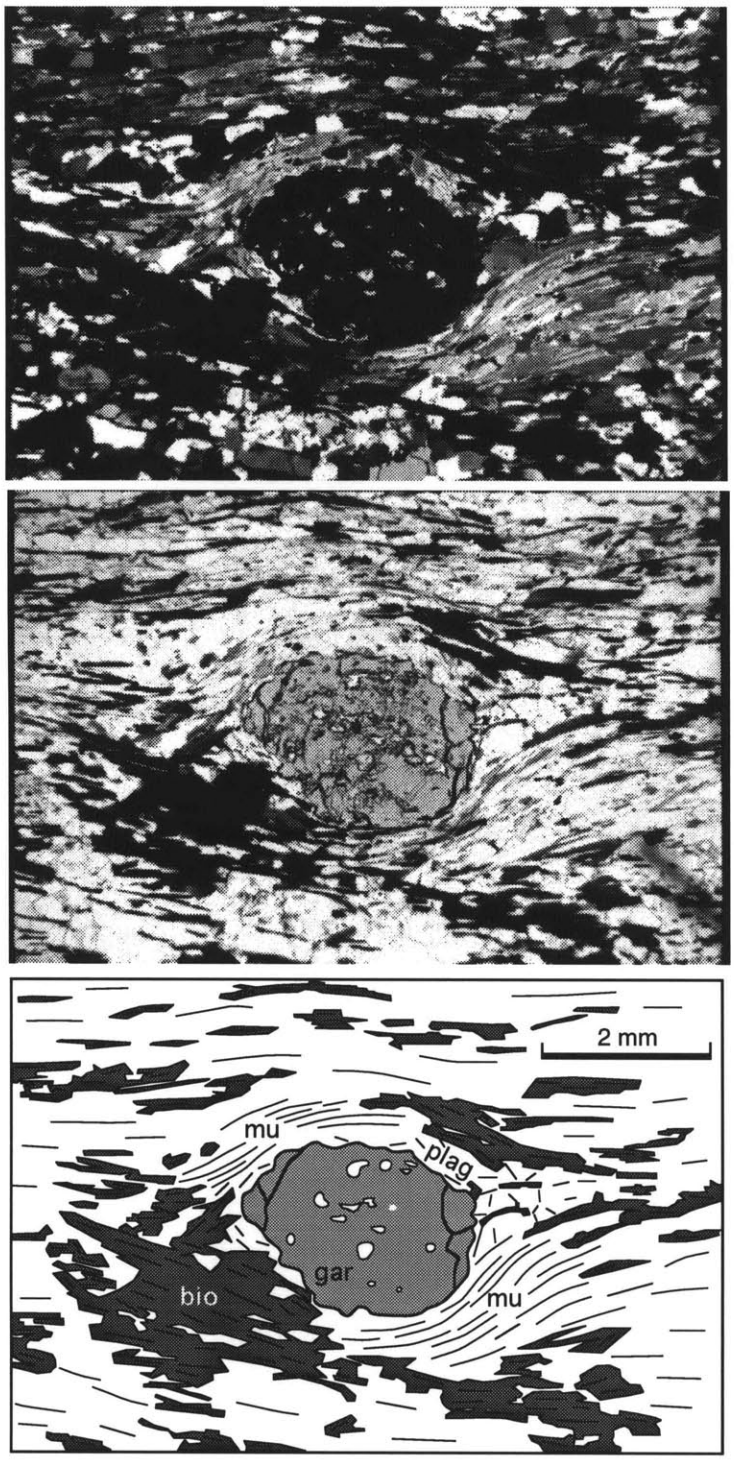

Figure 9: Photomicrographs of a garnet porphyroblast in the psammitic schist (sample 92SC-91a). The section is cut purpendicular to foliation (S2) and parallel to stretching lineation (L2); the view is looking North. Note the irregular, embayed morphology, consistent with resorption of the garnet. Adjacent to the garnet, the pressure shadows are filled with plagioclase ± biotite (upper-right & lower-left quadrants), and the high-pressure zones contain abundant muscovite (upper-left and lower-right quadrants).

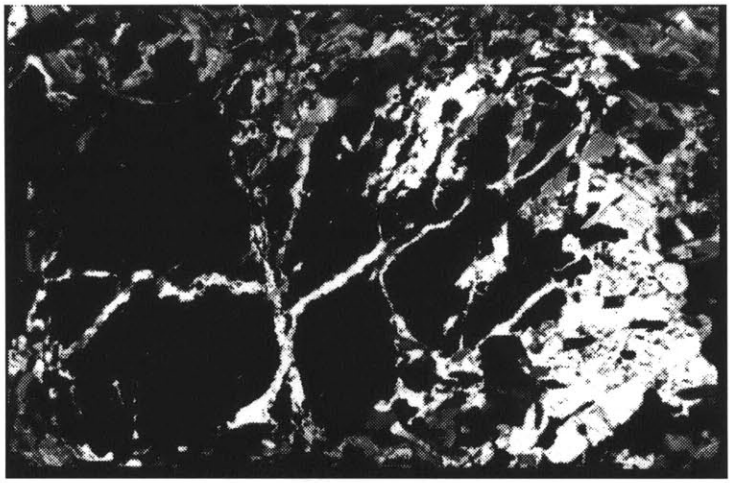

cross-polarized
illumination

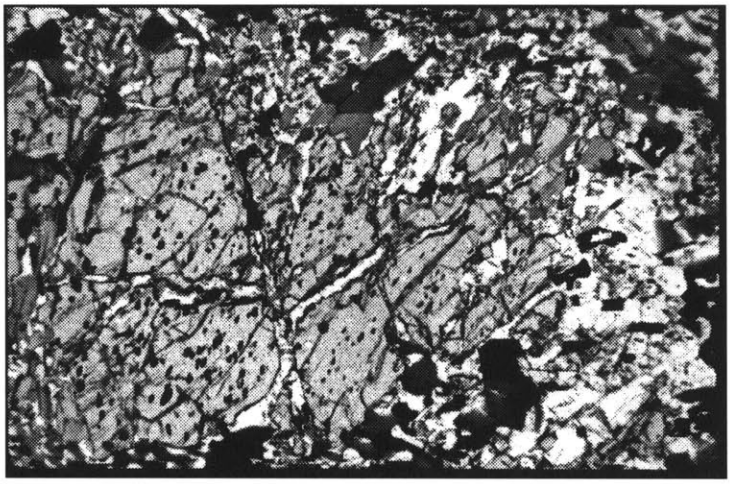

plane-polarized
illumination

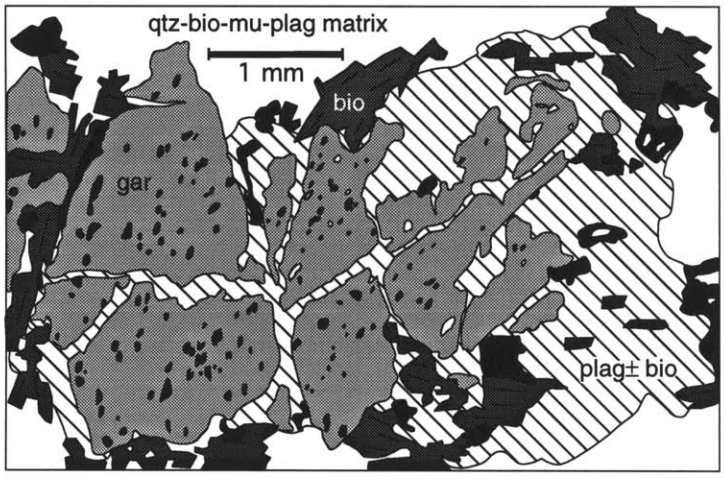

Figure 10: Photomicrographs of a garnet porphyroblast in the psammitic schist, sample 92SC-102. The garnet has been resorbed, mechanically broken, and overgrown by optically continous plagioclase.

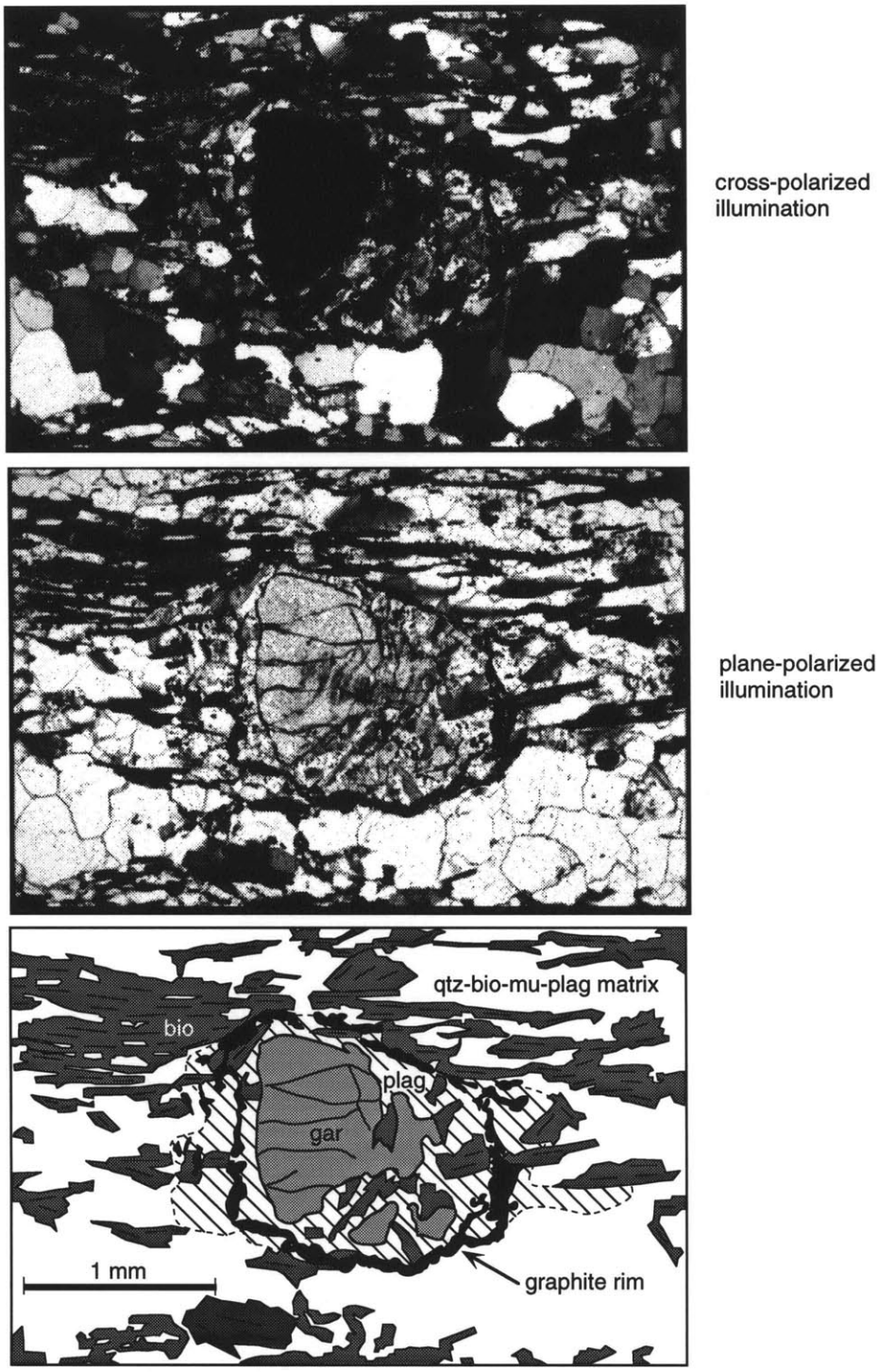

Figure 11: Photomicrographs and sketch of a garnet in the psammitic schist (sample 92SC-102). The section is cut purpendicular to foliation (S2) and parallel to stretching lineation (L2). The opaque material is graphite. The graphitic rind marks the original extent of garnet which has been largely resorbed and replaced by plagioclase ± biotite.

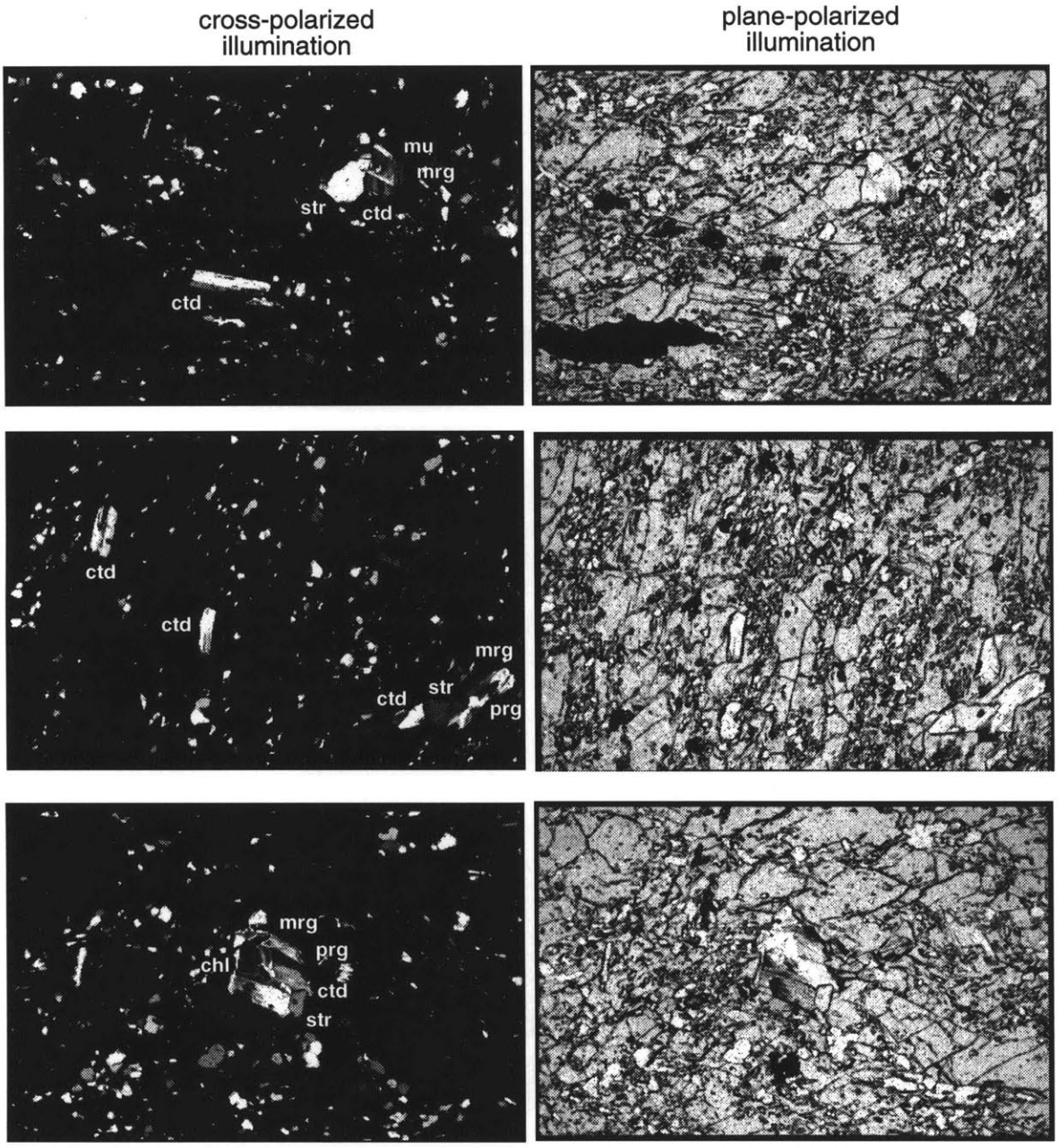

Figure 12: Photomicrographs of polymineralic inclusions within garnet porphyroblasts from sample 93SC-24. Petrogenetically significant minerals found as inclusions include chloritoid (ctd), chlorite (chl), staurolite (str), margarite (mrg), and paragonite (prg).

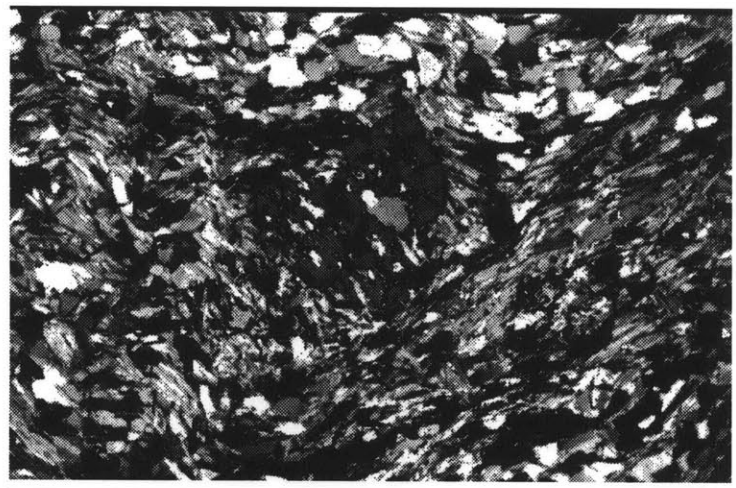

cross-polarized illumination

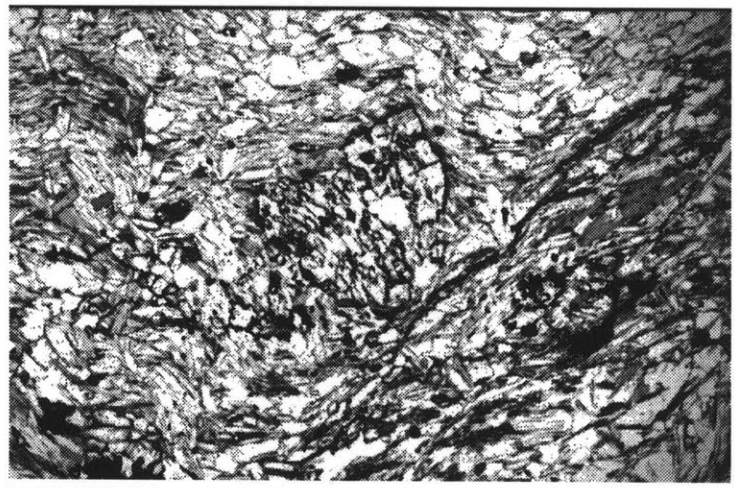

plane-polarized illumination

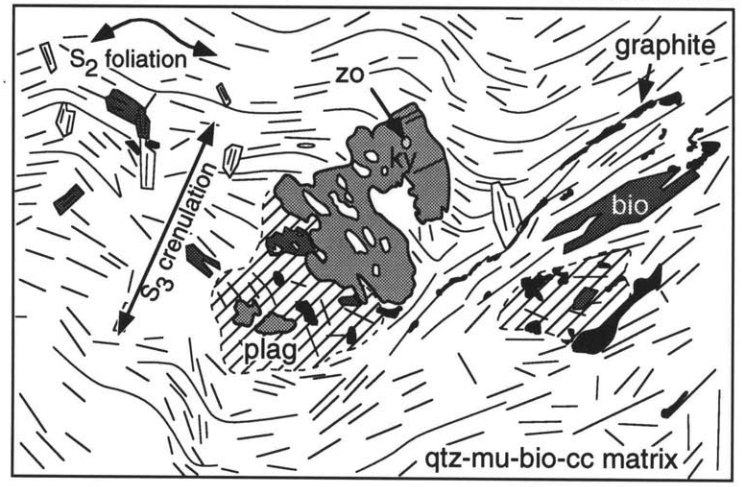

Figure 13: Photomicrographs and sketch of textural relationships in the calc-pelitic schist, sample 93SC-25. Section is cut perpendicular to foliation (S2), perpendicular to stretching lineation (L2), and nearly perpendicular to late crenulation (S3). Minerals present include kyanite (ky), plagioclase (plag), biotite (bio), zoisite (zo), muscovite (mu), quartz (qtz) and calcite (cc). Note the inclusion of zoisite in kyanite, and the growth of plagioclase against a resorbed margin of the kyanite porphyroblast.

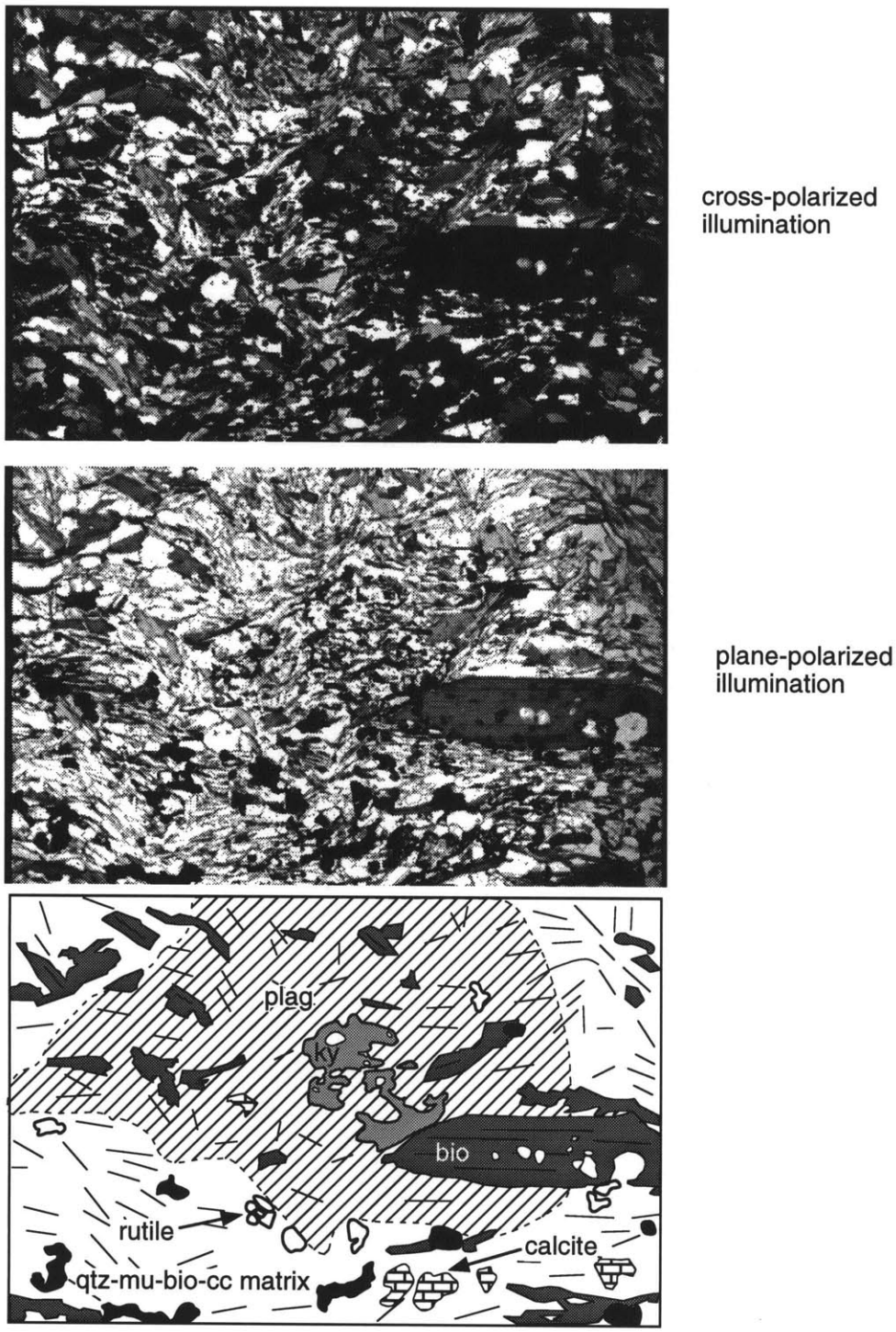

Figure 14: Photomicrographs and sketch of textural relationships in the calc-pelitic schist, sample 93SC-25. Section is cut perpendicular to foliation (S2), perpendicular to stretching lineation (L2), and nearly perpendicular to late crenulation (S3). Minerals present include kyanite (ky), plagioclase (plag), biotite (bio), muscovite (mu), quartz (qtz) and calcite (cc). Note the growth of plagioclase over a resorbed kyanite porphyroblast, and the partial inclusion of a large biotite porphyroblast.

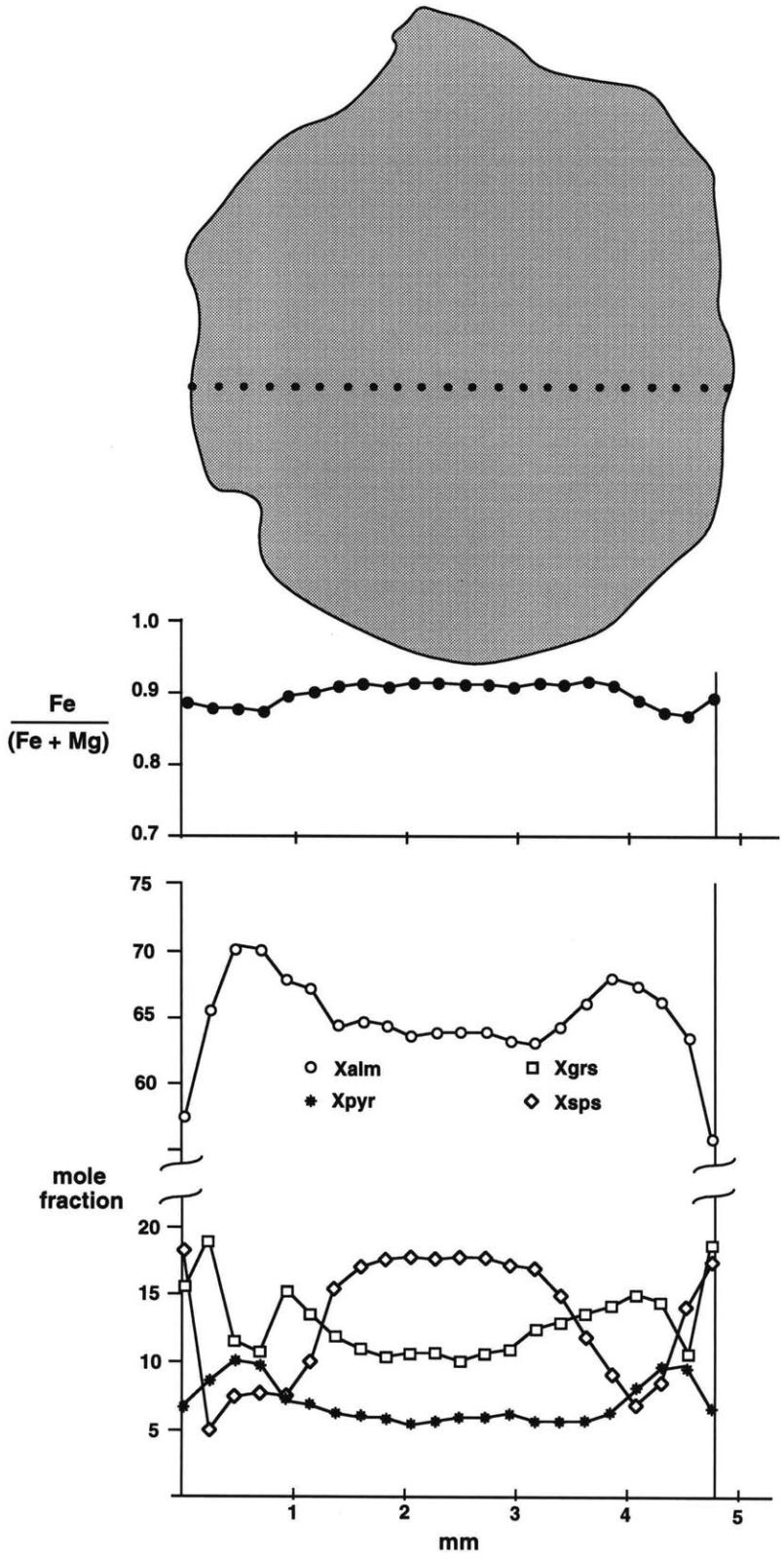

Figure 15: Rim-to-rim analytical traverse across a garnet porphyroblast from the psammitic schist, sample 92SC-102.

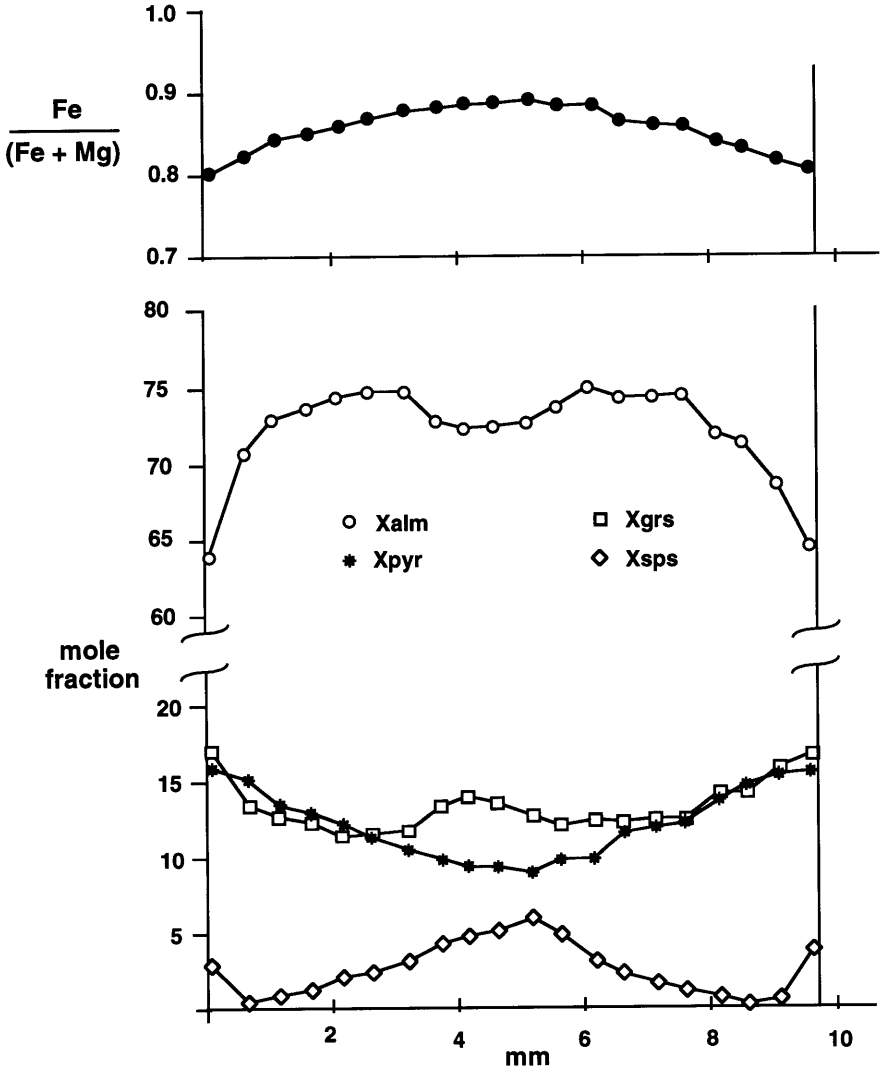

Figure 16: Rim-to-rim analytical traverse across a garnet porphyroblast from the calc-pelitic schist, sample 92SC-25.

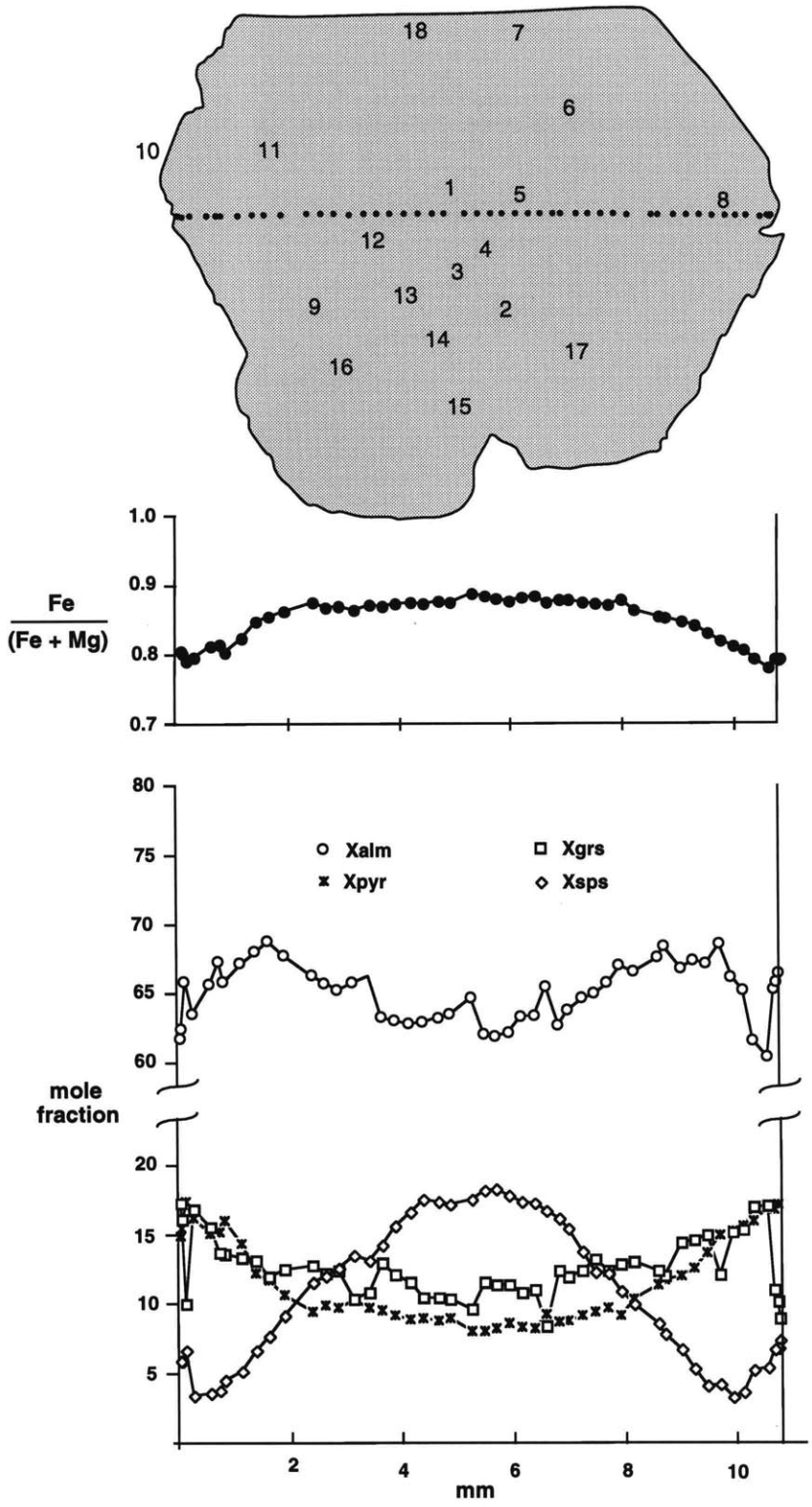

Figure 17: Rim-to-rim analytical traverse across a garnet porphyroblast from the calc-pelitic schist, sample 92SC-24. The numbers in the sketch show the locations of polymineralic inclusions within the garnet porphyroblast described in Table 1.

Table 1

Composite inclusions in garnet porphyroblast, 93SC-24

inclusion location	minerals present (± qtz, mus): ctd	str	chl	bio	mrg	prg
1	-	√	√	-	-	√
2	√	-	-	-	√	√
3	-	-	-	-	-	√
4	√	-	-	-	√	√
5	-	√	√	-	√	√
6	√	-	-	-	√	√
7	-	√	√	-	√	√
8	√	√	-	-	-	-
9	-	-	√	√	-	√
10	(rim location)					
11	-	-	√	-	-	-
12	-	√	√	-	√	√
13	√	-	√	-	-	√
14	-	√	√	-	√	√
15	-	-	-	-	√	√
16	(muscovite)					
17	-	√	√	-	-	√
18	-	√	√	-	-	-

Mineral assemblage of sample: gar-ky-bio-mus-plag-cc-qtz ± str, with accessory rutile, zoisite, and alanite.

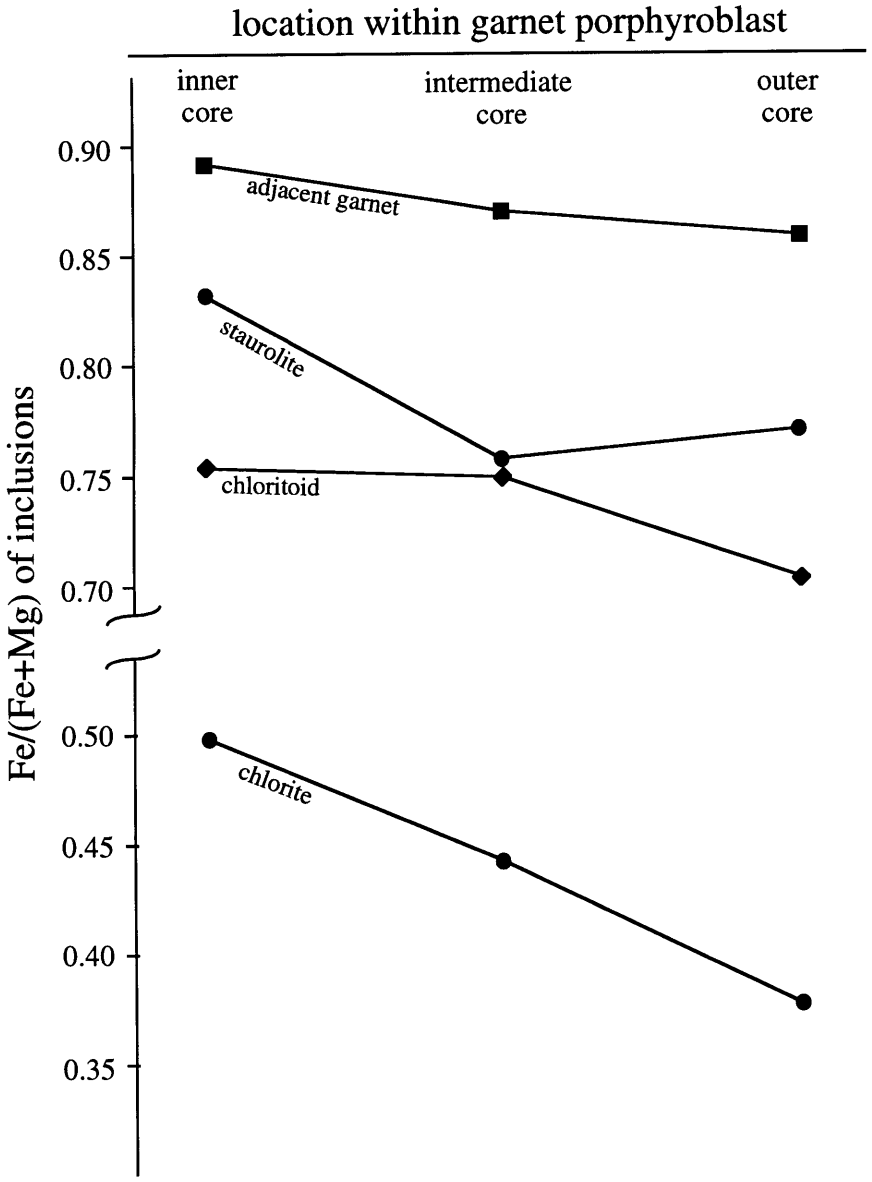

Figure 18: Variations in the Fe/(Fe+Mg) ratio of ferromagnesian mineral inclusions as a function of location within a garnet porphyroblast. Compositions are from the garnet illustrated in figure 17.

"Inner core" data are averaged from inclusions at locations 1, 4, and 5.
"Intermediate core" data are averaged from inclusions at locations 2, 6, 12, 13, and 14.
"Outer core" data are averaged from inclusions at locations 7, 8, 15, and 18.

Samples from Vargfjellet

Sample	T (°C)	P (kbar)
92SC-50	488 ±54	5.34 ±1.12
92SC-55	539 ±40	9.42 ±0.99
92SC-75	589 ±30	9.77 ±0.71
92SC-87	605 ±49	8.84 ±1.04
92SC-91a	542 ±49	7.27 ±1.25
92SC-91b	514 ±58	6.66 ±2.06
92SC-102	520 ±56	6.59 ±1.09

Samples from E. Hinnøya

Sample	T (°C)	P (kbar)
93SC-22	545 ±27	8.84 ±0.98
93SC-24	533 ±36	8.36 ±0.74
93SC-25	539 ±37	8.81 ±0.91
93SC-26	534 ±42	8.82 ±0.93
93SC-33	539 ±48	7.30 ±1.17

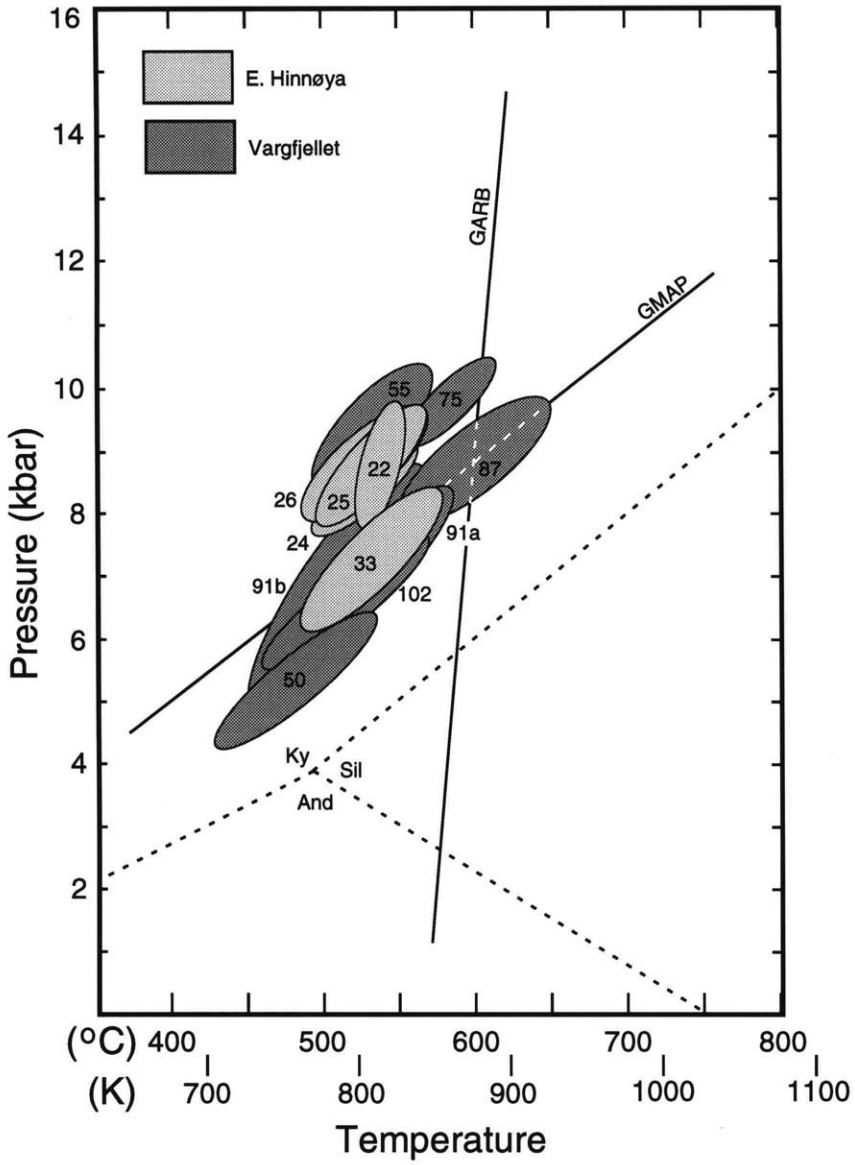

Figure 19: Results of simultaneous solution of the GARB and GMAP thermobarometers for samples of the metasedimentary cover on Baltica. Sample locations are given in figures 4 and 5.

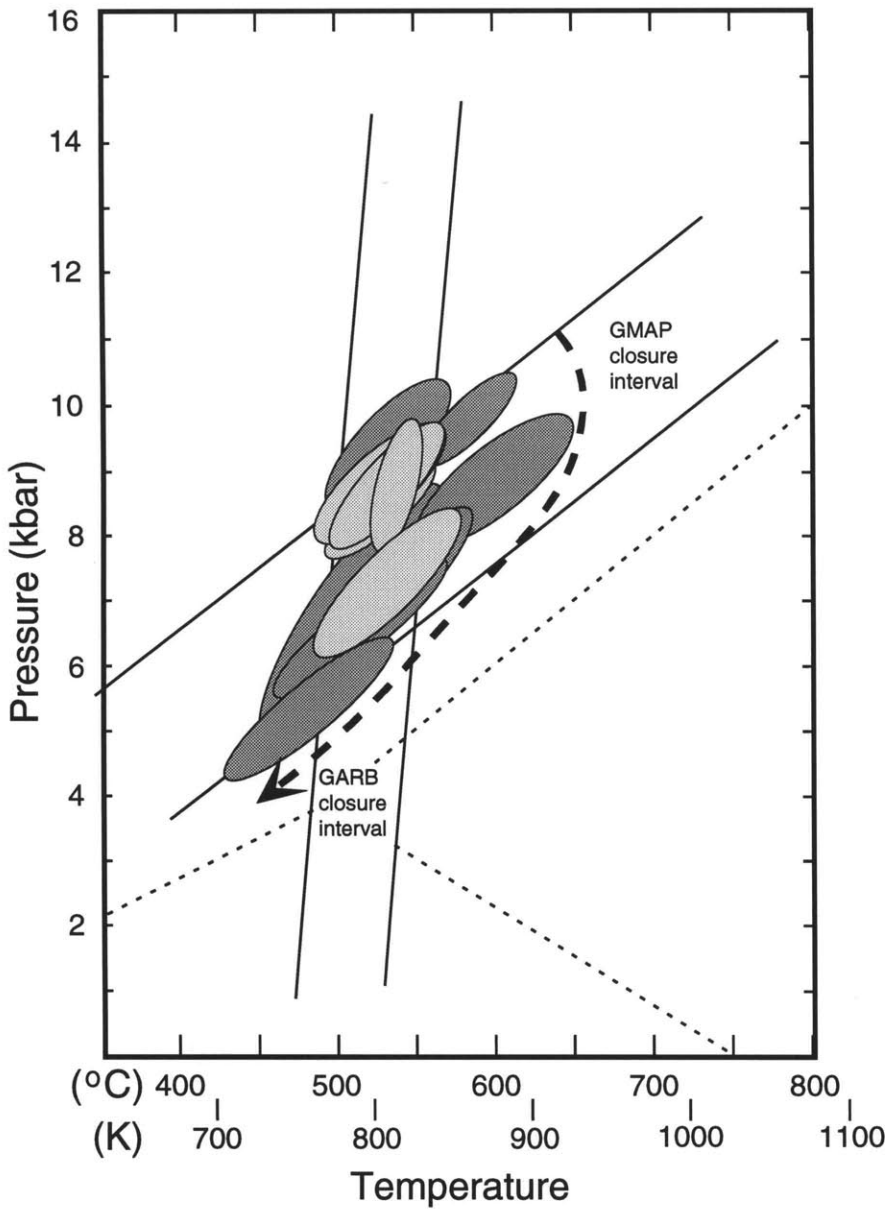

Figure 20: Generation of the array of P-T estimates in this study through independent equilibration of the GARB and GMAP thermobarometer reactions at different stages of a hypothetical P-T path (dashed arrow).

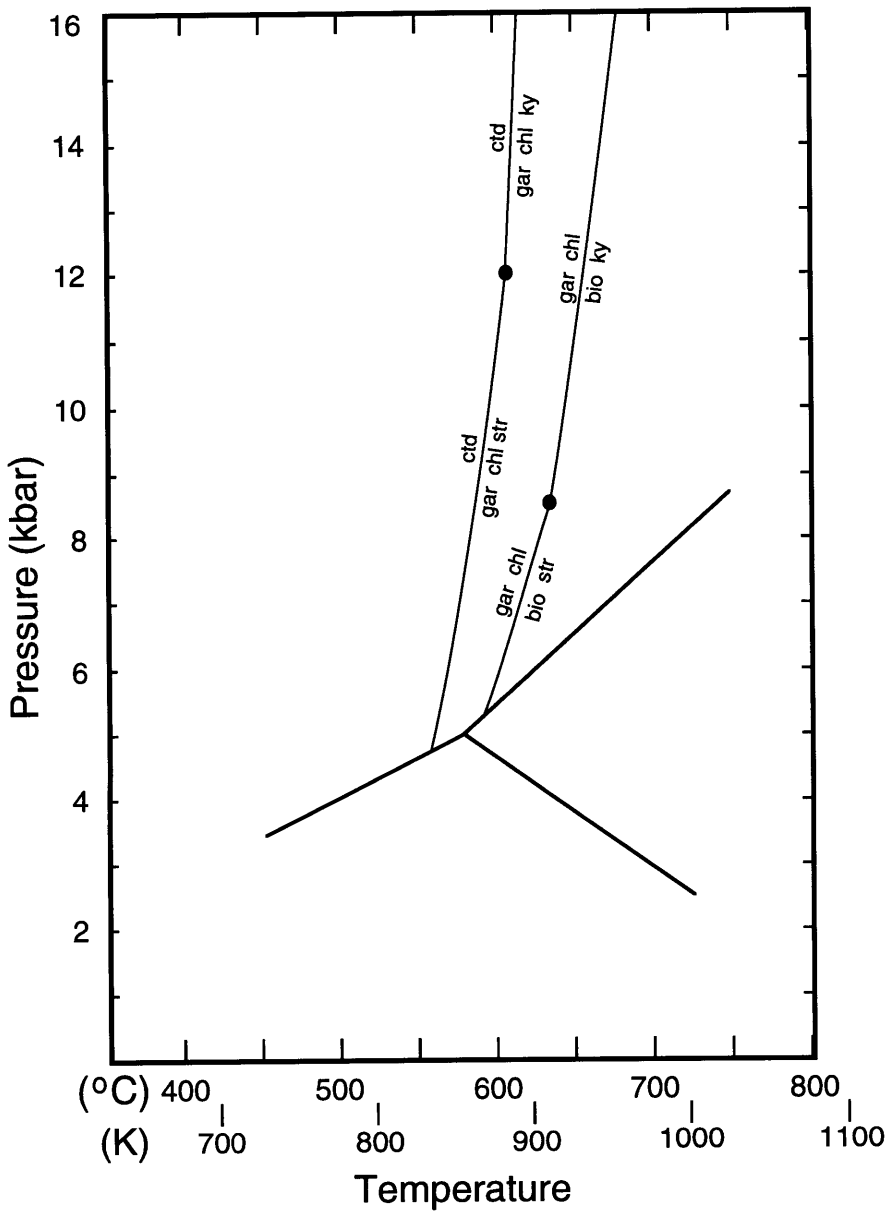

Figure 21: Stability fields of the aluminum silicate polymorphs and the upper stability limits of chloritoid and garnet + chlorite ± kyanite parageneses in the KFMASH system as calculated by Holland and Powell (1990).

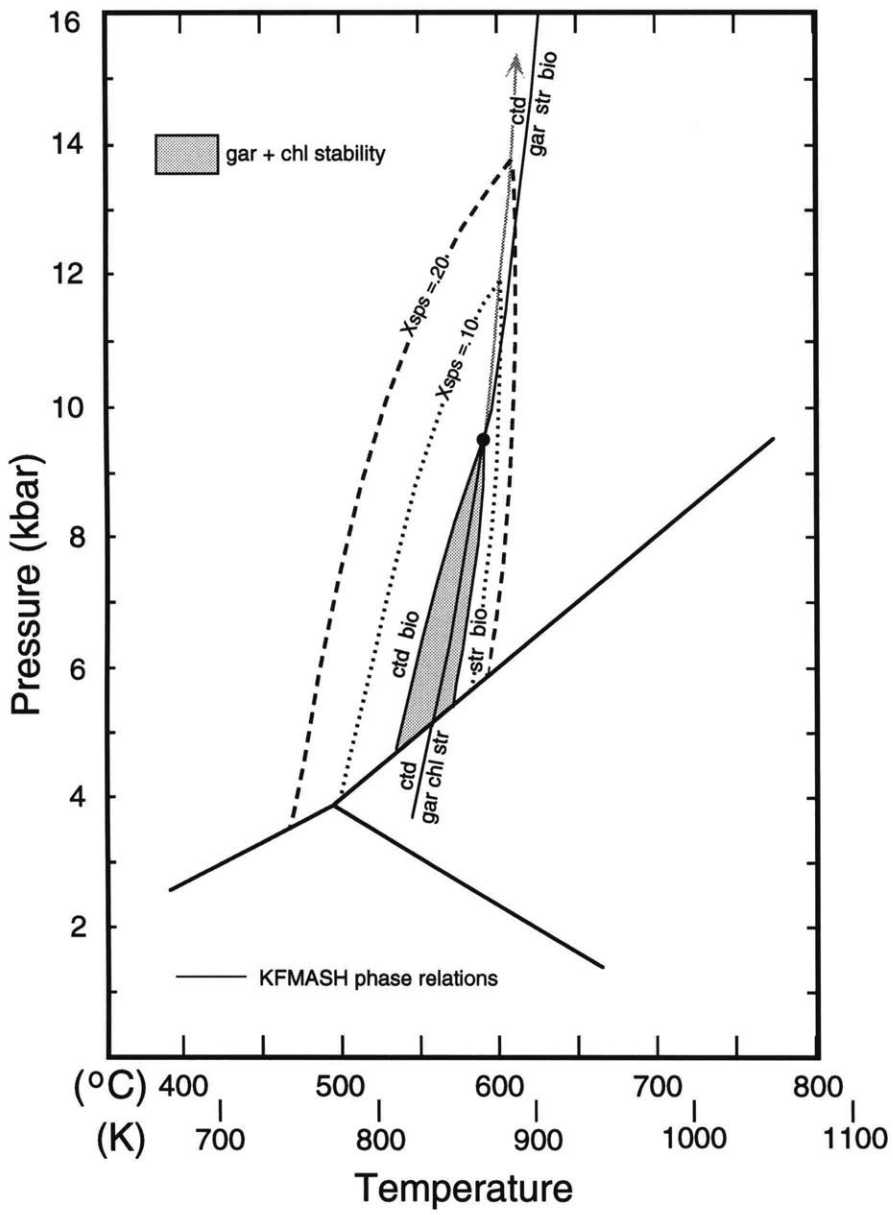

Figure 22: Upper stability limits of chloritoid and garnet + chlorite ± kyanite parageneses in the KFMASH system and the effects of increasing Xsps in garnet, as calculated by Spear and Cheney (1989).

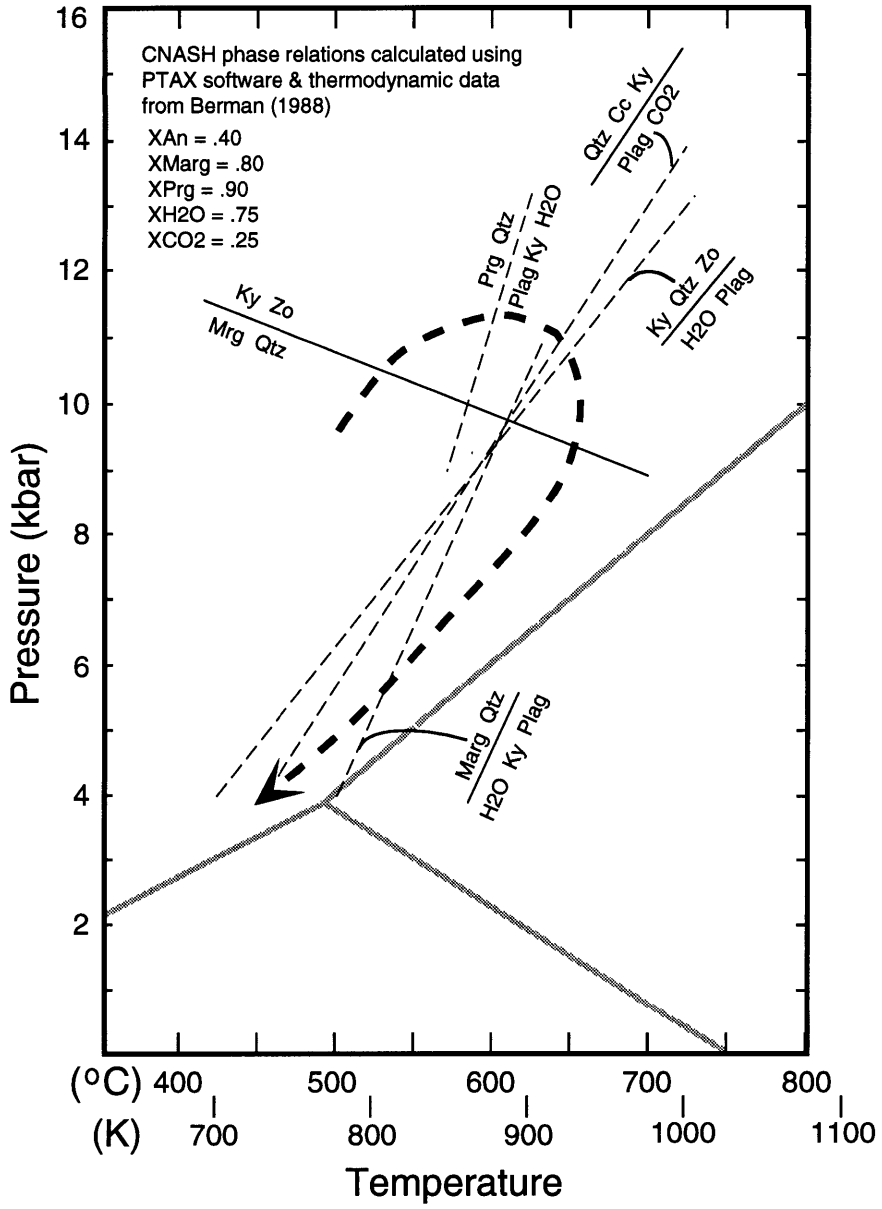

Figure 23: Reactions in the CNASHC composition system inferred or indicated texturally to have occurred in the calc-pelitic schist. The dashed arrow illustrates a hypothetical P-T path consistent with the relative sequence of reactions suggested by textural relations in the schist. Note that all reaction boundaries shown are fluid sensitive and, therefore, are not rigorously located in P-T space.

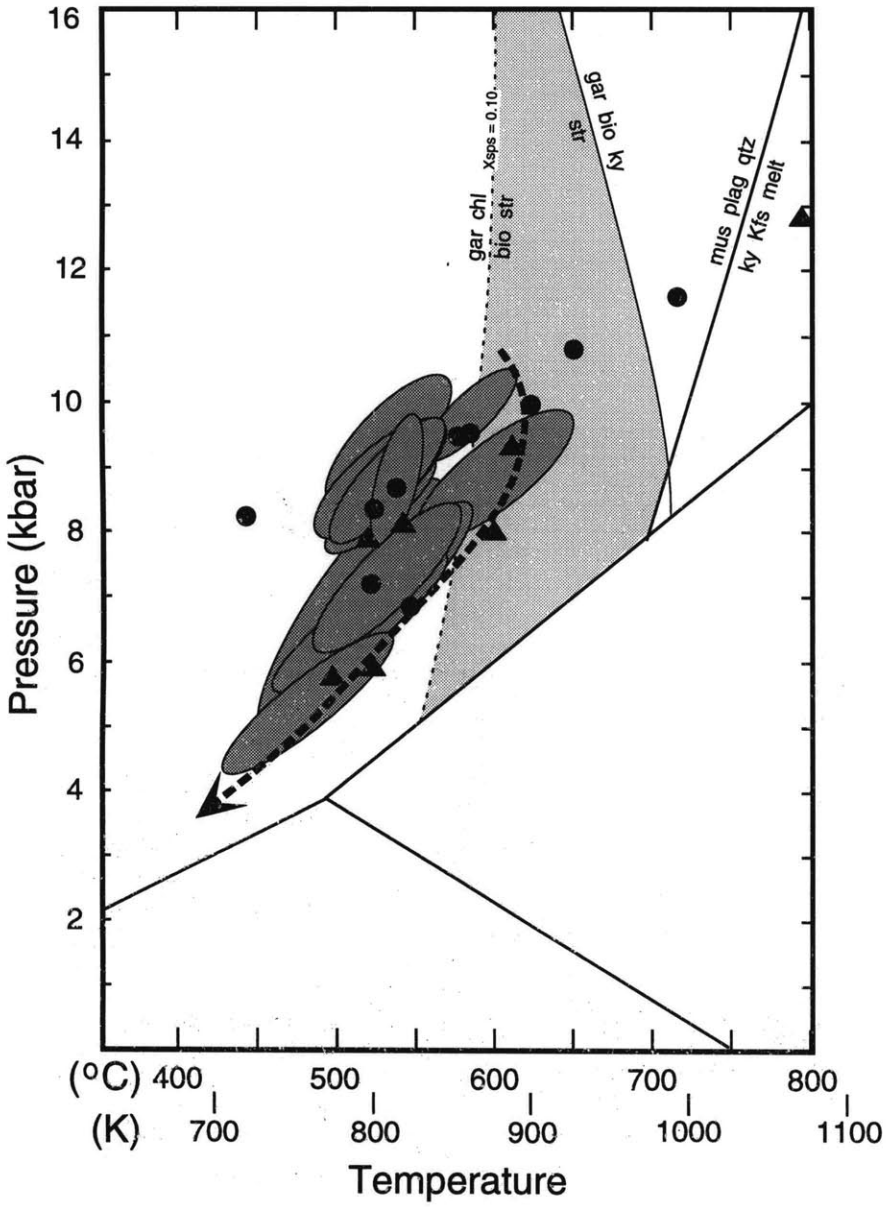

Figure 24: Summary of constraints on the conditions of peak metamorphism in the footwall of the Caledonian A-type subduction zone from quantitative thermobarometry and KFMASH petrogenetic considerations (Phase relations after Spear and Cheney, 1989). Black triangles and dots show P-T estimates for samples from the overlying allocthhon, recalculated from the data of Hodges and Royden (1984) and Steltenpohl and Bartley (1987), respectively. The dashed arrow illustrates one possible P-T path for the footwall consistent with the data.

Plate 1

16°25'E

16°35'E

68°35'N

68°30'N

TJELSUND

OFOTFJORDEN

RESTRICTED ACCESS

Explanation

Lithologic units:

- oe — Evenes marble
- oa — amphibolite schist ± tonalite

Ofoten Nappe Complex

- n — Narvik Nappe Complex (undifferentiated): pelitic schist and amphibolite with felsic dikes

- sp — calc-pelitic schist
- sm — impure marble; in some locations identified as lower (m1) or upper (m2) marble
- sg — psammitic schist
- sq — banded or vitreous quartzite ± mica schist; contains garnet in some locations (sqg)
- sa — arkosic quartzite ± mica schist

Storvann Group metasedimentary cover sequence

- pCg — Proterozoic granite
- pCs — Proterozoic schist, amphibolite, and epidote-amphibolite gneiss

Baltic craton

Symbols:

- orientation of tectonic foliation (S_2) (dipping, vertical, horizontal)
- orientation of stretching lineation (L_2) (extra half-arrow on shaft shows transport direction infered from S-C fabric, asymetric porphyroclasts, or shear bands)
- thrust fault (ornament on hangingwall, dashed where approximate, dotted where inferred)
- lithologic contact (dashed where approximate, dotted where inferred)
- normal fault (ornament on hangingwall, dashed where approximate, dotted where inferred)

0 1 2 km

contour interval = 100 m

Plate 2

16°20'E 16°30'E 68°25'N 68°20'N

Explanation

Lithologic units:

Ofoten Nappe Complex
- ob — Bogen group (undifferentiated quartzite, schist and marble)
- oe — Evenes marble ± calcareous schist
- oc — heterogeneous, metamorphosed clastic sedimentary rocks with local conglomerate and/or amphibolite

Narvik Nappe Complex
- np — pelitic schist
- nb — amphibolite and biotite schist
- nu — ultramafic rock
- nm — impure marble and dolomite

Storvann Group Metasedimentary Cover Sequence
- sp — calc-pelitic schist
- sm — impure marble
- sg — psammitic schist
- sq — banded or vitreous quartzite ± mica schist
- sa — arkosic quartzite ± mica schist

Baltic Craton
- pCg — Proterozoic granite
- pCs — Proterozoic schist, amphibolite, and epidote-amphibolite gneiss

Symbols:
- orientation of tectonic foliation (S_2) (dipping, vertical)
- orientation of stretching lineation (L_2) (extra half-arrow on shaft shows transport direction infered from S-C fabric, asymetric porphyroclasts, or shear bands)
- orientation of crenulation (S_3) (dipping, vertical)
- thrust fault (ornament on hangingwall, dashed where approximate, dotted where inferred)
- lithologic contact (dashed where approximate, dotted where inferred)

0 1 2 km

contour interval = 100 m

N

OFOTFJORDEN

EFJORDEN

A A'

NE A

A' SE

1000
sea level
1000
2000
3000
4000

oe
oc
np
nb
sg
sq
sa
pCg
pCs

Plate 3

Explanation

Lithologic units:

- n — Narvik Nappe Complex (undiferentiated schist, amphibolite, marble and quartzite)
- mz — mylonitic sliver zone
- sg — psammitic schist ± pelitic schist and marble
- sq — banded or vitreous quartzite ± mica schist

Storvann Group Metasedimentary Cover Sequence

- pCg — Proterozoic granite
- pCs — Proterozoic schist, amphibolite, and epidote-amphibolite gneiss

Baltic Craton

Symbols:

- orientation of tectonic foliation (S_2) (dipping, vertical)
- orientation of stretching lineation (L_2) (extra half-arrow on shaft denotes transport direction infered from S-C fabric, asymetric porphyroclasts, or shear bands)
- thrust fault (ornament on hangingwall, dashed where approximate, dotted where inferred)
- lithologic contact (dashed where approximate, dotted where inferred)
- glacial cover
- trace of Efjord antiform

0 1 2 km

contour interval = 100 m